GEOFISICA
PURA E APPLICATA

PURE AND APPLIED GEOPHYSICS
REINE UND ANGEWANDTE GEOPHYSIK
GÉOPHYSIQUE PURE ET APPLIQUÉE
GEOFISICA PURA Y APLICADA

Comitato di redazione - Editorial Consulting Board

M. Båth, Uppsala - J. Bartels, Göttingen - A. Belluigi, Roma - H. P. Berlage, De Bilt - H. R. Byers, Chicago - M. Cadez, Beograd - S. Chapman, Alaska - J. Coulomb, Paris - H. Ertel, Berlin - G. Fanselau, Potsdam - F. Gassmann, Zürich - W. A. Heiskanen, Helsinki - K. Kondratiev, Leningrad - J. C. Jaeger, Canberra - K. Jung, Kiel - E. Lahaye, Uccle - K. Ledersteger, Wien - P. Melchior, Uccle - F. Möller, München - T. Nagata, Tokyo - L. W. Pollak, Dublin - C. H. B. Priestley, Aspendale - P. Raethjen, Hamburg - K. Rawer, Breisach - A. E. Scheidegger, Calgary - O. Schneider, Buenos Aires - V. P. Starr, Cambridge, Mass. - A. Tárczy-Hornoch, Sopron - A. & E. Vassy, Paris - J. R. Wait, Boulder - J. T. Wilson, Toronto.

Direttore - Editor
Mario Bossolasco

VOL. 48 (1961/I)

UNIVERSITY OF HAWAII
LIBRARIES
NOV 30 1983
LIBRARY USE ONLY
PERIODICAL ROOM
LIBRARY

...NO - ISTITUTO GEOFISICO ITALIANO - MILANO
...za Leonardo da Vinci 12 - Casella Postale 3689

GEOFISICA
PURA E APPLICAT

PURE AND APPLIED GEOPHYSICS
REINE UND ANGEWANDTE GEOPHYSIK
GÉOPHYSIQUE PURE ET APPLIQUÉE
GEOFISICA PURA Y APLICADA

Comitato di redazione - Editorial Consulting Board

M. BÅTH, Uppsala - J. BARTELS, Göttingen - A. BELLUIGI, Roma - H. P. BERLAGE, De Bilt - H. R. BYERS, Chicago - M. CADEZ, Beograd - S. CHAPMAN, Alaska - J. COULOMB, Paris - H. ERTEL, Berlin - G. FANSELAU, Potsdam - F. GASSMANN, Zürich - W. A. HEISKANEN, Helsinki - K. KONDRATIEV, Leningrad - J. C. JAEGER, Canberra - K. JUNG, Kiel - E. LAHAYE, Uccle - K. LEDERSTEGER, Wien - P. MELCHIOR, Uccle - F. MÖLLER, München - T. NAGATA, Tokyo - L. W. POLLAK, Dublin - C. H. B. PRIESTLEY, Aspendale - P. RAETHJEN, Hamburg - K. RAWER, Breisach - A. E. SCHEIDEGGER, Calgary - O. SCHNEIDER, Buenos Aires - V. P. STARR, Cambridge, Mass. - A. TÁRCZY-HORNOCH, Sopron - A. & E. VASSY, Paris - J. R. WAIT, Boulder - J. T. WILSON, Toronto.

Direttore - Editor
MARIO BOSSOLASCO

VOL. 48 (1961/I)

MILANO - ISTITUTO GEOFISICO ITALIANO - MILANO
Piazza Leonardo da Vinci 12 - Casella Postale 3689

PRINTED IN ITALY

PROPRIETÀ RISERVATA — ALL RIGHTS RESERVED

This volume or any part thereof must not be reproduced in any form without the written permission of the publisher.

FUMIGATED 1995 FUMIGATED 1995

GEOFISICA PURA E APPLICATA

VOL. 48 (1961/1)

CONTENTS - INHALT - SOMMAIRE - INDICE - SUMARIO

Attmannspacher W.: Nullschicht und Tropopause ..... Pag. 151
Bary (De) E. (*und K. Bullrich & D. Lorenz*): Messungen der Himmelsstrahlung und deren Polarisationsgrad während der Sonnenfinsternis am 15.2.1961 in Viareggio (Italien) ..... » 193
Bossolasco M. (*and A. Elena & A. Caneva*): On the Geomagnetic Effect of the Solar Eclipse of 1961, February 15th at Genova ..... » 102
Bullrich K. (*und E. De Bary & D. Lorenz*): Messungen der Himmelsstrahlung und deren Polarisationsgrad während der Sonnenfinsternis am 15.2.1961 in Viareggio (Italien) ..... » 193
Burkard O.: Studies of the new Ionospheric Model: II ..... » 57
Caneva A. (*and M. Bossolasco & A. Elena*): On the Geomagnetic Effect of the Solar Eclipse of 1961, February 15th at Genova ..... » 102
Chakraborty S. K.: Disturbances in a Viscoelastic Medium due to Impulsive Forces on a Spherical Cavity ..... » 23
Coroniti S. C.: The Effect of Aerosols on the Electrical Conductivity in the Atmosphere ..... » 124
Das Gupta S. C.: On Pressure Waves in the Coastal Region ..... » 49
Elena A. (*and M. Bossolasco & A. Caneva*): On the Geomagnetic Effect of the Solar Eclipse of 1961, February 15th at Genova ..... » 102
Gherzi E.: Some Querries concerning Tropical Cyclones and their Origin » 199
Lorenz D. (*und E. De Bary & K. Bullrich*): Messungen der Himmelsstrahlung und deren Polarisationsgrad während der Sonnenfinsternis am 15.2.1961 in Viareggio (Italien) ..... » 193
Montefinale A. (*& H. M. Papée*): Correlation of Precipitable Water Vapour Values over the United States with Physical and Chemical Parameters. Part I: Seasonal Trends with Precipitation and its Nitrate Content. Geographic Changes of Nitrate ..... » 203
Part II: Seasonal Trends with Physical Variables ..... » 224
Mueller I. I.: The Determination of the Regional Part of the Vertical Gradient Anomaly by a Geodetic Method ..... » 1
Nag K. R.: On the Propagation of Rayleigh Waves in three Dimensions in Alluvial Soils ..... » 16
Paetzold H. K. (*& H. Zschörner*): An Annual and a Semiannual Variation of the Upper Air Density ..... » 85

Paffrath D.: Ein einfacher Niederschlagsindikator ..... Pag. 138
Papée H. M. (& *A. Montefinale*): Correlation of Precipitable Water Vapour Values over the United States with Physical and Chemical Parameters. Part I: Seasonal Trends with Precipitation and its Nitrate Content. Geographic Changes of Nitrate ..... » 203
Part II: Seasonal Trends with Physical Variables ..... » 224
Paul M. K.: On Computation of Second Derivatives from Gravity Data » 7
Rasool S. I.: Effects de l'activité solaire sur l'ozone atmosphérique et la hauteur de la tropopause ..... » 93
Reuter H.: Mittelfristige Wettervorhersagen mit synoptisch-statistischen Methoden ..... » 167
Saltzman B.: Perturbation Equations for the time-average State of the Atmosphere including the Effects of Transient Disturbances .... » 143
Shifrin K. S.: Spectral Properties of Clouds ..... » 129
Simojoki H.: On the Secular Change in Water Level of Lakes in Finland » 53
Stacey F. D.: Dielectric Anisotropy and Fabric of Rocks ..... » 40
Starr V. P.: Hydrodynamical Red-Shift Phenomena in Geophysics .. » 109
Tárczy-Hornoch A.: Ein neuer automatischer Libellenprüfer für Sekundenlibellen ..... » 27
Thams J. C.: Der Einfluss von Bewölkungsmenge und -art auf die Grösse der diffusen Himmelsstrahlung ..... » 181
Weber M.: Ein exakter Seismometer ..... » 35
Wegener K.: Der Neubau der Meteorologie ..... » 178
Zschörner H. (& *H. K. Paetzold*): An Annual and a semiannual Variation of the Upper Air Density ..... » 85
Libri Nuovi - Reviews - Buchbesprechungen - Nouveaux Livres - Nuevos Libros ..... » 240

GEOFISICA PURA E APPLICATA

Vol. 48 Gennaio-Aprile 1961

THE DETERMINATION OF THE REGIONAL PART OF THE VERTICAL GRADIENT ANOMALY BY A GEODETIC METHOD

by Ivan I. Mueller (*)

Summary — The significance of the vertical gradients of gravity is great in geophysics and also in geodesy. In geophysics the observed vertical gradients can give valuable information about mass distributions close to the surface of the earth and in geodesy they may be used in determining the shape of the equipotential surfaces. The observed vertical gradients are very sensitive to masses close to the surface of the earth and they change very rapidly. Therefore, they should not be used for purposes such as the reduction of the observed gravity to the sea level. The normal vertical gradients are not the best either for this purpose because they are much too uniform on the surface of the earth. The best values for practical purposes are probably the regional vertical gradients.

This paper presents a method to determine the regional vertical gradient anomalies in large areas from geodetic observations which, added to the normal part, will give the regional vertical gradients.

In geodetic and gravimetric computations the coordinate system generally used is a local coordinate system. The x axis at such a system is oriented towards the North, i.e., it is tangent to the local meridian; the z axis coincides with the direction of the local gravity; and the y axis is perpendicular to both x and z and it is positive towards East. Therefore, the relative orientation of the coordinate system is different at each observation station. For the sake of simplicity let us use only one coordinate system for a small area.

We choose an arbitrary station, O, with astro-coordinates, Φ and L, as our reference station and we use the coordinate system based on this point over the whole area. Hence at any point the z axis is parallel to the vertical at point O and the x axis is parallel to the tangent to the meridian at point O.

Figure 1 shows the xz plane of a coordinate system as defined above and through an arbitrary point, A_1. The origin of the system is at A_1. The z axis is parallel to the vertical at the reference station O; therefore, it does not coincide with the direction of the gravity vector g at point A_1. The vector A_1G is the projection of the gravity vector on to the xz plane. The difference between the vector A_1G and the gravity vector is negligible. In this case the A_1H vector is the g_x compo-

(*) Dr. Ivan I. Mueller, Assistant Professor, The Ohio State University, Department of Geodetic Science, *Columbus* 10, *Ohio*, U.S.A.

nent of g. The line $E - E$ is the intersection of the equatorial plane and the xz plane. If the astro-latitude of the reference station is Φ and the angle between the vertical at O and at A_1 is $\Delta\Phi_1$, then the latitude at A_1 is $\Phi_1 = \Phi + \Delta\Phi_1$. From Figure 1 it is obvious that

$$-g_x = g \sin \Delta\Phi_1$$

or since $\Delta\Phi_1$ is a small angle

$$\Delta\Phi_1 = -\frac{g_x}{g} . \tag{1}$$

After a similar approach the angle difference in the yz plane, i.e., in the prime-vertical plane is

$$\Delta L_1 \cos \Phi_1 = -\frac{g_y}{g} \tag{2}$$

where ΔL_1 is the astro-longitude difference between the reference station O and A_1.

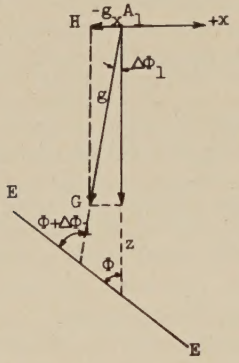

Fig. 1

Expressions (1) and (2) give the North and the East components of the angle between the true verticals at O and at A_1 respectively. We can similarly determine the North and East components of the angle between the verticals at O and another arbitrary point, A_2, $\Delta\Phi_2$ and ΔL_2. The quantities $(\Delta\Phi_2 - \Delta\Phi_1)$ and $(\Delta L_2 - \Delta L_1)$ are the North and the East components of the angle between the true normals at A_2 and at A_1.

$$\begin{cases} \Delta\Phi_2 - \Delta\Phi_1 = -\dfrac{1}{g_m}\left[(g_x)_2 - (g_x)_1\right] = -\dfrac{1}{g_m}\left[\left(\dfrac{\partial W}{\partial x}\right)_2 - \left(\dfrac{\partial W}{\partial x}\right)_1\right] \\ (\Delta L_2 - \Delta L_1)\cos \Phi_m = -\dfrac{1}{g_m}\left[(g_y)_2 - (g_y)_1\right] = -\dfrac{1}{g_m}\left[\left(\dfrac{\partial W}{\partial y}\right)_2 - \left(\dfrac{\partial W}{\partial y}\right)_1\right] \end{cases} \tag{3}$$

where g_m and Φ_m are the mean gravity and the mean astro-latitude between A_1 and A_2. The quantities $(\Delta\Phi_2 - \Delta\Phi_1)$ and $(\Delta L_2 - \Delta L_1)$ are the *astro*-latitude and longitude differences between points A_2 and A_1. The $(g_x)_1$, $(g_x)_2$, etc. are the gravity components in the x or y directions at A_1 and A_2. W is the potential function of the gravity (geopotential function).

Similar expressions can be derived for the North and the East components of the angle between the ellipsoidal normals, i.e., between the directions of the normal gravity, at A_1 and A_2.

$$\begin{cases} \Delta\varphi_2 - \Delta\varphi_1 = -\dfrac{1}{\gamma_m}\left[\left(\dfrac{\partial U}{\partial x}\right)_2 - \left(\dfrac{\partial U}{\partial x}\right)_1\right] \\ (\Delta\lambda_2 - \Delta\lambda_1)\cos\varphi_m = -\dfrac{1}{\gamma_m}\left[\left(\dfrac{\partial U}{\partial y}\right)_2 - \left(\dfrac{\partial U}{\partial y}\right)_1\right] \end{cases} \tag{4}$$

where the quantities $(\Delta\varphi_2 - \Delta\varphi_1)$ and $(\Delta\lambda_2 - \Delta\lambda_1)$ are the *geodetic*-latitude and longitude differences, γ is the normal gravity and U is its potential function (spheropotential function). The differences between expressions (3) and (4) are the differences of the deflection components between A_1 and A_2. Without any loss of accuracy we can assume that within the surveyed area $\gamma_m = g_m$ and $\Phi_m = \varphi_m$. Subtracting expressions (4) from (3)

$$[(\Delta\Phi_2 - \Delta\varphi_2) - (\Delta\Phi_1 - \Delta\varphi_1)]\, g_m = -\left[\left(\frac{\partial W}{\partial x}\right)_2 - \left(\frac{\partial W}{\partial x}\right)_1\right] + \left[\left(\frac{\partial U}{\partial x}\right)_2 - \left(\frac{\partial U}{\partial x}\right)_1\right]$$

$$[(\Delta L_2 - \Delta\lambda_2)\cos\varphi_m - (\Delta L_1 - \Delta\lambda_1)\cos\varphi_m]\, g_m = -\left[\left(\frac{\partial W}{\partial y}\right)_2 - \left(\frac{\partial W}{\partial y}\right)_1\right] + \left[\left(\frac{\partial U}{\partial y}\right)_2 - \left(\frac{\partial U}{\partial y}\right)_1\right]$$

or by using the usual symbols $\xi = \Delta\Phi - \Delta\varphi$, $\eta = (\Delta L - \Delta\lambda)\cos\varphi$, and $\Delta W = W - U$ we get

$$\begin{aligned} -g_m(\xi_2 - \xi_1) &= (\Delta W_x)_2 - (\Delta W_x)_1 \\ -g_m(\eta_2 - \eta_1) &= (\Delta W_y)_2 - (\Delta W_y)_1 \end{aligned} \tag{5}$$

where we used the symbols ΔW_x for $\partial\Delta W/\partial x$, and ΔW_y for $\partial\Delta W/\partial y$, which are the anomalies of the first partial derivatives of the potential. ξ_1, ξ_2, η_1, and η_2 are the deflection components at A_1 and A_2.

Let $(x_2 - x_1)$ and $(y_2 - y_1)$ be the distances between A_1 and A_2 in the directions x and y, respectively. Dividing the equation in (5) by $(x_2 - x_1)$ and again by $(y_2 - y_1)$ we get

$$\begin{cases} -g_m\dfrac{\xi_2 - \xi_1}{x_2 - x_1} = \dfrac{(\Delta W_x)_2 - (\Delta W_x)_1}{x_2 - x_1} \\ -g_m\dfrac{\eta_2 - \eta_1}{y_2 - y_1} = \dfrac{(\Delta W_y)_2 - (\Delta W_y)_1}{y_2 - y_1}\,. \end{cases} \tag{6}$$

Bringing the two points infinitely close to each other equations (6) become

$$\begin{cases} -g_m\dfrac{\partial\xi}{\partial x} = \dfrac{\partial}{\partial x}\Delta W_x = \Delta W_{xx} \\ -g_m\dfrac{\partial\eta}{\partial y} = \dfrac{\partial}{\partial y}\Delta W_y = \Delta W_{yy}\,. \end{cases} \tag{7}$$

The Laplace equation is valid not only for the second partial derivatives of the potential, but also for the anomalies; therefore, we get

$$\Delta W_{zz} = -(\Delta W_{xx} + \Delta W_{yy}) . \tag{8}$$

Substituting (7) into (8) we get

$$\Delta W_{zz} = g_m \left(\frac{\partial \xi}{\partial x} + \frac{\partial \eta}{\partial y} \right) . \tag{9}$$

Applying this equation to a grid system (Fig. 2) where the deflection components ξ and η were determined ad the intersection points we get the vertical

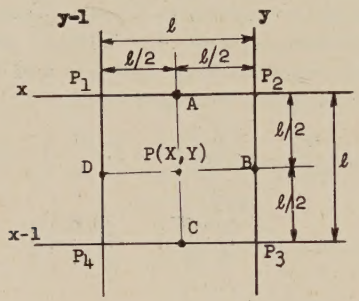

Fig. 2

gradient anomaly at the center of the square from the following equation

$$(\Delta W_{zz})_{X,Y} = \frac{g_m}{2l} [(\xi_{x,y} - \xi_{x-1,y}) + (\xi_{x,y-1} - \xi_{x-1,y-1}) + (\eta_{x,y} - \eta_{x,y-1}) + (\eta_{x-1,y} - \eta_{x-1,y-1})] . \tag{10}$$

Another form of this equation is

$$(\Delta W_{zz})_{X,Y} = \frac{g_m}{2l} [(\xi + \eta)_{x,y} - (\xi - \eta)_{x-1,y} + (\xi - \eta)_{x,y-1} - (\xi + \eta)_{x-1,y-1}] \tag{11}$$

where $(\Delta W_{zz})_{X,Y}$ is the vertical gradient anomaly at the center of the square $P_1P_2P_3P_4$,

ξ, η are the deflection components at the cornerpoints indicated by the indices of the parentheses,

g_m is the average gravity value within the square,

l is the length of one side of the square.

The length l should be selected carefully because in the derivation of (10) it is assumed that the variation of the deflection components is linear over that distance. The length l can vary in the computation but depends upon the variation of the deflections. The normal gravity value can be substituted for the gravity value without any loss of accuracy.

The deflection components at the cornerpoints can be determined by interpolation from any relative deflection of the vertical net. We do not need absolute values because in equation (10) we have deflection differences only. Thus, the deflection net can be astro-geodetic. If the deflections were reduced to the geoid

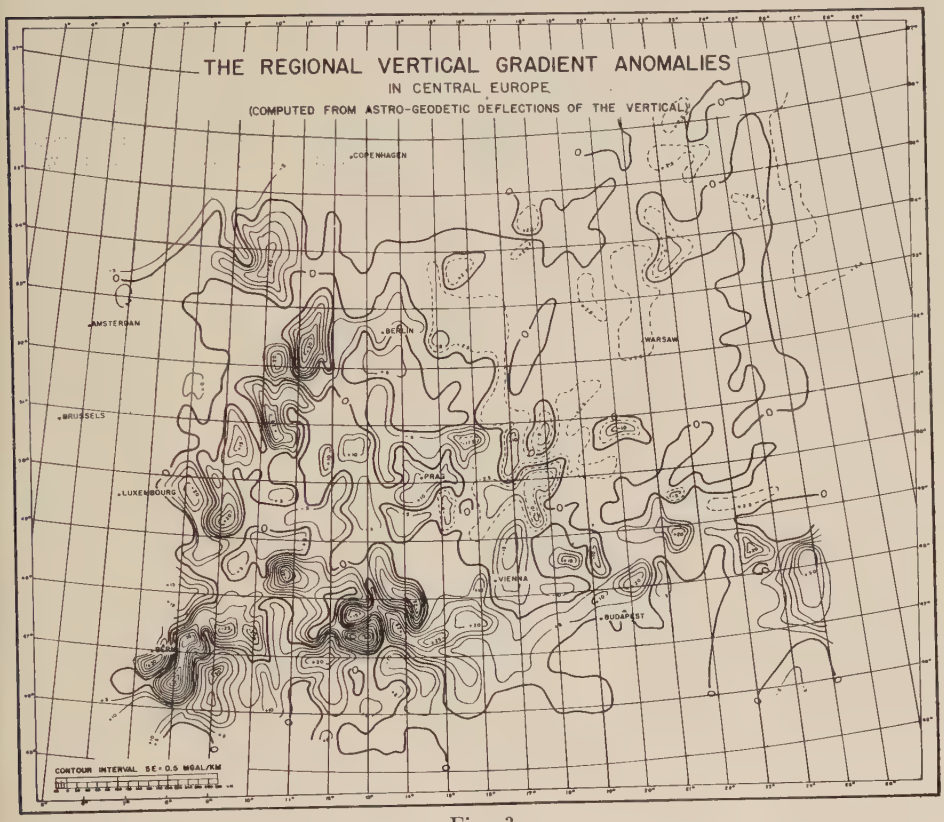

Fig. 3

then the anomaly computed from (10) or (11) and added to the normal vertical gradient $U_{zz} = 0.3086$ mgal/m would give the vertical gradient:

$$\frac{\partial^2 W}{\partial z^2} = \frac{\partial^2 U}{\partial z^2} + \frac{\partial^2 \Delta W}{\partial z^2} = U_{zz} + \Delta W_{zz}\,.$$

The vertical gradient is very sensitive to the masses directly below the computation point. Naturally, the astrogeodetic deflections do not reflect the influence of these masses. Therefore the vertical gradient anomaly computed by this method can be considered only as *the regional part of the total anomaly*.

Fig. 3 shows the regional vertical gradient anomalies in Central Europe as computed by this method. The astrogeodetic deflection components used were

taken from the maps, Number 1 and Number 3, of the publication by WOLF ([1]). The computation using about 2,000 squares has been carried out by the students of The Ohio State University as a laboratory exercise in Physical Geodesy under the supervision of the writer. Similar computation is under progress for the United States.

REFERENCES

([1]) WOLF H.: *Versuch einer Geoidbestimmung im mittleren Europa aus Astronomisch-Geodätischen Lotabweichungen.* Deutsche Geod. Komm. bei der Bayerische Ak. d. Wiss., Reihe A, Heft 18, 1956.

(*Received 8th March* 1961)

ON COMPUTATION OF SECOND DERIVATIVES FROM GRAVITY DATA

by M. K. Paul (*)

Summary — Second derivative formulae of Elkins and Rosenbach are developed from a unified approach and their merits and demerits are discussed. Some new formulae are suggested, which, from theoretical considerations it is felt, will prove more efficient.

The second derivative method of gravity interpretation has gained its importance from the fact that the second derivative contour maps give clearer picture of local shallow subsurface anomalies, at the expense of broad regional ones, than what the normal Bouguer anomaly maps furnish.

Peters (1949), Elkins (1951) and Rosenbach (1953) have developed formulae for determinations of second derivative in terms of gravity values over the surface.

If we take the horizontal plane of the ground as the plane $z = 0$, and z-axis positive vertically downwards and if G be the vertical downward component of gravity, then $\frac{\partial^2 G}{\partial z^2}$ is the second derivative of gravity, we are interested in.

Here, we shall, first develop the same formulae, as obtained by Elkins and Rosenbach, from a unified approach and then deduce some formulae for simple grid spacings.

Gravitational potential, V, at free space, just over the surface of earth satisfy Laplaces equation

$$\frac{\partial^2 V}{\partial x^2} + \frac{\partial^2 V}{\partial y^2} + \frac{\partial^2 V}{\partial z^2} = 0 . \tag{1}$$

Differentiating both sides of (1) partially with respect reference to z and remembering that $\frac{\partial V}{\partial z} = -G$ we have

$$\frac{\partial^2 G}{\partial x^2} + \frac{\partial^2 G}{\partial y^2} + \frac{\partial^2 G}{\partial z^2} = 0 . \tag{2}$$

Thus G is a harmonic function and hence can be expanded in the neighbourhood

---

(*) Mathematician, Geological Survey of India, 5 Middleton Street, *Calcutta*-16, India.

of origin in a convergent power series in x, y, z:

$$G(x, y, z) = \sum_{i=0}^{\infty} \sum_{j=0}^{\infty} \sum_{k=0}^{\infty} a_{ijk}\, x^i y^j z^k . \tag{3}$$

Replacing a_{ij_0} by a_{ij}, we have on the plane $z = 0$

$$G(x, y) = \sum_{i=0}^{\infty} \sum_{j=0}^{\infty} a_{ij}\, x^i y^j \tag{4}$$

and, if we take $x = r \cos\theta$, $y = r \sin\theta$, we obtain,

$$G(r, \theta) = \sum_{i=0}^{\infty} \sum_{j=0}^{\infty} a_{ij}\, r^{i+j} \cos^i\theta \sin^j\theta . \tag{5}$$

Now if the origin of our axes of reference be taken at the point where second derivative is sought, which is represented by $\left(\frac{\partial^2 G}{\partial z^2}\right)_0$ then by (2) and (4) we obtain

$$\left(\frac{\partial^2 G}{\partial z^2}\right)_0 = -2\,(a_{20} + a_{02}) . \tag{6}$$

This equation will be utilised in obtaining the numerical formula for second derivative.

Average over Circle.

As defined by Peters (1949), average gravity over a circle of radius r, $\overline{G}(r)$, is given by

$$\overline{G}(r) = \frac{1}{2\pi} \int_0^{2\pi} G(r, \theta)\, d\theta \tag{7}$$

substituting in (7) from (5) we obtain,

$$\overline{G}(r) = \frac{1}{2\pi} \sum_{i=0}^{\infty} \sum_{j=0}^{\infty} a_{ij}\, r^{i+j} \int_0^{2\pi} \cos^i\theta \sin^j\theta\, d\theta \tag{8}$$

$$= \sum_{p=0}^{\infty} r^{2p} \sum_{m=0}^{\infty} \frac{a_{2p,2p-2m}}{2^{2p}} \frac{(2m)!\,(2p-2m)!}{p!\,m!\,(p-m)!} \tag{9}$$

since

$$\int_0^{2\pi} \cos^{2m+1}\theta \sin^j\theta\, d\theta = \int_0^{2\pi} \cos^i\theta \sin^{2n+1}\theta\, d\theta = 0$$

$$\int_0^{2\pi} \cos^{2m}\theta \sin^{2n}\theta\, d\theta = \frac{\pi}{2^{2m+2n-1}} \frac{(2m)!\,(2n)!}{m!\,n!\,(m+n)!} \tag{10}$$

and correct up to r^4, we have

$$\overline{G}(r) = a_{00} + \frac{a_{20} + a_{02}}{2} r^2 + \frac{3a_{40} + a_{22} + 3a_{04}}{8} r^4 . \tag{11}$$

From (6) and (11) we note that the coefficient of r^2 in the expansion of $\overline{G}(r)$, multiplied by (-4) is equal to the values of second derivative at the centre. Thus, if we obtain the series for $\overline{G}(r)$, we can compute therefrom the second derivative.

Average over Discrete Points on Circle.

Let us take 4ν points on the circle of radius r, their positions being defined by the polar coordinates,

$$(r, \theta_k), \quad k = 1, 2 \ldots\ldots 4\nu, \quad \text{and let} \quad \overline{G'}(r)$$

be their average.

Then

$$\overline{G}'(r) = \frac{1}{4\nu} \sum_{k=1}^{4\nu} G(r, \theta_k) . \tag{12}$$

By application of (5) in (12), we have

$$\left.\begin{aligned} \overline{G}'(r) &= \frac{1}{4\nu} \sum_{k=1}^{4\nu} \sum_{i=0}^{\infty} \sum_{j=0}^{\infty} a_{ij} r^{i+j} \cos^i \theta_k \sin^j \theta_k \\ &= \frac{1}{4\nu} \sum_{i=0}^{\infty} \sum_{j=0}^{\infty} a_{ij} r^{i+j} \sum_{k=1}^{4\nu} \cos^i \theta_k \sin^j \theta_k . \end{aligned}\right\} \tag{13}$$

Now θ_k's are so selected that

i) $\theta_k < \pi/2 , \qquad k = 1, 2, \ldots\ldots \nu,$

ii) $\theta_{\nu+k} = \pi/2 + \theta_k , \qquad k = 1, 2 \ldots\ldots 3\nu$

and iii) when θ_k is not equal to either of 0 and $\pi/4$, corresponding to k, there is some value of

$$k' \; (k \leq \nu , \quad k' \leq \nu , \quad k \neq k')$$

such that

$$\theta_{k'} = \pi/2 - \theta_k .$$

When $\theta_k = \pi/4$, the contribution C, for θ_k, $\theta_{k+\nu}$, $\theta_{k+2\nu}$, $\theta_{k+3\nu}$ in the summation $\Sigma \cos^i \theta_K \sin^i \theta_K$ is given by

$$C = 2^{-\frac{(i+j)}{2}} [1 + (-1)^i + (-1)^j + (-1)^{i+j}]$$

i) 0, when either i or j is odd

ii) 4 $\cos^i \theta_k \sin^i \theta_k$ when both i and j are even.

When $\theta_k = 0$, the corresponding contribution in the summation is given by

$$C = \sum_{\mu=0}^{3} \cos^i \mu\pi/2 \sin^j \mu\pi/2$$

i) 2, when one of (i, j) is zero and other even,

ii) 0, for all other pairs of (i, j).

Now let us calculate the contribution of eight angles

$$\theta_k\,,\ \theta_{k+\nu}\,,\ \theta_{k+2\nu}\,,\ \theta_{k+3\nu} \quad \text{and} \quad \theta_{k'}\,,\ \theta_{k'+\nu}\,,\ \theta_{k'+2\nu}\,,\ \theta_{k'+3\nu}$$

in the summation.

This contribution

$$= [1 + (-1)^i][1 + (-1)^j](\cos^i \theta_k \sin^j \theta_k + \cos^i \theta_{k'} \sin^j \theta_{k'})$$

i) 0, when either i or j is odd,

ii) 4 $(\cos^i \theta_k \sin^i \theta_k + \cos^i \theta_k, \sin^i \theta_k,)$

when both i and j are even.

Thus when θ_k's $\neq 0$ we have

$$\sum_{k=1}^{4\nu} \cos^i \theta_k \sin^j \theta_k = \tag{14}$$

i) 0, when either i or j is odd,

ii) 4 $\Sigma \cos^i \theta_k \sin^i \theta_k$ when both i and j are even.

Combining (13) and (14) we obtain

$$\begin{aligned} \overline{G}'(r) &= \frac{1}{\nu} \sum_{m=0}^{\infty} \sum_{n=0}^{\infty} a_{2m,2n}\, r^{2m+2n} \sum_{k=1}^{\nu} \cos^{2m} \theta_k \sin^{2n} \theta_k \\ &= \frac{1}{\nu} \sum_{p=0}^{\infty} \sum_{m=0}^{p} a_{2m,2p-2m}\, r^{2p} \sum_{k=1}^{\nu} \cos^{2m} \theta_k \sin^{2(p-m)} \theta_k \end{aligned} \tag{15}$$

and when r^6 and other higher powers of r are neglected we obtain,

$$\begin{aligned} \overline{G}'(r) &= a_{00} + \left\{ a_{20} \frac{1}{\nu} \sum_{k=1}^{\nu} \cos^2 \theta_k + a_{02} \frac{1}{\nu} \sum_{k=1}^{\nu} \sin^2 \theta_k \right\} r^2 \\ &+ \left\{ \frac{a_{40}}{\nu} \sum_{k=1}^{\nu} \cos^4 \theta_k + \frac{a_{22}}{\nu} \sum_{k=1}^{\nu} \cos^2 \theta_k \sin^2 \theta_k + \frac{a_{04}}{\nu} \sum_{k=1}^{\nu} \sin^4 \theta_k \right\} r^4. \end{aligned} \tag{16}$$

This is the form when all θ_k's are different from zero. When one of θ_k's, say

θ_1, is $= 0$, (16) takes the form

$$(17)\quad \left.\begin{aligned} \overline{G'}(r) = a_{00} &+ \left[\frac{a_{20}}{\nu}\left(\frac{1}{2} + \sum_{k=2}^{\nu}\cos^2\theta_k\right) + \frac{a_{02}}{\nu}\left(\frac{1}{2} + \sum_{k=2}^{\nu}\sin^2\theta_k\right)\right] r^2 \\ &+ \left[\frac{a_{40}}{\nu}\left(\frac{1}{2} + \sum_{k=2}^{\nu}\cos^4\theta_k\right) + \right. \\ &\left. + \frac{a_{22}}{\nu}\sum_{k=2}^{\nu}\cos^2\theta_k \sin^2\theta_k + \frac{a_{04}}{\nu}\left(\frac{1}{2} + \sum_{k=2}^{\nu}\sin^4\theta_k\right)\right] r^4 . \end{aligned}\right\}$$

Again for all sets of θ_k's satisfying the three condition given above, we have

$$\sum_{k=1}^{\nu}\cos^2\theta_k = \sum_{k=1}^{\nu}\sin^2\theta_k = \frac{\nu}{2}, \qquad \text{when } \theta_1 \neq 0$$

and

$$\sum_{k=2}^{\nu}\cos^2\theta_k = \sum_{k=2}^{\nu}\sin^2\theta_k = \frac{\nu-1}{2} \qquad \text{when } \theta_1 = 0 .$$

Thus the formulae for $\overline{G'}(r)$ are modified as

$$(18)\quad \left.\begin{aligned} \overline{G'}(r) = \text{ i) } a_{00} &+ \frac{(a_{20}+a_{02})}{2} r^2 + \frac{1}{\nu}\left[a_{40}\sum_{k=1}^{\nu}\cos^4\theta_k + a_{22}\sum_{k=1}^{\nu}\cos^2\theta_k\sin^2\theta_k\right. \\ &\left. + a_{04}\sum_{k=1}^{\nu}\sin^4\theta_k\right] r^4 , \qquad \text{when } \theta_1 \neq 0 \\ \text{ii) } a_{00} &+ \frac{a_{20}+a_{02}}{2} r^2 + \frac{1}{\nu}\left[a_{40}\left(\frac{1}{2} + \sum_{k=2}^{\nu}\cos^4\theta_k\right) + \right. \\ &+ a_{22}\sum_{k=2}^{\nu}\cos^2\theta_k\sin^2\theta_k \\ &\left. + a_{04}\left(\frac{1}{2} + \sum_{k=2}^{\nu}\sin\ \theta_k\right)\right] r^4 , \qquad \text{when } \theta_1 = 0 . \end{aligned}\right\}$$

Comparing (11) and (18) we note that the error in replacing $\overline{G'}(r)$ by $\overline{G'}(r)$ is of

the order of r^4. But, as will be shown below, the formula for second derivative can be built up without introducing the concept of $\overline{G'}(r)$.

ELKINS' *formula.*

To deduce ELKINS' formula, we calculate $\overline{G'}(s)$, $\overline{G'}(s\sqrt{2})$, $\overline{G'}(s\sqrt{5})$ from (18) by taking

i) $r = s$ $\quad \nu = 1, \quad \theta_1 = 0$

ii) $r = s\sqrt{2}, \quad \nu = 1, \quad \theta_1 = \pi/4$

iii) $r = s\sqrt{5}, \quad \nu = 2, \quad \theta_1 = \cos^{-1}\frac{2}{\sqrt{5}}, \quad \theta_2 = \cos^{-1}\frac{1}{\sqrt{5}}$

and obtain,

$$(19)\quad \begin{cases} \overline{G'}(s) = a_{00} + \dfrac{a_{20}+a_{02}}{2}s^2 + \dfrac{a_{40}+a_{04}}{2}s^4 \\ \overline{G'}(s\sqrt{2}) = a_{00} + (a_{20}+a_{02})s^2 + (a_{40}+a_{22}+a_{04})s^4 \\ \overline{G'}(s\sqrt{5}) = a_{00} + 5/2\,(a_{20}+a_{02})s^2 + \dfrac{1}{2}(17a_{40}+8a_{22}+17a_{04})s^4 \end{cases}$$

and also $G(0) = a_{00}$.

ELKINS neglected terms involving s^4 in the above equations and then, applying the method of least squares arrived at the following expression

$$(20)\quad \left(\frac{\partial^2 G}{\partial z^2}\right)_0 = -2(a_{20}+a_{02}) = \frac{2}{7s^2}[2G(0) + \overline{G'}(s) - 3\overline{G'}(s\sqrt{5})]$$

and assigning the weights 1/2 to $G'(s\sqrt{5})$ and 1 to others, he also obtained by the same method

$$(21)\quad \left(\frac{\partial^2 G}{\partial z^2}\right)_0 = \frac{1}{31s^2}[22G(0) + 8\overline{G'}(s) - 6\overline{G'}(s\sqrt{2}) - 24\overline{G'}(s\sqrt{5})]\,.$$

ROSENBACH'S *Formula.*

ROSENBACH used two sets of points on the circle $r = s$ and built up two averages $\overline{G'}_1(s)$ and $\overline{G'}_2(s)$ and also $\overline{G'}(s)/\sqrt{2}$ on the circle $r = s/\sqrt{2}$. These we calculate by taking

i) $r = s, \quad \nu = 1, \quad \theta_1 = 0,$

ii) $r = s, \quad \nu = 3, \quad \theta_1 = 0, \quad \theta_2 = \cos^{-1}\frac{\sqrt{3}}{2}, \quad \theta_3 = \cos^{-1}\frac{1}{2}$

iii) $r = \frac{s}{\sqrt{2}}, \quad \nu = 1, \quad \theta_1 = \pi/4$

and obtain

$$(22)\quad \begin{cases} \overline{G_1}'(s) = a_{00} + \frac{1}{2}(a_{20} + a_{02})\, s^2 + \frac{1}{2}(a_{40} + a_{04})\, s^4 \\ \overline{G_2}'(s) = a_{00} + \frac{1}{2}(a_{20} + a_{02})\, s^2 + \frac{1}{8}(3a_{40} + a_{22} + 3a_{04})\, s^4 \\ \overline{G}'(s/\sqrt{2}) = a_{00} + \frac{1}{4}(a_{20} + a_{02})\, s^2 + \frac{1}{16}(a_{40} + a_{22} + a_{04})\, s^4 \\ \text{and } G(0) = a_{00}\,. \end{cases}$$

If s^4 be not sufficiently small to be neglected, then these equations can be looked upon as four linear equations involving four unknowns, which are a_{00}, $(a_{20} + a_{02})$, $(a_{40} + a_{04})$ and a_{22}.

Solving these equations for $(a_{20} + a_{02})$ and using (6), we obtain,

$$(23)\quad \left(\frac{\partial^2 G}{\partial z^2}\right)_0 = \frac{1}{s^2}\left[12G(0) - 4\,\overline{G_1}'(s) + 8\overline{G_2}'(s) - 16\overline{G}'(s/\sqrt{2})\right]$$

which is ROSENBACH's formula.

Their Merits and Demerits.

The sources of error in a result arrived at through numerical operations on a set of observed data are:

i) random errors in the data observed,

ii) errors involved in the simplified approximate formulations in the place true theoretical ones (e.g. error for truncation of an infinite series to a polynomial),

iii) round-off errors in actual numerical operations.

Second derivatives calculated by ELKINS' formula will be affected by the error of the second type because the series for $\overline{G}'(r)$ has been approximated by neglecting terms involving r^4 and higher powers of r. But as the method of least squares has been applied to solve the linear equations, the effect of the error of the first type is minimized. Thus this formula will produce satisfactory results with field data provided the station separation is sufficiently small.

On the other hand, ROSENBACH's formula has been built up by taking into consideration the effect of terms involving r^4, which introduce less amount of error of second type. But, at the same time, as the exact method of solutions has been applied to solve the linear equations, the contribution of the error of the first type is greater. Moreover, the error of interpolation for calculating gravity values at points other than stations of observations may have some contribution in the final result. Thus this formula is likely to introduce greater error with field data, although it can be applied where the stations of observations are comparatively less dense. This formula will, of course, produce more satisfactory results with gravity values calculated theoretically.

New Formulae.

Now, if we solve ELKINS' set of equations using ROSENBACH's approach (i.e.

including terms involving r^4 and applying the method of exact solutions, we get

$$\left(\frac{\partial^2 G}{\partial z^2}\right)_0 = \frac{1}{3s^2}\left[12G(0) - 9\overline{G}'(s) - 4\overline{G}'(s\sqrt{2}) + \overline{G}'(s\sqrt{5})\right]. \tag{24}$$

Except for effect of error of interpolations this formula will have the same merits and demerits as ROSENBACH'S one.

Some average of (20) and (24) will be, in general, a more effective formula than either of the two individually; because, some effect of r^4 being taken into accounts, the average formulae can be applied for bigger station inervals at the same time, effect of random error will be less compared to ROSENBACH'S formula. Simple arithmetic mean of (20) and (24) gives

$$\left(\frac{\partial^2 G}{\partial z^2}\right)_0 = \frac{1}{42\,s^2}\left[96G(0) - 57\overline{G}'(s) - 28\overline{G}'(s\sqrt{2}) - 11\overline{G}'(s\sqrt{5})\right]. \tag{25}$$

Again if we incluce the equation for $\overline{G}'(2s)$ (for which $r = 2s$, $\nu = 1$, $\theta' = 0$) with (19).

We have

$$\left\{\begin{aligned}
G(0) &= a_{00} \\
\overline{G}'(s) &= a_{00} + \frac{1}{2}(a_{20} + a_{02})s^2 + \frac{1}{2}(a_{40} + a_{04})s^4 \\
\overline{G}'(s\sqrt{2}) &= a_{00} + (a_{20} + a_{02})s^2 + (a_{40} + a_{22} + a_{04})s^4 \\
\overline{G}'(2s) &= a_{00} + 2(a_{20} + a_{02})s^2 + 8(a_{40} + a_{04})s^4 \\
\overline{G}'(s\sqrt{5}) &= a_{00} + \frac{5}{2}(a_{20} + a_{02})s^2 + \frac{1}{2}(17a_{40} + 8a_{22} + 17a_{04})s^4.
\end{aligned}\right. \tag{26}$$

As the number of unknowns in these equations are less than number of equations, they are solved by the method of least squares and the formula

$$\left\{\begin{aligned}
\left(\frac{\partial^2 G}{\partial z^2}\right)_0 = \frac{1}{114s^2}&\left[333G(0) - 55\overline{G}'(s) - 316\overline{G}'(s\sqrt{2})\right. \\
&\left. - 41\overline{G}'(2s) + 79\overline{G}'(s\sqrt{5})\right]
\end{aligned}\right. \tag{27}$$

is deduced.

To obtain this formula, we have selected grid spacings in such a manner that the application of method of least squares has been possible with terms containing r^4 included. Thus, this formula is expected to be more effective with actual field gravity data, especially when stations are widely separated.

The interpretations of the second derivative maps in terms of subsurface masanomalies are usually carried out in empirical and qualitative ways based on experience and controlled by the information on local geology. So the author is no making any a priori claim for the practical use of the new formulae, from the standpoint

of better interpretation, over the old ones. He has attempted in the present paper to give a clearer mathematical exposition of the second derivative method.

Acknowledgement.

The author expresses his indebtedness to Sri L. N. Kailasam, Chief Geophysicist, Geological Survey of India, Calcutta for his valuable advice and suggestions and thanks the Director, Geological Survey of India, Calcutta, for his kind permission to publish this paper.

REFERENCES

Elkins Thomas A. (1951): *The second derivative method of gravity interpretation*, Geophysics, Vol. 16, pp. 29-50. — Peters Leo J. (1949): *The direct approach to magnetic interpretation and its practical application.* Geophysics, Vol. 14, pp. 290-320. — Rosenbach Otto (1953): *A contribution to the computation of « Second derivative » from gravity data.* Geophysics, Vol. 18, pp. 894-912.

(*Received 28th January* 1961)

ON THE PROPAGATION OF RAYLEIGH WAVES IN THREE DIMENSIONS IN ALLUVIAL SOILS

by K. R. Nag (*)

Summary — The propagation of Rayleigh waves in three dimensions in alluvial soils which do not behave like ordinary isotropic elastic solids have been discussed in this paper. The frequency equation has been solved for different soil constants.

Introduction — Soils do not behave like ordinary isotropic elastic solids. Weiskopf (1945) states that due to the slipping of granules on each other the resistance to shear is much less than that in a solid, and the resulting shearing deflection much greater. So in a soil we shall have $E/G > 2\,(2 + \sigma)$ instead of $E/G = 2\,(1 + \sigma)$ where

E = modulus of elasticity in compression,

G = modulus of elasticity in shear, and

σ = the Poisson's ratio.

In order to investigate the different aspects of the ground motion in the Gangetic alluvium first of all we consider the propagation of Rayleigh waves in three dimensions in such soils. The stress strain relations are taken as taken by Weiskopf (1945), and the analysis is similar to that of Das Gupta (1955).

The frequency equation obtained has been solved for different values of the soil constant E/G satisfying the required condition for soils. With slight modification the ordinary frequency equation for Rayleigh waves is deduced as a check.

Basic equations. — Let $z = 0$ be the bounding surface of the semi infinite medium and z axis in the medium.

The equations of motion are

$$(1)\qquad \left.\begin{aligned} \frac{\partial \sigma_x}{\partial x} + \frac{\partial T_{xy}}{\partial y} + \frac{\partial T_{xz}}{\partial z} &= \rho \frac{\partial^2 u}{\partial t^2} \\ \frac{\partial T_{yx}}{\partial x} + \frac{\partial \sigma_y}{\partial y} + \frac{\partial T_{yz}}{\partial z} &= \rho \frac{\partial^2 v}{\partial t^2} \\ \frac{\partial T_{zx}}{\partial x} + \frac{\partial T_{zy}}{\partial y} + \frac{\partial \sigma_z}{\partial z} &= \rho \frac{\partial^2 \omega}{\partial t^2} \end{aligned}\right\}$$

(*) K. R. Nag, Assistant Geophysicist, Geological Survey of India, 5 Middleton Street, *Calcutta*-16, India.

where

$$(2)\qquad \left.\begin{aligned} \sigma_x &= \frac{E}{(1+\sigma)}\frac{\partial u}{\partial x} + \frac{E\sigma}{(1+\sigma)(1-2\sigma)}\left(\frac{\partial u}{\partial x}+\frac{\partial v}{\partial y}+\frac{\partial \omega}{\partial z}\right)\\ \sigma_y &= \frac{E}{(1+\sigma)}\frac{\partial v}{\partial y} + \frac{E\sigma}{(1+\sigma)(1-2\sigma)}\left(\frac{\partial u}{\partial x}+\frac{\partial v}{\partial y}+\frac{\partial \omega}{\partial z}\right)\\ \sigma_z &= \frac{E}{(1+\sigma)}\frac{\partial \omega}{\partial z} + \frac{E\sigma}{(1+\sigma)(1-2\sigma)}\left(\frac{\partial u}{\partial x}+\frac{\partial v}{\partial y}+\frac{\partial \omega}{\partial z}\right) \end{aligned}\right\}$$

and

$$(3)\qquad \left.\begin{aligned} T_{xy} &= \frac{E}{2(1+\sigma)}\gamma_{xy}\\ T_{xz} &= G\gamma_{xz}\,; \qquad T_{yz} = G\gamma_{yz}\,. \end{aligned}\right\}$$

Here T_{xy} is related to γ_{xy} according to the conventional theory for solids and in the xz and yz planes the more general relation applying to soils is used (c.f. Weiskopf, 1945).

Solution — Let us now define

$$(4)\qquad \left.\begin{aligned} u &= \frac{\partial \varphi}{\partial x} + \frac{\partial^2 \psi}{\partial x \partial z}\\ v &= \frac{\partial \varphi}{\partial y} + \frac{\partial^2 \psi}{\partial y \partial z}\\ \omega &= \frac{\partial \varphi}{\partial z} + \frac{\partial^2 \psi}{\partial z^2} + k\psi \end{aligned}\right\}$$

k to be determined suitably.

Substituting from (2), (3) & (4) in (1) we see that the equations (1) are satisfied if φ & ψ satisfy the following equations:

$$(5a)\qquad \left.\begin{aligned} &\frac{\partial}{\partial x}\left[a_1\left(\frac{\partial^2}{\partial x^2}+\frac{\partial^2}{\partial y^2}\right)\varphi + (a_2+2G)\frac{\partial^2 \varphi}{\partial z^2} - \rho\frac{\partial^2 \varphi}{\partial t^2}\right]\\ &+\frac{\partial^2}{\partial x \partial z}\left[a_1\left(\frac{\partial^2}{\partial x^2}+\frac{\partial^2}{\partial y^2}\right)\psi + (a_2+2G)\frac{\partial^2 \psi}{\partial z^2} + k(a_2+G)\psi - \rho\frac{\partial^2 \psi}{\partial t^2}\right] = 0 \end{aligned}\right\}$$

$$(5b)\qquad \left.\begin{aligned} &\frac{\partial}{\partial y}\left[a_1\left(\frac{\partial^2}{\partial x^2}+\frac{\partial^2}{\partial y^2}\right)\varphi + (a_2+2G)\frac{\partial^2 \varphi}{\partial z^2} - \rho\frac{\partial^2 \varphi}{\partial t^2}\right]\\ &+\frac{\partial^2}{\partial y \partial z}\left[a_1\left(\frac{\partial^2}{\partial x^2}+\frac{\partial^2}{\partial y^2}\right)\psi + (a_2+2G)\frac{\partial^2 \psi}{\partial z^2} + k(a_2+G)\psi - \rho\frac{\partial^2 \psi}{\partial t^2}\right] = 0 \end{aligned}\right\}$$

and

$$\frac{\partial}{\partial z}\left[(a_2+2G)\left(\frac{\partial^2}{\partial x^2}+\frac{\partial^2}{\partial y^2}\right)\varphi + a_1\frac{\partial^2 \varphi}{\partial z^2} - \rho\frac{\partial^2 \varphi}{\partial t^2}\right] +$$

$$(5c)\qquad +\frac{\partial^2}{\partial z^2}\left[(a_2+2G)\left(\frac{\partial^2}{\partial x^2}+\frac{\partial^2}{\partial y^2}\right)\psi+a_1\frac{\partial^2\psi}{\partial z^2}-\rho\frac{\partial^2\psi}{\partial t^2}\right]$$

$$+\left[kG\left(\frac{\partial^2}{\partial x^2}+\frac{\partial^2}{\partial y^2}\right)\psi+a_1k\frac{\partial^2\psi}{\partial z^2}-k\rho\frac{\partial^2\psi}{\partial t^2}\right]=0$$

where

$$(6)\qquad \begin{cases} a_1=\dfrac{E(1-\sigma)}{(1+\sigma)(1-2\sigma)} \\ a_2=\dfrac{E\sigma}{(1+\sigma)(1-2\sigma)}\,. \end{cases}$$

Let u, v, ω be proportional to e^{ipt} and we suppose that

$$(7)\qquad \begin{cases} \varphi = AJ_0(\alpha r)\,e^{-\alpha qz+ipt} \\ \psi = BJ_0(\alpha r)\,e^{-\alpha qz+ipt} \\ p^2/\alpha^2 = c^2 \end{cases}$$

where A, B, α & q are constants, q is positive, and $r^2=x^2+y^2$.

Now equations (5a) & (5b) are satisfied if

$$(8)\qquad A[-a_1+(a_2+2G)q^2+\rho c^2]=\alpha qB[(a_2+2G)q^2+\rho c^2]$$

where

$$k=\frac{a_1}{a_2+G}\alpha^2$$

and since

$$\frac{\partial^2}{\partial x^2}+\frac{\partial^2}{\partial y^2}=\frac{1}{r}\frac{\partial}{\partial r}+\frac{\partial^2}{\partial r^2}$$

and

$$J_0''(\alpha r)+\frac{1}{r}J_0'(\alpha r)+\alpha^2J_0(\alpha r)=0\,.$$

Equation (5c) is satisfied if

$$(9)\qquad \begin{aligned} &A[(a_2+2G)-a_1q^2-\rho c^2]\alpha q=B\alpha^2\left[\left\{(a_2+2G)-a_1q^2-\rho c^2\right\}q^2\right. \\ &\qquad\left.+\frac{a_1G}{a_2+G}-\frac{a_1^2q^2}{a_2+G}-\frac{a_1\rho c^2}{a_2+G}\right]. \end{aligned}$$

Now eliminating A & B from (8) & (9) we get

$$(10)\quad \left.\begin{aligned} &[(a_2+2G)\,q^2+\rho c^2-a_1]\left[\left\{(a_2+2G)-a_1q^2-\rho c^2\right\}q^2+\right.\\ &\left.\frac{a_1G}{a_2+G}-\frac{a_1^2q^2}{a_2+G}-\frac{a_1\rho c^2}{a_2+G}\right]= \end{aligned}\right.$$

$$=q^2\,[(a_2+2G)\,q^2+\rho c^2]\,[(a_2+2G)-a_1q^2-\rho c^2]\,.$$

or simplifying we get

$$(11)\quad \left.\begin{aligned} &q^4-q^2\left[\frac{a_1}{G}\cdot\frac{a_2+2G}{G}\cdot\frac{a_2}{a_1}-\frac{\rho c^2}{G}-\frac{\rho c^2}{a_1}\right]\\ &+\left(\frac{\rho c^2}{G}-1\right)\left(\frac{\rho c^2}{a_1}-1\right)=0\,. \end{aligned}\right.$$

Let q_1^2 & q_2^2 be the two roots of (11) and let

$$\tau=\frac{\rho c^2}{G}\;;\quad \frac{a_1}{G}=\nu\;;\quad \frac{a_2}{G}=\gamma\,.$$

Then

$$(12)\qquad q_1^2+q_2^2=\left(\nu^2-2\gamma-\gamma^2-\tau\,(1+\nu)\right)/\nu$$

and

$$(13)\qquad q_1^2q_2^2=(\tau-1)\,(\tau-\nu)\,/\,\nu\,.$$

Now we take, omitting the time dependent factor

$$(14)\quad \left.\begin{aligned} \varphi&=J_0(\alpha r)\,[A_1\,e^{-\alpha q_1 z}+A_2\,e^{-\alpha q_2 z}]\\ \psi&=J_0(\alpha r)\,[B_1\,e^{-\alpha q_1 z}+B_2\,e^{-\alpha q_2 z}] \end{aligned}\right.$$

where A_1, A_2, B_1, B_2 are constants and they are connected by the relations

$$(15)\quad \left.\begin{aligned} A_1&=B_1\alpha q_1 m_1\\ A_2&=B_2\alpha q_2 m \end{aligned}\right.$$

where

$$(16)\quad \left.\begin{aligned} m_1&=\frac{(a_2+2G)\,q_1^2+\rho c^2}{(a_2+2G)\,q_1^2+\rho c^2-a_1}\\ m_2&=\frac{(a_2+2G)\,q_2^2+\rho c^2}{(a_2+2G)\,q_2^2+\rho c^2-a_1}\,. \end{aligned}\right.$$

In this case we are not considering the form of the source and taking as free Rayleigh wave we have the boundary conditions

$$\left.\begin{aligned} \hat{rz} &= 0 \\ \hat{zz} &= 0 \end{aligned}\right\} \qquad \text{at } z = 0$$

i.e. we have

$$\left(2\frac{\partial\varphi}{\partial z} + 2\frac{\partial^2\psi}{\partial z^2} + k\psi\right)_{z=0} = 0 \tag{17}$$

and

$$\left.\begin{aligned} & a_1\left(\frac{\partial^2\varphi}{\partial z^2} + \frac{\partial^3\psi}{\partial z^3} + k\frac{\partial\psi}{\partial z}\right)_{z=0} \\ & + a_2\left[\left(\frac{1}{r}\frac{\partial}{\partial r} + \frac{\partial^2}{\partial r^2}\right)\varphi + \frac{\partial}{\partial z}\left(\frac{1}{r}\frac{\partial}{\partial r} + \frac{\partial^2}{\partial r^2}\right)\psi\right]_{z=0} = 0\,. \end{aligned}\right\} \tag{18}$$

Hence from the boundary condition (17) with the help of (15) we get

$$B_1\left[2(1-m_1)q_1^2 + \frac{a_1}{a_2+G}\right] + B_2\left[2(1-m_2)q_2^2 + \frac{a_1}{a_2+G}\right] = 0 \tag{19}$$

and similarly from (18) we get

$$\left.\begin{aligned} & B_1\left[(m_1-1)q_1^3 - \frac{a_2}{a_1}q_1m_1 + q_1\left(\frac{a_2}{a_1} - \frac{a_1}{a_2+G}\right)\right] \\ & + B_2\left[(m_2-1)q_2^3 - \frac{a_2}{a_1}q_2m_2 + q_2\left(\frac{a_2}{a_1} - \frac{a_1}{a_2+G}\right)\right] = 0\,. \end{aligned}\right\} \tag{20}$$

Now eliminating B_1 & B_2 from (19) & (20) we get the frequency equation as

$$\left.\begin{aligned} & \left[2(1-m_1)q_1^2 + \frac{a_1}{a_2+G}\right]\left[(m_2-1)q_2^3 - \frac{a_2}{a_1}q_2m_2 + q_2\left(\frac{a_2}{a_1} - \frac{a_1}{a_2+G}\right)\right] \\ & = \left[2(1-m_2)q_2^2 + \frac{a_1}{a_2+G}\right]\left[(m_1-1)q_1^3 - \frac{a_2}{a_1}q_1m_1 + q_1\left(\frac{a_2}{a_1} - \frac{a_1}{a_2+G}\right)\right]. \end{aligned}\right\} \tag{21}$$

Now putting the values of m_1 & m_2 and $q_1^2 + q_2^2$ & $q_1^2q_2^2$ we get

$$(\nu\tau - \nu^2 + \gamma^2)^2(\tau - 1) - \nu\tau^2(\tau - \nu) = 0\,. \tag{22}$$

As a check to the correctness of the frequency equation we see that for an isotropic elastic solid we get

$$\left.\begin{aligned} & G = \mu\,; \quad \mu = \frac{E}{\alpha(1+\sigma)}\,; \quad \lambda = \frac{E\sigma}{(1+\sigma)(1-2\sigma)} \\ & \alpha^2 = \frac{\lambda+2\mu}{\rho}\,; \quad \beta^2 = \frac{\mu}{\rho}\,; \quad \tau = \frac{c^2}{\beta^2}\,. \end{aligned}\right\} \tag{23}$$

Substituting in terms of α, β & c we have from (22) after cancelling some

factors

$$\frac{c^6}{\beta^6} - 8\,\frac{c^4}{\beta^4} + c^2\left(\frac{24}{\beta^2} - \frac{16}{\alpha^2}\right) - 16\left(1 - \frac{\beta^2}{\alpha^2}\right) = 0 \tag{24}$$

which is the well-known Rayleigh wave frequency equation.

Discussion — Now data about the modulus of elasticity and rigidity of the Gangetic alluvium are very much lacking. Though KAILASAM (1953) has given the velocity of P waves as nearly equal to 1.62 km/sec in the Gangetic alluvium near Calcutta from seismic observations values of the shear wave velocity are lacking so that a determination of E/G is not possible. For a comparative study we note from the table given by HEILAND (1946) for unconsolidated formations.

TABLE I.

Locality	Investigator	E/G
Los Angeles, Calif.	HEILAND	3.0
Leine Valley, Germany	RAMSPECK	3.0
Werra Valley, Germany	RAMSPECK	2.9

If the perfect isotropic elastic condition prevailed these values of E/G should have given $\sigma = 1/2$. But for most of the substances near the crust we can take $\sigma = 1/4$.

« Poissons ratio seems to increase not quite regularly with depth inside the mantle from about 1/4 in the crust to about 0.3 near the core; inside the mantle, in general, 0.27 is a good approximation. Inside the core it is probably not far from 1/2 » (c.f. GUTENBERG, 1949).

WEISKOPF (1945) has given the value of E/G equal to 5.35 for sand. Thus we see that $E/G > 2\,(1 + \sigma)$ for unconsolidated formations.

The frequency equation (22) can be written as a function of τ and $\eta = E/G$, assuming σ to be equal to 1/4.

Thus we have

$$f(\tau, \eta) = 5.12\eta^3\,(\tau - 1) - 9.60\eta^2\tau\,(\tau - 1) + 4.50\eta\tau^3 - 3.75\tau^3 = 0\,. \tag{25}$$

In table II, solving (25) we have given some possible values of τ with different values of $\sigma > 2.5$. We note that for $\tau \geq 1$ there is no root of $f(\eta) = 0$, where $\eta > 2.5$. It is also observed that $0 < \tau < 1$.

TABLE II.

τ	0.85	0.88	0.90	0.92	0.94	0.96	0.98
η	2.54	2.87	3.17	3.56	4.12	5.02	7.03

For an isotropic body $\tau = 0.8453$ when $E/G = 2.5$ and $\sigma = 0.25$. From the above table we see that if we take $\eta = 3.0$ then τ becomes equal to 0.889 approximately.

Acknowledgement — I wish to thank Sri L. N. Kailasam, Chief Geophysicist, Geological Survey of India, for his kind encouragement and the Director, Geological Survey of India, for permitting me to publish this paper.

REFERENCES

Das Gupta S. C. (1955): Trans. Am. Geophys. Union Vol. 36, pp. 675-78. — Gutenberg B. (1949): *Internal Constitution of the Earth.* Dover Pub. pp. 349. — Heiland C. A. (1946): *Geophysical Exploration.* Prentice-Hall pp. 468. — Kailasam L. N. (1953): G. S. I. *Report on experimental reflection seismic investigations in the Gangetic Alluvium near Calcutta.* — Weiskopf W. H. (1945): Jour. Franklin Inst. Vol. 239, pp. 445-65.

(*Received* 23*rd January* 1961)

DISTURBANCES IN A VISCOELASTIC MEDIUM DUE TO IMPULSIVE FORCES ON A SPHERICAL CAVITY

by Sakti Kanta Chakraborty (*)

Summary — The disturbances produced in a visco-elastic medium by impulsive forces on the surface of a spherical cavity inside the medium have been studied.

1. — While problems of attenuation of waves in visco-elastic media have been considered in some simple cases [Ref. (1), (2)], it is found that the interesting problem of disturbances produced by impulsive forces has not yet been studied. In this paper, the medium surrounding a spherical cavity has been taken to be the Voigt type of visco-elastic solid. Approximate solution of the resulting disturbances has been obtained on the assumption of small viscosity.

2. — The stress-strain relations in a visco-elastic medium may be taken as

$$\tau_{ij} = \left(\lambda + \lambda' \frac{\partial}{\partial t}\right) \Delta \delta_{ij} + 2\left(\mu + \mu' \frac{\partial}{\partial t}\right) e_{ij}\,, \tag{2.1}$$

where λ, μ are elastic constants,

λ', μ' are the viscosity constants,

τ_{ij}, e_{ij} $(i, j = 1, 2, 3)$ are the stress, strain tensors respectively,

$$e_{ij} = \frac{1}{2}\left(\frac{\partial u_i}{\partial x_j} + \frac{\partial u_j}{\partial x_i}\right) \quad \text{in cartesian co-ordinates,}$$

$$\Delta = \text{dilatation} = \operatorname{div} u_i\,,$$

u_i $(i = 1, 2, 3)$ being the displacement components,

δ_{ij} being the usual Kronecker delta symbol.

The equations of small motion in the absence of body forces, are

$$\frac{\partial \tau_{ij}}{\partial x_j} = \rho \frac{\partial^2 u_i}{\partial t^2}\,. \tag{2.2}$$

Substituting for τ_{ij} from (2.1) in (2.2), we obtain

$$\left\{(\lambda + \mu) + (\lambda' + \mu')\frac{\partial}{\partial t}\right\} \operatorname{grad} \Delta + \left(\mu + \mu' \frac{\partial}{\partial t}\right) \Delta^2 u_i = \rho \frac{\partial^2 u_i}{\partial t^2}\,, \tag{2.3}$$

(*) Department of Mathematics, University of Burdwan, *Burdwan, India.*

where

$$\Delta^2 = \frac{\partial^2}{\partial x_1^2} + \frac{\partial^2}{\partial x_2^2} + \frac{\partial^2}{\partial x_3^2} .$$

Substituting

$$u_i = \text{grad } \Phi + \text{curl } \Psi_i$$

in equation (2.3), it reduces to

$$\left(c^2 + b^2 \frac{\partial}{\partial t}\right)\Delta^2\Phi = \frac{\partial^2\Phi}{\partial t^2} \tag{2.4}$$

where

$$c^2 = \frac{\lambda + 2\mu}{\rho}, \qquad b^2 = \frac{\lambda' + 2\mu'}{\rho} .$$

3. — Let us suppose that an impulsive pressure of magnitude $P\delta(t)$ acts uniformly on the inner surface of a spherical cavity of radius a inside the medium, $\delta(t)$ being impulsive DIRAC delta function.

If r, θ, Φ be the spherical polar co-ordinates referred to the centre of the cavity as origin, then the boundary condition may be written as

$$(\widehat{rr})_{r=a} = -P\delta(t) . \tag{3.1}$$

The resulting motion is, because of symmetry, purely radial and the only non-zero component of displacement is the radial one, u_r.

Therefore,

$$u_r = \frac{\partial}{\partial r}\Phi(r, t), \qquad \Delta^2\Phi = \frac{1}{r}\frac{\partial^2}{\partial r^2}(r\,\Phi),$$

and equation (2.4) becomes

$$\left(c^2 + b^2 \frac{\partial}{\partial t}\right)\frac{\partial^2}{\partial r^2}(r\,\Phi) = \frac{\partial^2}{\partial t^2}(r\,\Phi) . \tag{3.2}$$

Taking a solution of the form $f(r)/r\left\{e^{-int}\right\}$ for Φ, we have from (3.2)

$$\frac{d^2f}{dr^2} + \frac{n^2(c^2 + inb^2)}{c^4 + n^2b^4} f(r) = 0 \tag{3.3}$$

i.e.

$$f(r) = \exp\left[-\gamma(r - a) + in\beta(r - a)\right]$$

where

$$\beta = \left[\frac{(c^4 + n^2b^4)^{\frac{1}{2}} + c^2}{2(c^4 + n^2b^4)}\right]^{\frac{1}{2}},$$

$$\gamma = n\left[\frac{(c^4 + n^2b^4)^{\frac{1}{2}} - c^2}{2(c^4 + n^2b^4)}\right]^{\frac{1}{2}} . \tag{3.4}$$

For the solution of our problem, we therefore take

$$\Phi(r,t) = \frac{1}{2\pi r}\int_{-\infty}^{\infty} N(n)\exp\left[-\gamma(r-a) - in\{t-\beta(r-a)\}\right] dn \tag{3.5}$$

where $N(n)$ is a function of n to be so chosen as to satisfy the boundary condition (3.1). Before substituting (3.5) in (3.1) we note that if we neglect the effect of order b^4 (b^2 being taken as small), (3.4) gives

$$\beta = \frac{1}{c}, \qquad \gamma = \frac{n^2b^2}{2c^3} \quad \text{approximately}.$$

Then on substituting (3.5) in equation (3.1), we obtain, after making the approximation

$$N(n) = \frac{Pa}{\rho C}[n + iA + B]^{-1}[n + iA - B]^{-1}$$

where

$$C = 1 + \frac{4\mu'\beta}{a\rho} - \frac{2b^2\mu}{c^3a},$$

$$AC = \frac{2\mu'}{\rho a^2} + \frac{2\mu\beta}{\rho a},$$

$$B^2C^2 = \frac{4\mu}{\rho a^2}\left\{1 - \frac{\mu\beta^2}{\rho} - \frac{2b^2\mu}{c^3a} + \frac{2\mu'\beta}{\rho a}\right\}.$$

Hence

$$\Phi(r,t) = \frac{Pa}{2\pi r\rho C}\int_{-\infty}^{\infty} \frac{\exp\left[-\frac{n^2b^2}{2c^3}(r-a) - in\tau\right]}{(n + iA + B)(n + iA - B)}\, dn \tag{3.6}$$

where τ stands for $t - \beta(r-a)$.

When $\tau < 0$, on integrating in the complex n-plane along the semicircular contour on the upper half plane we obtain

$$\Phi(r,t) = 0.$$

When $\tau > 0$, on integrating in the complex n-plane along the semi-circular contour in the lower half plane, we have

$$\left.\begin{aligned} \Phi(r,t) &= \frac{Pa}{\rho CB}\cdot\frac{1}{r}\exp\left[-A\tau\right. \\ &\quad \left. - \frac{b^2}{2c^3}(r-a)(B^2 - A^2)\right]\sin B\left\{\tau - \frac{b^2}{c^3}(r-a)A\right\} \\ u_r &= 0 \quad \text{for} \quad \tau < 0, \end{aligned}\right\} \tag{3.7}$$

$$
\left.
\begin{aligned}
u_r = \frac{\partial \Phi}{\partial r} = & -\frac{Pa}{\rho CB} \exp\left[-A\tau - \frac{b^2}{2c^3}(r-a)(B^2-A^2)\right] \times \\
& \left[\left\{\frac{1}{r}\left(\frac{A}{\beta} - \frac{b^2}{2c^3}(B^2-A^2)\right) - \frac{1}{r^2}\right\} \sin B\left\{\tau - \frac{b^2}{c^3} A (r-a)\right\}\right. \\
& \left. - \frac{B}{r}\left(\frac{1}{\beta} + \frac{b^2 A}{c^3}\right) \cos\beta\left\{\tau - \frac{b^2}{c^3}(r-a) A\right\}\right],
\end{aligned}
\right\} \tag{3.8}
$$

for $\tau > 0$.

4. — It follows therefore that the disturbance propagates with velocity $1/\beta$ which, correct to first order approximation is equal to velocity of propagation of longitudinal waves in elastic media.

The damping effect due to viscosity on the displacement at a point increases with distance from the cavity.

REFERENCES

(1) Mattice H. C. & Paul Lieber (1954): *On attenuation of waves produced in a visco-elastic medium.* Transactions of American Geophysical Union Vol. 35, pp. 618-622. — (2) Chakraborty Sakti Kanta: *Rotational Waves in a viscoelastic medium due to a twist on the surface of a spherical cavity.* Journal of Science and Engineering Research, Vol. II, Part 2, 1958.

(*Received* 15*th March* 1961)

EIN NEUER AUTOMATISCHER LIBELLENPRÜFER FÜR SEKUNDENLIBELLEN

von A. Tárczy-Hornoch (*)

Zusammenfassung — Es wird ein neuer automatischer Libellenprüfer für Sekundenlibellen beschrieben, der im Geodätischen Forschungslaboratorium der Ung. Akademie der Wissenschaften entwickelt wurde. Bei der Beschreibung des Libellenprüfers werden auch die Konstruktionsgrundsätze angeführt und zum Schluß die Prüfung des Libellenprüfers selbst angegeben.

Summary — A new automatic bubble-level test set for levels of high sensibility is described which was constructed by the Geodetical Research Laboratory of the Hungarian Academy of Sciences. By the description of the bubble-level test set the construction fundamentals also are given, and finally the checking of the bubble-level test set described too.

Besonders bei der Bestimmung der Lotabweichungen und bei der Messung der Polhöhenschwankungen, die auch im Programm des Internationalen Geophysikalischen Jahres als eine wichtige Aufgabe angesehen wurde, spielen die Sekundenlibellen noch immer eine wesentliche Rolle. Um die erforderliche Genauigkeit zu erzielen, müssen diese Libellen entsprechend geprüft werden. Es sind deshalb im Laufe der Zeit verschiedene Libellenprüfer, oder mit anderem Namen Libellenwaagen entwickelt worden, von denen der in der berühmten Hannoverschen Schule entstandene, mit Lichtinterferenz arbeitende Hannoversche Libellenprüfer ([1]) eigens hervorgehoben werden möge.

Das Geodätische Forschungslaboratorium zu Sopron der Ung. Akademie der Wissenschaften hat sich gleichfalls mit dem Problem entsprechend genauer Libellenprüfern beschäftigt und es wurden hier unter wesentlicher Beteiligung von Gy. Alpár und A. Bummer, von 1953 angefangen, im Laufe der Zeit vier Typen von Libellenprüfern für hochempfindliche Libellen entwickelt, von denen die letzten zwei automatisch arbeiten und diese wohl die ersten automatischen Libellenprüfer überhaupt sind. Die letzte Type entstand in 1959 und wurde — wie die früheren — in der eigenen Werkstatt hergestellt. Da über diese letztere im Druck noch nirgends berichtet wurde, dürfte es nicht ohne Interesse sein, einiges darüber zu veröffentlichen, zumal selbst von den vorangegangenen Libellenprüfern bis jetzt nur ein vorläufiger Bericht ([2]), und dieser ungarisch. erschienen ist.

(*) Geodätisches und Geophysikalisches Laboratorium der Ung. Akad. d. Wissenschaften, *Sopron* (Ungarn).

Wir sehen eine Gesamtansicht von dem automatischen Libellenprüfer II in Abb. 1. Unten an einem Pfeiler ist der eigentliche Libellenprüfer, im vorliegenden Fall mit einer Achsenlibelle. Rechts im Bilde ist eine vom Pfeiler unabhängige Säule zwischen Boden und Decke sichtbar. Diese Säule trägt etwa in der Höhe

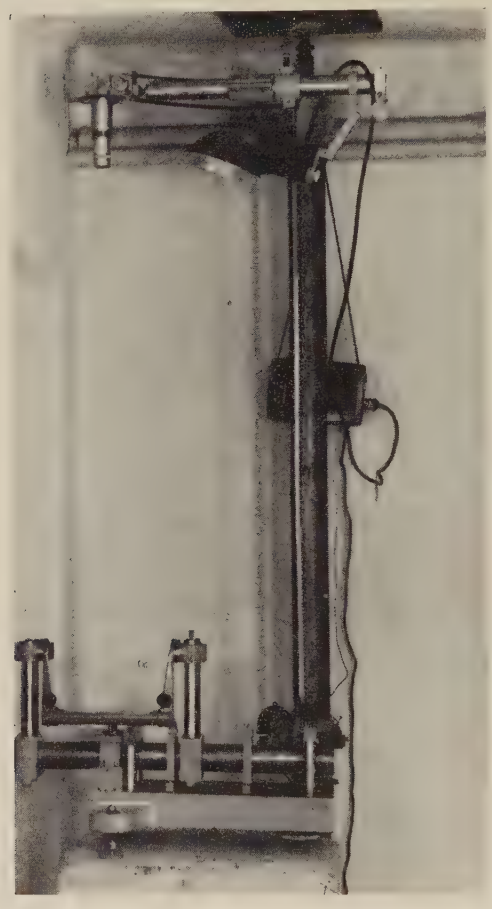

Abb. 1 - *Gesamtansicht des automatischen Libellenprüfers.*

des Libellenprüfers einen zur zeitweiligen Hebung des Prüferarmes erforderlichen kleinen Elektromotor (der in den Bildern 2 und 4 besser wahrnehmbar ist), weiter etwa in der Mitte der Säule ein zum Blitzlicht gehöriges Zusatzgerät und oben einen zur Festlegung der Blasenlagen erforderlichen fotografischen Apparat (besser sichtbar in Abb. 5) mit einer zur Aufnahme zeitweilig eingeschalteten Blitzlichtlampe und dem Mechanismus, der für die Aufnahmen den Film automatisch weiterbewegt. Die Verbindung zwischen dem Motor und dem fotografischen Apparat besorgt eine drehbare vertikale Stange, die in Bild 1 am linken Rand der Säule zu sehen ist und deren Wirkungsweise später noch erklärt wird. Der Motor mit dem drehenden Teil des Antriebmechanismus befindet sich mithin auf einer vom Pfeiler des Libellenprüfers unabhängigen Säule, sodass keine Erschütterungen auf den Pfeiler übertragen werden.

Der eigentliche Libellenprüfer ist in Abb. 2 dargestellt. Das Untergestell des Libellenprüfers kann mit drei Fußschrauben horizontiert werden. Der Prüfarm des Libellenprüfers ist eine etwa 80 cm lange Stahlhülse mit einem Durchmesser von rund 7 cm. Diese Abmessungen wurden zur Abschätzung der übri-

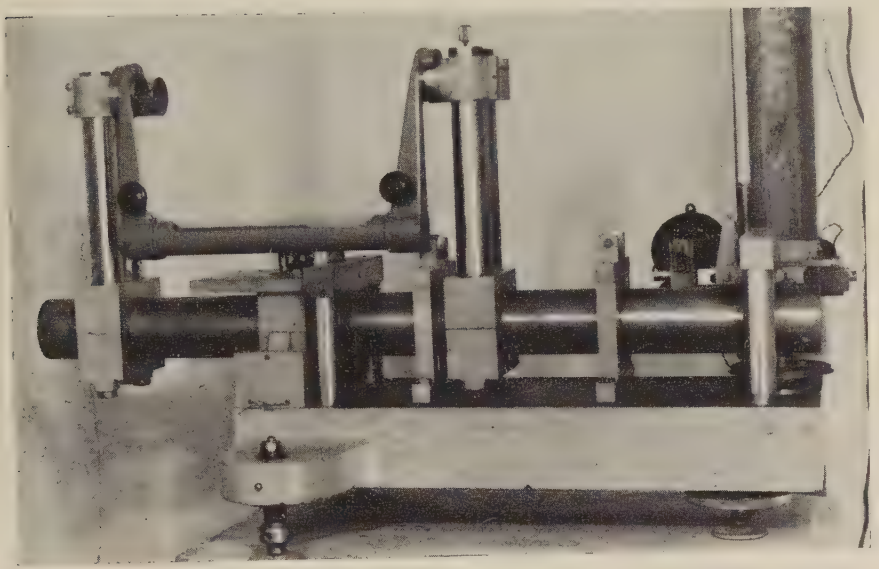

Abb. 2 - *Der eigentliche Libellenprüfer mit aufgesetzter Achsenlibelle.*

gen angegeben. Die horizontale Drehachse des Prüfarmes ist keine Schneide, sondern wird durch zwei Präzisionskugellager von 12mm Durchmesser gebildet. Die entsprechenden Lager im Untergestell und in dem Unterteil des Prüfarmes sind sehr sorgfältig hergestellt, sodass dadurch eine eindeutige Drehachse erreicht wurde. Die Lage der Drehachse ist dabei in bezug auf den Prüfarm so gewählt, dass beiderseits die Massendrehmomente möglichst nicht sehr unterschiedlich sind und dieser Unterschied unbeschadet der Belastung immer derselbe ist. Dadurch erreichen wir u.a., dass im Bilde rechts die das Ende des Prüfarmes hebende oder senkende Meßschraube keine besondere Belastung aufzunehmen braucht, daher leicht verstellt werden kann und sich nicht abnützt.

Für das Aufhängen der Achsenlibellen hat der Prüfarm zwei, der Länge der zu prüfenden Libelle entsprechend verstellbare Träger, die andererseits je zwei kurze zylinderförmige Ansätze besitzen, auf die zur Prüfung zwei gleich lange Libellen gehängt werden können. Die Platte für Horrebow-Libellen befindet sich unmittelbar oberhalb des Prüfarmes; es kann auch ein Instrument mit zu prüfender Libelle daraufgesetzt werden.

Die Scheibe der Meßschraube des Libellenprüfers ist, wie aus Abb. 3 ersichtlich, als Zahnrad ausgebildet, in dessen Zähne in später zu erörternder Weise in bestimmten Zeitabschnitten eine Klinke eingreift und die Meßschraube so verdreht, dass die Neigung des Prüfarmes sich um einen bestimmten einstellbaren Betrag

von 1″ bis 4″ ändert. Im übrigen hat die Meßschraube eine Ganghöhe von 0.4 mm und die Scheibe der Meßschraube 180 Zähne.

Um die erforderliche Änderung der Neigung des Prüfarmes zu erreichen, treibt der Motor mit zweifacher Übersetzung ein auf einer vertikalen Welle befindliches Schneckenrad an (Abb. 4). Unten an dieser Welle sitzt ein Nocken, der bei jeder Umdrehung einmal einen waagrechten, um eine vertikale Achse drehbaren

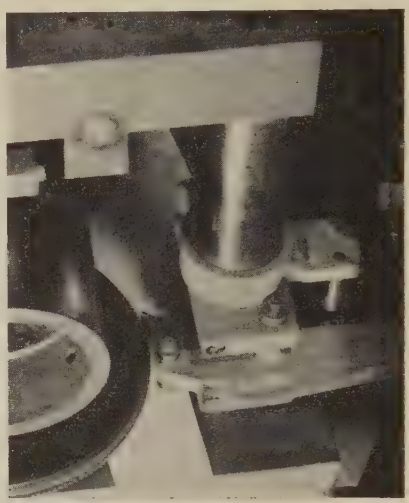

Abb. 3 - *Antrieb der Scheibe der Messschraube durch die Klinke.*

Arm (der nach Abb. 3 auch eine die Drehung der Meßschraube bewirkende Klinke enthält) aus seiner Ruhelage bringt. Die Größe der Verdrehung, die die Klinke der Meßschraube erteilt, wird durch einen nach unten gerichteten Anschlagsbolzen geregelt und begrenzt, der an einem vom Untergestell des Libellenprüfers

Abb. 4 - *Antriebsmotor mit Schneckenrad und Nocken zur Bewegung der am drehbaren Arm befindlichen Klinke.*

herunterragenden Zapfen (der auch die Drehachse des waagrechten Armes trägt) drehbar und nachher festklemmbar (S. Abb. 3) angeordnet ist. Mit der entsprechenden Einstellung des Anschlagbolzens können dann die den Winkeln 1″, 2″, 3″ und 4″ entsprechenden Verdrehungen mit einer Zahnbreite, mit zwei oder drei bzw. vier Zahnbreiten erreicht werden.

Die obere Fortsetzung der das Schneckenrad haltenden drehenden Welle (Abb. 4) bildet eine gleichfalls mitgedrehte — bereits am Anfang kurz erwähnte — Stange, die nach Abb. 1 und 5 die Drehbewegung auf ein Zahnrad und dieses durch eine Kette auf ein weiteres, am fotografischen Apparat befindliches Zahnrad überträgt. Die mit dem letzteren Zahnrand in Verbindung stehende, im Inneren des fotografischen Apparates befindliche Welle besorgt eine langsame, aber kontinuierliche Weiterbewegung des Filmes. Die Übersetzungen der Zahnräder sind so berechnet, dass bei einer Umdrehung der Welle der Film genau mit einer Bildgrösse weiterbewegt wird.

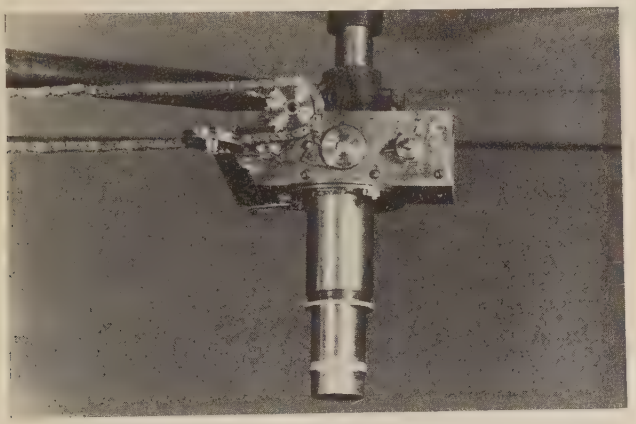

Abb. 5 - *Automatisch betätigter fotografischer Registrier-Apparat.*

Die Prüfung der Libellen erfolgt in einem verdunkelten Raum und so kann der Verschluss des fotografischen Apparates ständig geöffnet sein. Der Libellenprüfer ist so eingerichtet, dass nach einer den Erfordernissen entsprechend einstellbaren Zeit von einer bis zwei Minuten nach erfolgter Verdrehung der Meßscheibe das Blitzlicht auf 0.001 sec Zeit eingeschaltet und dadurch die bereits beruhigte Blase am Bild festgehalten wird. Das Einschalten des Blitzlichtes geschieht so, dass an der oberen Seite des Schneckenrades der Abb. 4 sich ein kleiner Kontaktansatz befindet, der mit einem kleinen Drehwinkel vor dem Nocken liegt, bei jeder Umdrehung kurz vor dem Eingreifen des Nockens das Blitzlicht einschaltet und so die Blasenlage festlegt. (Die Zuführungsdrähte zur Lampe sieht man auf Abb. 1). Bald darauf folgt die Verdrehung der Meßscheibe. Bis zur nächsten Einschaltung des Blitzlichtes kann sich nachher die Libellenblase wieder beruhigen.

Die ganze Prüfung der Libellen erfolgt bisher vollkommen automatisch. Man setzt den Libellenprüfer mit dem Blasenende nahe dem einen Rand der Libelle in Gang und nach entsprechender Zeit (bei einer Umdrehungszeit der Nockenwelle von einer Minute etwa nach 30-35 Minuten) stellt man den Motor des Libellenprüfers ab, entwickelt den Film und mißt an ihn die Lagen der Blasenenden in einem geeigneten Raum unter einer Handlupe oder kleinerem Mikroskop ab, was sehr rasch geschehen kann. Wir können diese Ausmessungen so sehr rasch auch wiederholen, wobei noch dazu die kontrollierbaren Unterlagen der Messungen erhalten bleiben. Dadurch, dass die Körperwärme des Beobachters während der

Messung weitgehend ausgeschaltet wird, kann die Genauigkeit merklich gesteigert werden. In dieser Beziehung ist auch das Blitzlicht ganz unschädlich, da es erstens etwa 2.5 m hoch über der Libelle angeordnet ist, und zweitens, weil die Belichtung, wie erwähnt, nur 0.001 sec dauert. Den großen Vorteil des fotografischen Festlegens der Blasenlagen betont bereits GIGAS in 1952 [Vgl. (3), S. 27].

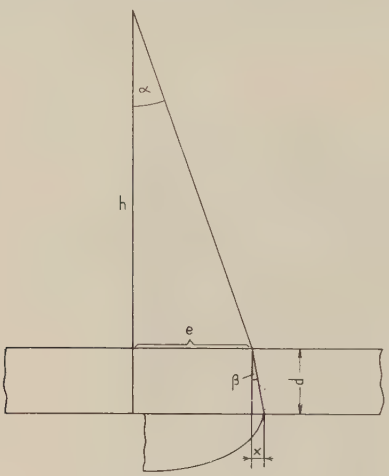

Abb. 6 - *Fehler infolge des schräg einfallenden Lichtstrahles.*

Eine Korrektion der ausgemessenen Blasenlagen ist allerdings erforderlich: Der das Blasenende an dem Film festlegende Lichtstrahl ist im Allgemeinen nicht normal zur äußeren Fläche des Glaskörpers, weshalb die Abbildung etwas verzerrt erscheint. Dazu kommt noch beim Eintreten in das Glas die Strahlenbrechung hinzu. Die Verhältnisse sind aus der nicht maßstabrichtigen Abb. 6 zu entnehmen, in der d die Glasdicke der Libelle, h die Höhe des Fotoobjektivs über der Libelle, e die Entfernung des Blasenendes von der Vertikalen durch den Objektivmittelpunkt und $n = \sin\alpha / \sin\beta$ den Brechungsexponenten bedeutet. Die am Film erhaltene Ablesung ist mit dem Betrag x zu verbessern, deren Größe aus

$$x = d\,\mathrm{tg}\,\beta \doteq d\sin\beta = \frac{d\sin\alpha}{n} = \frac{e\cdot d}{n\cdot h}$$

berechnet werden kann. Wenn

$$h_{min} = 2m,\ e_{max} = 70\,\mathrm{mm}\ \text{und}\ d = 1\,\mathrm{mm}$$

sowie $n = 1.6$ angenommen wird, so erhält man:

$$x_{max} = 0.022\,\mathrm{mm}.$$

Wir ersehen, dass selbst dieser maximale Wert oft vernachlässigt werden kann, da er kaum mehr als den Hundertstelteil des 2 mm großen Skalenintervalls bedeutet. Gegebenenfalls können die Korrektionen einer berechneten kleinen Tabelle entnommen werden.

*

Zu einem einwandfreien und genauen Arbeiten des automatischen Libellenprüfers ist das Gerät vor der eigentlichen Inbetriebnahme sorgfältig zu prüfen. Die wichtigste Prüfung ist dabei die der Meßschraube und der damit zusam-

menhängenden Hebevorrichtung. Dies kann am einfachsten mit einem Präzisionsnivellierinstrument mit verdrehbarem planparallelen Vorsatz geschehen, das durch ein Zwischenstück an die Libellenträger gesetzt wird. In einer Entfernung von 20.626 m stellen wir eine geeichte mm-Skala vertikal auf: wenn bei Beginn der Überprüfung die Ziellinie des Nivellierfernrohres auf ein ganzes mm eingestellt wird, so entsprechen für je 10″ jetzt 1 mm. Aber auch die einzelnen Sekunden können überprüft werden, da ja mit der planparallelen Platte noch 0.01 mm erfaßt werden kann. Gegebenenfalls müssen die Abweichungen festgestellt und als Korrektionen berücksichtigt werden. Bei uns traten solche nicht auf. Unsere diesbezügliche Überprüfungsmethode hat sich gut bewährt. Mit Rücksicht auf den beschränkten Bereich der Prüfung und auf die geringe Abweichung der Zielung von der Horizontalen kann die Änderung an der Latte proportional der Neigungsänderung genommen werden.

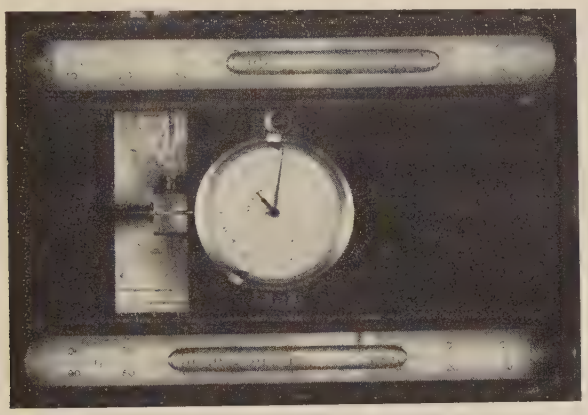

Abb. 7 - *Ein Feld des Registrierfilms.*

Um bei den Libellenprüfungen noch weitere Kontrollen zu haben, wurde an dem Libellenprüfer noch eine Fühlhebeluhr mit Umsetzungen so angeordnet, dass sie mit den Libellen mitfotografiert wird (Abb. 7). Die Differenzen der Ablesungen auf zwei nacheinander folgenden Abbildungen geben das Maß der Erhöhung in Zehntausendstelmillimetern an, woraus die Winkel auf etwa 0.05″ genau bestimmbar sind. Die Fühlhebeluhr dient mithin nicht allein zur Kontrolle, sondern kann auch zur Bestimmung der Neigungsänderung nach einer zweiten, von der ersteren unabhängigen Methode benützt werden.

Wir ordnen vorteilhaft auf dem Untergestell des Libellenprüfers noch eine genaue Setzlibelle an, die aber nicht mitfotografiert wird: es genügt am Anfang und am Ende der Aufnahmen sich zu überzeugen, dass das Untergestell selbst seine Neigung nicht geändert hat.

*

Mit dem beschriebenen automatischen Libellenprüfer wurden im Laufe der letzten 2 Jahre zahlreiche bewährte Libellenprüfungen, auch im Ausland, vorgenommen, die es ermöglichten, zu den Messungen höchster Genauigkeit die hierfür

entsprechenden Sekundenlibellen auszusuchen bzw. Verfahren auszuarbeiten, die geeignet sind, auch durch Sekundenlibellen mit zeitlich und örtlich veränderlichen Parswerten gute oder zumindest zufriedenstellende Ergebnisse zu erzielen. Die Behandlung letzterer Fragen überschreitet aber den Rahmen dieser Abhandlung.

LITERATUR

([1]) Höpcke: *Der Hannoversche Libellenprüfer.* Niedersächsisches Landesvermessungsamt, Hannover (1953). — ([2]) *Nagyérzékenységü libellák vizsgálata.* Magy. Tudom. Akadémia Müszaki Tud. Oszt. Közleményei, Bd. XXIII, S. 287-302 (1959). — ([3]) Deutsche Geodätische Kommission: *Wissenschaftliche Referate.* Reihe A, Heft 3 (1952).

(*Eingegangen am* 18. *April* 1961)

EIN EXAKTER SEISMOGRAPH

von Max Weber (*)

Zusammenfassung — Es wird ein exakter Seismograph beschrieben.

Summary — An exact seismograph is described.

1. *Einleitung* — Das Prinzip des exakten Seismographen ist einfach. Verwendet man einen Schwinger, dessen Bewegungsgleichung die Form

$$\ddot{x} + 2h\omega_0\dot{x} + \omega_0^2 x = -\ddot{s}$$

hat, einen elektromechanischen Umformer, der der Beziehung

$$E_1 = a\dot{x}$$

unterliegt und führt das Signal E_1 über einen aktiven Vierpol, der E_1 vermöge

$$E_3 = b\left[E_1 + 2h\omega_0 \int_0^t E_1 dt_1 + \omega_0^2 \int_0^t \int_0^{t_2} E_1 dt_1 dt_2\right]$$

entzerrt, einem hinreichend trägheitslosen Registriergerät zu, so erhält man für den Seismogrammausschlag z

$$z = -abcs\,,$$

d.h. der Seismograph ist ein exakter Geschwindigkeitsmesser, also ein Messgerät, das weder Einschwingvorgängen och einen Amplituden- oder Phasengang aufweist.

Natürlich ist in der Praxis die Bandbreite beschränkt, denn keine der Ausgangsgleichungen kann exakt realisiert werden. Die erreichbare Annäherung ist aber bemerkenswert, und der Einsatz des neuen Gerätes gibt zu berechtigten Hoffnungen Anlass.

2. *Der Entzerrverstärker* — Das neue Element ist der Entzerrverstärker.

Schaltet man das erste System einer Doppeltriode als Verstärker und das zweite als Kathodenfolger und legt die Spannung E_1 über einen Widerstand R an das erste Gitter und führt die Ausgangsspannung E_2 über einen Widerstand R_1 und

---

(*) Priv.-Doz. Dr. Max Weber, Eidg. Technische Hochschule, *Zürich*.

eine Kapazität C_1 in Reihe auf das erwähnte Gitter zurück, so gelten ersichtlich folgende Gleichungen

$$E_1 = \alpha E_2 + RJ_1$$

$$E_1 + E_2 = RJ_1 + R_1 J_1 + \int_0^t J_1 dt_1 / C_1 .$$

α ist der reziproke Verstärkungsfaktor des ersten Systems. Der Widerstand des Kathodenfolgers als Last ist in R_1 berücksichtigt, während sein Innenwiderstand als Quelle vernachlässigt wurde.

Damit erhält man für E_2 die VOLTERRA'sche Integralgleichung mit konst. Kern

$$E_2 = f(t) - \frac{\alpha}{k_1 C_1 R} \int_0^t E_2 dt_1$$

mit

$$f(t) = \frac{1}{k_1}\left(\frac{R_1}{R} E_1 + \frac{1}{C_1 R} \int_0^t E_1 dt_1\right)$$

$$k_1 = 1 + \alpha + (R_1 \alpha / R) .$$

Ihre allgemeine Lösung hat die Gestalt

$$E_2 = f(t) - \frac{\alpha}{k_1 C_1 R} \int_0^t f dt_1 + \left(\frac{\alpha}{k_1 C_1 R}\right)^2 \int_0^t \int_0^{t_2} f dt_1 dt_2 + \ldots\ldots$$

und für $\alpha \ll 1$ gilt angenähert

$$E_2 \cong f(t) .$$

Die stationäre Lösung lautet mit

$$E_1 = u_1 \exp i\omega t$$

$$E_2 = u_2 \exp i(\omega t + \varphi)$$

mit

$$u_2 = u_1 \sqrt{1 + (R_1 C_1 \omega)^2} \,/\, \sqrt{\alpha^2 + (k_1 C_1 R \omega)^2}$$

$$\cong u_1 \sqrt{1 + (R_1 C_1 \omega)^2} \,/\, C_1 R \omega$$

$$\operatorname{tg} \varphi = (\alpha R_1 C_1 \omega - k_1 C_1 R \omega) / (\alpha + R_1 C_1^2 k_1 R \omega^2)$$

$$\cong -1/R_1 C_1 \omega .$$

Nun kann das Signal E_2 nochmals auf gleiche Weise wie E_1 entzerrt werden.

Dies führt auf

$$E_3 \cong \frac{1}{k_2}\left(\frac{R_2}{R}\,E_2 + \frac{1}{C_2 R}\int_0^t E_2 dt_1\right)$$

und durch Einsetzen des Ausdruckes für E_2 erhält man

$$E_3 \cong \frac{R_1 R_2}{k_1 k_1 R^2}\left[E_1 + \left(\frac{1}{\tau_1} + \frac{1}{\tau_2}\right)\int_0^t E_1 dt_1 + \frac{1}{\tau_1\tau_2}\int_0^t\int_0^{t_2} E_1 dt_1 dt_2\right]$$

mit den Abkürzungen

$$\tau_1 = R_1 C_1 \quad \text{und} \quad \tau_2 = R_2 C_2 .$$

Werden nun die Entladezeiten τ_1 und τ_2 durch die Gleichungen

$$2h\omega_0 = (1/\tau_1) + (1/\tau_2)$$

$$\omega_0^2 = 1/\tau_1\tau_2$$

festgelegt, so folgt mit $b = R_1 R_2/k_1 k_2 R^2$ die angestrebte Entzerrung

$$E_3 \cong b\left[E_1 + 2h\omega_0\int_0^t E_1 dt_1 + \omega_0^2\int_0^t\int_0^t E_1 dt_1 dt_2\right],$$

und zu den Schwingerkonstanten h und ω_0 gehören die Entladezeiten

$$\tau_1 = h\left(1 + \sqrt{1 - (1/h^2)}\right)/\omega_0$$

und

$$\tau_2 = h\left(1 - \sqrt{1 - (1/h^2)}\right)/\omega_0.$$

ω_0 kann also beliebig gewählt werden, während $h \geq 1$ sein muss. Diese Einschränkung ist aber ersichtlich belanglos.

3. *Aufbau und Eigenschaften des exakten Seismographen* — Der Seismograph besteht im wesentlichen aus drei Elementen:

Einem Pendel, dessen doppeltgeführte Masse an einer Spiralfeder aufgehängt und als Tauchspule ausgebildet ist, einem Differenz- und Entzerrverstärker und einem Registriergerät.

Die Eigenfrequenz des schwach überaperiodisch gedämpften Pendels liegt bei 2.45 Hz. Das relativ hochohmige Tauchspulensystem, dessen Ringmagnet in einem Spaltvolumen von rund 43.10^3 mm^3 eine Feldstärke von angenähert 5000 Gauss erzeugt, arbeitet praktisch im Leerlauf.

Zum Aufbau der Verstärker wurde nur ausgesuchtes Material, wie zum Beispiel speziell rauscharme Widerstände und Röhren und Kondensatoren mit Entladezeiten von einigen Monaten, verwendet.

Registriert wird mit einem SIE-Schleifenoszillographen oder mit einem ergänzten Askania-Registriergerät. Dazu stehen verschiedene Galvanometer zur

Verfügung. Ihre Eigenfrequenzen liegen zwischen 10 und 350 Hz. Ein Zweikanalkathodenstrahloszillograph mit grossem Schirm und ein Blauschreiber ergänzen die Registriereinrichtung. Natürlich können alle Geräte ohne gegenseitige Beeinflussung gleichzeitig eingesetzt werden.

Die gemessene lineare Verzerrung geht aus folgender Tabelle, in der zur Ab-

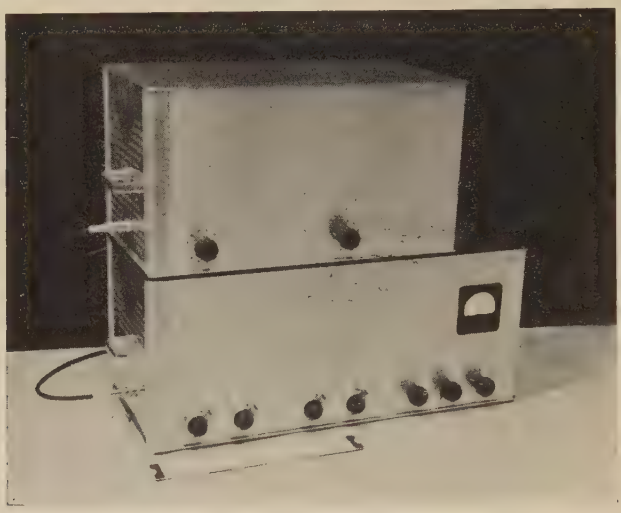

Abb. 1 - *Differenz- und Entzerrverstärker.*

kürzung die Messfrequenz in Hz mit ν, die Phasenverschiebung in Grad mit G und die Amplitudenüberhöhung in % mit Δu bezeichnet ist, hervor.

ν	0.1	0.2	0.3	0.4	0.5	0.6	0.7	0.7 → 40
G	+ 26	+ 12	+ 7	+ 3.5	+ 1	0	0	0
Δu	— 5	— 1	0	0	0	0	0	0

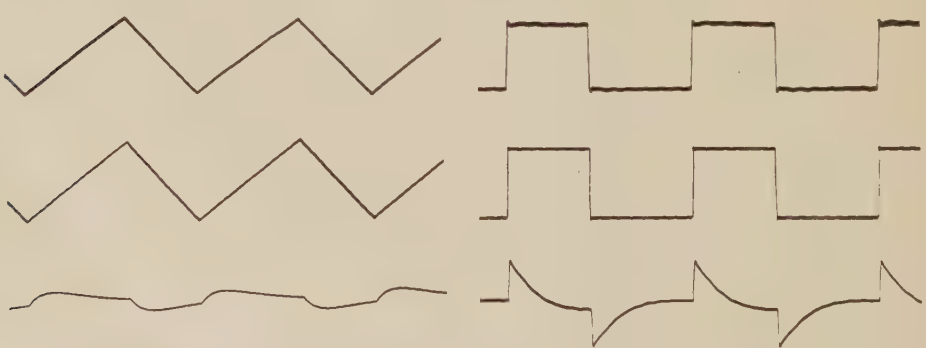

Abb. 2 - *Zur Illustration der Bandbreite des exakten Seismographen* (Erläuterungen siehe Text).

Zur Illustration dieser Bandbreite, die angenähert 7 Oktaven umfasst, dient Fig. 2. In dieser stellt durchgehend die mittlere Spur die Geschwindigkeit des Eichtisches, die obere Spur das entsprechende Seismogramm des exakten Seismographen, und die untere Spur vergleichsweise die entsprechende Signalspannung E_1 an den Tauchspulenklemmen dar. Die Grundfrequenz ist 4 Hz.

Die Empfindlichkeit ist bei Verwendung eines 350 Hz Galvanometers mit der Spitzenempfindlichkeit üblicher P.G.-Seismographen ([1,2]) vergleichbar.

Ich danke den Herren R. Berger und M. Dietiker für ihre Mitarbeit beim Aufbau des Seismographen.

LITERATURVERZEICHNIS

([1]) *First report by the commitee on seismological stations. Specifications for a world-wide network of standardized seismographs.* Washington, D. C. 1960. — ([2]) Weber Max: *P. G. - Seismographen und ihre Eichung.* Geofisica pura e applicata, Bd. 46, 1960.

(*Eingegangen am 15. Februar 1961*)

DIELECTRIC ANISOTROPY AND FABRIC OF ROCKS

by F. D. Stacey (*)

Summary — Measurements have been made of the dieletric anisotropies of a number of rocks for which magnetic anisotropy data have been obtained previously. The purpose was to examine the possible usefulness of dielectric anisotropy as a physical property indicative of rock fabrics. Its advantage over the magnetic method is that it measures an average alignment of crystals of the dominant minerals, whereas magnetic anisotropy is due only to the ferromagnetic grains. Disadvantages are an extreme sensitivity to specimen shape and difficulty in distinguishing the several types of alignment which can give rise to dielectric anisotropy. In a number of strongly foliated rocks the axes of dielectric anisotropy were found to coincide with the axes of magnetic anisotropy. Specimens from a magnesian-pyroxene rich layer in a Tasmanian dolerite sill and from the olivine rich layer of the Palisades dolerite sill, New York, were found to have no systematic anisotropy. The pyroxenes in the Tasmanian dolerite are elongated crystals (about 2 : 1) so that the dielectric measurements show that they do not have a preferred horizontal alignment and therefore have probably not settled as individual crystals. Most of the olivines in the Palisades dolerite are more nearly equidimensional so that the absence of measurable anisotropy in this rock is less conclusive evidence against crystal settling.

1. *Introduction* — Optical work on rock fabrics is based on the statistical treatment of large numbers of measurements of the optic axes of individual mineral grains and is particularly laborious if the grain alignment is slight. In many cases sufficient information about the fabrics of rock samples may be obtainable from measurements of the anisotropies of macroscopic physical properties, whereby the net alignment in any specimen of all the grains of a particular type or an appropriately weighted mean of several types is obtained directly. In principle almost any physical property could be used, but only a few are likely to be of pratical interest. Of these magnetic anisotropy has received considerable attention recently ([1, 2, 3, 4, 5]). While the magnetic methods are direct, simple and sensitive, two limitations arise from the fact that they observe only the ferromagnetic grains:

(i) some rocks contain too little magnetic material for the measurements to be significant;

(*) Geophysics Department, Australian National University, *Canberra*, Australia, now Gassiot Fellow in Geomagnetism, Meteorological Office, *Edinburgh*, Scotland.

(ii) it is possible that in some rock types the magnetic grains may be distributed randomly and therefore isotropically, while other minerals are strongly aligned; a possible example arises in the problem of crystal settling, considered in Section 4.

The measurement of dielectric anisotropy avoids these particular limitations and may therefore provide another useful fabric element. When this possibility was first considered a collection of foliated rock specimens was already available, having been used to study the relationship between magnetic anisotropy and fabric ([5]). The same specimens have been used in the measurements reported in Section 3.

As in the case of magnetic anisotropy, dielectric anisotropy is due to two types of grain alignment, the alignment of grain elongations, which leads to anisotropy by virtue of differences in dielectric constant between the grains, and crystallographic alignment, which results in anisotropy because the dielectric constant of each mineral is, in general, a function of the direction of measurement with respect to the crystallographic axes. The dielectric constants of minerals vary very widely, from about 4.3 for quartz to about 170 for rutile parallel to its axis ([6]) and this is probably not the extreme range. The differences between minerals are generally much greater than the difference between the dielectric constants measured in different directions in any one mineral ([6]). We must therefore expect that the alignment of grain elongations predominates in determining dielectric anisotropy.

2. *The Measurement of Dielectric Anisotropy.* — The dielectric constant of a material is most conveniently measured by determining the capacity of a calibrated condenser into which the material is inserted. The dielectric cell used in this work consisted of two square copper plates of side 7.5 cm held in a plastic framework so that the spacing of the plates was adjustable between 0 and 3.5 cm. Cylindrical specimens were stuck to a plastic rod which was fixed to a 360° scale and could be turned with respect to the plates. The cell was operated standing on a bench with its plates vertical and the specimens were suspended with their cylindrical axes vertical and as nearly as possible half way between the centres of the plates. As the specimens were rotated the variation of dielectric constant was measured in the plane perpendicular to the axes. No attempt was made to screen the cell which was merely placed on a bench remote from all moving objects and current-carrying wires, and the lead to each plate was a coaxial cable about 2 metres long with the screen earthed. This was sufficient to prevent movements of the experimenter from influencing the capacity, which was measured with a Wayne-Kerr universal bridge operated at 1592 cps.

With each specimen the cell capacitance, C was measured at a series of specimen angles, θ; the data obtained with a sample of adamellite of mean dielectric constant 20 are plotted in Figure 1.

The data obtained with other samples were similar except that with rocks of higher mean dielectric constant the variation in capacitance was smaller. The data in Figure 1 show substantial regular differences between the values of C observed at $\theta = 0°$ to 180° and $\theta = 180°$ to 360°, which appear as a $\sin\theta$ term in the curve $C(\theta)$, and are due to a slight asymmetry in setting the specimen in the cell. The dominant $\sin 2\theta$ term is due to the anisotropy of the rock, which in this case is quite clear. However, for specimens in which the anisotropy is much less pronounced the $\sin\theta$ and $\sin 2\theta$ terms may be of comparable magnitudes and in

these cases the sin 2θ terms cannot be unambiguously attributed to anisotropy. They may also be due to asymmetry of the system or possibly to inhomogeneity of the specimens. These spurious effects set a limit to the usefulness of the method.

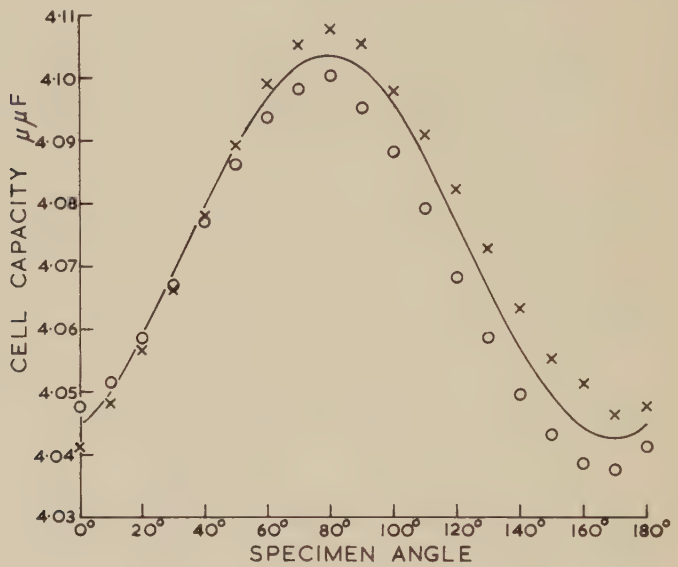

Fig. 1 - *Capacitance of dielectric cell with a specimen of Tharwa Adamellite plotted as a a function of the angle of the specimen.* Crosses are measurements 0° — 180°, circles are measurements 180° - 360°, solid line is closest fitting sin 2θ curve. Axis of anisotropy from magnetic data was 80° ± 3°, axis from dielectric data 79° ± 3°.

The cell was calibrated for each size of specimen by measuring its capacity with a series of standard specimens of the same size and known dielectric constants k: no specimen ($k = 1$), polythene ($k = 2.3$), glassbonded mica ($k = 7.8$) and copper (effective $k = \infty$). A large scale graph was then plotted of cell capacity C vs $1/k$, so that the value of k for each specimen was found by interpolation. The method is rather insensitive to variations in dielectric constant for high values, so that for many of the rocks, for which the dielectric constants were found to be very high, the absolute values were obtained only approximately. Assuming accuracy of the calibration, experimental errors were such that the nominal measured values of k are reliable within the limits indicated in Table 1. It is possible that systematic errors of comparable magnitude occur in the calibration. However, this did not lead to any difficulty in determining the directions of maximum and minimum k for each specimen as the accuracy of measurement of the small differences in C was much greater than the accuracy of the absolute calibration.

Owing to dielectric losses and the dissipation of power by conduction in the specimens the balance of the bridge gave values for the conductance of the cell as well as for its capacitance. With some specimens the maximum conductance was found with the specimen in the same direction as for the maximum capacitance but with others the conductance was greatest in the direction of the minimum

capacitance. This presumably depends upon the relative importance of the dielectric and conduction losses. When the conductance is greatest perpendicular to the maximum capacitance the dielectric losses are probably predominant. When the two balance conditions give maxima at the same angle, conduction losses *may* be more important, in spite of careful drying of the specimens.

TABLE 1 - *Uncertainties in the Estimation of Absolute Dielectric Constant.*

Measured value of k	Range of possible absolute values
10	9.1 to 11.2
20	17.4 to 23.5
50	38 to 71
100	67 to 200
200	100 to 1000
∞	250 to ∞

It is also possible to find the axis of dielectric anisotropy of a cylinder of rock by means of a torque meter. This was demonstrated with several of the specimens of section 3 which had volumes of approximately 3.5 cm^3 and were suspended between square copper plates of side 15 cm on a 90 cm length of 0.004 cm wire. When exposed to a field of 1000 volts/cm they turned with their axes perpendicular to field, as expected. However, this appears to be less convenient way of measuring dielectric anisotropy and may involve uncertainties arising from transient effects due to conduction.

3. *Results of Measurements on Foliated Rocks* — Dielectric anisotropies have been measured for all the specimens used by STACEY, JOPLIN & LINDSAY ([5]), except a few which had been destroyed in making thin sections. The dielectric experiments also included two groups of specimens which were collected at the same time but were found to have too little magnetic material for useful magnetic measurements to be made. The two types are a rhyolite from Bredbo, N.S.W., and a graphic pegmatite from Cooma, N.S.W. The rhyolite occurs in the Bransby Beds of the Upper Ordovician sequence, described by BROWNE ([7]) and JOPLIN ([8]) and most specimens show a well marked schistosity, the rocks varying from a slightly sheared rhyolite to a higly crushed rock, almost a mylonite. The pegmatite occurs as a group of dykes invading amphibolite. It is genetially related to the Cooma gneiss and has been described by BROWNE ([9]) and JOPLIN ([10, 11]). Movement is indicated by contortion of feldspar lamellae and by composite aggregates of feldspar up to 10 mm across with grains approximately 0.4 mm across, suggesting partial recrystallization. The feldspar aggregates are regularly intergrown with quartz.

Results of the measurements are summarised in Table 2, except for the Murrumbucka Tonalite and included xenoliths, of which specimens were cut at various angles so that the results are not suitable for tabulation in the same way. In all cases measurements were made only in planes perpendicular to the cylindrical axes of the specimens; measurements at other angles are not possible on account of the

TABLE 2 - *Summary of Dielectric Data.*

Rock	k_{max}	k_{min}	$\frac{k_{max}}{k_{min}}$	Alignment of Maximum Conductance with max or min Capitance	Angle between k max and foliation*
Tharwa Adamellite 1	16.1	11.5	1.40	k max	0° ± 5°
	15.8	13.4	1.18	k max	
	15.9	13.2	1.23	no variation	
	15.8	11.9	1.33	no variation	
Tharwa Adamellite 2	30.3	18.5	1.64	no variation	0° ± 5°
	26.9	16.4	1.64	k max	
	34.0	21.5	1.58	k min	
	26.3	17.9	1.47	k max	
Bunyan Leucogranite	71	17	4.1	k min	0° ± 5°
	143	34	4.1	k min	
Paragneiss (Cooma)	135	75	1.5	k min	0° ± 10°
	41	25	1.6		
	143	108	1.3		
	96	58	1.7		
	93	61	1.5		
« Injection Gneiss » (Cooma)	88	60	1.5	k min	0° ± 5°
	125	72	1.7		
	137	108	1.3		
Ordovician Rhyolite (Bredbo)	217	200	Very slight	k min	0° ± 20°
	250	217			
	1000	300			
Pegmatite (Cooma)	30	23	1.3	k min	No evident correlation with planes of veins
	54	54	1.0	no variation	
	39	31	1.2	no variation	

* In all cases except the rhyolite and pegmatite, for which no magnetic data were obtained, the foliation considered is the magnetic foliation, i.e. the direction of maximum elongation of magnetic grains as seen in the plane of the dielectric measurements. For the rhyolite the observed foliation was used and the pegmatite specimens were referred to the planes of the veins from which they were taken.

extreme sensitivity of cell capacitance to specimen shape. The specimens had been cut with their axes in the observed planes of foliation of the rocks, so that the table compares the values of dielectric constant observed in the planes of foliation and perpendicular to them, but gives no indication of any variations within the planes of foliation.

Most of the observed values of dielectric constant are remarkably high, even allowing for errors of the magnitude indicated in Table 1. It may be noticed also that the results indicate that the ratio k_{max}/k_{min} is greater in rocks which have high average dielectric constants. If this is due partly to an error in the method or in calibration it implies that all the quoted values are too high. However in all the specimens in Table 2 the existence of a real anisotropy was clear and in all cases except the pegmatite, the axes of anisotropy coincided with the directions expected from field observations and from the magnetic data. The origin of the anisotropy of the pegmatite is not known, but it may be statistical effect due to large crystals or aggregates of crystals which are randomly oriented but are of such a size that one or two can dominate the anisotropy of each specimen.

In the Murrumbucka Tonalite values of k from 50 to 150 were found. In the plane of foliation, which coincides both with the magnetic foliation and with the plane of maximum elongation of the xenoliths, there were only very slight variations in k, in contrast with the magnetic observations which indicated a strong preferred orientation within the plane. k_{max} coincided with the plane and values of k_{max}/k_{min} up to 3 were observed.

4. *The Problem of Crystal Settling* — Differentiation commonly occurs in thick cooling sheets of intrusive magma. The early formed crystals are usually the more dense ones and tend to settle through the magma, so that, after solidification, rock of higher than average density appears near the bottom of the intrusion. However the mechanism of settling is uncertain. In considering thick dolerite sills, Jaeger & Joplin ([12]) pointed out that there are serious physical objections to the supposition that individual crystals settle through a large depth of magma and suggested that roof-stoping was more probable, but Joplin ([13]) has pointed out that large blocks leaving the roof may break up into smaller ones before reaching the floor of the sill. Hess ([13]) suggested a mechanism of irregular convection whereby cool liquid, containing early crystals accumulating at the roof of a sill, is drawn off periodically by spontaneous but irregular convective overturn and flows to the bottom of the sill where it then spreads out; alternatively the cooler liquid might move downwards as « tear-droplike masses ».

It is important to consider the process by which settling crystals reach their final positions. Thus if they settle as individual crystals through the last centimetre or so of magma, then the fabric of the solidified rock will be characteristic of individually settled crystals, even though the crystals may have been transported through hundreds of metres of magma by some other process. It may be supposed that individual crystals of olivine or magnesian pyroxene will tend to settle with their longest axes horizontal and that even if the downward motion is more complicated a preferred horizontal alignment of long axes would be observed. In spite of the jumble which would result from accumulation at the bottom the alignment would be partially preserved as an igneous lamination in the finally solidified rock. Hess ([14]) regards the absence of preferred orientation of crystals in dolerite sheets as the main objection to the hypothesis of individual crystal settling in them.

However it is not clear what degree of alignment must be expected to result from crystal settling, so that even a slight but regular alignment would constitute evidence of settling. The measurement of dielectric anisotropy appears to be a method of looking for slight crystal alignments. Magnetic anisotropy is less useful as the magnetic grains would almost certainly appear principally in the isotropic matrix surrounding the settled crystals and hence would not indicate any alignment.

The Great Lake dolerite sheet in Tasmania is a good example of a thick intrusion which has differentiated, and it has been conveniently sampled by diamond drill hole no. 5084 of the Hydro-Electric Commission of Tasmania, which penetrated the lower contact at a depth of 360 m. Except for the chilled margin, the lowest 115 m is a zone of magnesia-pyroxene enrichment, and above this layer the basic dolerite passes progressively into more acid dolerites ([15]). The lower pyroxene-rich zone of this sheet has been interpreted by EDWARDS ([16]) as a zone of accumulation of early pyroxenes, which have settled through the magma from higher in the intrusion (i.e., from near the upper surface of crystallization). The pyroxene and associated plagioclase occur as elongated crystals (dimension ratio approximately 2 : 1) so that if they had settled individually they would almost certainly have a preferred horizontal alignment. The possibility of such alignment has been examined by measuring the dielectric anisotropies of 10 specimens of the bore core which were taken at 1.5 m intervals at about 100 m above the lower contact and were all well inside the pyroxene-rich zone. Cylindrical specimens, with axes which would have been horizontal in the original rock, were cut from each of the 10 lengths of core, so that measurements were of variations in dielectric constant in planes which would have been vertical in the original rock. Any regular differences between the dielectric constants in the vertical and horizontal directions would reflect an alignment of crystals.

The $C(\theta)$ curves (as Figure 1) were analyzed into $\sin\theta$ and $\sin 2\theta$ components which were of comparable magnitudes and random orientations. If the $\sin 2\theta$ terms represented real anisotropy then its magnitude was $k_{max}/k_{min} \approx 1.05$, but the fact that the axes of anisotropy were randomly oriented and not systematically horizontal means that it was either a statistical effect due to finite crystal sizes or, more probably, a result of asymmetry of the measuring system and inhomogeneities in the rock (as was the $\sin\theta$ term). Thus no preferred horizontal alignment of crystals has been found in this rock and there is therefore no evidence of individual crystal settling.

Similar measurements have also been made on four cores from a single hand specimen of dolerite from the olivine-layer of the Palisades sill, New York, which were also found to be isotropic within the limits of the experiment In this case the randomly oriented $\sin 2\theta$ terms in the $C(\theta)$ curves were rather smaller than those found with the Tasmanian dolerite, possibly because the olivine crystals are more nearly equidimensional than the pyroxenes in the Tasmanian dolerite or because greater care was taken to put the specimens symmetrically into the dielectric cell. The dielectric anisotropy of the olivine dolerite is less than 2-3 per cent. In this case the negative result is less conclusive evidence against the settling of individual cristals because most of the olivines are nearly equidimensional. In a single thin section, which was cut in a vertical plane, 50 idiomorphic olivine crystals were counted. The maximum elongation within the plane was 2.6 : 1, 10 of the smaller grains having elongations of 2.0 : 1 or greater. 12 of the grains had elongations between 1.5 : 1 and 2.0 : 1 and in 28 grains the elongation was less than 1.5 : 1.

The largest of the grains measured 1.12 mm × 0.64 mm and the smallest 0.16 mm × 0.14 mm.

5. *Conclusion* — Dielectric anisotropy is a readily measurable property of rocks and can be used in petrofabric work. More accurate and more sensitive methods than the one described here could be developed by using slices of rock with electrodes in contact on opposite faces, but this would require the cutting of a larger number of specimens from each rock. Even with cylindrical specimens three mutually perpendicular specimens are required for complete anisotropy data on a single rock sample; in this respect dielectric anisotropy is therefore less convenient as a petrofabric tool than magnetic anisotropy, for which a single specimen is sufficient. A further disadvantage in the method as reported in this paper is that, as in Section 4, a 5% dielectric anisotropy could not be distinguished from experimental errors, whereas in the same specimens 1% magnetic anisotropy is both readily measured and statistically significant.

The consistent difference between the mean dielectric constants of the two adamellites (Table 2) suggests a correlation of dielectric constant with the content of ferromagnesian minerals. If this correlation is a direct one then the dielectric and magnetic measurements may be less independent than they might appear to be. In any case the magnetic and dielectric data have been shown to give very similar results.

For a detailed examination of the problem of crystal settling the method of dielectric anisotropy appears to be very suitable but it would probably be advantageous in subsequent experiments to cut vertical and horizontal slices rather than cylindrical specimens. Although this would limit the measurements to the determination of dielectric constants in the horizontal and vertical directions, it would be more accurate and sensitive.

Model experiments to determine the degree of alignment of elongated crystals, which have settled individually would assist in the interpretation of dielectric measurements. If it can be assumed that settling does produce appreciable alignment then the dielectric measurements show that the pyroxene-rich layer of the Great Lake dolerite has not been formed by the settling of individual crystals.

Acknowledgments — The examination of the crystal settling problem by the dielectric method was suggested by Professor J. C. Jaeger, Dr. Germaine Joplin examined thin sections of most of the rocks used in this work and Dr. Ian McDougall communicated data from his petrological study of the Tasmanian dolerites.

REFERENCES

([1]) Graham J. W.: *Magnetic susceptibility anisotropy, an unexploited petrofabric element.* Bull. Geol. Soc. America, 65, 1257 (1954). — ([2]) Balsley J. R. & Buddington A. F.: *Magnetic susceptibility anisotropy and fabric of some Adirondack granites and orthogneisses.* Am. J. Sci. 258 A, 6 (1960). — ([3]) Fuller M. D.: *Anisotropy of susceptibility and the natural remanent magnetization of some Welsh slates.* Nature, 186, 791 (1960). — ([4]) Stacey F. D.: *Magnetic anisotropy of igneous rocks.* J. Geophys. Res., 65, 2492 (1960). — ([5]) Stacey F. D., Joplin Germaine & Lindsay J.: *Magnetic anisotropy and fabric of some foliated rocks from S E. Australia.* Geofisica pura e applicata, Vol. 47, pp. 30-40, 1960. — ([6]) *Handbook of Chemistry and Physics* (40th Edition), p. 2521, Che-

mical Rubber Publishing Company, Cleveland, Ohio, (1958). — ([7]) Browne W. R.: *The geology of the Cooma district, N.S.W. II. The country between Bunyan and Colinton.* J. Roy. Soc. N.S.W., 77, 159 (1944). — ([8]) Joplin G. A.: *Petrological studies in the Ordovician of N.S.W.* II. *The northern extension of the Cooma Complex.* Proc. Linn. Soc. N.S.W., 78, 164 (1943). — ([9]) Browne W. R.: *The geology of the Cooma district, N.S.W.I.* J. Roy. Soc. N.S.W., 48, 172 (1914). — ([10]) Joplin, G. A.: *Studies in metamorphism and assimilation in the Cooma district of N.S.W.*, 73, 86 (1939). — ([11]) Joplin G. A.: *Petrological studies in the Ordovician of N.S.W. I. The Cooma Complex.* Proc. Linn. Soc. N.S.W., 67, 187 (1942). — ([12]) Jaeger J. C. & Joplin Germaine: *Rock magnetism and the differentiation of dolerite sill.* J. Geol. Soc. Australia, 2, 1 (1955). — ([13]) Joplin G. A.: *The Problem of the quartz dolerites: some significant facts concerning mineral volume, grain size and fabric.* Papers and Proceedings Roy. Soc. Tasmania, 93, 129 (1957). — ([14]) Hess H. H.: *Stillwater igneous complex, Montana — a quantitative mineralogical study.* Geol. Soc. of America, Memoir 80, (1960). — ([15]) McDougall I.: *A note on the petrography of the Great Lake dolerite sill.* Symposia of the Geology Department of the University of Tasmania, Vol. 4 - Dolerite, (University of Tasmania, Hobart 1958). — ([16]) Edwards A. B.: *Differentiation of the dolerites of Tasmania.* Journal of Geol., 50 451 and 579 (1942).

(*Received* 1*st March* 1961)

ON PRESSURE WAVES IN THE COASTAL REGION

by S. C. Das Gupta (*)

Summary — Several authors have tried to explain the different aspects of pressure waves in water including the phenomenon of « Singing » by assuming another fluid layer below the water column. In this note an attempt has been made to determine the thickness of such a layer.

Recently seismic studies have been made by several observers such as Burg & al. (1951), Werth & al. (1959), Liu (1958) and others by detonating inside the liquid in the offshore area. They have generally observed a spectrum of waves with an interesting not infrequent exception. In many areas offshore, the conventional seismic record has the appearance of a series of sine waves or simple odd harmonic combinations of sine waves with a fundamental wavelength four times the water depth. This case was called by the above mentioned observers as « singing ». Burg in a ray theory treatment ascribe this oscillatory phenomenon to guided energy travelling in the water layer. He found from the time of arrival of

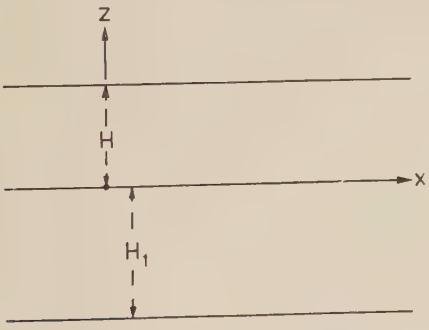

Fig. 1

waves that depth in which the energy is trapped is a little greater than the water column. Pekeris (1948) included this by considering the water layer to be lying over a medium which also acts as a fluid with a different higher sound velocity. We shall consider here the depth of semiliquid layer from the time during which the arrivals of waves persist. Minimum group velocity has been shown to be suf-

(*) Professor of Mathematics, Bengal Engineering College, *Howrah, West Bengal*, India.

ficiently small so that the duration of wave arrivals is not large. The purpose of this paper is to have an idea of the depth of the lower layer which will be utilised in a subsequent paper in order to explain by proper mathematical method the cause of « singing » and its relation to semi-liquid sediment thickness.

We take the origin at the interface which is taken to be horizontal which may not be true in the coastal region. The axis of x- is in the horizontal direction and z-axis is vertically upwards.

The pressure field $p\,(z, t)$ is determined from the wave equation

$$\frac{\partial^2 p}{\partial x^2} + \frac{\partial^2 p}{\partial z^2} = \frac{1}{c^2}\frac{\partial^2 p}{\partial t^2}$$

with

$$-\frac{\partial p}{\partial z} = \rho \frac{\partial u}{\partial t},$$

where u is the particle velocity.

Pressure wave equation for the upper layer is

$$\frac{\partial^2 p}{\partial x^2} + \frac{\partial^2 p}{\partial z^2} = \frac{1}{c_1^2}\frac{\partial^2 p}{\partial t^2} \tag{1}$$

where c_1 is the sound velocity in water. Let p be proportional to $e^{ik(x-ct)}$. Then

$$\frac{d^2 p_1}{dz^2} - k^2 p_1 = -\frac{k^2 c^2}{c_1^2} p_1$$

or

$$\frac{d^2 p_1}{dz^2} + k^2\left(\frac{c^2}{c_1^2} - 1\right) p_1 = 0. \tag{2}$$

Solution of equation (2) is given by

$$p_1 = A \cos(sz) + B \sin(sz), \tag{3}$$

where $s^2 = k^2\,(c/{c_1}^2 - 1)$ and A, B are constants. If s be real $c > c_1$.

In the lower layer the pressure wave equation is

$$\frac{\partial^2 p}{\partial x^2} + \frac{\partial^2 p}{\partial z^2} = \frac{1}{c_2^2}\frac{\partial^2 p}{\partial t^2},$$

where c_2 is the velocity of sound in the lower layer. Putting p proportional to $e^{ik(x-ct)}$,

$$\frac{d^2 p_2}{dz^2} - k^2\left(1 - \frac{c^2}{c_2^2}\right) p_2 = 0. \tag{4}$$

Solution of (4) is given by

$$p_2 = C\, e^{s'z} + D\, e^{-s'z}, \tag{5}$$

where $s'^2 = k^2\,(1 - c^2/{c_2}^2)$ and C, D are constants. If s' be real $c < c_2$.

The boundary conditions are that at $z = H$, $p_1 = 0$ and at

$$z = -H_1, \quad \frac{\partial p_2}{\partial z} = 0 .$$

At $z = 0$,

$$\frac{1}{\rho_1}\frac{\partial p_1}{\partial z} = \frac{1}{\rho_2}\frac{\partial p_2}{\partial z}$$

and $p_1 = p_2$ where ρ_1, ρ_2 are the densities of water and the lower layer respectively.

From the boundary conditions we get

$$A \cos(sH) + B \sin(sH) = 0 \tag{6}$$

$$C e^{-s'H_1} - D e^{s'H_1} = 0 \tag{7}$$

$$A = C + D \tag{8}$$

$$\frac{s}{\rho_1} B = \frac{s'}{\rho_2}(C - D) . \tag{9}$$

Eliminating A, B, C, D from (6), (7), (8) and (9),

$$\begin{vmatrix} \cos(sH) & \sin(sH) & 0 & 0 \\ 0 & 0 & e^{-s'H_1} & -e^{s'H_1} \\ 1 & 0 & -1 & -1 \\ 0 & \dfrac{s}{\rho_1} & -\dfrac{s'}{\rho_2} & \dfrac{s'}{\rho_2} \end{vmatrix} = 0$$

or

$$\tan(sH) = \frac{s\rho_2}{s'\rho_1} \coth(s'H_1)$$

or

$$\tan\left[kH\left\{\left(\frac{c^2}{c_1^2} - 1\right)^{1/2}\right\}\right] = \frac{\left(\dfrac{c^2}{c_1^2} - 1\right)^{1/2} \rho_2}{\left(1 - \dfrac{c^2}{c_2}\right)^{1/2} \rho_1} \coth\left[kH_1\left\{\left(1 - \frac{c^2}{c_2^2}\right)^{1/2}\right\}\right]. \tag{10}$$

The frequency equation (10) has real roots when $c_1 < c < c_2$.

Near the coast we take $H = 150$ ft. H_1 is taken to be 2000 ft which is probably too high. c_1 is 5000 ft/sec and c_2, 8300 ft/sec. The following table I gives the group velocities for different c/c_1. ρ_2 is taken to be 2.6.

TABLE I.

c/c_2	$(c^2/c_1^2 - 1)^{1/2}$	$(1 - c^2/c_2^2)^{1/2}$	$\frac{\rho_2 s}{\rho_1 s'}$	kH	$\frac{d(kH)}{d(c/c_2)}$	C/c_2
1.00	1.33	0	∞	1.19		
.96	1.241	.280	11.523	1.198	— 1.3	.04
.94	1.198	.341	9.134	1.226	— 1.3	.03
.92	1.156	.392	7.667	1.250	— 1.4	.03
.90	1.110	.436	6.619	1.283	— 1.7	.05
.602	0	.84	0	3.1		

We follow then the method of JEFFREYS (1925). Minimum group velocity occurs when $c/c_2 = .93$ and $C/c_2 = .03$ or $C/c_1 = .05$. So waves of any two periods within the range defined by minimum group velocity and higher group velocities on the right, will separate by one wavelength when the waves have moved by 1.05 wavelengths. If waves traverse a distance of 15.000 ft taking about 3 sec to cross the path, the whole train of waves will cross the observing position in about 2 sec. This time agree well with the observation of LIU. Sometimes the duration time is longer than 2 sec. This may involve a smaller thickness for the lower layer. 2000 ft is just the thickness when the effect of it is little felt in the frequency equation. 1000 ft is probably a good approximation to the true picture.

REFERENCES

(1) BURG K. E., EWING M., PRESS F. & STULKEN E. J.: Geophysics, Vol. 16, pp. 594-612 (1951). — (2) JEFFREYS H.: M.N.R.A.S. (Geo. Suppl.), Vol. 1, pp. 282-292 (1925). — (3) LIU D. T.: Geophysics, Vol. 24, pp. 658-666 (1959). — (4) PEKERIS C. L.: Geological Soc., Memoir 27, pp. 1-117. — (5) WERTH G. C., LIU D. T. & TROREY A. W.: Geophysics, Vol. 24, pp. 220-232 (1959).

(*Received* 10*th April* 1961)

ON THE SECULAR CHANGE IN WATER LEVEL OF LAKES IN FINLAND

by H. Simojoki (*)

Summary — In some larger lakes in Finland continuous lowering of the water level can be established. This is presumed to be chiefly the consequence of secular changes in climate.

For establishing secular changes in the water level the following observation series, the longest and the most reliable which are accessible in Finland, were used:

Lake	Gauge	Period	Lake area km²	Drainage area km²
Saimaa	Lauritsala	1851-1959	1460	61265
Kallavesi	Konnus	1871-1959	505	16270
Päijänne	Kalkkinen	1881-1959	1090	26480
Vanajavesi	Lempäälä	1881-1959	179	8515

The position of the gauges is given in Fig. 1.

The investigation is based upon the yearly mean values of water level calculated, as a rule, from daily observations. These yearly mean values of water level may vary considerably (Fig. 2). In lake Saimaa, the observations of which are mainly used in the following, the dispersion during the period 1851-1959 is 39 centimeters. In data for consecutive years rhythmic fluctuations may be observed. In the water level data of lake Saimaa, e.g. a rhythm of about 30 years has appeared ([2]).

A possible secular change is assumed to be linear. By the method of least squares the constants of the equation $y = a + bx$ were determined, y indicating the yearly mean value of the water level, and x the number of the year. Fig. 2 represents the yearly mean values of lake Saimaa, and the straight line computed

(*) Finnish Hydrological Office, *Helsinki*.

in the manner mentioned above. From the Figure it is also evident that the water level of lake Saimaa has a tendency to decrease.

The computed values of b, actually showing the secular change of the water level, and their maximum errors are as follows:

Saimaa, Lauritsala	— 1.92 ± 0.06	mm per year	1851-1959
	— 6.31 ± 0.14	»	1881-1959
	— 1.77 ± 0.08	»	1851-1948
	— 8.94 ± 0.20	»	1881-1948
	— 0.78 ± 0.51	»	1851-1920
Kallavesi, Konnus	— 1.11 ± 0.01	»	1871-1959
Päijänne, Kalkkinen	— 1.00 ± 0.08	»	1881-1959
Vanajavesi, Lempäälä	— 0.06 ± 0.08	»	1881-1959

From the observations of Lauritsala the values of b were calculated for different periods. Owing to the regulation of lake Saimaa after 1948 the observations prior to that time were, moreover, treated separately. The values given above indicate

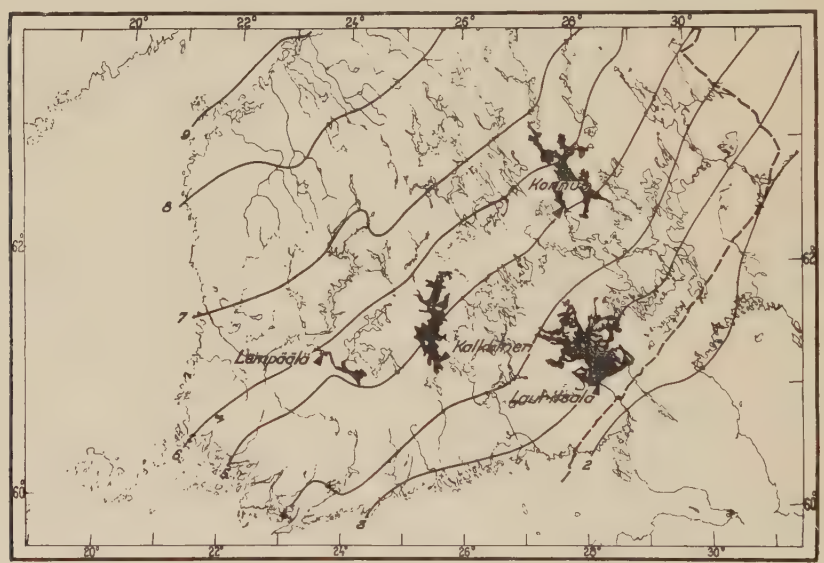

Fig. 1 - *Location of the gauges and mean land uplift* (mm per year) *according to* KÄÄRIÄINEN (1953).

that the changes in water level varied considerably during different periods. Maximum value for the average decrease of the water level in lake Saimaa is obtained for the period 1881-1948 whereas the calculated average change in the water level for the period 1851-1920 is the least marked and very insignificant. Further it may be noticed that in all the examined lakes the change has a similar trend. How-

ever, the value of Vanajavesi remains within the limits of error. The lake area of Vanajavesi as well as its drainage area is considerably smaller than that of other lakes under examination.

Looking for the reason of the changes mentioned above,and if human action is not considered, the possible causes may be grouped as follows:

1) Vertical land uplift caused by geological factors:

2) Changes caused by other geological factors, such as erosion and sedimentation.

3) Changes caused by meteorological factors.

From isobases illustrating the land uplift (Fig. 1) it may be seen that the lake plateau tilts in the direction NW-SE. According to Sirén [3] land uplift also appears in the differences of the water level observations carried out simultaneously at the ends of the same lake. Because of land uplift one may presume a continuous rise in water level in the SE, and a lowering in the NW end of the same lake. For instance, the NW shore of lake Saimaa rises as regards to Lauritsala in SE 1.2 mm per year. However, in Lauritsala the water level has lowered, on an average,

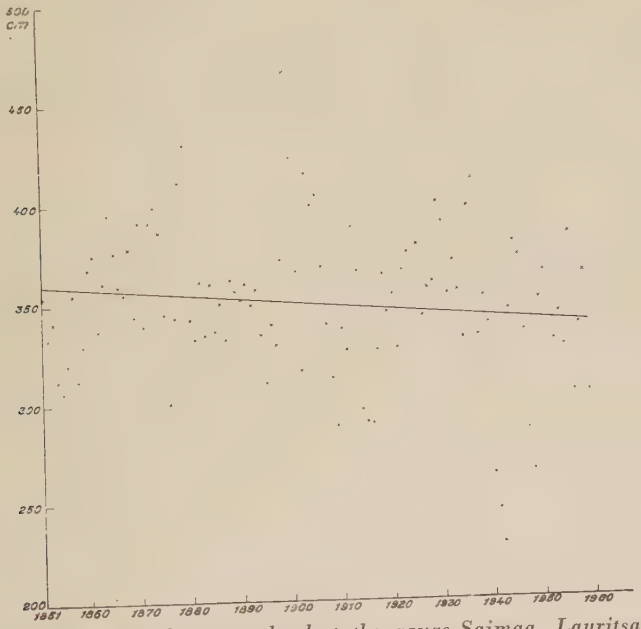

Fig. 2 - *Yearly means of the water level at the gauge Saimaa, Lauritsala,* 1851-1959.

1.9 mm per year (period 1851-1959). Although land uplift does not occur according to our presumption, it is possible that in connexion with an increase in differences of height it slowly causes a general decrease in the amount of water in the lakes.

The part of the other geological factors in contributing possibly to the phenomenon, such as erosion and sedimentation, is difficult to be determined. In wide outlets which eventually may be taken into consideration, no notable changes were proved. As, on the other hand, values of different magnitude were obtained for the changes in the water level of lake Saimaa during different periods it is hard-

ly probable that these factors could be of any significance for the problem in question.

The influence of meteorological factors appears primarly in the amount of precipitation and evaporation. The precipitation observations of earlier date are uncertain to such a degree that a reliable picture of a possible secular change in the amount of precipitation can not be proved. For the period 1911-1959 observations of sufficient reliability are available for the water systems used above. However, according to them no distinct change can be established although there appear rhythmical fluctuations regarding the amount of precipitation.

For evaporation no direct measurements are available. In the course of the air temperature which greatly regulates evaporation, slow increase has occurred. It is general knowledge that since the middle of last century climate began to warm up. For the secular change of the temperature of Helsinki 0.016° C per year is obtained by methods of calculations similar to those used for water levels above. A consequence of the increase in temperature is the fact that the time with no ice covering the lakes has increased.

No definitive explanation can be given for the decreasing tendency established in the water level. It is possible that increase in evaporation is one of the causes for the phenomenon. The opinion that this phenomenon is chiefly the consequence of long-term changes in meteorological elements is supported also by the fact that the change in water level has the same trend in different lakes, and that the magnitude of the change has varied similarly in the course of different periods.

REFERENCES

([1]) Kääriäinen Erkki, 1953: *On the recent uplift of the earth's crust in Finland.* Fennia 77, No. 2, pp. 56-57. — ([2]) Simojoki H., 1954: *Long rhythmic water level variations in lake Saimaa compared with the fluctuations in some climatological elements.* Geophysica, Vol. 5. No. 2 pp. 107-111. — ([3]) Sirén Allan, 1951: *On computing the land uplift from lake water level records in Finland.* Fennia 73, No. 5.

(*Received 9th February* 1961)

STUDIES OF THE NEW IONOSPHERIC MODEL: II (*)

by O. Burkard (**)

Zusammenfassung — Die vom Central Radio Propagation Laboratorium (National Bureau of Standards, Boulder) seit einiger Zeit veröffentlichten $N(h)$-Profile für die Station Puerto Rico wurden dazu benutzt, die seinerzeitigen Modellvorstellungen weiter auszubauen. Als eine wertvolle Ergänzung hierzu wird die Variation der Elektronenkonzentration mit der Höhe herangezogen, wie sie mit Hilfe von Mondreflexionen oder mittels der Radar-Streuecho-Methode beobachtet wurde. Die wichtigsten, so gewonnenen Erkenntnisse sind:

a) Der Vorgang der Elektronenvernichtung kann rein formal dargestellt werden durch den Ansatz

$$L = \alpha_0 \cdot \sqrt{p} \cdot N \quad \text{bei Quasi-Anlagerung,}$$

$$L = \alpha_0 \cdot T \cdot N^2 \quad \text{bei Quasi-Wiedervereinigung,}$$

worin L die pro Zeit- und Raumeinheit verschwindende Anzahl von Elektronen, p den Druck, T die absolute Temperatur und N die Elektronenkonzentration bedeuten. *Beide* Ansätze ergeben jedoch in ihrer Ausdeutung, daß die Zahl der verschwindende Elektronen direkt proportional der Temperatur T gesetzt werden muß.

b) Die Skalenhöhe H weist im Bereich von rund 200 km Höhe tagsüber ein markantes Maximum auf. Oberhalb dieses Bereiches findet man daher einen negativen Gradienten dH/dh. Erst im Bereich des $F2$-Maximums geht der Betrag dieses Gradienten auf sehr kleine Werte zurück; man wird dort praktisch mit einer von der Höhe unabhängigen Skalenhöhe rechnen können.

c) Die Skalenhöhe für diese räumlich annähernd isotherme Region variiert mit der Jahres- und Tageszeit. (Höchste Werte etwa Sommer-Mittag).

d) Das Maximum der Skalenhöhe wächst bis etwa Mittag ungefähr proportional $\sqrt{\cos \chi}$ (χ = Zenithwinkel der einfallenden Strahlung) an, nimmt hingegen am Nachmittag nur langsam ab. Gleichzeitig ändert sich auch die Höhenlage, in der dieses Maximum auftritt: Am Vormittag findet man eine rasche Verlagerung in größere Höhen, am Nachmittag ein nur langsames Absinken.

e) Dichte-Profile zeigen diesem Skalenhöhe-Maximum entsprechend in rund 200 km Höhe einen Wendepunkt-ähnlichen Verlauf, wie er auch aus Satellitenbahnen errechnet wurde.

f) Die Vorgänge bei Ionosphärenstürmen können derzeit noch nicht mit voller Sicherheit erfaßt werden. Es wären hierfür laufende Mondecho-Beobachtungen (mit der Zweifrequenzen-Methode) dringend erforderlich.

(*) Part I: Geofisica pura e applicata, Vol. 41, 133-140, 1958.

(**) Prof. Dr. Otto Burkard, Vorstand des Institutes für Meteorologie u. Geophysik der Universität *Graz*, Halbärthgasse 1.

Summary — Starting-point for our study was the static balance equation where the electron production is equated to the effective recombination. For the latter process we use the generally valid formula

$$L = \alpha_0 \cdot p^k \cdot T^n \cdot N^{m+2}$$

as introduced by Burkard. It was one of our first tasks to find appropriate numerical values for the constants k, m, n. Thereby the following possibility presented itself: The $N(h)$ profiles derived from observations are represented in power series, that is in powers of « x », where x designates the height from the layer peak upwards. Similarly, we can also set up such power series for the scale height H, the pressure p and the density ρ. A comparison of coefficients thus should enable us to compute $H(h)$ profiles.

It turned out, however, in the course of this study that the accuracy of the observational material [e.g. the $N(h)$ profiles at hand] is not sufficient for such a comparison of coefficients, so that we had to look for other ways.

We were finally successful in determining from the observational material the numerical values for the hitherto undefined constants k, m, n. Here two different possibilities result, according as we assume quasi-recombination or quasi-attachment. In many cases, so for instance in the derivation of $H(h)$ profiles, it did not prove necessary to decide upon one of these two possibilities, so that the computed values are valid for both models.

One fact is probably of special importance, namely that the process of electron loss is found as a linear function of the temperature of the neutral gas (or the electron gas). Here further studies will be necessary, in order to interpret this result on the basis of molecular or atomic theory.

The model presented in this study is mainly based on $N(h)$ profiles, but agreement is also excellent with observations obtained by the moon-echo method, moreover, with determinations of density derived from satellite orbits. In this connection valuable information is obtained from $H(h)$ profiles which were computed for many cases and which show the diurnal variation of the scale height. Additional calculations were performed in order to determine the seasonal variation of the scale height at least basically.

The $H(h)$ profiles show that at a height of about 200 km a considerable increase in temperature can be observed in the daytime. There the scale height varies between about 80 km and 170 km (Station Puerto Rico, July). At higher altitudes, however, those variations are considerably smaller, amounting to only about 30 km. In these altitudes we also find gradients of the scale height whose derivation from zero is very slight. Calculation of an $N(h)$ profile obtained by the Scatter-Radar-Method (Bowles) yielded an almost constant scale height from a height of about 340 km upwards to altitudes of 700 km. Seasonal variations, however, proved to be much higher. For the layer maximum under consideration relatively small values for the scale height were found for winter-time and values 1.4 times larger for summer-time. Also the diurnal variation at a height of about 200 km is much less noticeable in the winter-time. The maximum of the scale height changes its height also with the time of the day and the year reaching its maximum at summer noons.

Since the present study deals with models only, some of the expressions used for calculation had to suffer a few neglects in order to avoid unnecessary complications. Thus the variation of gravity with height was neglected. Also the diffusion of electrons was not taken into account and present results indicate that those processes of diffusion do not prove as important as is generally assumed.

In conclusion we make a few suggestions as to an effective continuation of the investigations reported here.

1. *Introduction* — The position of the physics of the ionosphere has been a peculiar one for a number of years: for, while on the one hand observational data currently collected have been accumulating to an extent where survey or even

compilation must become next to impossible, we are on the other hand still lacking more accurate knowledge of fundamental physical quantities allowing a complete understanding of conditions and physical processes prevailing in the ionosphere.

This discrepancy between extensive observational material on the one hand and very unsatisfactory knowledge of physical conditions on the other hand has been brought about above all by the fact that up to recently the numerous ionospheric observations (here I am having vertical soundings in mind especially) were only yielding the electron-concentration as dependent upon the — less usefull — virtual height (h'). Moreover, in spite of satellites and high-range rockets we have not even today been able to determine *directly*, i.e. by measurement, a quantity as important for the physics of the upper atmosphere as for instance temperature. Especially the latter fact has resulted in a situation where already for years we have trying by means of models to draw conclusions from numerous observational data at hand as to all those quantities and laws which at least for the time being cannot be determined otherwise. Such a model will have to meet two basic requirements: firstly, the underlying assumptions should be as simple as possible in order to permit a good survey of the *essential* characteristics of the processes, and, secondly, it should be stated with the broadest general validity possible in order not to cause any uncalled-for limitations of the problem on account of too specialized expressions. Having once gained insight into the fundamental principles of prevailing conditions it will not prove difficult in most cases to modify such a model according to subsidiary conditions. We shall see that the better such a model represents as many observational data as possible the closer its underlying principles and assumptions will come to actual conditions in nature.

Based on several concepts of models developed by BURKARD [1] within the past years this paper for the first time exploits to a greater extent the $N(h)$ profiles being at our disposal already for a number of stations. With their help we have been able to evaluate numerically two model constants not determinable hitherto enabling us to further extend the above mentioned model conceptions and offering a deeper insight into the physical processes of the ionosphere.

2. *Derivation of Basic Equations* — It is generally assumed that due to a monochromatic component of solar radiation a single component of the atmosphere is ionized. The number of electrons per ccm and sec thus produced is to be represented by q. Excluding conditions at sunrise and sunset we can neglect the curvature of the earth's surface and thus the solar radiation S when entering the atmosphere decreases according to equation

$$dS/dh = A \cdot \varrho \cdot S / \cos\chi . \tag{1}$$

The height above the ground is represented by h; ϱ stands for the density of that component of the air which is ionized. Moreover, A characterizes the process of absorption and χ is the zenith angle of incident solar radiation. For the density we can also write

$$\varrho = p/gRT \tag{2}$$

where p is the pressure, R the specific gas constant (measured in km/degrees) of the ionized air component. T stands for the gas temperature measured in degrees Kelvin assumed to be equal for all components of the air (with the exception of electron gas). Finally g stands for the gravity, whose variation with the height is neglected.

With regard to the decrease of pressure with height the following relation is valid:

$$dp/dh = -\frac{p}{R_0 \cdot T} . \tag{3}$$

The air being composed of several different types of gases a certain state of diffusion will generally prevail. Since, however, the degree of diffusion is unknown we do best to work with the two extremes:

a) Complete mixture corresponding approximately to conditions prevailing in the lowest atmosphere. In this case a mean value would have to be inserted in eq. (3) for the gas constant R_0

$$R_0 = \frac{\Sigma n_i \cdot R_i}{\Sigma n_i} \tag{4a}$$

where n_i are the concentrations and R_i the gas constants of the constituent parts of atmosphere.

b) Diffusive equilibrium. As gas constant R_0 we would now have, to take the gas constant of that component of the air which is ionized; we must write, therefore

$$R = R_0 . \tag{4b}$$

The question from which height on such a diffusive equilibrium in the ionosphere may be assumed is still somewhat disputed; YONEZAWA [2] supports the view that a height of 110 km may be this lower boundary. So we use only eq. (4-b); we may be sure that it is valid for the entire upper ionosphere examined here.

Using eq. (2) and (3) equation (1) can be integrated and we get

$$S = S_0 \cdot \exp\left(-\frac{A \cdot p}{g \cos \chi}\right) \tag{5}$$

where S_0 is the radiation energy outside the atmosphere of the earth.

The number of electrons produced in time and space unit by the absorbed radiation is thus given by

$$q = B \cdot A \cdot \varrho \cdot S$$

where B is a factor of proportionality of no further interest in this connection. Introducing the formulas derived above we may also write

$$q = \frac{B \cdot A \cdot S_0}{g \cdot R} \cdot \frac{p}{T} \cdot \exp\left(-\frac{Ap}{g \cos \chi}\right) = q_0 \cdot \frac{p}{T} \cdot \exp\left(-\frac{Ap}{g \cos \chi}\right) . \tag{6}$$

This permanent production of electrons by means of solar energy is opposed by processes causing a loss of free electrons; the number of electrons disappearing per time and space unit on account of recombination and/or attachment is to be represented by L (= loss) and according to an expression in BURKARD [3] is given by:

$$L = \alpha_0 \cdot p^k \cdot T^n \cdot N^{m+2} = \alpha \cdot N^2 . \tag{7}$$

Finally — as first approximation — we assume the two processes determined by eq. (6) resp. (7) to be in equilibrium, hence

$$q = L . \tag{8}$$

3. *Representation of the Relative Electron Concentration N/N^* by Means of an Exponential Series* — The $N\,(h)$ profiles derived from observations determine the electron concentration as dependent upon the true height. It has been the object of our investigations to be dealt with in this section to determine the extent to which from here also $p\,(h)$- and $T\,(h)$-profiles can be computed.

Eq. (6), (7) and (8) yield for the electron concentration N at any height h the expression

$$(9) \qquad N = \left(\frac{q_0}{\alpha_0}\right)^{1/m+2} \cdot (p)^{(1-k)/(m+2)} \cdot (T)^{-(1+n)/(m+2)} \cdot \exp\left(-\frac{A \cdot p}{g\,(m+2)\cos\chi}\right)$$

if, moreover, we are marking all quantities relating to the point of maximum electron concentration with asterisks (*) we also get

$$(10) \qquad N^* = \left(\frac{q_0}{\alpha_0}\right)^{1/m+2} \cdot (p^*)^{(1-k)/(m+2)} \cdot (T^*)^{-(1+n)/(m+2)} \cdot \exp\left(-\frac{A \cdot p^*}{g\,(m+2)\cos\chi}\right)$$

with the additional stipulation that at height $h = h^*$, resp. at pressure $p = p^*$ there must be valid

$$\frac{d \lg N}{dp} = 0\,.$$

Since in those formulas certain expressions are constantly recurring we are introducing abbreviations by writing

$$(11) \qquad \frac{1-k}{m+2} = P \quad \text{and} \quad \frac{1+n}{m+2} = Q\,.$$

With these reductions eq. (9) may be written somewhat shorter in logarithmized form

$$\lg N = \frac{1}{m+2} \lg \frac{q_0}{\alpha_0} + P \cdot \lg p - Q \cdot \lg T - \frac{A \cdot p}{g\,(m+2)\cos\chi}$$

thus from the maximum condition mentioned above it follows

$$(12) \qquad P + Q \cdot \left(\frac{d\,RT}{dh}\right)^* = \frac{A \cdot p^*}{g\,(m+2)\cos\chi} = Z$$

taking eq. (3) into account and introducing also the letter Z by means of abbreviation. Using eq. (9) and (10) the relative electron concentration is thus given by

$$(13) \qquad N/N^* = (p/p^*)^P \cdot (H^*/H)^Q \cdot e^Z \cdot \exp\left(-Z \cdot \frac{p}{p^*}\right).$$

At the right-hand side of this equation only the relative presure p/p^* and the relative scale-height values H/H^* do still occur. ($R \cdot T = H$). All variable quantities of eq. (13), however, are apparently functions of the height h. Thus it proves to be quite reasonable to relate also this height h to the marked value h^* by introducing

$$(14) \qquad h - h^* = x\,.$$

At this point it will not prove difficult to represent the three quantities dependent on height (namely p/p^*, H/H^* and N/N^*) in power series $\Sigma a_n \cdot x^n$. The simplest

way seems to be to start from the series for pressure by writing

$$\lg \frac{p}{p^*} = -\frac{1}{H^*}\,x - \frac{a}{H^{*2}}\,x^2 - \frac{b}{H^{*3}}\,x^3 - \frac{c}{H^{*4}}\,x^4 - \frac{d}{H^{*5}}\,x^5 - \ldots \tag{15}$$

where no conditions are laid down concerning the constants a, b, c, d, ... thus rendering eq. (15) generally valid. Taking eq. (3) into account also the series for $\lg (H/H^*)$ can be determined from here. Thus we find

$$\lg \frac{T}{T^*} = \lg \frac{H}{H^*} = -\frac{2a}{H^*} \cdot x + \frac{2a^2 - 3b}{H^{*2}}\,x^2 - \frac{8a - 18ab + 12c}{2H^{*3}}\,x^3 + \tag{16}$$

$$+ \frac{8a^4 - 24a^2b + 9b^2 - 10d}{2H^{*4}} \cdot x^4 \ldots$$

If we differentiate the latter equation with respect to x we obtain the quantity needed

$$(dH/dh)^* = -2a \tag{17}$$

so that eq. (12) can be rewritten

$$P - 2aQ = Z\ . \tag{18}$$

If, moreover, we also logarithmize eq. (13) and introduce the series eq. (15) and (16) then also $\lg (N/N^*)$ can be represented in an exponential series

$$\lg \frac{N}{N^*} = -K_2 \cdot \left(\frac{x}{H^*}\right)^2 + K_3 \cdot \left(\frac{x}{H^*}\right)^3 - K_4 \cdot \left(\frac{x}{H^*}\right)^4 + \ldots \tag{19}$$

The coefficients K_i ($i = 2, 3, 4, \ldots$) have been presented in the following Table I on grounds of a better survey. Above all several special cases with simpler assumption as to the course of temperature within the region of the F-layer-maximum have been shown. It shall not surprise us that the series eq. (19) begins only with the quadratic term so that $K_0 = K_1 = 0$ is valid if we take into consideration that at the point $x = 0$, $N = N^*$ must be valid. The coefficients K_2 and K_3 can be taken from the Table I. Since the series is progressing with the powers of (x/H^*) its properties of convergence depend entirely upon this ratio $x : H$ since the coefficients K_i taken by themselves do not converge generally. Thus this series only represents a useful approximation for $x < H^*$.

In computing $N(h)$ profiles the electron concentration in the vicinity of the F-layer-maximum is usually represented approximately by a comparatively simple expression. We usually write according to BECKER [4]

a) the EPSTEIN-layer with

$$\frac{N}{N^*} = \frac{4e^{3x/2y}}{\left(1 + e^{3x/2y}\right)^2} \quad \text{resp.} \quad \lg \frac{N}{N^*} = -\frac{9}{16y^2} \cdot x^2 + 0 \cdot x^3 - \ldots \tag{20a}$$

b) The cosine-layer with

$$\frac{N}{N^*} = \frac{1 + \cos 3\pi x/8y}{2} \quad \text{resp.} \quad \lg \frac{N}{N^*} = -\frac{9\pi^2}{256y^2} \cdot x^2 + 0 \cdot x^3 - \ldots \tag{20b}$$

Table I.

H	dH/dh	a	b	K_2	K_3
H	0	0	0	$P/2$	$P/6$
$H + \gamma Rx$	γR	$-\frac{\gamma R}{2}$	$\frac{(\gamma R)^2}{3}$	$\frac{P + \gamma RQ}{2}$	$\frac{(P + \gamma RQ)(1 + 3\gamma R)}{6}$
$H + \delta \cdot x^2$	$2\delta \cdot x$	0	$-\frac{\delta}{3} H$	$\frac{P + 2\delta \cdot QH}{2}$	$P/6$
eq. (16)		a	b	$\frac{P - 2Q(a - 4a^2 + 3b)}{2}$	$\frac{P(1 - 6a) - 2Q(a - 6a^2 - 8a^3 + 24ab - 12c)}{6}$

c) the parabolic layer with

$$\frac{N}{N^*} = 1 - \left(\frac{x}{2y}\right)^2 \tag{20c}$$

resp.

$$\lg \frac{N}{N^*} = -\frac{1}{4y^2} \cdot x^2 + 0 \cdot x^3 - \ldots$$

where $2y$ measures the half layer thickness of the parabolic profile, the quantity y thus corresponding to the value called « SCAT » by NBS (National Bureau of Standards, Boulder). If we compute the resp. logarithms for these three models and develop the latter in an exponential series in x we notice that those series only contain terms with even exponents and that the terms with odd exponents of x are missing. Of course, also the terms with x^0 and x^1 are missing in all three cases.

A comparison of coefficients for the series eq. (19) and (20) thus leads to the condition $K_3 = 0$ and Table I already shows us that under these conditions the assumption $H = H^* =$ constant is impossible. For then also K_2 would have to become zero which is not the case.

Assuming a constant temperature gradient $(dH/dh)^* = \gamma R =$ constant (second line, Table I), however, we obtain the solution

$$\gamma R = -\frac{1}{3}$$

again taking into account that $K_3 = 0$ but $K_2 = 0$. We are very much hesitating to assume a general validity for $dH/dh = -0.33$. Those doubts are augmented by the fact that apparently the expressions for a layer symmetrical to $x = 0$ as stated in eq. (20) comprise a certain measure of constraint asking for property of symmetry in the N (h) profile not corresponding to the actual electron distribution. Considering the degree of accuracy for N (h) profiles attainable at present it seems quite

possible that the coefficient K_3 cannot be determined with sufficient accuracy any more. Therefore, we want to limit the comparison of coefficients between the exponential series of eq. (19) and (20) to the single coefficient K_2. In order to work with as little constraint as possible we are using the generally valid presentation of line 4 (Table I) for a comparison of the coefficient K_2 with the one pertaining to the parabolic layer:

$$H^* = y \cdot \sqrt{2P - 4Q\,(a - 4a^2 + 3b)}\,. \tag{21}$$

From this relation we can easily see that the SCAT-value stated by NBS in their tables of $N\,(h)$ profiles ([5]) is identical with the scale height in the layer-maximum only if the expression below the square root becomes equal to unit. As we shall see later the root is often greater or smaller than one, from where result corresponding values for the scale height being in part considerably greater or smaller than generally assumed.

In closing this section we must state that by means of presenting $\lg\,(N/N^*)$ as exponential series the corresponding exponential series for $\lg\,(H/H^*)$ or $\lg\,(p/p^*)$ *cannot* be determined since every time we add an additional coefficient K_i for the comparison of coefficients also a new unknown quantity must be added. (For instance for K_3 the constant c, for K_4 the constant d, etc.).

With regard to computing $N\,(h)$ profiles it seems desirable that in future the approximation in the vicinity of the F-layer-peak is not performed by means of a common parabola but at least by means of a asymmetrical parabola of the third order.

4. *The Constants P and Q* — Considering what has been said above evaluation of P and Q would be of great importance for two reasons: possible models basically depend upon these quantities and, moreover, we would thus gain further insight into the process of electron loss. Up to now we unfortunately had to work with assumptions and the most we were able to do was to show within about what limits P and Q would have to be situated. The numerous $N\,(h)$ profiles at our disposal have now been offering a new way of evaluating P and Q numerically. Using eq. (11) and (12) we may thus rewrite eq. (10) in logarithmical form

$$\lg N^* = \frac{1}{m+2}\,\lg\,(q_0/\alpha_0) + P \cdot \lg p^* - Q \cdot \lg T^* - Z\,. \tag{22}$$

Moreover, we assume that in the course of the day the quantities a, b (eq. 15) and also $(dH/dh)^*$ (eq. 12) and also (q_0/α_0) can be regarded as constants. Thus all quantities remaining unchanged during the day can be comprised in a constant C and there remains

$$\lg N^* = C + P \cdot \lg \cos\chi - Q \cdot \lg y \tag{23}$$

that is in other words $\lg\,(N^*)$ only remains a function of the zenith angle of incident solar radiation and a function of the quarter-of-layer thickness y, varying according to observations in the course of the day. It is thus possible to determine P and Q either already from this equation or to compute the difference quotients in addition, thus arriving at

$$\frac{\Delta \lg N^*}{\Delta \lg \cos\chi} = P - Q \cdot \frac{\Delta \lg y}{\Delta \lg \cos\chi} \tag{24}$$

where the differences refer to observational data with intervals of an hour or half-an-hour. If in a diagram we take $\Delta \lg y / \Delta \lg \cos \chi$ for abscissa and $\Delta \lg N^* / \Delta \lg \cos \chi$ for ordinate we would have to get a straight line the slope of which determines Q and which is intercepting the distance P on the y-axis. Fig. 1 shows the result of such a calculation. The material used have been the N^* and y data for the Station Puerto Rico as published by NBS ([5]). (March 1960, only days with sunspot-number $R < 90$, 7 : 00 a.m. to 10 : 00 a.m.). Here we have been limiting ourselves to the early morning hours since scatter has been too heavy otherwise. One of the reasons for this scatter might be found in the fact that towards noon the denominator $\Delta \lg \cos \chi$ is growing very small thus enlarging out of proportion smaller deviations of the quantities $\Delta \lg N^*$ and $\Delta \lg y$ in the numerators. In the diagram the variations of $\cos \chi$ and also of $\Delta \lg \cos \chi$ during the month have not been considered.

Considering that P and Q represent the exponents of pressure and temperature at least for Q a « simple » number is probable for physical reasons. From Fig. 1 we think to be able to read

(25) $$P = 0.5 \qquad \text{and} \qquad Q = 1 .$$

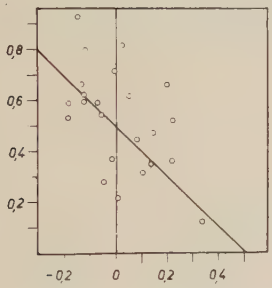

Fig. 1 - *Determination of P and Q*; Station Puerto Rico, March 1960.

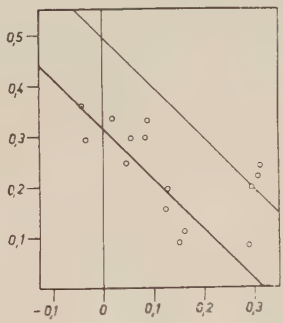

Fig. 2 - *Determination of P and Q*; Station Adak, July 1959 (5-day-averages, morning hours).

The scatter of values entered in the diagram is obviously caused by the fact that our assumption concerning the constancy of a, b, $(dH/dh)^*$ and (q_0/α_0) does not prove to be completely true. If according to eq. (17) we use $(dH/dh)^* = -2a$ then a « perturbation term » would have to be added on the right-hand side of the form

(26) $$\frac{1}{m+2} \cdot \frac{\Delta \lg q_0}{\Delta \lg \cos \chi} + \frac{Q^2}{P - 2Q\,(a - 4a^2 + 3b)} \cdot \frac{\Delta\,(a - 4a^2 + 3b)}{\Delta \lg \cos \chi} + + 2Q \cdot \frac{\Delta a}{\Delta \lg \cos \chi} .$$

Here according to our investigations especially those items seem to be decisive containing Δa. Since $(dH/dh)^*$ often shows a slight but still noticeable diurnal

variation — the noon values being larger than those for morning and night hours — we may possibly get a wrong value too small for P if using the simplified eq. (24). Such a situation is shown in Fig. 2 derived from $N(h)$ profiles as computed by the Station ADAK for July 1959. (For providing these $N(h)$ profiles yet unpublished we are indebted to Mr. J. W. Wright of NBS-Boulder). Here, too, we think to be able to read

$$Q = 1$$

as to P, however, we get a value $P = 0.3$ on account of neglecting the « perturbation term » according eq. (25).

Since in the two figures we have only been using the morning values Fig. 3 is presenting all values observed during the day excepting hours late in the afternoon. Thereby we are using equation (23) by plotting log N^* as a function of (1/2 log cos χ — log SCAT). It became evident, however, that monthly averages of $N(h)$ profiles published by NBS have been leading to a heavy scattering of points in such a diagram in all those cases where mean values had been computed from very inhomogenous observational material. (In some months there are only a very few days for which observations for every hour of the day are available). On the other hand, we may say that the better the homogeneity of the observational material the better the agreement of plotted values with the straight line to be expected. Two further proofs of validity of eq. (25) are adduced in section 8 and 9.

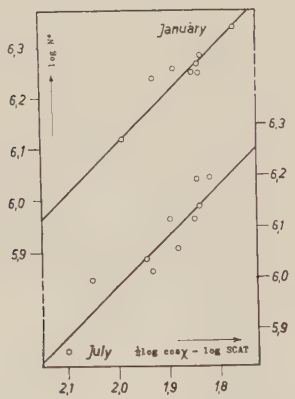

Fig. 3 - *The relation log* $N^* = C + 1/2$ log cos χ — log y. Station Puerto Rico, 1960. (The figures of abscissa to be read with negative sign).

5. *The Process of Electron Loss* — In section 1 we have determined in eq. (7) the number of free electrons disappearing per time and space unit with

$$L = \alpha_0 \cdot p^k \cdot T^n \cdot N^{m+2}$$

thereby introducing the three « model constants » k, m and n. From here there results that

$m = 0$ corresponds to a quasi-recombination (square law)
$m = -1$ corresponds to a quasi-attachment (linear law).

It is, however, striking that those three model constants always occur in the formulas in the same combination thus enabling us to introduce the new quantities

P and Q (eq. 11) by means of abbreviation of equations and formulas. Thus every simple model of the upper ionosphere is reduced to the choice of two parameters (P, Q) and to the assumptions of the course of temperature with height: $T = T(h)$. We are, however, not able to decide upon the two possibilities $m = 0$ or $m = -1$ as long as we have no additional observational material at our disposal (e.g. behavior during solar eclipses etc.).

Before dealing further with the physical importance of the values computed for P and Q we want to make a few critical remarks on those expressions for electron loss to be found frequently in relevant literature. It is a well-known fact that in a great number of studies an isothermal layer (atmosphere) is assumed whose characteristic feature is that the resulting $N(h)$ profile is independent of the choice of a numerical value for Q. In many other cases the so-called CHAPMAN-layer is used, characterized by the following assumptions:

$$T = \text{constant}, \quad \alpha = \text{constant} \quad \text{and} \quad L \propto \alpha \cdot N^2.$$

It is surprising to see that among the great number of possibilities four statements are leading to the same CHAPMAN-like $N(h)$ profile — appropriate assumptions as to the temperature-variation with height provided. (See Table II).

From the last two lines of this Table we can see that a CHAPMAN-like $N(h)$ profile is also obtained for an anisothermal layer if we express the process of electron loss in the manner stated in the third column.

TABLE II.

Type	T	L	P	Q
I	constant	$\propto N^2$	0.5	any value
II	constant	$\propto (p)^{1/2} \cdot N$	0.5	any value
III	$T = T(h)$	$\propto T^{-1} \cdot N^2$	0.5	0
IV	$T = T(h)$	$\propto (p)^{1/2} \cdot T^{-1} \cdot N$	0.5	0

RATCLIFFE & Co. [6] have introduced a linear law of loss given by

$$L = 10^{-4} \cdot N \cdot \exp\left(\frac{300 - h}{50}\right) \quad \text{and} \quad T = \text{constant}.$$

This model thus corresponds to

$$P = \frac{50 - H}{50} \quad \text{and} \quad Q = \text{not defined}$$

and would pass into a CHAPMAN-like layer of type II if we assume $H = 25$.

WRIGHT [7] uses the same expressions assuming, however, $H = 100$ km thus obtaining the model constant

$$P = -1.$$

While WRIGHT still adheres to an isothermal layer with $T \neq T(h)$, RISBETH & BARRON ([8]) assume for their studies a scale height possessing a constant gradient where again a process of loss is expressed by

$$P \approx -1 .$$

Moreover, in my opinion, the latter paper puts too much stress on processes of diffusion. Finally also HIRSH ([9]) starts from well-defined ideas as to the process of recombination so that he must necessarily arrive at a value for P to be found between zero and (-1).

This paper, however, tackles the problem from the opposite side by not stating any limiting assumptions as to the process of recombination. On the contrary the process effective in electron loss is to be derived from the numerical values computed for P and Q. Since our calculations have yielded the numerical values

$$P = 1/2 \quad \text{and} \quad Q = 1$$

the process of electron loss can be stated in the following way:

linear law	or	square law
$m = -1$		$m = 0$
$k = 0.5$		$k = 0$
$n = 0$		$n = 1$
$L \propto (p)^{\frac{1}{2}} \cdot n(e)$		$L \propto T \cdot n^2(e)$

(Here for the time being the somewhat longer symbol $n(e)$ has been used in denoting electron concentration in order to avoid confusions with N, the chemical symbol for nitrogen atoms). Now this result is apparently inconsistent with postulations for the rate of removal made by different workers hitherto and it must be our task to give an interpretation which is physically valid. At first we want to make a few remarks on the decrease of pressure with height for the different components of the air, assuming — as stated in section 1 — an atmosphere with diffusive equilibrium. For every constituent (i) of the atmosphere pressure thus decreases with height according to a law of the form

$$p(i) \propto \exp\left(-\int \frac{dh}{H_i}\right).$$

Taking as scale height of the oxygen molecule $H(O_2) = H_0$ we obtain for atomic oxygen, resp. for nitrogen:

$$\begin{aligned} H(O) &= 2.00\, H_0 \\ H(N_2) &= 1.14\, H_0 \\ H(N) &= 2.28\, H_0 . \end{aligned}$$

Thus also the pressure-variation with height for atomic resp. molecular components will be in mutual relation:

$$\begin{aligned} p(N_2) &\propto p^2(N) \\ p(O_2) &\propto p^2(O) \\ p(N_2) &\propto p^{1.75}(O) . \end{aligned}$$

In analogy to the duplication of the scale height of molecular gas by way of dissociation we find such a duplication of the scale height also for the process of ioniza-

tion for the single ionized gas as shown by JOHNSON ([10]). Thus the following is also valid

$$H(O_2^+) = 2H(O_2)$$
$$H(O^+) = 2H(O)$$
and so on.

Complete diffusive equilibrium provided, we would thus again obtain relations between the pressure of a non-ionized and an ionized air component similar to the relations for dissociation derived above. As to ionized gas components, however, we will have to take into account that a distribution of positive ions corresponding to diffusive equilibrium must necessarily have as a consequence electrostatic fields in that part of the ionosphere where electrons are not distributed according to diffusive equilibrium, i.e. in the entire lower region of the layer as far as a region slightly above the layer maximum. We might, on the other hand, also assume that the electric powers of attraction between positive ions and electrons are that powerful that positive ions are diffusing with height much the same as electrons. Then, of course, the $N(h)$ profile would correspond to the one of positive ions.

a) Let us assume that the linear law of loss is valid. The resulting proportionality to the root of the pressure p then only indicates that-diffusive equilibrium provided — the electron loss is proportional to the density of the *ionized* gas (with double scale height) while the electron production is proportional to the density of the same but non-ionized gas (with single scale height). Then, moreover, the process of electron loss must be proportional to the gas temperature T.

This might lead to the assumption that the electron production is a consequence of the ionization of nitrogen molecules while the loss would thus represent only a quasi-recombination of those ionized molecules by writing

$$N_2 + h\gamma \quad \text{electron production}$$
$$N_2^+ + e \quad \text{electron loss} = L \propto T \cdot n(N_2^+) \cdot n(e) .$$

Likewise we could also assume that the oxygen-atom is ionized and that the density of these positive oxygen-atom-ions is decisive for the capture of electrons:

$$O + h\gamma \quad \text{electron production}$$
$$O^+ + e \quad \text{electron loss} = L \propto T \cdot n(O^+) \cdot n(e) .$$

Whatever it might be the novelty is contained in our result that the process of electron loss is dependent on temperature and is proportional to the absolute temperature of the atmospheric gas. Since, moreover, no absolute values but only proportionalities can be determined in this connection it might also be possible that the process of electron loss is proportional to the temperature of electron gas which can be assumed proportional but not equal to the gas temperature for vast regions of the ionosphere.

b) We will now proceed to the second possibility: Now the square law shall be valid according to which L is proportional to the temperature T and the square of the electron concentration $n(e)$. Interpretation in this case is very simple since it is only necessary to assume electric neutrality in the ionized gas so that in all cases the density of positive ions can be assumed equal to the density of electrons. We would so have a recombination before us where the process is again dependent on temperature: again we find proportionality to the temperature T.

Since up to now hardly any detailed studies on a possible thermal influence in similar processes of (quasi-) recombination have been made a theoretical and also a experimental study of this problem would be very desirable.

6. *Calculation of $H(h)$-Profiles* — Since in computing the constants P and Q only data of the layer-maximum have been used those values are, of course, only valid for the region near the maximum of electron concentration in the upper ionosphere that is near the F-layer-peak. The region for which the numerical values computed for P and Q are valid being unknown we are able to extend it to the whole upper ionosphere. This assumption provided we go back to the relations derived in section 3 and using equations (13) and (25) compute the integral

$$\int_{h}^{h^*} \frac{N}{N^*}\, dh = -H^* \cdot e^{Z} \int_{p}^{p^*} \sqrt{\frac{p}{p^*}}\, e^{-Z \cdot p/p^*} \cdot \frac{dp}{p}$$

writing

$$Z \cdot \frac{p}{p^*} = t^2 \tag{27}$$

and obtaining the result

$$\int_{h}^{h^*} \frac{N}{N^*}\, dh = e^{Z} \cdot \sqrt{\frac{\pi}{Z}} \cdot H^* \cdot \left[\Phi(t) - \Phi(\sqrt{Z})\right] \tag{28}$$

if we write the error function Erf (x) in the form:

$$\mathrm{Erf}(x) = \int_{0}^{x} e^{-t^2} \cdot dt = \frac{\sqrt{\pi}}{2} \cdot \Phi(x) \quad . \tag{29}$$

If we succeed in stating Z and H^* appropriately we are now able to compute Erf (t) and thus, of course, also t for any height h as long as $N(h)$ profiles are available:

$$\mathrm{Erf}(t) = \mathrm{Erf}(\sqrt{Z}) + \frac{\sqrt{Z}}{2H^*} \cdot e^{-Z} \int_{h}^{h^*} \frac{N}{N^*}\, dh \,. \tag{30}$$

From equation (27) also a $p(h)$ profile for the pressure variation with height can determined.

On the other hand, we obtain from eq. (13) also the $H(h)$ profile, for

$$H = H^* \cdot \frac{N^*}{N} \cdot \frac{e^{Z}}{\sqrt{Z}} \cdot t \cdot e^{-t^2} \,. \tag{31}$$

As long as Z and H^* are not determined, however, every $N(h)$ profile yields a system of curves $t(h)$ with two parameters (H^*, Z) which can be computed from $\Phi(t)$ by means of tables ([11]). It is thus not possible to obtain unambiguous $p(h)$ and $H(h)$ profiles since also in this case systems of curves with two parameters are resulting.

Since hardly any other quantity seems to be more suitable for characterizing an ionospheric model than the scale height H we have been studying in detail

the variation of $H(h)$ profiles which can be computed for different values (H^*, Z) but for only one $N(h)$ profile and we have made special efforts to determine those parameters in a reasonable way which are that important for the final calculation of $H(h)$ profiles. Since we think that our experiences in this respect will prove useful also for other workers in their future studies and since they, moreover, offer a good insight into existing mathematical relations we are in the following stating some results of calculations intended above all to solve the questions to the limits within which the two parameters H^* and Z can be reasonable varied. Also in this place we want to mention a result to be dealt with later in more detail to the effect that the two parameters in question are not independent of each other. As long as no appropriate observational material is at hand, however, these relations cannot be exploited.

Fig. 4 first shows some $H(h)$ profiles computed from $N(h)$ profiles of the Station Puerto Rico using the monthly averages for July 1959, noon, as published by the Central Radio Propagation Laboratory, NBS, Boulder. In all cases the value 0.5 has been used for the parameter Z and thus on account of eq. (12) the gradient of the scale height becomes zero: $(dH/dh)^* = 0$.

For the second parameter namely H^*, however, we have been using various numerical values in order to show the dependence of this parameter. For the system of curves shown here

$$67 \text{ km} \leq H^* \leq 110 \text{ km}$$

is valid. Now H^* values which are too small yield $H(h)$ profiles making a decisive turn to the left already at a relatively great height there leading to H values that small that they do not agree with H values observed otherwise. On the other hand, H^* values which are too large result in $H(h)$ profiles turning decisively to the right in lower layers thus again not corresponding with the observational material at hand. Thus only a small range is left for choosing an appropriate H^* value.

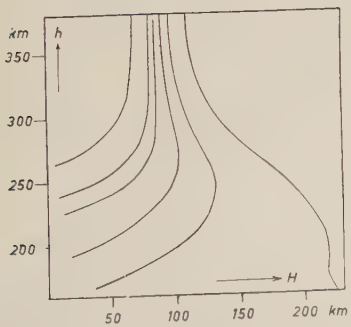

Fig. 4 - *Computed $H(h)$ profiles for fixed Z and variable H^*.* Station Puerto Rico, July 1959, noon.

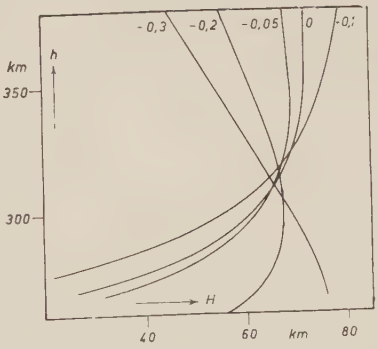

Fig. 5 - *Computed $H(h)$ profiles for variable H^* and Z.* Station Puerto Rico, July 1959, noon.

We have a similar situation before us if we use various values for H^* and Z. This case is shown as an illustration in Fig. 5 for the same initial values (Puerto

Rico, July 1959, noon) where Z varies between 0.2 and 0.6. This corresponds to values of $(dH/dh)^*$ between -0.3 and $+0.1$. In the vicinity of the layer maximum those curves are showing either a positive gradient $(dH/dh)^*$ — if $Z > 0.5$ has been chosen — or a negative gradient for $Z < 0.5$. Considering our present state of knowledge and the theoretical expressions at hand, however, it is hardly probable that this gradient deviates from zero considerably, thus limiting the «possible» cases.

As far as the $H(h)$ profiles shown in the two figures above can be said to follow a reasonable course, they have without exception a surprising and striking feature in common: around 200 km height we find a maximum of the scale height which we think to be justified in considering a temperature maximum related to the point of inflection in the density profile $\rho(h)$ found by PRIESTER & MARTIN ([12]).

At this stage of our investigations we have made special efforts to find clues to the right choice of the parameters H^* and Z. Beyond that we were having certain doubts as to the use of averaged $N(h)$ profiles, for — as we know ([5]) — before the averaging process the individual profiles are extrapolated above h^* by a CHAPMAN distribution of 100 km scale height. Extrapolation is necessary in order to calculate homogenous averages near h^*. Thus, a certain error in the $N(h)$ profiles will result on account of using in the averaging process already a fixed value for H^* which should only be obtained from calculations of $H(h)$ profile.

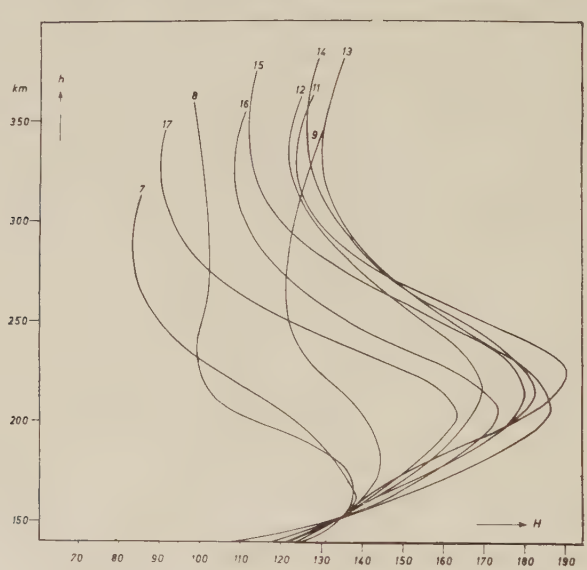

Fig. 6 - *$H(h)$ profiles computed from $N(h)$ profiles*: Puerto Rico, July 1, 1959.

Another problem with regard to these monthly averages for $N(h)$ has been the question in how far $N(h)$ profiles are reproducing themselves from day to day, in other words to what extent monthly averages can be said to represent the single curves. We also been hoping to be able to draw conclusions from the diurnal variation of $N(h)$ profiles as to possible relations between Z and H^*. Thus we have again been computing $H(h)$ profiles for number of magnetically quiet days.

The calculations show that variations from day to day usually found in $N(h)$

profiles are not very conspicuous in $H\,(h)$ profiles and that the diurnal variation of $H\,(h)$ looks much the same for every day. This result has removed most of our doubts as to the use of monthly averages; any new idea useful in the choice of parameters has not resulted, however. Therefore, we have been trying several other ways; on account of these calculations being trials it has been necessary to use new statements every time. It did, therefore, not pay to use bigger (possibly electronic) computers, but calculations with a small electro-mechanical computer proved to be very time-consuming.

With regard to the $H\,(h)$ profiles as shown in Fig. 6 another method has been used, namely introduction of a mutual «adaptation» of curves for the hours of the day in a way that for the height range between 140 and 160 km the quantities t and H are to be constant (if taken the averages). This statement has been based on the thought that for the lowest layer of the ionosphere no great temperature variations should result in the course of the day and that for this region the gradient of the scale height can be considered to be at least approximately constant. For Z_{12} (at noon) we used the value 0.7. In fact, those curves look quite reasonable and it is especially striking that the maximum of scale height is to be found in the morning and afternoon hours at a height of about 170 km (with $H \approx 140$ km) while the noon values of H rise to about 180 km accompanied by a simultaneous shift of this maximum to a height of about 210 km. It is also striking that within the region of the layer maximum the gradient $(dH/dh)^*$ is smaller in the morning and afternoon hours than at noon. We have, however, abandoned the above mentioned conditions since they did not seem to have a sound physical basis.

Physically reasonable conditions did not prove successful in solving the problems in question: thus, for instance, assumption of constant temperature and constant pressure for the lowest region of the layer during the whole day.

7. *Some Extensions of Formulas* — We have finally been able to arrive at a deeper insight into prevailing conditions by computing the integral eq. (28) for two special cases obviously suggesting themselves, inserting for h one time zero and one time infinity. In the first case we get

$$J_b = \int_0^{h^*} \frac{N}{N^*} \cdot dh = e^Z \cdot \sqrt{\frac{\pi}{Z}} \cdot H^* \cdot [1 - \Phi(\sqrt{Z})] \qquad (32)$$

where

$$N^* \cdot J_b = n_b$$

is the total number of electrons/cm^2 column *below* the maximum. In the other case we similarly obtain the total number of electrons/cm^2 column *above* the layer maximum, where

$$J_a = \int_{h^*}^{\infty} \frac{N}{N^*} \cdot dh = e^Z \cdot \sqrt{\frac{\pi}{Z}} \cdot H^* \cdot \Phi(\sqrt{Z}) \qquad (33)$$

and

$$N^* \cdot J_a = n_a \,.$$

Moreover, it might be useful to state that we thus get

$$J_b + J_a = \int_0^\infty \frac{N}{N^*}\, dh = e^Z \cdot \sqrt{\frac{\pi}{Z}} \cdot H^* \tag{34}$$

and

$$\frac{n_a}{n_b} = \frac{J_a}{J_b} = \frac{\Phi(\sqrt{Z})}{1 - \Phi(\sqrt{Z})}\,. \tag{35}$$

As we can easily see from the latter equations certain relations exist between the parameters Z and H^* whose exploitation is only a question of possibility to observe the two integrals J_a and J_b.

8. *Total Electron Content below the Layer Maximum* — The Tabulations of Electron Density Data published by CRPL-Boulder in Ionospheric Data (Part A) also contain the integral

$$\text{SHMAX} = \int_{0^-}^{h^*} N \cdot dh$$

(called « SHMAX » by CRPL). On the other hand, we can compute the right-hand-side terms of eq. (32):

$$e^Z \cdot \sqrt{\frac{\pi}{Z}} \cdot H^* \cdot N^* \cdot [1 - \Phi(\sqrt{Z})]$$

for those two parameters Z and H^* which have been used by us. Agreement of these two numerical values (namely SHMAX and the term above) has been surprisingly good. Thereby, we must consider that those SHMAX-values start integration not from zero but from the height h_{min}, h_{min} being determined by the ionograms in question. Moreover, it is evident that also the electrons of the E-layer and those of a possible $F1$-layer have been included while our eq. (32) refers, of course, only to those electrons produced by the process of ionization stated in section 1. This good agreement seems to be a further proof of the appropriateness of our model constants determined by eq. (25), so that we think to be justified in using the SHMAX-values derived from direct observations in order to determine the still undefined parameters Z and H^*. From eq. (32) results that those parameters cannot be chosen as independent of each other any more; a « free » choice can thus only concern either H^* or Z. Here, we will always have to see, however, that in J_b only those electrons are taken into account which have been produced by one single process of ionization according to derivation eq. (6) seq. Thus, electrons pertaining to the normal or sporadic E-layer must be left out of consideration with certainty.

Another problem concerns electrons possibly constituting an $F1$-layer. Here several processes are possible. Thus the $F1$-maximum of electron concentration can be the result of absorption and ionization of another radiation component (with different wave lenght) in this region. Another possibility would be the ionization of another component of the air deviating from conditions in the $F2$-layer. Finally, Burkard [1] has shown, that a certain variation of temperature with height can cause a stratification of the layer and it is striking that the course of tempera-

ture deduced from our $H(h)$ profiles meets the postulations of BURKARD. We are, however, at present unable to differentiate between these possibilities with certainty. One possibility for future studies, however, can already be indicated here: During years with very small solar activity — again in about five years — the critical frequencies of the $F1$-layer and the $F2$-layer do not diverge too much from each other. Thus, of course, the electrons belonging to the F1-layer contribute much more to the computation of the SHMAX-value than the present $N(h)$ profiles, where the critical frequency of the $F2$-layer on account of a strong solar activity is several times greater than the one of the $F1$-layer. It is to be hoped, however, that at that time the two important questions in this respect can be finally solved, namely:

a) Is the process of ionization responsible for the $F2$-layer also responsible for the $F1$-layer?

b) May we assume that in this lower region of the ionosphere the same process of loss is valid as in the $F2$-layer?

Present data seem to indicate a positive answer to these two questions; it might also be possible, however, that the influences of the $F1$-layer prove to be that slight that their influence on the resulting integral SHMAX is not noticeable.

Finally, I want to mention a result obtained from eq. (21) and (32) offering further proof of the validity of my finding

$$Q = 1 .$$

From the equations mentioned above there follows that the integral J_b must be proportional to the first power of H^*. We are now using in place of the integral the observational value SHMAX available through publications and in place of H^* — which cannot be observed directly — the value « SCAT » (= y according to our designation) of the Tabulations. For Fig. 7 I have taken corresponding values of log (SHMAX/N^*) as ordinate dependent upon log (SCAT) (= abscissa) from CRPL-Data and have plotted them in a diagram. The slope of the straight line to be drawn through the points is fairly equal to one which would be not possible if we had chosen a different value for Q. This straight line according to the equations stated above must correspond to the relation:

$$\log J_b = \log y + \log \left(e^Z \cdot \sqrt{\frac{\pi}{Z}} \cdot [1 - \Phi(\sqrt{Z})] \cdot \sqrt{1 - 4(a - 4a^2 + 3b)} \right) . \tag{36}$$

It is surprising that the latter term on the right-hand-side of this equation apparently varies only very slightly from day to day for a certain, fixed hour of the day, though y and also J_b are subject to considerable variations. On the other hand, the different straight lines are clearly superimposed so that a definite daily variation for the expression

$$\log e^Z \cdot \sqrt{\frac{\pi}{Z}} \cdot [1 - \Phi(\sqrt{Z})] \cdot \sqrt{1 - 4(a - 4a^2 + 3b)}$$

can be ascertained.

9. *Total Electron Content above the Layer Maximum and of the entire Layer* — As already mentioned eq. (35) provides a possibility of determining the parameter Z not defined accurately hitherto, provided the ratio J_a/J_b can be obtained from observations. Here, we have to stress again the fact that these integrals refer only

to those electrons produced by processes stated in section 1. On the other hand, it is to be feared that observational data yield too large numerical values for both integrals since also electrons will be included which have not entered the layer on account of the assumed single process of ionization. Thus, observational data for the two integrals will only present an upper limit.

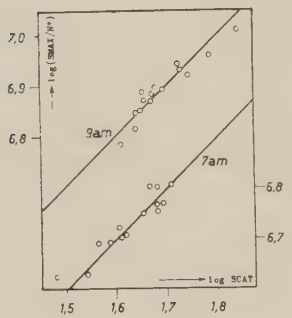

Fig. 7 - log (SHMAX/N^*) *plotted against* log (*SCAT*). Puerto Rico, March 1 to 15, 1960.

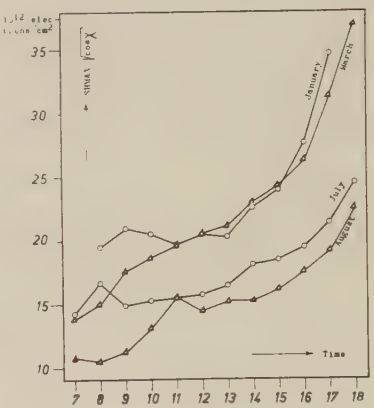

Fig. 8 - *Diurnal variation of* SHMAX / $\sqrt{\cos\chi}$. Puerto Rico, 1960.

According to data in Bauer & Daniels ([13]) about the following is valid in daytime

$$\frac{J_a}{J_b} < 3$$

the minimum being reached at noon and the numerical value increasing at night. By inserting this numerical value in eq. (35) we obtain:

$$\Phi(\sqrt{Z}) < 0.75 \quad \text{and} \quad Z < 0.662 .$$

This implies that at noon the gradient of the scale height in the region of the F-layer-peak cannot be much larger than $+0.16$ at the most.

It would, of course, be very interesting to have a more accurate knowledge for the diurnal variation of Z. We have, however, no possibility of determining it from $N(h)$ profiles. But the diurnal variation of the quantity

$$1 - \Phi(\sqrt{Z})$$

can be computed — with the exception of a factor of proportionality — if we combine the equations (10), (12) and (32) to a product. Hence

$$1 - \Phi(\sqrt{Z}) \propto \frac{J_b \cdot N^*}{\sqrt{\cos\chi}} = \frac{\text{SHMAX}}{\sqrt{\cos\chi}} . \tag{37}$$

In Fig. 8 SHMAX / $\sqrt{\cos\chi}$ has been computed from tables of $N(h)$ profiles for the station Puerto Rico for the months of January, March, July and August

1960 and has been plotted as a function of the time of the day. This representation shows a continuous decrease of the quantity Z from morning to night. Compared with the common diurnal variation of $\cos\chi$ we thus find a considerable asymetry in the diurnal variation of Z obscuring the relation with $\cos\chi$. A somewhat different result is obtained if we compute the averages of morning and afternoon values belonging to about the same position of the sun and then plot them as a function of $\cos\chi$ in a diagram. (See Fig. 9). For the winter months we thus obtain a clear maximum of Z at noon, corresponding to data in DYCE ([14]), for the summer months, however, Z remains almost constant. It is obvious that this result needs considerable extension since at present nothing can be said about a variation of data with the geographical latitude and a possible influence of the variable solar activity.

W. J. Ross ([15]) has recently published observational data obtained from satellites by using the Doppler effect, where also the diurnal variations for the integrals $\int_0^{800} Ndh$ resp. $\int_0^{950} Ndh$ are contained. These two integrals show a marked increase from morning to night, whereas according to relations eq. (10) and (34) derived by me proportionality to $\sqrt{\cos\chi}$ would have to be expected, provided we may replace $\int_0^{800}$ by $\int_0^{\infty}$. According to the equations stated above there must be

$$\int_0^{\infty} Ndh = n_0 \propto \sqrt{\cos\chi}\,. \tag{38}$$

We are indebted to HILL & DYCE ([16]) for observational data on the total electron content of the ionosphere. They have however, been computing their values by the moon-echo method. Unfortunately the data under consideration could be determined only with the exception of a undeterminable initial-value. Thus, a direct comparison with my equations is impossible: it can, however, be conducted

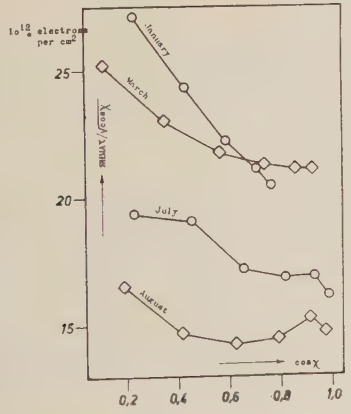

Fig. 9 - *Variation of* $SHMAX / \sqrt{\cos\chi}$ *with* $\cos\chi$. (Averages). Puerto Rico, 1960.

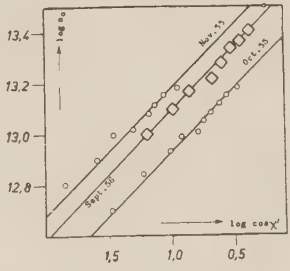

Fig. 10 - *Variation of total electron content* (Moon-echo, EVANS) *with* $\cos\chi'$. Jodrell Bank, 1955 and 1956. (The figures of abscissa to be read with negative sign).

for the moon-echo data (obtained with *two* transmitter frequencies) published by EVANS ([17]). For the three months of October and November, 1955 and September 1956 these n_0-values for the morning hours are at hand which we have been using in examining the validity of eq. (38). In Fig. 10 we have plotted $\log n_0$ as a function of $\log \cos \chi'$, and have obtained in all three cases straight lines the slope of which is given by

$$\frac{\Delta \log n_0}{\Delta \log \cos \chi'} = 1/2 = P .$$

Our equation (38) has thus been fully confirmed by the observational material of EVANS. Since part of the observations by EVANS were made already at sunrise we had to take into account that our formulas had been derived for a flat surface of the earth, although with such a low position of the sun the curvature of the earth's surface must not be neglected. As shown by CHAPMAN ([18]) and later on MALLINGER ([19]) in this case a « virtual » $\cos \chi'$ must take the place of the true $\cos \chi$-values. The relation used by me is shown in Fig. 11.

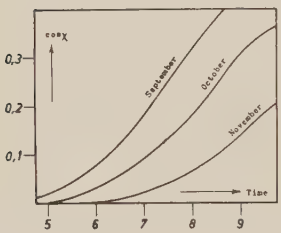

Fig. 11 - *Variation of* $\cos \chi'$ *with morning hours.*

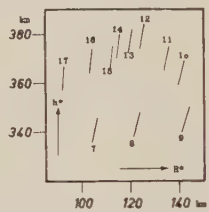

Fig. 12 - H^* *and* $(dH/dh)^*$, Puerto Rico, July 1959.

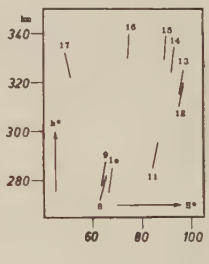

Fig. 13 - H^* *and* $(dH/dh)^*$, Puerto Rico, January 1960.

10. *Diurnal Variation of* H^* *and* $(dH/dh)^*$ — Using the equations stated in the preceding sections the diurnal variation of H^* and $(dH/dh)^*$ can be estimated in the following way: We start from noon observations and assume

$$n_a/n_b = 3$$

(Final results are only changed slightly if according to HILL & DYCE ([16]) we use the numerical value 2.5). Then, as has been shown, from eq. (35) there follows

$$1 - \Phi_{12}(\sqrt{Z}) = 0.25 .$$

For all the other hours of the day we can then assume according to equation (10) and (32)

$$\frac{1 - \Phi_i}{1 - \Phi_{12}} = \frac{\mathrm{SHMAX}_i}{\mathrm{SHMAX}_{12}} \cdot \sqrt{\frac{\cos \chi_{12}}{\cos \chi_i}} . \tag{39}$$

Thus for every hour of the day also Z_i can be determined. Going back to eq. (10)

we can also write

$$\frac{H_i^*}{H^*_{12}} = \frac{N^*_{12}}{N_i^*} \cdot \sqrt{\frac{Z_i \cos \chi_i}{Z_{12} \cos \chi_{12}}} \cdot e^{Z_{12}-Z_i} \,. \tag{40}$$

In using this equation, however, we will have to take into account that it works with the assumption of a constant solar radiation during the day, it can thus be used for monthly averages but must be used for single days with certain restrictions only. Above all we have doubts with regard to its use on days with ionospheric disturbances.

Fig. 12 shows values for July, 1959 (Station Puerto Rico) computed as described above and plotted in a h^*-H^*-diagram. Since, according to eq. (12) from Z also $(dH/dh)^*$ can be determined also these gradients of the scale height have been marked by short lines.

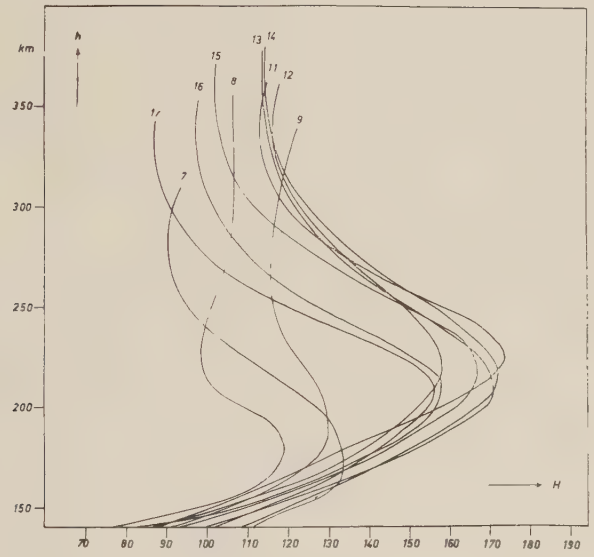

Fig. 14 - *H(h) profiles computed from N(h) profiles*: Puerto Rico, July 1, 1959 (Adapted to the condition $J_a/J_b = 3$ at noon).

In Fig. 13 we are showing by way of completion the H^* and $(dH/dh)^*$ values computed for January, 1960 dependent upon the height h^* where the F-layer-peak was situated. These two diagrams show fairly well the diurnal variations of these quantities.

In Fig. 14 finally all the $H(h)$ profiles for July 1, 1959 have been plotted obtained from the parameters (H^*, Z) determined in this way. Those curves have been adjusted to each other and adapted to the certain value for $J_a/J_b = 3$ (at noon).

11. *Seasonal Variation of* H^* — In order to compute the seasonal variation of H^* only an equation can be considered which does not contain q_0; otherwise

it would be impossible to take variations of S_0 and q_0 due to the variable solar activity into account. As we may easily see eq. (32) meets these postulations and we obtain

$$H^* = F(Z) \cdot \frac{\text{SHMAX}}{N^*} \tag{41}$$

where $F(Z)$ is a function of Z only, which, for the range $Z \approx 0.5$ in question, proves to be almost constant and which can, moreover, be equated to about unit. We thus completely neglect $F(Z)$ in equation (41). If thus the seasonal variations

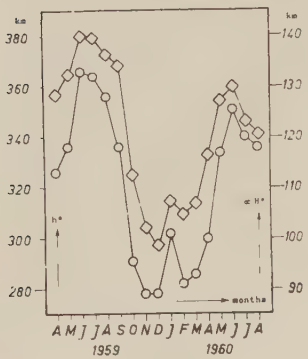

Fig. 15 - *Seasonal Variation of* H^* (o o o) *and* h^*: Puerto Rico.

of H^* (for Puerto Rico, noon values) cannot be determined accurately, we do yet obtain initial informations about these variations. In Fig. 15 the H^*_{12} values (right-hand scale) and the heights h^*_{12} of the layer maximum (left-hand scale) for the months of April, 1959 to August, 1960 have been plotted in two curves. The H^*-maxima are to be found in June, the H^*-minima with an H^* value about 40 km smaller in November-December. The parallel course of H^* and h^* is rather striking; it almost corresponds to a linear relation between H^* and h^*. We must caution, however, against drawing conclusions as to a corresponding gradient of the scale height.

12. *Profiles for Scale Height H and Density* ϱ — K. L. Bowles ([20]) has obtained $N(h)$ profiles reaching up to altitudes of about 700 km by means of the Scatter-Radar-Method. We have been using his data (February 27, 1959, 11 h 35 a.m.) to compute also a $H(h)$ and $\varrho(h)$ profile following the method described above in section 10. The first step in this direction has been determination of the integrals J_a and J_b. Since the $N(h)$ profile is neither reaching down to the height $h = 0$ nor up to $h = \infty$ those integrals had to be extrapolated, thus introducing a factor of uncertainty into the calculation. In order to estimate it at least approximately we have been trying to state an upper and lower limit for J_a and J_b, thus obtaining according to eq. (35) two values for $\Phi(\sqrt{Z})$ resp. Z and similarly two limiting values for H^* from eq. (34). From these initial values two curves for $H = H(h)$ have been computed (Fig. 16) and we may expect the « actual » $H(h)$ profile to be situated somewhere between these two limiting curves. Furthermore, taking into consideration scattering of measurements we seem to be quite justified in assuming that from a height of about 350 km upwards the scale height amounts to constant ≈ 90 km.

The idea is now close at hand to calculate also the density variation with height and to compare this $\rho\,(h)$ profile with observations which were computed from satellite orbits. By using eq. (30) we obtain the quantity $\Phi\,(t)$ and according to eq. (27) from here the pressure ratio p/p^*. Since, however, the absolute pressure p cannot be determined also the density ρ can only be calculated relatively; according to eq. (2) we obtain:

$$\frac{\rho}{\rho^*} = \frac{p}{p^*} \cdot \frac{H^*}{H} \tag{42}$$

where ρ^* is the density at height h^*. Here we have computed only one curve for ρ/ρ^* (corresponding to the $H\,(h)$ profile in Fig. 16 with approximately constant H

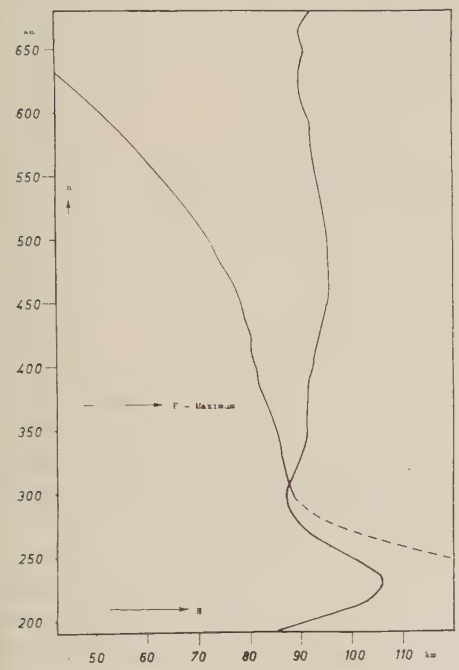

Fig. 16 - *H (h) profile for the whole F-layer*: Long Branch, February 27, 1959, 11h35m a.m.

in the upper layer) and have plotted it in a diagram (Fig. 17) where log ρ/ρ^* resp. log ρ have been used as abscissa and h as ordinate. Moreover, those density profiles have been plotted in the diagrams, which Priester & Martin ([12,21]) have deduced as model 1960 and 1961 from satellite observations. Agreement is fair, especially the slight decrease of density with height in the region about 200 km is clearly noticeable. H. K. Paetzold ([22]) has interpreted this point of inflection in the $\rho\,(h)$ profile as an effect of temperature; Burkard ([23]), on the other hand, by means of $H\,(h)$ profiles described in this paper has been able to prove directly the existence of high temperatures within the region of the $F1$-layer.

13. *$q\,(h)$- and $\alpha\,(h)$-Profiles.* — Those profiles are of interest since they afford a deeper insight into the processes of ionization and electron removal. Due to

the impossibility of determining the pressure absolutely we can also in this case only state the variation of q/q^* and α/α^* with height, where the quantities marked with an asterisk again refer to the height h^*. For the course of the effective recombination coefficient we obtain two curves according as we insert in eq. (11) for $m = 0$ or $= -1$. These results and above all the value to be chosen for m will, however, not be discussed in this place.

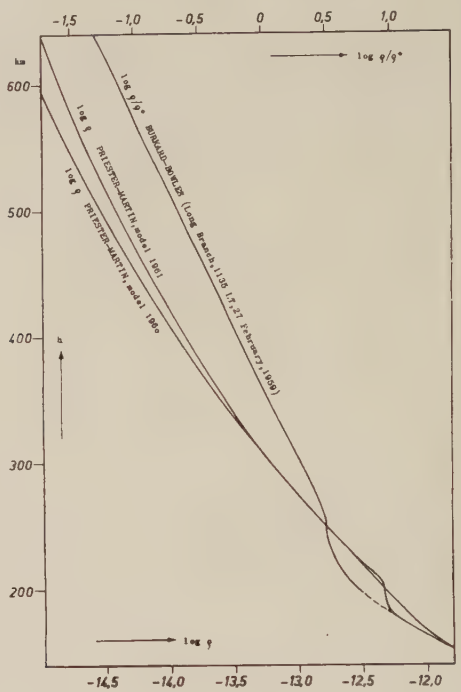

Fig. 17 - *Profiles for Density.*

14. *Conclusion* — The object of the preceding sections has been to prove the effectiveness of our ionospheric model. We are, however, quite aware of the fact that it is by no means perfect as yet. From the statement in eq. (8) we can already see that our model is static and does not take motion processes into account. An extention of our model concepts by adding terms of the form dN/dt in eq. (8) seems, therefore, highly desirable for future studies. On the other hand, we think that diffusion terms might be considered less important in general than terms taking variations of electron concentration with temperature (e.g. dN/dT) into account. Only after having obtained a model concept thus extended it will be possible to investigate the observations made on days with ionospheric disturbances and during solar eclipses.

Intensification of moon-echo observations seems to be highly important; they will, however, yield really valuable material only in those cases where they been conducted with two frequencies. By way of completion simultaneously also Scatter-Radar-observations according to the method of Bowles should be made as well as the usual vertical soundings of the electron distribution up to the *F*-layer-peak.

As far as theoretical studies are concerned, we want to suggest that the temperature dependence of the recombination (attachment) process as stated in this paper should be given special consideration.

The bibliographical references given in this paper are in no way complete since a systematical consideration of relevant literature would have by far surpassed the scope of this paper even if we been limiting ourselves to recent publications only.

Acknowledgements: For the many and extensive calculations I am indebted to: Frau Dr. W. Triebl, Frau Dr. E. Rauscher, Fräulein cand. phil. M. Wenzl, Herrn Dr. H. Repp, Herrn cand. phil. F. Saller.

The research reported here has been made possible through the support and sponsorship of the U.S. Government (European Research Office, Contract PCF 3983 - S).

Symbols

A	absorption constant (cm^2/g)
B	factor of proportionality
$a, b, c, \ldots$	any constants
e	base of natural logarithms
g	gravity
h	height (km)
J_a	$= \int_{h^*}^{\infty} N/N^* \cdot dh$ (km)
J_b	$= \int_{0}^{h^*} N/N^* \cdot dh$ (km)
H	scale height (km)
K_i	coefficients of a power series
L	number of electrons disappearing per ccm and sec
k, m, n	constants
$N = n\,(e)$	electron concentration (cm^{-3})
$n\,(\ )$	particle concentration (cm^{-3})
n_a	$= \int_{h^*}^{\infty} N \cdot dh$ (cm^{-2})
n_b	$= \int_{0}^{h^*} N \cdot dh$ (cm^{-2}) = SHMAX
n_0	$= \int_{0}^{\infty} N \cdot dh$ = SHINF (cm^{-2})
N, N_2	Nitrogen (atomic, molecule)
O, O_2	Oxygen (atomic, molecule)
p	pressure
P	$= (1 - k) / (m + 2)$
q	electron production ($cm^{-3}\ sec^{-1}$)
Q	$= (1 + n) / (m + 2)$
R	specific gas constant (km/degrees Kelvin)
S	radiation energy

ι $= \sqrt{Z \cdot \frac{p}{p^*}}$

T temperature (degrees Kelvin)
x $= h - h^*$
y = SCAT, one half of the half-thickness of a parabolic layer
Z see eq. (12)
α recombination coefficient
ρ density
$\Phi(x)$ $= 2 / \sqrt{\pi} \cdot \mathrm{Erf}(x)$ (error function)
χ angle of incident solar radiation.

REFERENCES

(1) Burkard O.: Arch. Met. Geophys. Biokl., A 2, 308-314, 1950; Geofisica pura e appl., 37, 145-164, 1957; Naturwissenchaften 45, 507, 1958; Geofisica pura e appl., 41, 133-140, 1958. — (2) Yonezawa T.: J. Radio Res. Lab. 7 (30), 69-84, 1960. — (3) Burkard O.: J. Atm. Terr. Phys. 8, 83-90, 1956. — (4) Becker W.: Mitt. Max-Planck-Institut f. Aeronomie, Nr. 4, 1960. — (5) National Bureau of Standards (NBS), Boulder: Ionospheric Data, Part A. — (6) Ratcliffe J. A. & Co.: Phil. Trans. A 248, 621-642, 1956. — (7) Wright J. W.: J. Geoph. Res. 65, 185-191, 1960. — (8) Risbeth H. & Barron D. W.: J. Atm. Terr. Phys. 18, 234-252, 1960. — (9) Hirsh A. J.: J. Atm. Terr. Phys. 17, 86-95, 1959. — (10) Johnson F. S.: J. Geophys. Res. 65, 2571-2575, 1960. — (11) Jahnke-Emde-Lösch: *Tables of Higher Functions.* 6th Edition 1960. — (12) Priester W., Martin H. A. & Kramp K.: Mitt. Univ. Sternwarte Bonn, Nr. 34a, 1960. — (13) Bauer S. J. & Daniels F. B.: J. Geophys. Res. 64, 1371-1376, 1959. — (14) Dyce R. B.: J. Geophys. Res. 65, 2617-2618, 1960. — (15) Ross W. J.: J. Geophys. Res. 65, 2607-2615, 1960. — (16) Hill R. A. & Dyce R. B.: J. Geophys. Res. 65, 173-176, 1960. — (17) Evans J. V.: J. Atm. Terr. Phys. 11, 259-271, 1957. — (18) Chapman S.: Proc. Phys. Soc. 43, 483-501, 1931. — (19) Mallinger F. & Co.: Geofisica pura e appl. 23, 43-59, 1952. — (20) Bowles K. L.: NBS-Report Nr. 6070, 1959. — (21) Priester W. & Martin H. A.: Mitt. Univ. Sternwarte Bonn (18.II.1960). — (22) Paetzold H. K.: Naturwissenschaften 48, 39-40, 1961. — (23) Burkard O.: Nature 189, 474, 1961.

(*Received* 31 *March* 1961)

AN ANNUAL AND A SEMIANNUAL VARIATION OF THE UPPER AIR DENSITY

by H. K. Paetzold & H. Zschörner (*)

Summary — The fluctuation of the acceleration are analysed for several satellites. For the density variations three predominant influences can be distinguished: 1) The varying solar short ultra-violet radiation; 2) The day-night-effect; 3) An annual variation. The latter suggests a significant interaction of the terrestrial upper atmosphere with the interplanetary matter. The annual variation gives some evidence for an interstellar wind due to the solar motion in the local stellar system.

It is well known that the acceleration of artificial satellites shows significant variations (King-Hele 1958, H. K. Paetzold 1958a, L. G. Jacchia 1958) from which large fluctuations of the upper air density could be derived. Meanwhile several influences could be distinguished. The most clear of them is the effect of the solar activity (short ultra-violet radiation) which is demonstrated by a narrow correlation of the monthly fluctuations to the sun spot number (Paetzold 1958b), and to the solar radio emission in the 20 cm- (Priester 1959a) and the 10 cm-region (Jacchia 1959a). Further, a pronounced day-night-effect exists which amplitude strongly increases with height (Jacchia 1959b). At least an influence of stronger solar corpuscle clouds can be distinguished by the observed enhancement of the acceleration of $1958\delta_1$ (Jacchia 1959c), and $1958\delta_2$ (Paetzold 1960a). Latitude and season seem to be of minor influence.

While the solar short wave effect can be well determined by its strong correlation to the sun spot number or the solar radioemission in the dm-region it is much more difficult to analyse accurately the day-night-effect. For the day-night-period of the perigee amounts at least to several months for the present satellites. If further effects exist with a similar time-scale, they will be mixed with the day-night-variation. The erratic enhancement of the accelerations of 1958α and $1958\beta_2$ from August to November 1958 gave some evidence for such an additional effect (Paetzold 1959b). It can be only distinguished by the analysis of several satellites which day-night-cycles differ in phase and period.

After the analysis of the observations the day-night-variation may be given

---

(*) Technische Hochschule, *München.*

by the equation:

$$\text{(1)} \qquad \text{Log} \frac{\rho(\theta)_{Max}}{\rho(\theta)} = \theta(h) f(\theta)$$

$\rho(\theta)_{max}$ means the daily maximal density which occurs at about 14.00 h local time after the observations.

The latitude term $A(h)$ seems to be a linear function of h below 700 km:

$$\text{(2)} \qquad \theta(h) = 0.002 \cdot h - 0.45 \qquad (h \text{ in km})$$

If the observations would agree to the equation (1) two conditions must be fulfilled:

1) For *one* satellite the same air density should be found for the same local time θ, if the solar wave effect and the corpuscle effect have been eliminated.

2) For *several* satellites the function $f(\theta)$ should be nearly identical at altitudes between 300 and about 800 km, because in this region the heat loss is very

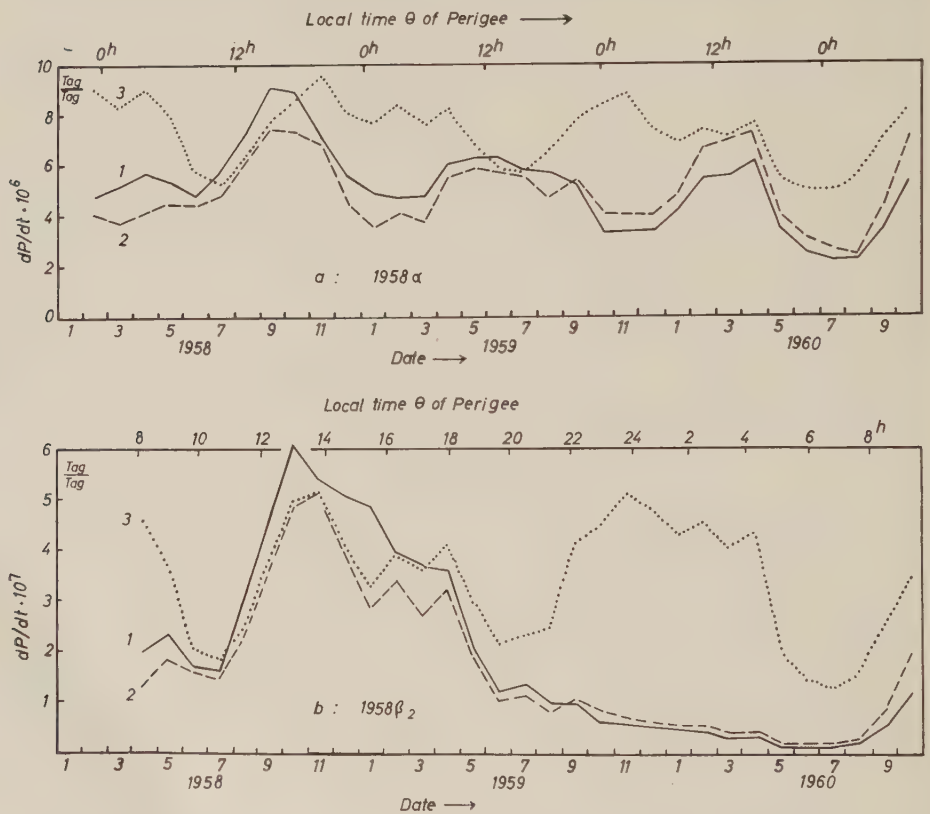

Fig. 1 - *Monthly means of the acceleration of Explorer I and Vanguard I.*
1: *Observed acceleration,*
2: *Normalized acceleration,*
3: *The residual annual effect.*

quick caused by molecular heat conduction, and the diurnal variation of the molecular weight of the air will be still small.

In Fig. 1 the monthly mean of the accelerations are given for 1958α and 1958β_2. It can be well seen that the acceleration of 1958α shows a clear additional influence besides the day-night-variations, because the for the solar activity normalized curve 2 does not agree at all with the condition 1 above. If the observed accelerations of the different satellites are normalized for the solar activity *and* for the day-night-effect by equ. (1) a horizontal strait line should result. Instead of it a further residual effect must be distinguished according curve 3 in Fig. 1.

This effect is also shown by other satellites. The acceleration of 1958β_1 e.g. decreased by the factor 4 from April 1960 to June 1960 while the local time θ of the perigee changes only slowly from 23.30 to 24.30 h so that the influence of the

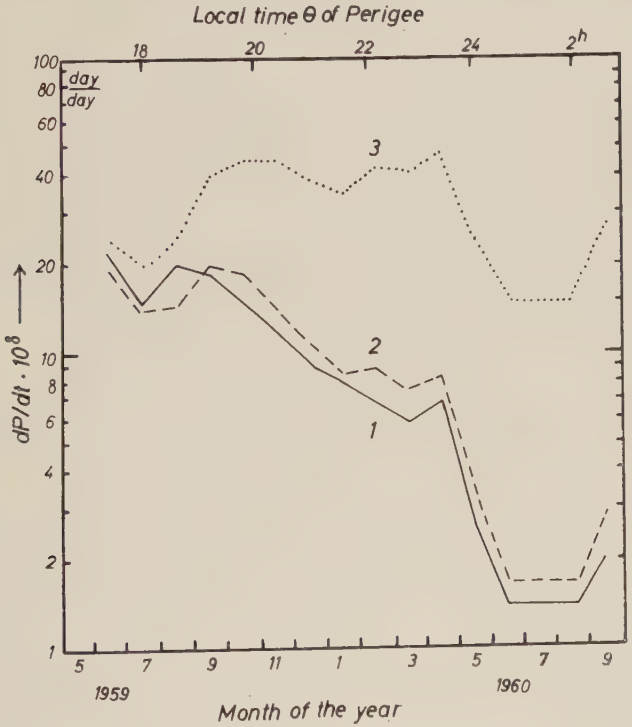

Fig. 2 - *Acceleration of* 1958 β_1. Explanation as in Fig. 1.

daily hour was small (Fig. 2). This residual effect is similar for ten satellites which has been analysed as Fig. 3 demonstrates for some examples. It must be pointed out that equ. (1) and (2) is the only used assumption for Fig. 1, 2, and 3. In Fig. 4 the day-night-function $f(\theta)$ is given, as it has been found identically for the different satellites. In Fig. 3 it is striking that the same residual effect is found for several satellites, which day-night-cycles strongly differs in period or phase. This agreement proves the two assumptions:

a) The day-night-function is valid as given in equ. (1) and (2),

b) The residual effect is real and significant.

An annual period seems to be evident with a narrow minimum from May to August, and a broad maximum during the rest of the year with a secondary minimum around January (Paetzold 1960b). The evidence of such an annual effect has been recently strengthened by independent whistler observations from which an extreme similar annual variation follows of the exospheric electron density (Helliwell 1960). Further, it is well known that the seasonal amplitude of the electron density in the F_2-layer is much more pronounced in the Northern hemisphere than in the Southern. For the explanation an unknown annual effect was suggested with a minimum in the middle fo the year in excellent agreement with our new result (Berkner & Wells 1938).

Densities were obtained by the numerical solution of the equ. (3):

$$\frac{dP}{dn} = -(1 + 2e)\ P\ \frac{F}{M} \oint \rho\,(h)\ ds \tag{3}$$

F : mean cross section, M : mass of satellite, e : excentricity of the orbit, P : revolution time.

In schedule 1 the density amplitudes are given caused by the different effects.

The last column gives a standard density for a flux of $220 \cdot 10^{-22}$ W/m^2 Hz of the solar 10 cm radiation, and for the maxima of the diurnal and annual effect. This value nearly represents the upper possible density of the upper atmosphere.

The altitude dependency of the amplitude of the annual effect markedly differs from that of the other influence (Schedule 1).

Schedule 1 - *Density variations.*

Height km	Solar effect $\rho\,(220) / \rho\,(100)$	Day-night ρ_{Max}/ρ_{Min}	Annual effect ρ_{Max} / ρ_{Min}	ρ_{stand} g/cm^{-3}
200	1.6	1.07	1.3	$4.3 \cdot 10^{-13}$
250	2.9	1.07	1.4	$1.6 \cdot 10^{-13}$
300	3.0	1.4	1.5	$5.9 \cdot 10^{-11}$
500	3.7	3.4	2.2	$4.7 \cdot 10^{-11}$
700	4.3	8.6	3.0	$7.1 \cdot 10^{-11}$

($\rho\,(220)$ means the air density normalized for a solar 10 cm-radio intensity of $220 \cdot 10^{-22}$ W/m^2 Hz).

No correlations of this effect seems to exist to the solar activity (Fig. 3). In the year 1958 the strange behaviour of the Berlin-Adlershof observations of the solar 20 cm emission seems to show the same long time shift as the annual effect. Therefore it has been suggested that the solar 20 cm emission is the most representative solar indicator for the variations of the upper air density (Priester & Martin 1960a). But in the following time the solar 20 cm emission didn't show anymore such long time shifts while the annual effect above existed in full

strength (*). It should be also mentioned that the radio observations between 3 cm and 30 cm of other stations, and also the 15 cm emission observed in Berlin don't show this strong long time shift during the year 1958. Further, the monthly

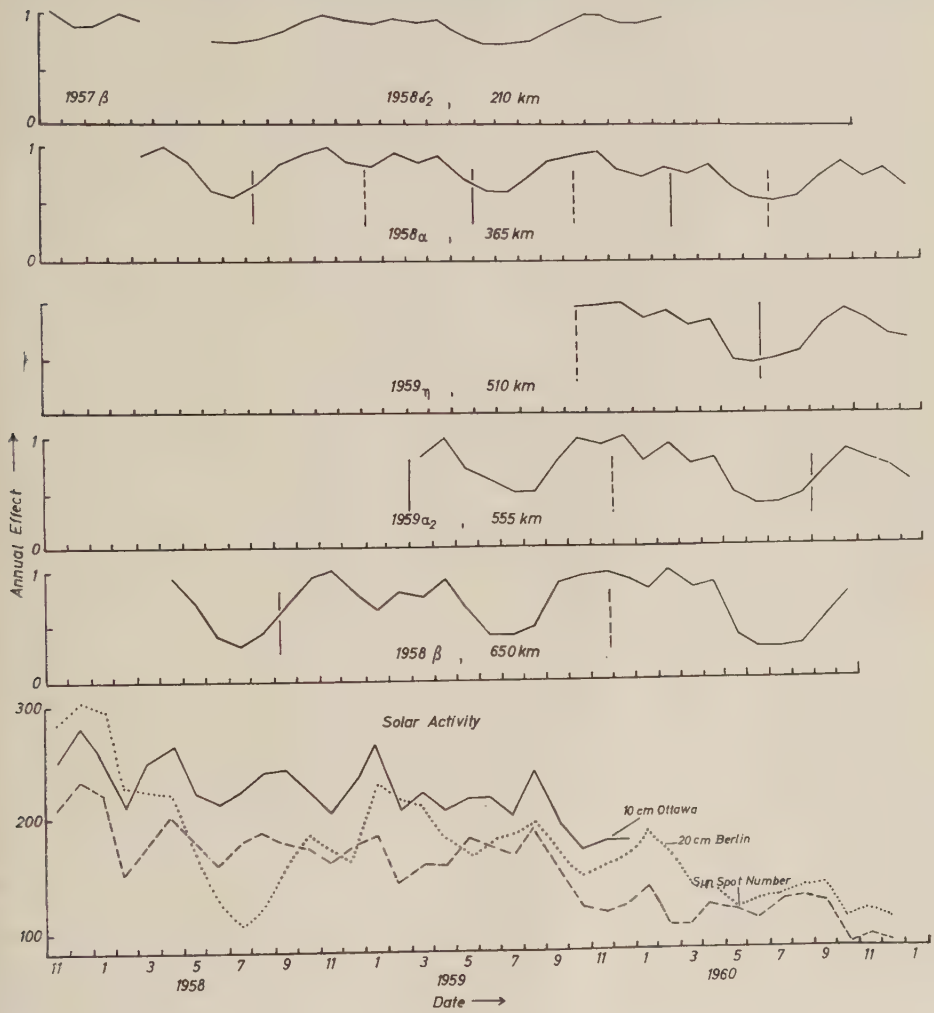

Fig. 3 - *Annual effect and solar activity.*

fluctuations of the satellites acceleration seem to show no better correlation to the solar 20 cm- than to the 10 cm-emission. So we have to conclude that no special correlation exists to the variations of the upper air density and the long time shift of the Berlin 20 cm-observation during 1958. It must be further mentioned

(*) Also from May to August 1960 no further deep minimum of the Berlin 20 cm radiation occured (Private communication from Dr. HACHENBERG, Berlin-Adlershof).

that all detailed analyses are affected by serious errors if this strong annual effect is ignored. This especially concernes to the relationship between density variation and the solar dm-radiation (PRIESTER & MARTIN, 1960a), and the accurate function of the day-night-effect (JACCHIA 1960; KING-HELE 1960).

If this annual effect of the air density is explained by a variable heating of the upper atmosphere an additional heat source must be assumed. Its annual fluctuation must amount to at least 0.1 erg/cm^2 sec, far too large to be explained by the annual variation of solar UV radiation due to the excentricity of the earths orbit. By this effect the air density of the upper atmosphere can only vary by about 5%. Therefore the most reasonable assumption is an interaction between the upper terrestrial atmosphere and the interplanetary matter.

If the density of the interplanetary plasma has a value of about 100 Proton/cm^3 and a relativ velocity to the earth of $3 \cdot 10^6$ cm/sec a sufficient energy influx seems to be possible. The special mechanism is not quite clear. The altitude dependency of the annual effect fits as well to the dissipation of hydromagnetic wave in the ionosphere originating from the outer boundary of the exosphere (A. J. DESSLER 1959) as to a heat influx from the outer part of the solar corona (S. CHAPMAN 1957). Hydromagnetic waves have been observed recently with a period of about 0.1 sec and an amplitude of 30 Γ at a distance of about 10 earth radii. This intensity would be sufficient. If the idea is valid that the interplanetary plasma contributes to the heating of the upper atmosphere the density of the plasma must systematically vary along the earth's orbit to explain the annual effect. With the assumption that this fluctuation is caused by the excentricity of the earth's orbit a very steep gradient of interplanetary plasma would follow in the vicinity of the earth's orbit which is hard to explain. For the density would vary by 50% for a difference of only 6 million km of the distance from the sun. But it should be mentioned that the minimum of the annual effect occurs when the earth moves on the foreside of the sun relative to its peculiar motion in the local stellar system. So the most simple explanation would be the assumption of an interplanetary wind. Its drag would shift the interplanetary plasma cloud somewhat excentric to the sun. A density of 0.5 Proton/cm^3 of the interstellar matter would be sufficient to explain this effect if a mean value of several Γ is assumed for the interplanetary magnetic field, as it has been recently measured with the Pioneer V space probe. In the proposed picture the *interstellar* wind would not directly produce the necessary heat influx but it would modulate the heating effect of the *interplanetary* plasma caused by its motion relative to the earth.

Another possibility is the interaction with the interplanetary dust. It is well known that the density of the ecliptical meteor streams markedly varies along the earth orbit. The intensity of HOFFMEISTERS Leuchtstreifen (*) seems to have the same annual variation as our annual effect if the satellites drag. But since the observations have been made at one place it is not clear whether this variation is seasonal or real annual. Unfortunately only crude estimations exist for the density of the interplanetary matter between the range from 10^{-21} to 10^{-23} g/cm^3. This values seem far too low to explain the amplitude of the annual effect. Even a density of 10^{-20} g/cm^3 produces an energy influx of only 0.003 erg/cm^2 sec. But there there may be also an increase of matter density in the upper atmosphere due to

(*) This phenomena has been explained by the influx of interplanetary dust.

the accumulation of the incoming dust. If we assume again a value of 10^{-20} g/cm^3 for the interplanetary dust, and a storage time of about 50 days a mean dust density of $5 \cdot 10^{-16}$ g/cm^3 would result in the region between 200 and 800 km height. This magnitude would be sufficient only for altitudes above 600 km. Greater storage times seem to be unreasonable because they would too strongly smooth the annual variation of the air density. Therefore the influence of the interplanetary dust seems to be much less probably than that of the plasma. But minor irregularities in Fig. 3 may be caused by the dust-effect.

The secondary minimum around January in Fig. 3 suggests that there must be superposed a semi-annual effect to the annual. Fig. 5 shows the harmonic analysis for the mean yearly variation from November 1957 to July 1960. Two harmonics fit well to the observations with periods of one year and a half year and

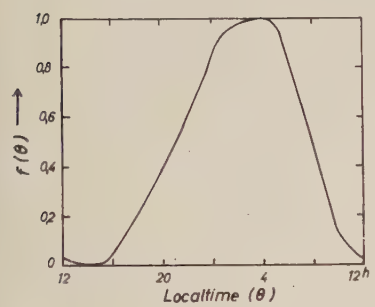

Fig. 4 - *The day-night function f* (θ).

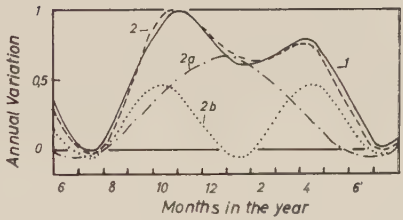

Fig. 5 - *Harmonic analysis of the annual variation.*

an amplitude ratio of 3 : 2. The maxima of the semi-annual effect are placed at about the 10th April and the 10th October. Such a world-wide semi-annual variation is already known from the magnetic activity (Bartels 1932) and recently, also from the *E*-layer (Minnis & Bazzard 1960). It depends perhaps on the location of the earth relative to the solar equatorial plane. This suggests an anisotropy of the interplanetary plasma to this plane due to the fact that solar matter will be more strongly ejected in the higher solar latitudes of the sun spot belts.

Long time variations of the amplitude of the annual and the semi-annual effect will be of extreme interest. The last observations till February 1961 show a considerable value of the relative amplitude and the absolute value of the plasma effect. From this it must be concluded that the density of the interplanetary plasma will considerably vary in the solar cycle. It is further worth to look for a correlation between the variations of the plasma effect and that of the extension and the intensity of the van Allen Belt.

Independently which explanation will be found valid the annual effect proves the existence for a further significant heat source of the upper atmosphere besides the solar short ultraviolet radiation. On the other side the influence of the interplanetary dust has to be carefully considerated. If it would be greater than supposed it would severly affect all determinations of the upper air temperature from vertical density distributions derived from satellite's acceleration.

REFERENCES

J. Bartels, 1932, Terr. Magn. 37, 24. — S. Chapman, 1957: *The Threshold of Space*, p. 65, London. — A. J. Dessler, 1959: J. Geophys. Res. 64, 397. — L. V. Berkner & H. W. Wells, 1938, Terr. Magn. 43, 13. — R. A. Helliwell, 1960: Aeronomie Symp. Copenhagen 1960. — L. G. Jacchia, 1958: IGY Satellite Rep. Nr. 4, 23. — L. G. Jacchia, 1959a: Nature 183, 327. — L. G. Jacchia, 1959b: Smiths. Astroph. Obs. Sp. Rep. Nr. 29. — L. G. Jacchia, 1959c: Nature 183, 1662. — L. G. Jacchia, 1960: Smiths. Astroph. Obs. Sp. Rep. Nr. 39. — D. G. King-Hele, 1958: Nature 181, 182. — D. G. King-Hele, 1960: Aeronomie Symp. Copenhagen 1960. — C. M. Minnis & G. H. Bazzard, 1960: J. Atmosph. Terr. Phys. 18, 306. — H. K. Paetzold, 1958a: Naturwissensch. 45, 485. — K. H. Paetzold & H. Zschörner, 1958b: Tagungsbuch Dtsch. Phys. Gesellsch. Essen 1958, 152. — H. K. Paetzold & H. Zschörner, 1959a: J. Atmosph. a. Terr. Phys. 16, 259. — H. K. Paetzold & H. Zschörner, 1959b: Proc. II. Int. Astronaut. Congress London 1959, 53. — H. K. Paetzold, 1960a: XII. Int. IUGG Ass. Helsinki 1960. — H. K. Paetzold, 1960b: Proc. I. Cospar Symp. Nice 1960, 24. — W. Priester, 1959a: Naturwiss. 46 197. — W. Priester & H. A. Martin, 1960a: Mitt. Univ. Sternw. Bonn Nr. 29. — W. Priester, H. A. Martin & H. Kramp, 1960b: Mitt. Univ. Sternw. Bonn Nr. 34.

(*Received* 10*th February* 1961)

EFFETS DE L'ACTIVITÉ SOLAIRE SUR L'OZONE ATMOSPHÉRIQUE ET LA HAUTEUR DE LA TROPOPAUSE

par S. I. Rasool (*)

Summary — A statistical study of experimental data concerning total ozone thicknesses and tropopause heights in several stations in Europe, Asia and Africa brings to the following preliminary results: 1) The height of the tropopause increases when the sunspot number increases, the increase being greater when the latitude is lower. The maximum of both effects seems to take place at the magnetic equator and not at the geographic equator; 2) Magnetic storms are in numerous cases connected with variations of ozone thickness; the thickness first decreases then increases before the storm; the ozone minimum is observed 24 or 36 hours before the maximum of magnetic activity. A two years study shows a similar variation for both phenomena.

La recherche de relations entre les phénomènes observés sur le soleil et ceux qui se produisent dans l'atmosphère terrestre a subi un brusque regain d'activité pendant ces dernières années. En ce qui concerne la haute atmosphère, il semble être bien établi que les phénomènes qui s'y produisent — aurores boréales — perturbations ionosphériques et géomagnétiques, etc. — sont directement liés aux brusques variations de l'activité solaire. Ces hypothèses ont été récemment confirmées et élargies par les observations effectuées à bord des fusées et des satellites mais il reste encore à préciser si ces éruptions solaires, électromagnétiques et corpusculaires, franchissent l'ionosphère et ont des répercussions dans la stratosphère et la troposphère.

De nombreuses études on été consacrées dernièrement à ce problème, parmi lesquelles on peut signaler les importants travaux de R. Shapiro ([1,2,3]) et de J. London ([4,5]) en Amérique et de Asakura & Katayama au Japon ([6]). Les conclusions tirées par ces auteurs sont diverses et quelquefois même opposées. Shapiro, par exemple, en analysant des données des Etats-Unis de 45 ans, trouve que 14 jours après un maximum d'activité magnétique (*Kp*), il y a abaissement notable de « l'indice de persistance », nombre qui indique dans quelle mesure se conservent des distributions de pression au sol.

Faisant les mêmes calculs pour les données provenant d'Europe, une telle corrélation n'a pas été trouvée ([3]). J. London ([5]), d'autre part, ne trouve aucune

(*) Laboratoire de Physique de l'Atmosphère, Faculté des Sciences de l'Université de *Paris*.

corrélation entre les orages magnétiques et les variations de l'altitude de la surface de 100 mb au-dessus des Etats-Unis. Au Japon, par contre, ASAKURA & KATAYAMA [6] ont démontré qu'environ 10 jours après un orage magnétique, l'indice A, qui est lié à la circulation méridionale à 500 mb et pour le cercle latitudinal de 50° N, présente une nette augmentation indiquant ainsi un important échange de l'énergie thermique entre les hautes et les basses latitudes.

MACDONALD & ROBERTS [7], d'autre part, viennent de constater que lorsque la Terre est bombardée par les intenses émissions corpusculaires en provenance du Soleil, les « talwegs » dans la circulation atmosphérique à 300 mb sont considérablement amplifiés. Ce phénomène est très fréquent surtout dans la région du Golfe d'Alaska.

Tout récemment, STRANZ [8] a signalé que la hauteur de la tropopause à Léopoldville (04° 04 S, 15° 00 E), croît en même temps que l'activité solaire (nombre de Wolf) pour les années 1955 à 1958.

Divers auteurs [9,10,11] ont également cherché une corrélation entre l'activité solaire ou magnétique et l'épaisseur réduite de l'ozone atmosphérique, mais ils n'ont pu apporter de résultat concluant. La plupart de ces études étaient relatives à des stations de latitude moyenne pour lesquelles les variations d'origine météorologique de l'ozone sont d'une telle importance qu'elles peuvent masquer l'influence d'autres phénomènes à variation rapide.

Pour la première fois, l'Année Géophysique Internationale a permis de disposer de nombreuses mesures d'ozone et de hauteur de la tropopause pour un réseau de stations mondiales assez serré, pendant une période d'activité solaire maximum et d'activité magnétique intense.

Nous avons donc fait une première étude en analysant les résultats de ces dernières années concernant la hauteur de la tropopause et l'épaisseur réduite d'ozone pour diverses stations d'Europe, d'Afrique, des Indes et du Japon, afin de chercher des relations avec certains phénomènes extraterrestres.

Tropopause — D'abord en partant des résultants obtenus par STRANZ [8], nous avons voulu voir si la hauteur de la tropopause augmente avec l'activité solaire aux stations de latitude différente de celle de Léopoldville et pour cela nous avons choisi une série de stations dont les longitudes ne soient pas trop différentes:

Trappes	(48° 46 N, 02° 02′ E)
Alger	(36° 48 N, 03° 00 E)
Colomb-Béchar	(31° 36 N, 02° 13 W)
Dakar	(14° 40 N, 17° 26 W)
Bangui	(04° 22 N, 18° 34 E)
Léopoldville	(04° 04 S, 15° 00 E)

Afin d'avoir des données suffisamment homogènes, nous avons dû les ramener aux mêmes valeurs; ainsi la hauteur de la tropopause est exprimée en mètres géopotentiels; la période d'observation s'étend de 1954 à 1958. Toutes les données (hauteur de tropopause et nombre de Wolf) ont été exprimées en moyennes mensuelles, puis on a effectué les moyennes glissantes sur 13 mois afin d'éliminer les fluctuations et aussi, au moins partiellement, la variation saisonnière de la hauteur de la tropopause. La variation du nombre de taches passe ainsi de 4 en 1954 à 190 à la fin de 1957, époque du maximum.

En portant en abscisses le nombre de Wolf et en ordonnées la hauteur de la tropopause pour une station, la variation de la hauteur de la tropopause se place assez bien sur une droite de pente positive (Fig. 1).

Bien entendu les hauteurs sont d'autant plus élevées que la latitude est plus basse, fait connu depuis longtemps. Mais on constate aussi que la variation relative avec le nombre de taches est d'autant plus grande que la latitude est plus basse.

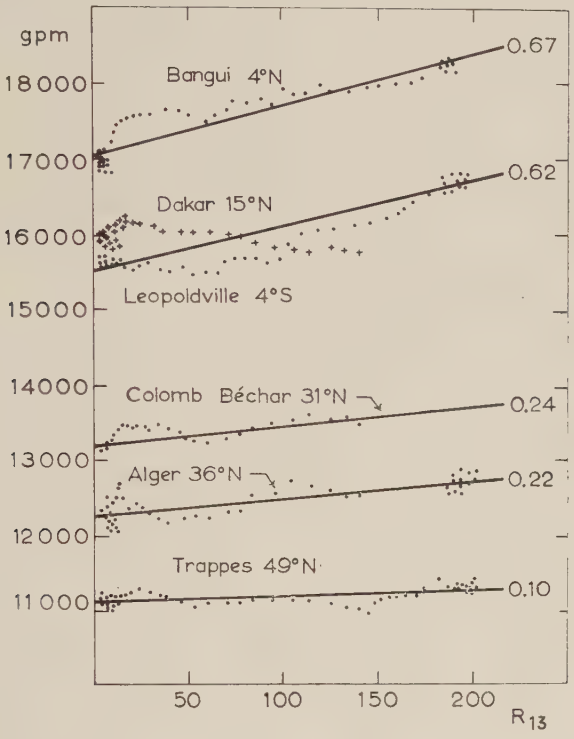

Fig. 1 - *Variation de la hauteur de la tropopause avec le nombre de taches.*

Ainsi à Trappes, il n'y a à peu près pas de variations; à Alger, la pente de la droite est faible: 0.22; à Colomb-Béchar: 0.24; à Bangui: 0.67; à Léopoldville: 0.62. Seul Dakar fait exception; on ne constate pas de variation, mais les données sont incomplètes (seulement jusqu'en 1956).

Mais en regardant les choses de plus près, nous voyons que ce n'est pas l'équateur géographique qui marque le maximum de la variation. En effet, la hauteur à Bangui est nettement plus élevée qu'à Léopoldville et les 2 stations sont à 4° N et S de l'équateur; et la pente à Bangui est plus forte qu'à Léopoldville. La hauteur moyenne à Léopoldville est la même qu'à Dakar (15° N). Or, sur le méridien de Bangui et de Léopoldville, l'équateur magnétique se trouve à 10° N environ.

Nous avons ensuite essayé de chercher par le test de Chree ([11]), le décalage en jours entre l'activité magnétique et ses répercussions éventuelles au niveau de la tropopause. Sur une période de deux ans (1957-1958), nous avons choisi les jours

de très forte activité magnétique ($C \geq 6$) pour lesquels les valeurs de la hauteur de tropopause ont été relevées. Dans chaque cas, nous avons également noté les hauteurs de tropopause pour le jour qui précède et les 12 jours qui suivent. En appelant chacun de ces jours actifs n_1, n_2, n_3 ..... n_r, nous avons fait un tableau des hauteurs de tropopause comme ci-dessous:

$$
\begin{array}{llllll}
t(n_1-1) \ldots t(n_1) \ldots t(n_1+1) \ldots t(n_1+2) \ldots\ldots t(n_1+j) \ldots\ldots t(n_1+s) \\
t(n_2-1) \quad t(n_2) \quad t(n_2+1) \quad t(n_2+2) \ldots\ldots t(n_2+j) \ldots\ldots t(n_2+s) \\
\vdots \quad \vdots \quad \vdots \quad \vdots \quad \vdots \quad \vdots \\
t(n_r-1) \quad t(n_r) \quad t(n_r+1) \quad t(n_r+2) \ldots\ldots t(n_r+j) \ldots\ldots t(n_r+s)
\end{array}
$$

Les moyennes de chaque colonne sont portées sur un graphique en fonction des jours $(n-1)$, n, $(n+1)$, ..., $(n+s)$. (Fig. 2). Le même travail a été fait pour les jours calmes et les valeurs ainsi obtenues sont aussi portées sur la Fig. 2.

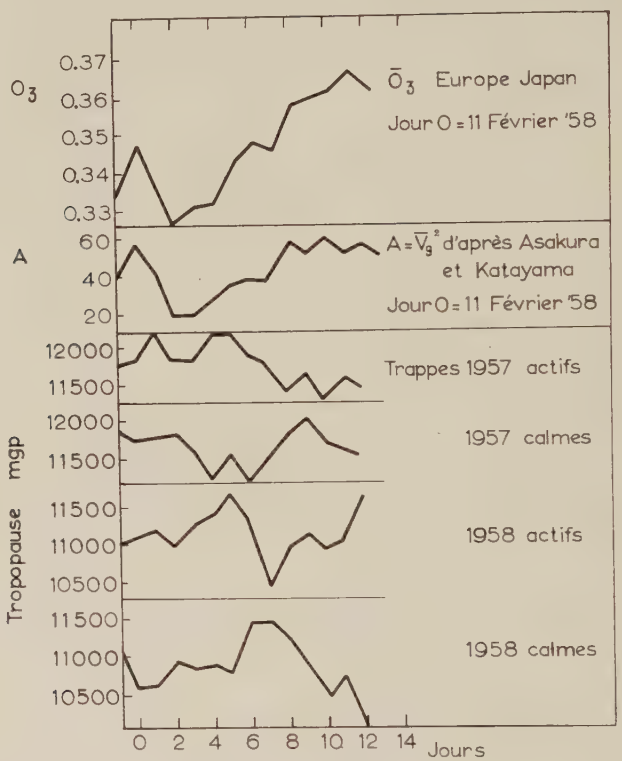

Fig. 2 - *Test de* CHREE.

Sur le même graphique est reproduite la courbe donnée par ASAKURA & KATAYAMA [6] qui montre la variation de l'indice A en fonction des jours après une forte activité magnétique.

A est la valeur moyenne de Vg^2 ($\overline{Vg}$ = flux géostrophique méridional) pour

le cercle latitudinal de 50° N et à 500 mb.

$$A = \frac{g^2}{2f^2R^2\cos^2\theta} \sum_{n=1}^{5} n^2 A_n^2$$

où R: rayon de la terre
θ: latitude: 50° N
f: paramètre de Coriolis
g: accélération de la pesanteur
A_n: amplitude de l'harmonique suivant l'équation:

$$Z = A_0 + \sum_{n=1}^{5} A_n \cos(n\lambda + \delta_n)$$

où Z est la hauteur moyenne de 500 mb sur 5 jours et
λ la longitude.

Cet indice A montre un maximum environ 10 jours après une manifestation d'activité magnétique, tandis que pour nos observations de Trappes, il y a une baisse de la tropopause 7 à 8 jours après cette manifestation.

Une augmentation de l'indice A signifie un fort échange de chaleur entre les hautes et les basses latitudes à 500 mb. Or, la baisse de la hauteur de tropopause pour les mêmes latitudes, en général, correspond à un flux de masses d'air polaire vers les basses latitudes, accompagné d'une augmentation d'ozone. Pour Paris, et sur une période de deux ans, nous avons noté qu'en moyenne une diminution en valeur d'ozone de l'ordre de 0.03 cm correspond à une augmentation de la hauteur de tropopause d'environ 1000 m et vice versa. Nous avons donc porté sur le même graphique les valeurs moyennes d'ozone mesurées en 10 stations d'Europe, et du Japon pour la période de 14 jours suivant l'intense orage magnétique du 11 février 1958. La courbe d'ozone a une allure semblable à celle de l'indice A et opposée à celle de la tropopause, ce qui confirmerait la conclusion de Asakura & Katayama, qu'environ dix jours après une forte activité magnétique, la circulation atmosphérique à 500 mb devient principalement méridionale.

Ozone — Des mesures simultanées de l'ozone atmosphérique et de l'activité magnétique ont été effectuées régulièrement en plusieurs stations pendant l'Année Géophysique Internationale. Nous en avons comparé les résultats pour diverses stations réparties à des latitudes différentes.

Ainsi, examinons d'abord le cas de Tamanrasset (22° 47 N, 05° 31 E). L'épaisseur réduite de l'ozone atmosphérique a été mesurée régulièrement avec un appareil Dobson 3 fois par jour. Nous comparons les moyennes journalières d'ozone pour les mois de mars, avril et mai 1959 et les valeurs du caractère magnétique « C » relevées sur les enregistrements continus du champ magnétique terrestre effectués à la même station pendant la même période (Fig. 3). On remarque quatre cas d'orages magnétiques forts ($C = 6$ ou 7, échelle française). A chaque orage correspond une augmentation d'ozone de l'ordre de 0.02 cm qui fait suite à une baisse lente; le minimum d'ozone précède de 24 ou 36 heures le maximum d'activité magnétique. Les dates de ces orages sont: 28 mars, 10 avril, 8 mai et 12 mai. Un autre orage a eu lieu le 23 avril, mais il n'y a pas d'observations d'ozone du 22 au 26 avril.

Examinons aussi le cas du violent orage magnétique du 11 février 1958 qui présente un début brusque à 01 h 25 T.U. enregistré à Chambon la Forêt avec une amplitude de 450 gammas sur H, 200 gammas sur Z et plus d'un degré sur D. A Alibag (Bombay) et à Kakioka (Japon) l'intensité de cet orage était aussi très grande. Nous avons examiné les valeurs d'ozone mesurées aux Indes, au Japon

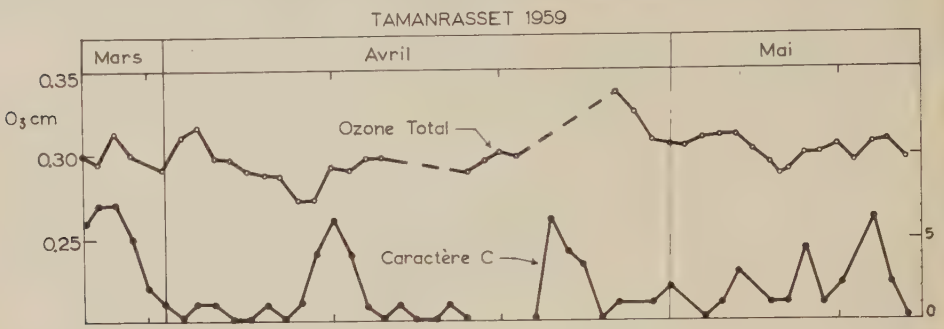

Fig. 3 - *Moyennes journalières d'ozone et caractère magnétique «C».*

et en Europe (Fig. 4) pendant la semaine entourant cette date. On observe un maximum d'ozone au Mont Abu, à Delhi, à Torishima et à Tateno le 10 février et à Srinagar, Sapporo, Rome, Paris et Oxford le 11 février. Tous ces maximums d'ozone sont précédés de minimums très nets 1 ou 2 jours auparavant. Le cas du 11 février 1958 est donc analogue à nos observations de Tamanrasset, mais l'étendue géographique du phénomène est considérable.

Nous avons aussi porté sur un graphique, les écarts entre les moyennes mensuelles des valeurs d'ozone mesurées à Paris, Oxford, Arosa en 1957 et 1958 et leurs moyennes mensuelles sur cinq ans (Fig. 5). Sur le même graphique étaient portées les sommes mensuelles du caractère « C » de l'activité magnétique enregistrée à Chambon la Forêt pour la même période. Les deux courbes ont une allure très semblable, semblant indiquer une relation directe entre l'activité magnétique terrestre et l'épaisseur réduite de l'ozone atmosphérique: maximum principal pour le mois de mars 1958, maximum secondaire en juin, septembre et novembre 1957, juin et octobre 1958 ([13]).

Bien entendu, la période d'observation est trop courte pour que la statistique puisse nous permettre de trouver un coefficient de corrélation. Nous pensons cependant que toutes les observations que nous venons de résumer sont l'indication d'une relation entre l'activité magnétique et l'ozone atmosphérique.

Calcul statistique — Les premiers calculs statistiques ont été faits pour examiner si les variations journalières d'ozone et de la tropopause sont dues au hasard, ou si l'on peut déceler dans leur répartition une certaine organisation comme la périodicité de 27 jours pour les taches solaires et l'activité magnétique.

Nous avons d'abord calculé les probabilités des maximums et des minimums par la formule du test KV ([14]).

$$Pc = \sum_{i=1}^{n} \alpha_i \left(\sum_{j=0}^{i-1} p_j \right)$$

où

$$\alpha_i = \frac{p_i}{1 - p_i}$$

et ensuite nous avons déterminé, pour les divers éléments, les limites des intervalles de confiance de 95% (τ_{max} et τ_{min}) à partir des valeurs moyennes théoriques.

Pour les mêmes éléments nous avons ensuite calculé les valeurs de τ d'après les observations. Le tableau I ci-dessous résume les résultats.

TAB. I: *Limites des intervalles de confiance.*

	Théorique		Expérimentale
	τ_{max}	τ_{min}	τ_{obs}
Taches solaires (1958)	0.3682	0.2592	0.181
Activité magnétique (Chambon-la-Forêt) (1958)	0.3309	0.2365	0.212
Ozone (Paris) (1958)	0.3260	0.2438	0.248
Tropopause (Trappes) (1958)	0.3585	0.2585	0.298
Tropopause (Tamanrasset) (1958) .	0.3492	0.2562	0.285

On voit que les séries des taches solaires et de l'activité magnétique présentent une organisation rigoureuse, celle de l'ozone une faible organisation, tandis que celle de la tropopause est due au hasard (la série de Tamanrasset est un peu plus organisée que celle de Trappes).

Nous espérons qu'en faisant les mêmes calculs pour un plus grand nombre d'observations de l'ozone et de la tropopause nous pourrons à l'avenir mieux connaître cette organisation.

Conclusion — Ces premières considérations nous ont conduit à croire que:

La hauteur de la tropopause croît quand le nombre de taches solaires augmente et d'autant plus que la latitude est plus basse. Le maximum de la hauteur de la tropopause au méridien de Greenwich se situe à l'équateur magnétique et non à l'équateur géographique. Il en est de même de la croissance de la hauteur avec le nombre de taches.

On a observé des orages magnétiques associés à une nette augmentation de l'épaisseur réduite de l'ozone atmosphérique précédée d'une diminution. Une étude portant sur deux ans montre également des variations semblables pour les deux phénomènes.

Discussion — Si l'existence d'une liaison entre les brusques variations de l'énergie solaire et les divers phénomènes météorologiques dans la troposphère a été démontrée par plusieurs chercheurs, le mécanisme de transport d'énergie des couches supérieures aux couches inférieures de l'atmosphère n'est pas encore établi.

L'augmentation de l'énergie reçue à la limite de l'atmosphère terrestre, pendant une forte activité solaire, est seulement de l'ordre de 0.3% de l'énergie que la Terre reçoit normalement (constante solaire). Or, l'énergie nécessaire pour déclencher un renversement de la circulation atmosphérique par exemple, est plusieurs

centaines de fois plus importante. Pour qu'une liaison entre les deux phénomènes soit explicable il faut envisager un système d'amplification de l'énergie, entre l'ionosphère et la troposphère.

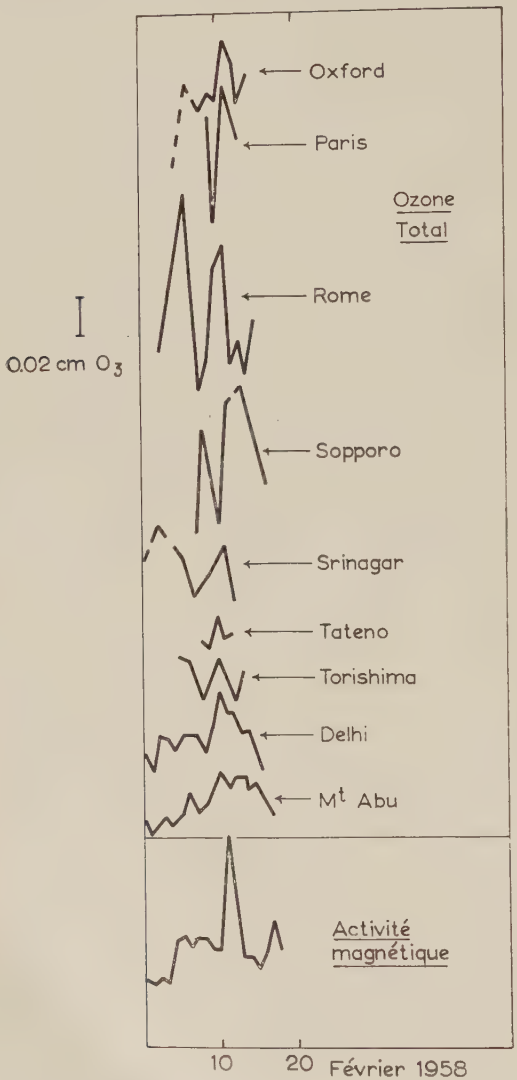

Fig. 4 - *Orage magnétique du 11 Février 1958.*

D'après MacDonald & Roberts (7), une émission corpusculaire du Soleil fournirait des noyaux de condensation à la stratosphère, qui seraient rendus beaucoup plus efficaces par la présence de rayons X pénétrant jusqu'à 20 Km après la manifestation d'une aurore boréale (15). Les phénomènes de condensation et de sublimation ainsi déclenchés pourraient affecter le régime de la circulation atmosphérique.

D'autre part, on peut aussi envisager un système d'amplification d'énergie par l'intermédiaire de l'ozone atmosphérique. Une forte activité solaire, donnant un flux beaucoup plus important de la radiation ultraviolette, peut déséquilibrer dans la stratosphère la production de l'ozone qui, ensuite, modifie son émission thermique dans la région de 9 μ 6, provoquant ainsi un déséquilibre dans le régime thermique de la troposphère. En effet, Murcray ([16]) a déjà observé une augmentation de

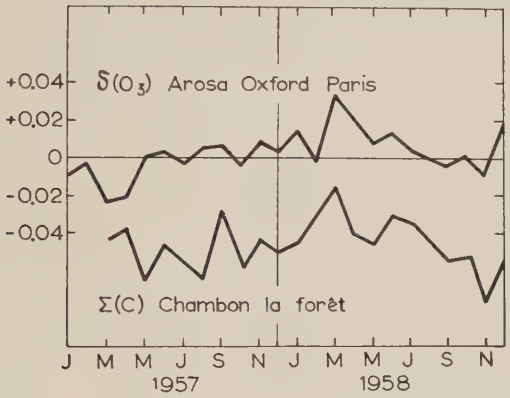

Fig. 5 - *Variations de l'ozone et de l'activité magnétique.*

l'émission d'ozone dans l'infrarouge pendant une aurore, ce qui signifierait, soit une augmentation de l'épaisseur réduite d'ozone, soit une baisse de sa hauteur ou bien les deux.

Il reste à apporter confirmation de ces hypothèses par un calcul approfondi relatif au transfert d'énergie à travers l'atmosphère.

BIBLIOGRAPHIE

([1]) Shapiro R., (1954): J. Meteor., 11, 424-425. — ([2]) Shapiro R., (1956): J. Meteor., 13, 335-340. — ([3]) Shapiro R., (1959): J. Meteor., 16, 569-572. — ([4]) London J., (1956): Trans. N.Y., Acad. Sci., 19, 138-146. — ([5]) London J., Ruff I. & Tick L. J., (1959): Jour. Geophys. Res., 64, 1827. — ([6]) Asakura T. & Katayama A., (1958): Pap. Meteor. Geophys., 9, 15. — ([7]) MacDonald N. J. & Roberts W. O., (1960): Jour. Geophys. Res., 62, 2, 529. — ([8]) Stranz D., (1959): Jour. Atm. Ter. Phys., 16, 180. — ([9]) Dobson G. M. B., (1930): Proc. Roy. Soc., (A), 129, 411-433. — ([10]) Fritz S., (1951): Archiv für Meteor. Geophys. Bioklimat. Ser. A., 4, 343-350. — ([11]) Götz F. W. P., (1951): *Compendium of Meteorology*, 275. — ([12]) Chree C., (1913): Phil. Trans. Roy. Soc. London, 212, 75-115. — ([13]) Vassy A. & Rasool I., (1960): C.R., 250, 3865. — ([14]) Kiveliovitch M. & Vialar J., (1957): *Les séries chronologiques et la théorie du hasard.* Publ. Scient. Tech. Minist. Air., Paris. — ([15]) Wincler J. R., Peterson L., Arnoldy R. & Hoffman R., (1958): Phys. Rev., 110, 1221. — ([16]) Murcray W. B., (1957): Nature, 180, 139.

(*Reçu le* 20 *Mars* 1961)

ON THE GEOMAGNETIC EFFECT OF THE SOLAR ECLIPSE OF 1961, FEBRUARY 15TH AT GENOVA (*)

by Mario Bossolasco, Antonio Elena & Azzio Caneva

Summary — The geomagnetic records obtained at Genova during the eclipse of February 15th, 1961 are quantitatively interpreted with the aim of separating the eclipse effect. Using the ionospheric observations also made at Genova, the result is well confirmed by the calculations carried out applying both the Chapman-model and the Volland-scheme for estimating the geomagnetic effect as originated by the changes of the current system flowing in the *E*-layer.

1. — For nearly a century several attempts have been made to determine the geomagnetic effect of solar eclipses and to evaluate it.

S. Chapman ([1]), considering the reduction of the ionization in the *E*-layer during solar eclipses, found that the geomagnetic effect consists in a diminution of the range of the solar daily variation on quiet days, i.e. of S_q. From the same point of view T. Nagata & Al. ([2]), H. Volland ([3, 4]), and Y. Yamaguchi ([5]) studied the phenomenon theoretically.

J. Egedal & N. Amboldt ([6, 7]) examined data of many observatories near the totality band of the solar eclipse of June 30th, 1954. The maximum geomagnetic effect was found near the projection on the earth's surface of the totality path of the eclipse in the *E*-layer, and occurred nearly at the time of the maximum obscuration. Recently, Y. Kato ([8]) has studied the geomagnetic effect of the solar eclipse of September 12th, 1958 at Suwarrow Island (South Pacific Ocean), making a good test of the validity of the Chapman model.

In many cases the treatment of observations for deducing the geomagnetic effect of solar eclipses has consisted in a comparison of the daily variation occurring on the eclipse day with the mean variation of some preceding and following days. However, as the daily variation may be different even on consecutive days, the reliability of this method is not always sufficient. Another method, consisting in an interpolation of the «unaffected» daily variation on the eclipse-day, is often preferable.

2. *The observational data* — For the eclipse of February 15th, 1961 the path of totality on the earth's surface was over Southern France, North-Central

---

(*) This report belongs to a set of investigations on geophysical effects of the solar eclipse of February 15th, 1961 carried out by the « Istituto Geofisico, Università di Genova », and made possible through a financial support of the « Consiglio Nazionale delle Ricerche ».

Italy (San Remo, Pisa-Livorno, Macerata), Yugoslavia, Southern Roumania and Southern Russia. The projection on the earth's surface of the totality path in the *E*-layer was displaced southwards of the totality path at ground by nearly 2° in latitude, for Italy. Thus, it follows that at Genova, while the obscuration at the maximum phase was 100% at ground, this was not the case for the *E*-layer and still less for the *F*-layer.

At ground, in Genova the eclipse began at 07h27m, reached its maximum on 08h36m and ended at 09h45m, 15° E Time.

The geomagnetic conditions during the eclipse at Genova (Monte Capellino) were not entirely quiet (*). In Fig. 1 we have reproduced the records of *D* and *H* for the eclipse hours, as well as the corresponding records obtained for two nearly quiet days, i.e. on 4th and 10th February 1961, taken as control days. Furthermore, the same figure contains also the variation of *D* and *H* recorded during the eclipse hours at Regensberg and Fürstenfeldbruck (deduced from copies of the records kindly supplied to us from the Swiss Meteorological Service and from the Geophysical Institute of the Munich University).

In Table I the geographical coordinates of the three stations, together with the corresponding maximum obscuration in % at ground are given:

Table I.

Station	Geogr. Lat.	Geogr. Long.	Maximum Obscuration in % at ground
Genova-Monte Capellino ...	44° 33′ N	8° 57′ E Gr.	100
Regensberg	47° 29′ N	8° 27′ E Gr.	97
Fürstenfeldbruck	48° 10′ N	11° 17′ E Gr.	93

Since the range of the daily S_q variation is small in winter, the geomagnetic effect due to the eclipse should be still smaller and therefore difficult to ascertain. Nevertheless, analysing in detail the *H*-variation in Fig. 1 it appears that during the eclipse hours a little diminution has occurred for the horizontal component in all the three stations considered, as against to the behaviour to be expected without eclipse (dashed lines in figure). Such a decrease seems to be anticipated nearly half an hour with respect to the occurrence of the eclipse at ground. This can be explained taking into consideration that on the eclipse-day the sunrays arrived in the

(*) Indeed, this results from the three-hourly planetary geomagnetic indices K_p from 0h to 12h U.T. reported here with the corresponding values in the control days:

	0-3h	3-6h	6-9h	9-12h
15th February 1961	3	2—	2—	3
4th » »	1+	2	2	1+
10th » »	2—	0+	1	0+

E-region (100 km height) over Genova nearly 1 hour before the sunrays at ground (See: J. Lugeon: *Tables Crépusculaires*, Warszawa 1934). Further, it should be remarked that the eclipse effect on the *E*-layer consists essentially in a change of the electrical conductivity of this layer as a consequence of the decay of ionization occurring in the obscured part of the same layer. Therefore, the changes in the electric currents over Genova should have been chiefly originated by the reduction of ionization provoked by the eclipse in the part of the *E*-layer situated west better or more accurately south-west of Genova. This means that the effective anticipation in time of the geomagnetic effect taking place in Genova can be

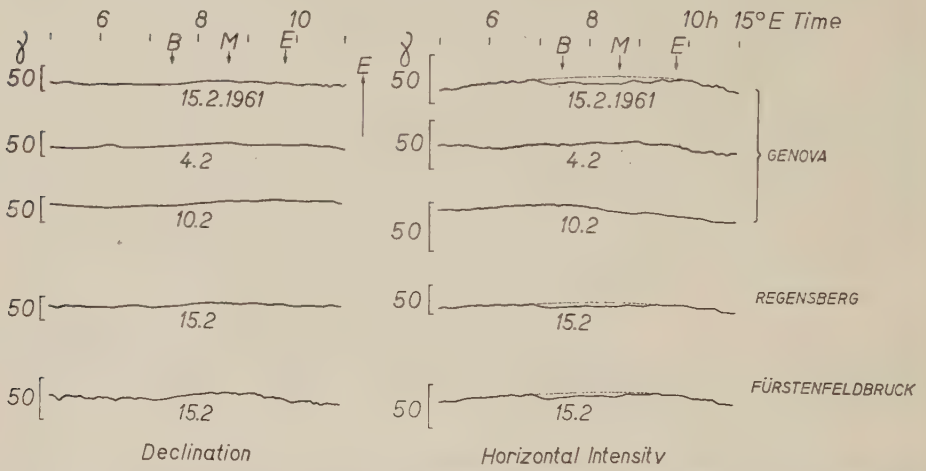

Fig. 1 - *Records of* D *and* H *at Genova* (*Monte Capellino*), *Regensberg and Fürstenfeldbruck on the eclipse day* (*February* 15th 1961). *Records of* D *and* H *on two nearly quiet days* (*Febr.* 4th *and* 10th, 1961) *at Genova.* (*B* = Beginning, *M* = Maximum and *E* = = End of the eclipse at ground in Genova).

little more than that calculated only as height effect on the Genova-vertical. Thus, although the changes provoked by the eclipse on the currents flowing in the *E*-layer cannot be precisely defined, we can deduce that the observed anticipation in time for the geomagnetic effect at Genova should be real and due chiefly to the early time of the eclipse occurrence, a short time after sunrise.

As the eclipse effect consists in a reduction of the amplitude of the S_q variation during the obscuration, it should be noted that at Genova the morning maximum of the unaffected S_q variation of H and D occurs about at the same time as the totality of the eclipse. This results from Fig. 2 where the mean solar daily variation of H and D on 5 international quiet days of each month is represented for the winter solstice (November and December 1960, January and February 1961). If we take as reference the mean values of H and D from 0h to 3h, at the time of totality, the amplitude of S_q in H is approximately 7 gammas, and 5 gammas in D. Therefore, at the time of the eclipse, normally the horizontal component $\mathfrak{H}_q$ of the field of the S_q current has a total amplitude of about 9 gammas.

More exactly, for the unaffected S_q variation it can be seen from Fig. 2 that the maximum in H occurs almost at the time of the beginning of the eclipse at ground (7h27m), while for D the maximum falls about 1 hour after the totality at ground (8h36m).

Now, if we inspect the records of H and D at Genova for the eclipse day (Fig. 1), we find that already half an hour before the beginning of the eclipse at the ground H ceases to increase, and only at about 10h does the same component recover its normal daily variation. Although it is possible that the effect of the eclipse on H has been somewhat masked by a slight perturbation present, we find that, during the eclipse, the mean deviation of H from the unaffected variation, interpolated with the aid of the two control days, is of the order of 5 gammas.

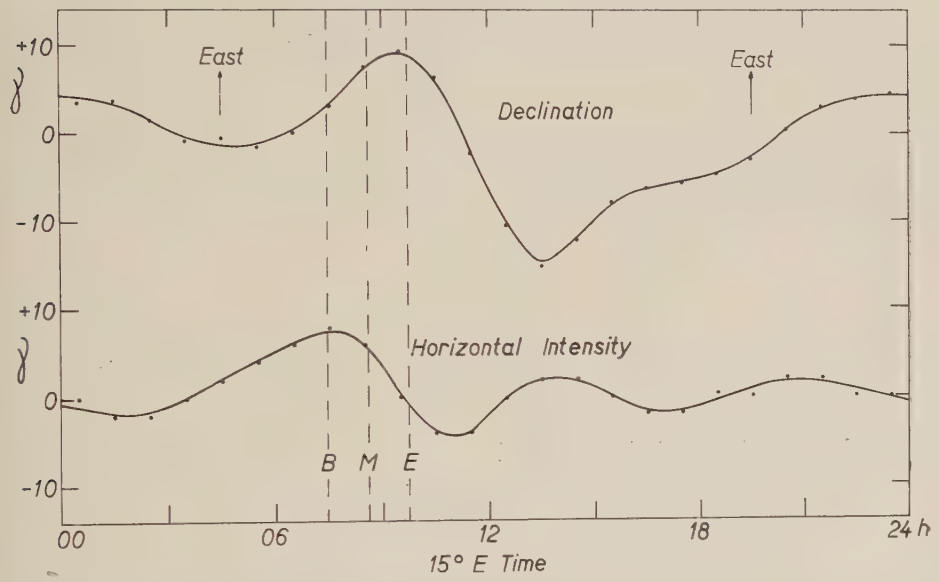

Fig. 2 - *Solar diurnal variation* S_q *of* D *and* H *at Genova, deduced from the five international quiet days in the winter solstice* 1960-61 (November & December 1960 with January & February 1961).

The eclipse effect on D is less evident; however, with reference to the control days a reduction of the order of 3 gammas with respect to the normal S_q can be deduced.

Concluding, a resultant reduction of about 6 gammas caused by the eclipse is found in the amplitude of the horizontal field of S_q.

In addition to the foregoing, we add some deductions from the magnetograms of Tortosa and Wingst (Hamburg), recently received by courtesy of the Observatorio del Ebro and of the Deutsches Hydrographisches Institut. During the eclipse, the H-variations at Tortosa (where the maximum obscuration at ground was 87%) show a similar but weaker depression to those recorded at Genova, while the corresponding variation at Wingst (83% max obscuration) reveals no appreciable depression, apart from a small step-like variation at about

7h (15°E), before the beginning of the eclipse. Thus, as Wingst, for the 100 km height, can be considered nearly outside the eclipse area, these data give a confirmation of the pictured geomagnetic effect. Only for the small step-like variation at Wingst it remains uncertain if it is due to the eclipse, on account of the anticipation of his effect on the E-layer, or if it represents a weak geomagnetic perturbation of general character. This latter interpretation, however, is more likely.

3. *Calculation of the eclipse effect* — For the purpose of estimating the changes in the electric currents flowing in the E-layer, as due to the eclipse, following T. Nagata & Al. ([2]), we can assume that the decrease in ions is proportional to that in electrons, and consequently the decrease of the conductivity is *proportional* to that of the electron density. Therefore, if K is the electrical conductivity of the E-layer, N its electron density, and f_0 its critical frequency

$$K \propto N \propto f_0^2 .$$

At Genova-Monte Capellino continuous records of ionospheric characteristics during the eclipse have been made. With these it was possible for us to deduce the variation of electrical conductivity during the eclipse, assuming

$$\frac{K'}{K} = \frac{N'}{N} ,$$

where K' and N' are respectively the electrical conductivity and the electron density of the E-layer during the eclipse. The variation of the ratio K'/K for the E-layer over Genova during the eclipse is represented in Fig. 3; for this purpose the days February 14th, 16th, and 17th were utilized for deducing, from the unaffected diurnal variation of f_0E, the values of K that would be expected on February 15th in the absence of the eclipse.

Although a detailed study of the ionospheric effects of the eclipse is still in progress, some deductions can already be drawn from Fig. 3. Firstly, the asymmetric behaviour of the electron density before and after the maximum obscuration cannot be explained only by the increase of the sun-height. Further, it follows that the minimum value of the ratio K'/K is about 0.375. This value agrees, at least in order of magnitude, with those found by K. Bibl & F. Delobeau from observations in Norway relative to the eclipse of June 30th, 1954 ([9]); taking into account that at Genova the eclipse at 100 km level was not total, but its effect has been more than 90% of that which would have occurred in case of totality.

After this premise, for the calculation of the eclipse effect we have followed the Chapman model ([10]).

Summarizing, the atmosphere is treated as a plane, thin, infinite conducting sheet, and, at first instance, uniformly conducting all over. The eclipse affects only a small area compared with any one circuit of the current system S_q; therefore, over this part of the current system the currents can be considered as uniform, and flowing through an uniformly conducting medium. Then, if in this medium an eclipse occurs, whereas the conductivity outside is uniformly K, the eclipse reduces the conductivity to some lower value K', again treated as uniform, over an area that can be considered as circular. Before the eclipse, there is an uniform electric field present, driving this current. Supposing that the forces driving the current persist, this uniform electric field will, during the eclipse, have to drive currents

through a sheet which is uniformly conducting except over the circular eclipsed region. If i_0 is the current intensity over the whole sheet before the eclipse, the current when the conductivity is reduced to K' becomes:

1) $$i' = i_0 \frac{2K'}{K + K'} .$$

This reduction of the current will cause a corresponding reduction of the magnetic field determined by the current at the surface of the ground below. The change in the magnetic field, as observed at the ground, will be perpendicular to the local direction of current flow.

Thus, we can now calculate the magnetic effect of the eclipse at Genova, taking into account the values of K'/K, as already found from our ionospheric data. We shall assume the approximate values of 7 gammas for the unaffected range of S_q variation of H and of 5 gammas for D, at the time when the maximum of the eclipse occurred.

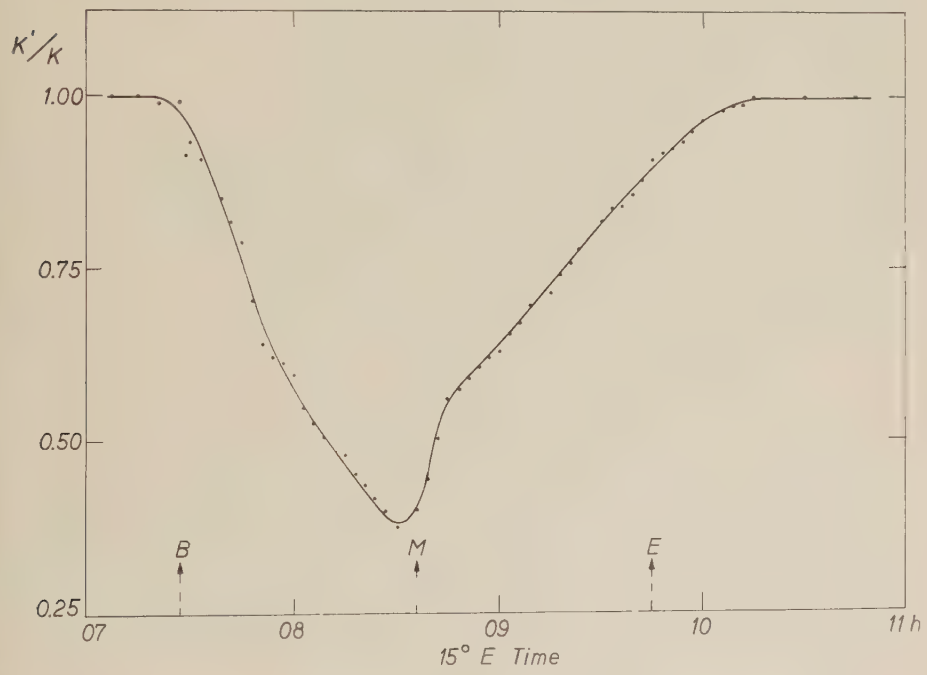

Fig. 3 - *Behaviour of the ratio* K'/K *i.e. between the electrical conductivity of the* E*-layer during the eclipse at Genova (Monte Capellino) and the conductivity of the* E*-layer which would be expected on the same day without the eclipse.*

Applying the formula (1), we obtain, therefore, an effect of nearly 4 gammas for H, and of about 3 gammas for D. It follows that the total eclipse effect on the horizontal field of S_q is about 5 gammas, a value which is the same as that deduced before, and derived from the geomagnetic data only.

H. VOLLAND has proposed another method for calculating the magnetic effect of an eclipse ([3, 4]), as produced by the deformation of the S_q current system by a current function related to the eclipse, moving itself with the latter, and superposed to the S_q system. The problem of induction in the earth's interior has also been considered.

The application of the VOLLAND method requires previous determination of the constant:

$$\varepsilon = \frac{K - K'_{min}}{K}$$

where K is the normal conductivity in the E-layer, corresponding to the S_q system, whereas K'_{min} is the minimum value of the conductivity K' during the eclipse, at the totality path in the E-layer According to VOLLAND, using a spherical coordinate system (θ, λ, r), with the center of the eclipsed area as its pole, the additional field at the time of the eclipse can be represented as follows:

$$(2) \qquad \begin{cases} H_\theta = \varepsilon \mathfrak{H}_q X(\theta) \sin \lambda \\ H_\lambda = \varepsilon \mathfrak{H}_q Y(\theta) \cos \lambda \\ H_r = -\frac{1}{2} \varepsilon \mathfrak{H}_q Z(\theta) \sin \lambda \end{cases}$$

where $\mathfrak{H}_q$ is the horizontal component of S_q field at the center of the eclipse area at ground, and $X(\theta)$, $Y(\theta)$, and $Z(\theta)$ are some functions of the polar distance θ. Assuming $\varepsilon = 0.7$ (*), and $\mathfrak{H}_q = 9$ gammas, as indicated above, from the two first formulae (2) a total effect of about 5 gammas results, in agreement with the interpretation of the geomagnetic records, as well as with the CHAPMAN model.

In conclusion, despite the smallness of the eclipse effect on the geomagnetic field, its detection can be considered as certain, as confirmed by the agreement with the corresponding results derived from ionospheric data.

REFERENCES

([1]) CHAPMAN S.: Terr. Magn., Vol. 48, 175 (1933). — ([2]) NAGATA T. & AL.: Rep. Ionosph. Res. Japan, Vol. 9, 121 (1955). — ([3]) VOLLAND H.: Journ. Atm. & Terr. Physics, Vol. 9, 131 (1956). — ([4]) VOLLAND H.: Journ. Atm. & Terr. Physics, Vol. 11, 1, (1957). — ([5]) YAMAGUCHI Y.: Mem. Kakioka Magn. Observ., Vol. 9, 41 (1959). — ([6]) EGEDAL J. & AMBOLDT N.: Journ. Atm. & Terr. Physics, Vol. 7, 40 (1955). — ([7]) EGEDAL J. & AMBOLDT N.: Journ. Atm. & Terr. Physics, Vol. 8, 105 (1956). — ([8]) KATO Y.: Sc. Rep. Tohoku Univ., Vol. 12, No. 1 (1960). — ([9]) BIBL K. & DELOBEAU F.: Zeits. f. Geophysik, Vol. 21, 215 (1955). — ([10]) CHAPMAN S.: *Solar Eclipses and the Ionosphere* (by W. J. G. BEYNON & G. M. BROWN), p. 221, London (1956).

(*) From our data we found $\varepsilon = 1 - 0.375 = 0.625$, but Genova was not in the totality zone; therefore, we have assumed as order of magnitude $\varepsilon = 0.7$, which is the same value as used by VOLLAND.

HYDRODYNAMICAL RED-SHIFT PHENOMENA IN GEOPHYSICS

by Victor P. Starr (*)

Summary — By the term red-shift is here meant a transfer of spectral energy from smaller disturbances to larger ones in particular regions of the spectrum. An instance of such action is cited in the behavior of certain wind systems of the atmosphere. It is suggested that this process is given a unique average direction through the agency of friction which prevents too large an accumulation of energy in the graver modes of motion. A second probable similar circumstance is cited in the case of the Gulf Stream, for which proper data have recently been obtained for the first time.

The possibility of the existence of a third instance of this type of red-shift is considered for the propagation of surface waves for long distances over deep water. The subject is treated from the standpoint of a nonlinear theory for wave propagation, investigated previously by the writer. An indication is obtained that a red-shift effect should be observed especially in the forward portion of a wave group which has travelled a large distance into new water.

Résumé — Par le terme « red-shift » on veut ici signifier un transfert d'énergie spectrale des plus petites perturbations aux plus grandes dans des régions particulières du spectre. Un exemple de telle action est cité dans le comportement de certains systèmes des vents dans l'atmosphère. On suggère qu'une direction unique soit donnée à ce procès par voie du frottement qui empêche une trop grande accumulation d'énergie dans les modes plus graves du mouvement. Une deuxième probable circonstance similaire est citée dans le cas du Courant du Golfe pour lequel les données convenables ont été récemment obtenues pour la première fois.

La possiblité de l'existence d'un troisième exemple de ce genre de « red-shift » est considérée pour la propagation des ondes de surface pour les grandes distances dans les eaux profondes. Le sujet est traité du point de vue d'une théorie nonlinéaire pour la propagation des ondes qui a été développée précédemment par l'auteur. Une indication est obtenue que l'effet d'un « red-shift » devrait être observé specialement dans la region frontale du groupe d'ondes qui a parcouru une grande distance dans des eaux nouvelles.

Zusammenfassung — Unter dem Ausdruck « Rot-Verschiebung » wird hier die Verschiebung der Spektral-Energie von kleineren zu grösseren Störungen in ausgesuchten Zonen des Spektrums verstanden. Ein Beispiel eines solchen Vorfalles ist hier besprochen in dem Verhalten von gewissen Wind-Systemen der Atmosphäre. Es wird

(*) Department of Meteorology, Massachusetts Institute of Technology, *Cambridge* 39, *Mass.* (U.S.A.).

angeraten, dass diesem Prozess eine einzige Durchschnittsrichtung durch Reibung gegeben wird, die eine zu grosse Anhäufung von Energie in den ernsteren Bewegungsarten verhindert. Ein zweiter, ziemlich gleicher Umstand wird im Falle des Golfstromes besprochen, für den zum ersten Mal ausführliche Daten vorhanden sind.

Die Möglichkeit des Vorhandenseins eines dritten Vorfalles von dieser Art der « Rot-Verschiebung » wird in der Fortpflanzung von Oberflächen-Wellen über längere Entfernungen an tiefem Wasser in Erwägung gezogen. Dieser Fall wird vom Gesichtspunkt einer nichtlinearen Theorie für Wellen-Fortpflanzung betrachtet, die früher vom Autor untersucht wurde. Man gewinnt den Eindruck, dass ein « Rot-Verschiebungs-Effekt » besonders in dem vorderen Teil einer Wellen-Gruppe beobachtet werden kann, besonders dann, wenn die Welle sich eine längere Strecke über frisches Wasser bewegt hat.

1. *Introduction* — Speaking of the more purely mechanical processes in the atmosphere one of the outstanding new developments has been the realization that there exist strong flows of kinetic energy from certain spectral bands of moderate wave length to those of longer wave length, the action being due to nonlinear coupling between the harmonics. Until very recently the best example of this process has been the maintenance of the mean zonal flow by the aggregate of the cyclone-scale disturbances in the atmosphere. In this example the transfer takes place to the zero wave number of the flow. The observational results just published by Saltzman & Fleisher (1960) extend the analysis so that the available range of the spectrum is divided into three equal bands of wave numbers in addition to the zero harmonic. They find that not only does energy flow to the zero mode, but also that a transfer takes place from the middle band of the three to the other two. Thus there exists an energy exchange among the eddies themselves from the moderate wave numbers (6-10 inc.) to the lower ones (1-5 inc.). The importance of results of this kind for the future of meteorology can scarcely be overestimated, because they tend to dislodge agelong prejudices and tacit oversimplifications which have hamstrung our efforts to arrive at a rational conception of basic meteorological processes.

I have borrowed the name « hydrodynamical red-shift phenomena » for anomalous spectral energy flows of this kind. Although the red-shift effects in modern physics involve similar energy displacements, (see e.g., Landau & Lifshits 1951), it is not to be understood that the causes are identical and any further analogous behavior, if it does exist, still remains to be demonstrated. On the other hand, it would be rather singular if such hydrodynamical red-shifts were entirely restricted to atmospheric motions. Indeed my main purpose at present is to bring together other cases in geophysics and to make comparisons among them. Before so doing, however, a review of some of the circumstances attending the atmospheric instance is needed.

2. *Some comments upon the atmospheric case* — The transfer of energy toward lower wave numbers — let us take flow into the zero harmonic — may be illustrated by various dynamic models, e.g., the theoretical treatments by Kuo (1953) showing the countergradient flux of momentum converging into the zonal mean jet stream causing the latter to gain energy at the expense of the disturbances. Such a model may of course be frictionless and barotropic, the action illustrated being a manifestation of nonlinear interaction arising from the inertia terms of the equations of motion. Although the action thus exemplified may be an actual

counterpart of what in fact operates in the atmosphere on the average, still it does not follow that the whole existing process does not vitally depend upon frictional dissipation. The same models teach us that long continued energy fluxes of this kind would lead, without limitations imposed by friction, to such strong mean jets that eventually these same mean zonal wind distributions would tend to become barotropically unstable, thus putting an end to the action. In crude terminology it could be said that presently the mean zonal motion would become choked up through an excessive accumulation of energy and momentum.

In spite of the fact that there is no good reason to suppose that at times the actual atmosphere may not be temporarily subject to such choking situations, representing passing abnormal states, the observational evidence points to the conclusion that on the average the atmosphere avoids the development of such strong mean zonal jets. Undoubtedly, the main reason for this is the action of frictional retardation on the mean zonal flow, although the action of the indirect mean meridional circulation in cutting down extreme velocities in the jet stream is not to be disregarded. These considerations help us in thinking about the possibility that here as well as in other instances of hydrodynamical red-shift phenomena friction may play a role, although this role might be one step removed from the actual nonlinear interaction process among the harmonics comprising the motions. Friction, in other words, may be an important factor in adjusting the motions so as to set the stage for the development of a reversal of the more familiar spectral cascade effects (which latter are of course still present for higher wave numbers, generally).

3. *Studies of the Gulf Stream* — For many years various workers have pointed to the similarities between the Gulf Stream and the atmospheric westerly flow, referring to kinematical features such as the ever-changing meander pattern, the cutting off of closed circulations, and contrasts of temperature across the current. These general facts have raised the interesting question as to whether similarity extends also to the basic dynamic processes which underlie the motions in the two instances. Unfortunately, the difficulty of obtaining information for the oceans, necessary to make studies of the kind already made in the atmosphere, is very great and only small beginnings have so far been made.

What is needed is a three-dimensional synoptic picture of the motions and other variables at fairly close intervals of time over a prolonged period, perhaps several months. Different portions of the Gulf Stream no doubt differ as to the basic dynamics, so that large geographical coverage would be desirable. The aim in more specific terms would be the delineation of the momentum and energy balances, to begin with along lines already followed in the atmospheric case, with however an ever-ready eye for the effects of special circumstances — lack of cyclic continuity around the earth, practically north-south orientation of the mean current, etc.

I am confident that the required work will be performed, perhaps sooner than one might expect. Actually, this line of investigation has already been started through the efforts of Webster (1961a, b), also reported in his doctoral dissertation (Mass. Inst. of Tech.).

Among certain other results, Webster computed the stress due to transient eddies, from velocity measurements taken at a fixed cross section normal to the mean current a little south of Cape Hatteras. The velocities used were obtained during

a cruise made by W. von Arx which included two round trips along the cross section per day for some thirty consecutive days. The current values themselves were the properly reduced observations from a geomagnetic current meter (Gek), which represent the motions of the uppermost several meters of the ocean. The stress, or cross-stream transport of upstream momentum, for obvious reasons could not include the effects of standing eddies, since observations at more than one cross section would be needed in order to measure standing eddy effects. However this may be, it would appear to me that the bulk of the eddy effects are probably contained in the action of the transient components.

The relation of the stress distribution to the mean downstream flow obtained by Webster was surprisingly analogous to that obtained by myself for the atmospheric case (Starr 1953, 1959b) and carries the same implications concerning energy flow from the eddies to the mean motion as does the latter. To wit, along the cross section the momentum is again transferred from regions of slow mean motion into the region of the maximum, the action thus being the reverse of a frictional effect. The expressions given by Osborne Reynolds (1895) may be used to calculate the mean rate at which kinetic energy is fed into the mean flow by the process (at the expense of the eddies).

Much still remains to be done in order to substantiate Webster's indications further, and to obtain a more rounded picture of the energy cycle for the more southern course of the Gulf Stream. Also it will be necessary to investigate processes at lower levels, not only for energy studies but also in order to secure a more complete determination of the momentum balance — a subject of importance in its own right. All in all it would nevertheless seem to me that the kinematic similarity previously recognized may already at present probably be extended considerably so as to include dynamic similarity in its grosser aspects.

Granting this view of the subject to be the correct one, we have here another beautiful example of a red-shift phenomenon. Kinetic energy is obtained from the wind or from the release of geopotential energy (more probably the latter) through the agency of eddies of certain scales and is then transferred to a graver mode of motion. A release of available potential energy could take place in a manner somewhat like that described for the atmosphere in Starr (1954). Nonadiabatic effects, and indirectly the wind action, no doubt are the ultimate sources of the available potential energy. Probably the mean flow is again kept within bounds through friction and, on the average at least, does not itself become (barotropically) unstable within the region considered. Farther downstream, in its course beyond Hatteras, the Stream may become thus unstable, but studies in that area have not as yet yielded answers to this question.

4. *The ocean wave problem* — As an empirical fact it has long been stated that a train of surface waves in the ocean, such as might be generated by some given storm, changes its characteristics progressively with time and distance after leaving its area of generation (see, e.g., Munk 1947). For our purpose the notable fact is that there seems to occur an increasing amount of energy in the lower frequency ranges of the spectrum and therefore a manifestation of long wave lengths traveling at correspondingly high speeds. This period-increase effect is more or less by definition a hydrodynamical red-shift phenomenon. For purposes of illustration an extreme example may be cited. As is known to oceanographers, waves with a period up to about thirty seconds are at times found in the vicinity of the coast

of southern California. The wave lengths reach perhaps a half a mile and the wave speed is upward to a hundred miles per hour in deep water. Suggestions have been made that their origin is from generating areas in certain storm regions of the southern hemisphere. Presumably marked alterations come about during the long travel time involved.

The efforts which have been made to explain the period-increase effect have often depended upon a purely frictional dissipation. It has been thought that viscosity might have a preferential action tending to destroy the higher harmonics more rapidly, thus leaving the long wave lengths to be more prominent at a later time. Such an explanation would imply that the long wave lengths and periods are present in the disturbance from the outset, and require no nonlinear spectral shifts of energy to make them apparent later. Neither are nonlinear spectral shifts involved in other explanations based on dispersion phenomena (see in this connection Rossby 1947). It is of course difficult to observe the details of the actual phenomenon in nature, and one cannot therefore judge the adequacy of these explanations directly. However, it is perhaps not amiss to consider other possible processes, particularly the one which naturally suggests itself from the other red-shift actions men tioned in the foregoing sections.

According to linear theory there can be no interaction between the spectral harmonics of a given wave system. If such interaction exists, it can be discussed only in terms of nonlinear theory which is not at all well developed due to the inherent complexity of the subject. Recourse could here be made, no doubt, to the numerical integration of the nonlinear governing equations with the aid of high speed electronic computers (*). Some suggestions for such a procedure are perhaps contained in similar integrations of meteorological equations recently carried out by Lorenz (1960). But even so, preliminary over-all discussion from a physical viewpoint is no doubt essential for the choices of suitable initial conditions and to gain a perspective on other questions.

While the simple frictional theory may not in itself be sufficient to account for the facts, it still may be that a fixed direction is given to the nonlinear spectral transfer of energy through an indirect frictional action, in a manner similar, in a sense, to that discussed in connection with the atmospheric case above. Thus a numerical nonlinear solution, however obtained, may possibly be inconclusive, showing no unidirectional spectral energy shift for the frictionless case. The proper illustrations may then be contained only in certain stages following immediately upon selected initial states, or else a suitably chosen form of dissipation might actually be included in the model.

All that can be done here is to speculate about the problem in a tentative fashion. If indeed a sense of direction is imparted to the process indirectly by friction, it would seem to me that one of the more vulnerable properties of the wave motion, more liable to derangement, is the momentum of the waves, first noted by Stokes (1847) as a characteristic of the higher order approximations for the problem. Since this attribute is a *necessary* one for periodic waves to be of the permanent type, it follows that if through some circumstance the waves become slowly deprived of their momentum, secular changes in other properties must

---

(*) See note at the end of this paper.

simultaneously take place. It is interesting to try to foretell qualitatively what some of these changes might be.

For a number of years I have made studies of the momentum and other properties of surface waves of finite height, these studies being summarized briefly in STARR (1959a), to which the reader is referred. Another recapitulation of them has been given recently by WEHAUSEN & LAITONE (1960). It turns out that the momentum per wave length, M, of a uniform wave train is related to the mass of water m transported across a fixed vertical during one wave period, by the rather simple equation (*)

$$M = cm \tag{1}$$

where c is the wave speed. For the present purpose it is desirable to use also another relationship involving energy (STARR 1951, 1959a), namely

$$E = mc^2 - \varepsilon \,. \tag{2}$$

Here E is the sum of the kinetic and potential energies $(e + v)$ per wave length, and ε is their difference $(e - v)$, the kinetic, e, being the larger of the two. The last term is of fourth order and for the time being may be dropped — a simplification which can, for the highest possible waves, cause an error of only a few per cent. We may now write (2) in the form

$$E = Mc \tag{3}$$

which is related to an equation due to LEVI-CIVITA (1924), and also discussed in STARR (1947a).

Customarily, although many equations describing wave-motion phenomena are derived for the case of a uniform train with various parameters fixed, the results once obtained are often applied approximately to modulated wave trains and to cases where the original parameters may actually vary. Use will be made of such freedom in the present discussion. In this way (3) may be differentiated logarithmically with respect to time t so that

$$\frac{1}{E}\frac{dE}{dt} - \frac{1}{M}\frac{dM}{dt} = \frac{1}{c}\frac{dc}{dt} \,. \tag{4}$$

The symbol d/dt is here used to denote in an approximate manner differentiation following an individual wave train.

Reverting at this point to the notion that friction may lead to a greater percentage rate of decrease of the momentum M than of the energy E, *the result is gotten that there must be an increase in the wave speed* c. For the instantaneous description of the state of the motion in general terms, some use may of course still be made of the linear theory, so that, nearly enough,

$$c^2 = \frac{gL}{2\pi} \tag{5}$$

in which g is the acceleration of gravity and L is the wave length. Or, since the

---

(*) For reasons of temporary expediency the notation in my previous articles cited among the references unfortunately has not always been consistent.

period $T = L/c$,

$$T = \frac{2\pi}{g} c \tag{6}$$

so that an increase in c is directly related to an increase in the wave length and period.

Thus far we have given consideration to the effect of a truly dissipative factor. Upon reflection one can see that the identical outcome would follow from (4) regardless of how one conceives that a relatively large percentage decrease in M might be occasioned. Such reductions in M might credibly be referred to causes other than friction — for example to air resistance, if this is not included under friction. Otherwise, it is possible that as the (limited) wave disturbance moves progressively into new water, there is a purely inertial resistance to the setting up of a concomitant momentum distribution, as contrasted with the conditions in the generating area where the wind stress can directly provide a supply (see STARR 1947a).

In order to examine the last hypothesis somewhat further, let us calculate the *transport* of horizontal momentum in the direction of an advancing wave train in the hope that this might throw some light upon the subject.

5. *Transport of momentum by gravity waves of finite height* — Let us consider the two-dimensional irrotational motions of an ideal incompressible and frictionless fluid, taking place in the x, z-plane as shown in Fig. 1. We shall focus atten-

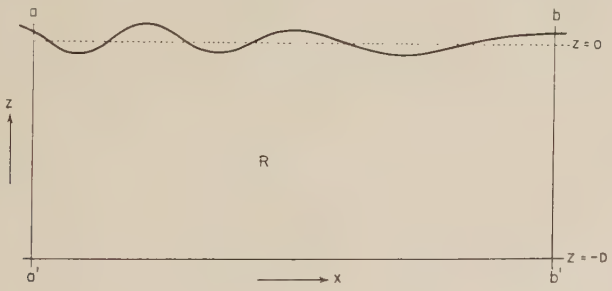

Fig. 1

tion upon the fluid within a region R bounded at the left by the vertical aa', at the right by the vertical bb', and below by the horizontal $a'b'$, the fluid being free to flow through each of the three line segments. At the top the region is bounded by the free surface of the fluid ab, which then comprises a material surface assumed to be continuous but of arbitrary shape except as specified at later stages of the development. The x-coordinate increases to the right and that of z upward, and the bottom boundary is at $z = -D$.

The x-momentum for the system is governed by the equation of motion for the horizontal direction

$$\rho \frac{du}{dt} = -\frac{\partial p}{\partial x} \tag{7}$$

and by the equation of continuity

$$\frac{\partial u}{\partial x} + \frac{\partial w}{\partial z} = 0 \tag{8}$$

in which u, w are the components of particle velocity in the x and z-directions respectively, ρ is the uniform and constant density of the fluid, p is pressure and the symbol d/dt signifies differentiation with respect to time t following an individual particle.

Upon expansion of the individual derivative into partials, the relations (7) and (8) may be combined so as to yield a continuity equation for x-momentum, namely,

$$\frac{\partial \rho u}{\partial t} + \frac{\partial}{\partial x}(\rho u^2 + p) + \frac{\partial}{\partial z}(\rho u w) = 0 . \tag{9}$$

This equation may be integrated with respect to area over the closed region R yielding, with obvious reductions,

$$\frac{d}{dt}\iint_R \rho u dz dx = \int_a^b \rho u_\zeta \frac{\partial \zeta}{\partial t} dx + \oint_R [\rho u w dx - (\rho u^2 + p) dz] \tag{10}$$

in which $\zeta = \zeta(x, t)$ denotes the height of the free surface and u_ζ the value of u at this value of z.

We may separate the cyclic integral of (10) into contributions from the four segments of the boundary of R. Since three of these segments are taken along coordinate directions, certain simplifications result. We have

$$\left\{ \begin{aligned} \frac{d}{dt}\iint_R \rho u dz dx = &\int_a^b \rho u_\zeta \frac{\partial \zeta}{\partial t} dx + \int_{a'}^{a} (\rho u^2 + p) dz - \int_{b'}^{b} (\rho u^2 + p) dz \\ &+ \int_{a'}^{b'} \rho u w dx + \int_a^b (\rho u^2 + p) dz - \int_a^b \rho u_\zeta w_\zeta dx . \end{aligned} \right. \tag{11}$$

We may further simplify (11) through the kinematic boundary condition for the free surface which states that this surface is to be a material surface. Thus (see, e.g., STARR 1945) w_ζ is given by

$$w_\zeta = \frac{\partial \zeta}{\partial t} + u_\zeta \frac{\partial \zeta}{\partial x} \tag{12}$$

enabling us to combine the three integrals along the free surface, giving

$$\left\{ \begin{aligned} \frac{d}{dt}\iint_R \rho u dz dx = &\int_{a'}^{a} (\rho u^2 + p) dz - \int_{b'}^{b} (\rho u^2 + p) dz \\ &+ \int_{a'}^{b} \rho u w dx + \int_a^b p_\zeta dz , \end{aligned} \right. \tag{13}$$

p_ζ being the pressure along ζ.

At this point it is clear that (13) represents in convenient form the principle of conservation of x-momentum for the region R. The four integrals on the right

represent one by one the fluxes of x-momentum into R across each of the segments of the boundary. To the extent that this sum may not be zero, it leads to an accumulation or deficit as measured by the left-hand term. Equation (13) is therefore a source-free continuity equation for momentum for R. It is to be noted that the fluxes do not necessarily all vanish even for equilibrium conditions with no motion and a level free surface, unless the pressure is zero — an impossibility with gravity present in our simple coordinate system.

What interests us most is the flux of momentum across the vertical at a, measured by the first integral on the right-hand side of (13), on the supposition that we have here regular periodic waves moving to the right without suffering a change of form in the immediate vicinity of aa'. These wave motions can be regarded as decreasing sensibly to zero at the depth $z = -D$ and having a mean level of the free surface at $z = 0$. Moreover we make it our object to seek the transport of momentum *due solely to the waves*, i.e., the excess of transport when the waves are present over and above what would obtain were the wave amplitude to be decreased to zero, other conditions remaining the same. In other words the desired instantaneous flux is

$$\int_{-D}^{\zeta} (\rho u^2 + p)\, dz - \int_{-D}^{0} p_h dz = \int_{-D}^{\bar{\zeta}} (\rho u^2 + p)\, dz - \frac{1}{2} g\rho D^2 - p_0 D\,, \tag{14}$$

where p_h is the hydrostatic pressure with no waves present, g is the constant acceleration of gravity acting in the negative z-direction and p_0 is the now constant and uniform surface pressure. The equality follows directly from hydrostatic principles.

It is desirable to calculate not the instantaneous flux of momentum, but rather the integrated transport M_t during one wave period T. In such a time integration it is permissible to use the transformation $dx = cdt$ in which c is the wave speed (Starr 1948). It now follows that, if L is wave length,

$$M_t = \frac{1}{c} \int_0^L \int_{-D}^{\zeta} (\rho u^2 + p)\, dz dx - \frac{g\rho D^2 L}{2c}\,. \tag{15}$$

No generality is lost by supposing henceforth from this point that the pressure p_0 at the free surface is zero, as has already been done in writing (15). By definition the integration of ρu^2 gives us twice the kinetic energy of the horizontal motions, e_x, per wave length so that

$$M_t = \frac{2e_x}{c} + \frac{1}{c} \int_0^L \int_{-D}^{\zeta} p\, dz dx - \frac{g\rho D^2 L}{2c}\,. \tag{16}$$

If U is defined as the steady x-component of particle velocity measured relative to the moving wave so that

$$U = u - c \tag{17}$$

it can easily be shown that

$$\frac{1}{2} \rho (U^2 + w^2) + g\rho z + p = \frac{1}{2} \rho c^2 \tag{18}$$

is the appropriate form of the Bernoulli equation under the conditions assumed (see LAMB 1932; STARR 1947b). From (17) and (18) it follows that

$$p = \rho uc - \frac{1}{2}\rho\,(u^2 + w^2) - g\rho z\,. \tag{19}$$

Upon insertion into the integral term in (16) this expression for p results in the following. The first term on the right of (19) gives the momentum per wave length, M. The second term gives minus the kinetic energy per wave length divided by c, namely, $-e/c$. The third term integrates out giving minus the potential energy per wave length divided by c, namely, $-v/c$, and also a residue $g\rho D^2L/2c$ which latter cancels the last term in (16). We now have for M_t

$$M_t = \frac{2e_x}{c} + M - \frac{E}{c} \tag{20}$$

in which E is the total energy per wave length, namely, $e + v$, as defined in the preceding section. With the aid of (1) and (2) it can be seen that

$$M_t = \frac{1}{c}\,(2e_x + \varepsilon) \tag{21}$$

ε being the difference between the kinetic and potential energies $e - v$ as stated previously. This is one form of the final result.

For purposes of discussion it is useful to form the ratio of the momentum transmitted during a wave period to the momentum per wave length. We have, using (1) and (2) and the definitions of E, ε, e, v,

$$\frac{M_t}{M} = \frac{2e_x + \varepsilon}{cM} = \frac{2e_x + \varepsilon}{E + \varepsilon} = \frac{1}{2} + \frac{2e_x - v}{2e}\,. \tag{22}$$

If now e_z is the kinetic energy of vertical motions per wave length so that $e = e_x + e_z$, the potential energy v may be expressed, according to a previously derived relation (STARR 1947b), as follows

$$v = \frac{1}{2}\,e_x + \frac{3}{2}\,e_z \quad \text{or} \quad \varepsilon = \frac{1}{2}\,(e_x - e_z)\,. \tag{23}$$

When (23) is combined with (22) the result may finally be written in the simple form

$$\boxed{\frac{M_t}{M} = \frac{1}{2} + \frac{3}{2}\,\frac{\varepsilon}{e}}\,. \tag{24}$$

According to PLATZMAN (1947) the quantity ε approaches zero for infinitesimal wave amplitudes, thus furnishing agreement with linearized theory, and increases to a positive maximum for the highest waves, so that for the extreme wave form

$$\varepsilon \equiv e - v = \frac{1}{8}\,v \tag{25}$$

approximately. The corresponding maximum of the transport ratio is

$$\frac{M_t}{M} = \frac{2}{3} \approx 0.67 . \tag{26}$$

It is of interest to compare (24) with a similar ratio of the energy E_t transmitted during one wave period, to the total energy E per wave length. This has been derived previously by STARR & PLATZMAN (1948) in the form

$$\frac{E_t}{E} = \frac{1}{2} + \frac{5}{2}\frac{\varepsilon}{E} . \tag{27}$$

Evaluation of this energy ratio for waves of the extreme form through the use of (25) yields a value of 11/17 or 0.65 approximately.

An item worthy of note is that both ratios approach the limit one half for waves of small amplitude.

6. *Discussion of inertial effects on gravity wave propagation* — The energy transport ratio mentioned at the close of the preceding section is closely connected to the dynamic interpretation of the concept of *group velocity*, as first pointed out by REYNOLDS (1877), for the case of waves of small amplitude. In fact, we may reagard the energy ratio given above as being equal to the ratio of a generalized *energy velocity* to the phase velocity, which replaces the ratio of group to phase velocity, when the effects of finite wave height are included.

Some of the connotations inherent in the notion of a group velocity are, however, no longer so simple in the present case. For one thing we are confronted not only with the presence of an energy velocity, but also on like terms with the presence of a *momentum velocity* as a consequence of (24). Moreover, these two velocities are not precisely the same in magnitude. It follows that the simple picture of the propagation of a group of waves is probably not strictly correct, requiring modification in certain respects. Perhaps the reasoning outlined in section (4) above contains a clue to the problem. That is to say, if the energy and momentum are propagated at different speeds the energy maximum of a given group of waves might become spacially separated from its original momentum concentration, thus leading to a secular change in the characteristics of the group. This change could then be reflected in a spectral shift of energy. On purely philosophical grounds these are problems of considerable intrinsic interest.

From the practical standpoint of looking at the actual phenomena in the oceans, there are nevertheless several things to be noted which make the applicability of the reasoning just given rather implausible. First of all the difference between the rates of propagation for momentum and energy is of the order of only three per cent *for the highest waves*, the momentum propagation moreover being indeed the swifter. For lesser waves, of moderate and small amplitude with respect to wave length, this difference rapidly becomes exceedingly small. Since the actual waves are irregular in various ways, and move under conditions that do not conform strictly to those presupposed in idealized theory, the consequences of such small effects as those here contemplated are no doubt rather completely obscured. We must search for factors whose effects are more gross, if we wish to deal with such coarse realities.

One of the special circumstances attending wave motions in the oceans sometimes commented upon by workers in this field is the fact that the medium is

one which participates in the rotation of the earth, and hence, in the most direct sense of the word, that the wave motions are rotational and not potential. Various general arguments may be adduced purporting to show that the derangement attributable to the earth's rotation, in the oscillatory components of the wave motion is small. These arguments envisage customarily only those wave phenomena encompassed within the scope of the linearized theory, and depend upon the large contrast between the wave frequencies and certain much lower frequencies linked with the earth's period of rotation.

Although such contentions may in the main be quite correct, serious questions arise in connection with the progressive components of particle velocity, associated with the momentum of the waves (see, e.g., STARR 1945 for a simple demonstration of this particle progression). In order for a mean transport velocity in the direction of wave propagation to persist, it would be necessary that the associated Coriolis acceleration, directed along the wave crests, should be balanced by a mean pressure force in the contrary sense, as is well known to oceanographers. In the absence of such a balancing pressure force, the deflective effect of the earth's rotation would cause the particles, rapid oscillatory wave motion components aside, to execute approximately circular horizontal orbits, only a few kilometers in radius, for speeds involved in the present case (the so-called inertia paths of dynamic oceanography).

It is, on the other hand, difficult to see how, as a group of waves advances into new water, a proper pressure force can systematically come into being. Although it would perhaps be possible in an *ad hoc* fashion to postulate some process which might tend in the direction of establishing this required attendant condition, still it would on the whole appear to me that this does not in actuality take place, and that therefore a strong barrier is interposed in this manner to the propagation of wave momentum into new water — a barrier which furthermore offers much less resistance to the propagation of wave energy, since this latter is due for the most part to the high frequency oscillatory components of the waves.

If the conclusions stated in the preceding paragraph are assumed correct, the further argument is thrown back once more to the considerations sketched in section (4.). Namely, it can be concluded that the propagation of energy tends to outstrip the propagation of momentum, and that progressively less momentum is associated especially with the forward portion of the onward moving area of significant wave energy. If the diminution of momentum in this active area is marked enough relative to the probable decrease in energy, then progressively larger wave lengths, phase speeds and periods should be found there as discussed in the statements made concerning frictional effects. For this final step in the reasoning the approximate equation (4) is once more sufficiently accurate to the purpose.

Through the instrumentality of the Coriolis effect we have thus been led to a chain of reasoning which purports to show that the waves, at least if they remain as waves, should change their fundamental parameters so as to show a red-shift purely as an inertia effect. It is true, of course, that no direct measurement of the interaction between harmonics has been made, but the inference is implied that such interactions do exist and act in the direction specified, regardless of which hemisphere is involved. The valid observation may however be made that this mode of explaining the period-increase phenomenon should lead to minimum effects for wave propagation in the direction of, and in the vicinity of, the equator.

It needs to be stated at this point, however, that at present information is

wanting in order to permit us to say whether any one of the several possible explanations for the red-shift effect predominates over the others.

7. *General remarks* — Unlike perhaps the intellectually most challenging instance of red-shift phenomena in cosmic physics — the theoretically predicted Einstein red-shift of general relativity — the anomalous hydrodynamic spectral shifts of energy discussed in this paper have been discovered through the analysis of observations pertaining directly to the processes under consideration. However, once things of this general kind are exhibited, it is usually found rather quickly that they are quite in accord with theory, which latter then receives a healthgiving stimulus from each such development. On this basis I therefore venture the guess that fairly soon we shall be confronted by the appearance of many novel theories for the Gulf Stream and other oceanic currents, embodying red-shift characteristics. This is indeed to be encouraged, but under the circumstances let it also not be forgotten what it was that first touched off the new lines of reasoning.

There probably are data in existence from which calculations like those of Webster could be made for the Japan Current. So far as I know this has as yet not been done, although my information about such work may not be up to date. The remaining counterparts of the Gulf Stream in the oceans of the southern hemisphere no doubt owe there existence to comparable processes, and hence also deserve to be studied in detail. The possibility that red-shift actions enter into the maintenance of some still other ocean currents cannot be ruled out except as adequate observational evidence accumulates.

In view of the increasing emphasis on the study of the oceans due to practical needs, more and more rapid strides are being made toward the materialization of a synoptic oceanography, portraying adequately the details of transient phenomena regarding ocean currents. It seems feasible in view of this situation to begin to make plans to investigate the energy budget for the oceans in terms of a separation of the total motion into standing eddies (mean circulations) and transient eddies, much as has been done for the atmospheric case during the last several years. Not only the motions but also the stored available potential energy could be resolved into these two components. Interactions between various pairs of such four quantities could then be studied, in order to secure a better conception of the transformations and fluxes of energy and momentum. This could be undertaken either for individual ocean basins or portions of such units, or ultimately for the entire ocean area of the earth — by seasons or otherwise in each case.

Actually the work of Webster is an initial excursion into this domain. As a further specific suggestion the recent work along these lines of my esteemed colleague Dr. T. Murakami (1961), for the atmosphere, could be copied by way of analogy as an initial framework for such schemes.

It is possible that surface waves, if deranged somewhat from their idealized symmetric form, transmit momentum (derived originally from the wind) downward to feed deeper oceanic currents. In order to do this, it is easy to show that the trough- and crest-lines in the relative streamlines would have to depart from the vertical so as to tilt *forward* with increasing depth. In this manner a portion of the downward momentum flow in the oceans, commonly attributed to turbulence, may in fact be transported by much more orderly processes associated with wave motions. This is perhaps more likely to happen in wave generating areas (see Starr 1947a).

8. *Note* — For the numerical integration of the generalized nonlinear surface wave problem it is necessary to use the basic hydrodynamical equations for these motions as a starting point. Unfortunately most discussions of the subject of gravity waves commence practically at the outset with the imposition of restrictive assumptions such as small amplitudes, motion periodic in x or t or both, motion without change of type, etc., so that a sufficiently general formulation is seldom set forth.

Let us suppose that the irrotational motions take place in the x, z-plane, and that the basin is one of infinite depth so that (from general considerations) the motion will die out as $z = -\infty$ is approached. For convenience but with some loss of generality, it might be conceived that the motions take place in a horizontally finite amount of fluid within a circular canal of large radius. The origin for z may then be taken at the mean level. The differential equation for the body of fluid is then

$$\frac{\partial^2 \Phi}{\partial x^2} + \frac{\partial^2 \Phi}{\partial z^2} = 0 \tag{28}$$

where

$$\Phi = \Phi(x, z, t)$$

is the velocity potential for the horizontal and vertical components of particle velocity,

$$u = -\partial \Phi / \partial x \; ;$$

$$w = -\partial \Phi \, \partial z \; .$$

Three more conditions must now be added to (28) for the deep water case. The first is the kinematic boundary condition at the free surface, stating that this surface remains a material surface, namely that if $\zeta = \zeta(x, t)$ is the height of this surface,

$$\frac{\partial \zeta}{\partial t} = \frac{\partial \zeta}{\partial x}\left(\frac{\partial \Phi}{\partial x}\right)_{z=\zeta} - \left(\frac{\partial \Phi}{\partial z}\right)_{z=\zeta} \tag{29}$$

derived from (12) above.

The second is the dynamic boundary condition stating that the pressure p should be spacially uniform at $z = \zeta$. This is guaranteed if p is kept constant in the Bernoulli equation so that

$$\left(\frac{\partial \Phi}{\partial t}\right)_{z=\zeta} + \frac{1}{2}\left[\left(\frac{\partial \Phi}{\partial x}\right)^2 + \left(\frac{\partial \Phi}{\partial z}\right)^2\right]_{z=\zeta} + g\zeta = \textit{constant} \; . \tag{30}$$

The third condition is the imposition of a desired initial state upon the system at, let us say, time $t = 0$. This step is closely connected with the technique to be followed in the process of solution, and will not be elaborated upon here. The final object is to specify Φ and ζ simultaneously so as to satisfy (28), (29) and (30). As a general reference Wehausen & Laitone (1960) may be consulted by those who are interested further.

REFERENCES

KUO H. L.: *On the production of mean zonal currents in the atmosphere by large disturbances.* Tellus, 5, 475-493 (1953). — LAMB H.: *Hydrodynamics.* Cambridge Univ. Press, sixth ed. 739 pp. (1932). — LANDAU L. & LIFSHITZ E.: *The classical theory of fields.* Addison-Wesley Press, Cambridge, Mass., 354 p. (1951). — LEVI-CIVITA T.: *Questioni di meccanica classica e relativista.* II. Zanichelli, Bologna (1924). — LORENZ E. N.: *The statistical prediction of solutions of dynamic equations.* International Symp. on Numerical Weather Prediction, Tokyo, Nov. 1960 (in press). — MUNK W.: *Increase in the period of waves travelling over large distances, with applications to tsunamis, swell, and seismic surface waves.* Trans. Am. Geo. Un., 28, 198-217 (1947). — MURAKAMI T.: *On the maintenance of kinetic energy of the annual mean stationary disturbances in the atmosphere for year* 1950. J. Met. (in press 1961). — PLATZMAN G.: *The partition of energy in periodic irrotational waves on the surface of deep water.* J. Mar. Res., 6, 194-202 (1947). — REYNOLDS O.: *On the rate of progression of groups of waves, and the rate at which energy is transmitted by waves.* Nature, 16, 343-344 (1877). — REYNOLDS O.: *On the dynamic theory of incompressible viscous fluids and the determination of the criterion.* Phil. Trans. Roy. Soc. of London (A) 186, 123-164 (1895). — ROSSBY C. G.: *Notes on the distribution of energy and frequency in surface waves.* J. Mar. Res., 6, 93-103 (1947). — SALTZMAN B. & FLEISHER A.: *The exchange of kinetic energy between large scales of atmospheric motions.* Tellus, 12, 374-377 (1960). — STARR V. P.: *Water transport of surface waves.* J. Met., 2, 129-131 (1945). — STARR V. P.: *A quasi-Lagrangian system of hydrodynamical equations.* J. Met., 4, 227-237 (1945). — STARR V. P.: *A momentum integral for surface waves in deep water.* J. Mar. Res., 6, 126-135 (1947a). — STARR V. P.: *Momentum and energy integrals for gravity waves of finite height.* J. Mar. Res., 6, 175-193 (1947b). — STARR V. P.: *Estimates of water transport produced by wave action.* J. Mar. Res., 7, 1-9 (1948). — STARR V. P.: *Review of progress in the study of gravity waves.* Hydrodynamics in Modern Technology, Mass. Inst. of Tech., 153-154 (1951). — STARR V. P.: *Note concerning the nature of the large-scale eddies in the atmosphere.* Tellus, 5, 494-498 (1953). — STARR V. P.: *Commentaries concerning research on the general circulation.* Tellus, 6, 268-172 (1954). — STARR V. P.: *Hydrodynamical analogy to* $E = mc^2$. Tellus, 11, 135-138 (1959a). — STARR V. P.: *Further statistics concerning the general circulation.* Tellus 11, 481-183 (1959b). — STARR V. P. & PLATZMAN G. W.: *Transmission of energy by gravity waves of finite height.* J. Mar. Res., 7, 229-238 (1948). — STOKES G. G.: *On the theory of oscillatory waves.* Trans. Camb. Phil. Soc., 8, 441-455 (1847). — WEBSTER T. F.: *A description of Gulf Stream meanders off Onslow Bay.* Deep-Sea Research (in press 1961a). — WEBSTER T. F.: *The kinetic energy balance of Gulf Stream meanders.* Tellus (in press 1961b). — WEHAUSEN J. V. & LAITONE E. V.: *Surface waves.* Handbuch der Physik, 9, 446-778 (1960).

(*Received 17th April* 1961)

THE EFFECT OF AEROSOLS ON THE ELECTRICAL CONDUCTIVITY IN THE ATMOSPHERE (*)

by S. C. Coroniti (**)

Summary — The value of the electrical conductivity of the free atmosphere is inversely related to the concentration of nuclei. Measurements made with an airborne conductivity meter illustrates this effect. It was found that for these particular meteorological conditions a change of 47 nuclei/cm^3 could be detected. It was also found that in one case nuclei from a smoke source were carried down wind for a distance of 400 miles. The concentration of nuclei varied from 14.6×10^3 nuclei/cm^3 near the source to $1{\cdot}3 \times 10^3$ at the distant location.

In 1948 a research program was initiated by USAF Cambridge Research Center to study the electrical conductivity of the atmosphere at altitudes ranging from sea level to approximately 40,000 feet. The development of an airborne conductivity meter ([1]) required hundreds of hours of flight testing under different meteorological conditions. It had been noted during this period of testing that the values of conductivity depends on the turbulence of, on the relative and absolute humidity of, and on the concentration of the contaminants within the sampled air. Some of these effects have been reported in the literature ([2,3,4]).

The object of this paper is to present two striking examples showing the effect of aerosols on the electrical conductivity of the atmosphere. They suggest possible applications of the airborne conductivity meter as an instrument not only to detect pollutants in the atmosphere but also to study their time-behavior.

The record shown in Figure 1 was taken on July 11, 1950 with an instrument installed in a B-17 aircraft. Its altitude was 2500 feet and its ground speed was 180 miles per hour. Figure 1 is a reproduction of the actual graph recorded on a « Brown Electronic Recorder ». It is a typical record taken under a particular meteorological condition, namely on a clear summer day, around noon. The air at 250 feet was slightly turbulent as evidenced by the bumpiness of the aircraft.

The graph shows that as the B-17 proceeds from right to left the value of conductivity increases until it reaches *C* where a slight but abrupt decrease in value

---

(*) This research was performed while the author was employed by USAF Cambridge Research Center, Bedford, Mass.

(**) Research and Advanced Development Division, AVCO Corporation, *Wilmington, Mass.* (USA).

occurs. At D an abrupt large decrease in value takes place. The decrease in value is attributed to the presence of smoke particles within the sampled air. At C the smoke was not visible; whereas, at D, approximately 1 mile distant from C a white cloud of smoke was present. The source of the smoke was a chimney below.

The electrical conductivity λ is defined as

$$\lambda = nek \tag{1}$$

where

n = the polar concentration of ions per cm^3,

e = the electrical charge in ESU,

k = mobility of ions in ESU.

The interval of measurement for events C and D are of the order of 5 seconds. During this short time interval the concentration of large ions N (nuclei) will not change perceptibly. Hence, equilibrium conditions can be assumed. Under these conditions, the concentration of small ions, n, is given by

$$q = \alpha n^2 + \beta N n \tag{2}$$

where

q = the rate of production of ions,

α = the recombination coefficient between small ions,

β = is a function of combination coefficients for collisions between small ions and nuclei and of the ratio of uncharged to charged nuclei (see Ref. [3])].

From equations (1) and (2) we get

$$\lambda = ek \frac{\beta N \pm (\beta^2 N^2 + 4\alpha q)^{\frac{1}{2}}}{2}. \tag{3}$$

Equation (3) shows that as the value of N increases, the value of conductivity decreases.

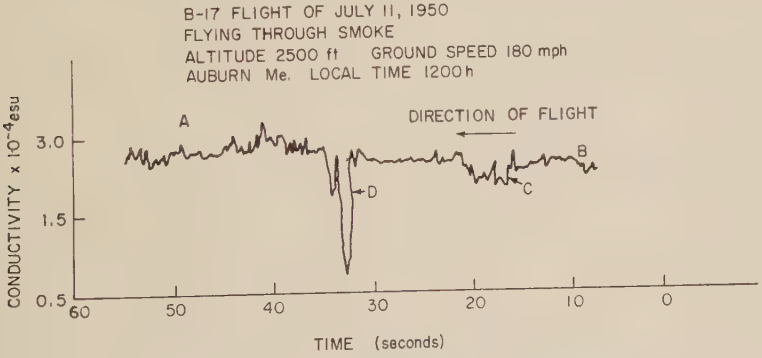

Fig. 1 - *Effect of Smoke on Conductivity.*

The computed value of N is shown in Table 1 for various sections of the curve of Figure 1 using equations (1) and (2). The value of q was taken from Figure 6, p. 195 of Fleming [5].

Table 1 shows that the source of smoke nuclei was at *D*. The change in value of nuclei from *A* to *D* was from 390 to 1210, an increase of 820. This change corresponds to a change in conductivity value of 1.7×10^{-4} ESU. The instrument can measure 0.1×10^{-4} ESU very accurately. Under these conditions the instrument is capable of detecting a change of 47 nuclei/cm³.

TABLE I - *Computed Values of N for Figure* 1.
$\alpha = 1.6 \times 10^{-6}$; $\beta = 2\alpha$; $q = 7.6$; $k = 1.5$ cm²/sec V

Part of curve	λ ESN	n ions/cm³	N nuclei/cm³
A	2.6×10^{-4}	13.8×10^{2}	390
B	2.25×10^{-4}	12.0×10^{2}	580
C	2.1×10^{-4}	11.1×10^{2}	710
D	0.9×10^{-4}	4.8×10^{2}	1210

C represents another pocket of smoke nuclei. These were not visible from the aircraft. The peak value of nuclei/cm³ at *C* is 710, a decrease of 500 from the peak value of *D*. In the interval of time required by the smoke to travel from *D* to *C*, a distance of 0.75 miles, the nuclei have suffered considerable dispersion or settling. In high concentrations, smoke and other aerosols tend to coagulate to form large particles which settle according to gravity and STOKES' Law. This rapid decrease indicates that the lapse rate was high which is to be expected for this particular meteorological condition around noontime, when the measurements were made. Generally, when the lapse rate is high, particles of smoke or aerosols will be diluted rapidly because the air is in a state of instability.

The other example illustrates night-time conditions. During the night the con-

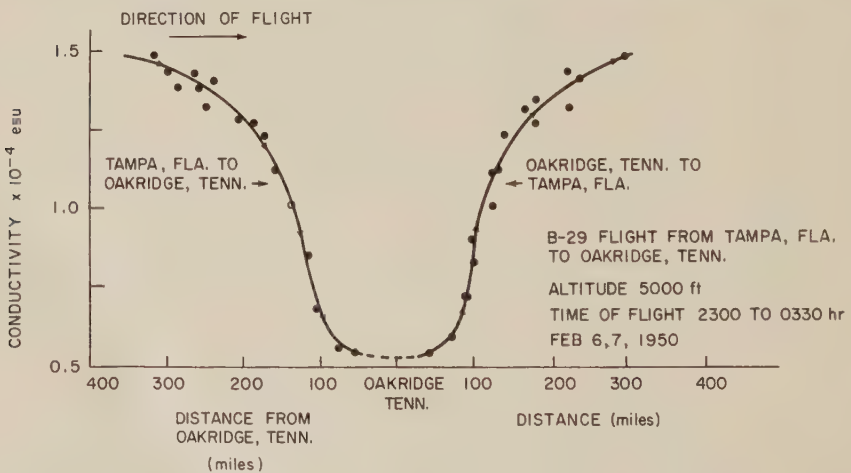

Fig. 2 - *Effect of Aerosols on Electrical Conductivity of the Atmosphere.*

taminants over large cities are trapped beneath and within the inversion layer ([6]). Furthermore, large scale atmospheric motion transport nuclei at an average speed of wind. The smaller the wind speed the more concentrated are the pollutants, provided the pollutant source is a continuous one ([7]). In other words, the concentration of pollutants away from the source decreases slowly with time. An excellent example of these principles is shown by the curve in Figure 1. This curve was plotted from a conductivity record obtained with the same airborne conductivity meter installed in a B-29 aircraft. The flight originated at McDill Air Force Base, Florida at approximately 2300 on February 6, 1950 and proceeded at a constant altitude of 5000 feet toward Oak Ridge, Tenn. at an average speed of 195 miles per hour. Soon after takeoff the conductivity value began to decrease slowly with time and became more rapid as we approached the source where the minimum value was obtained. At this point, the aircraft changed the direction of its course by 180° and headed back for McDill Air Force Base, Florida. During this segment of the flight the conductivity value increased with increasing distance from Oak Ridge. The duration of the flight was 5 hours and 30 minutes.

The remarkable feature of the data is that during a period of up to 4 1/2-hours the concentration of nuclei for any particular volume along the flight path remained constant. In other words, the divergence of the nuclei concentration was zero, indicating an extremely stable atmosphere. Furthermore, it indicates although no radiosonde data have been analyzed that the aircraft was immersed throughout its flight path in or below the inversion layer where the nuclei were trapped.

The computed values of nuclei concentration for distance from the source are shown in Table II.

The value of $q = 5$ ions/sec; $k = 1.5$ cm^2/sec-volt, $\alpha = 2.1 \times 10^{-6}$ cm^3 sec^{-1}; $\beta = 2\alpha$.

TABLE II - *Computed Values of Nuclei/cm^3 versus Distance From Source* (Oak Ridge).

Distance From Source Miles	Nuclei/cm^3 $\times 10^3$
50	14.6
100	4.8
150	1.9
200	1.6
300	1.4
400	1.3

Near the source the nuclei concentration is very high. Its value decreases by a factor of 3 for the next two successive 50 miles after which the decrease is gradual.

It has been shown that since there exists an inverse relationship between electrical conductivity and nuclei concentration [see equation ([3])] the airborne conductivity meter can be employed as a method for measuring the degree of air pollution and for estimating the effectiveness of atmospheric diffusion in dispersing particulate contaminants. It can also be used to measure turbulence.

REFERENCES

([1]) Coroniti S. C.: Geofisica pura e applicata, Vol. 47, 79-83, 1960 — ([2]) Sagalyn R. C. & G. A. Faucher: Jour. of Atmospheric and Terrestrial Physics, 5, 453-273, 1954. — ([3]) Sagalyn R. C. & G. A. Faucher: Quart. Jour. of the Royal Met. Soc., Vol. 84, 428-445, 1956. — ([4]) Sagalyn R. C. & G. A. Faucher: *Recent Advances of Atmospheric Electricity*, edited by L. G. Smith, Pergamon Press, N. Y., 97-123, 1957. — ([5]) Fleming J. A.: *Terrestrial Electricity and Magnetism*, Dover Publication, N. Y. p. 195, 1939. — ([6]) Katz M.: *The Distribution and Dispersion of Contaminants in the Atmosphere*, Proc. 12th International Congress Pure and Applied Chemistry, N. Y., 1951. — ([7]) Magill P. T., F. R. Holden & C. Ackley: *Air Pollution Handbook*, McGraw-Hill Book Co., Inc. N. Y. 1956.

(Received 18th February 1961)

SPECTRAL PROPERTIES OF CLOUDS

by K. S. Shifrin (*)

РЕЗЮМЕ — В коротковолновой области спектральные свойства облаков вызваны только изменениями оптических характеристик воды. Это приводит к небольшим изменениям в индикатриссе рассеяния. В длинноволновой области рассеяние и поглощение носит существенно дифракционный характер. Сообщаются результаты расчетов для типично облачной капли, анализируется точность метода «слоя осажденной воды», исследуются толщины облачных слоев, где входящий в облако поток, постепенно деформируется в поток черного излучения.

Summary — In the shortwave region the variations of the spectral properties of clouds are due only to the variations of optical characteristics of water. It results in small variations in the scattering pattern. In the longwave region scattering and absorption are of essentially diffraction character. Results of computation for a typical cloud drop are given; the accuracy of «the layer of precipitated water» method is analysed; thicknesses of cloud layers are investigated when the flux incoming into a cloud gradually deforms into the blackbody radiation flux.

1. *Introduction.*

It is the aim of the present paper to analyse theoretically spectral properties of clouds on the ground of a detailed analysis of scattering and absorption of radiation by a separate cloud drop.

From the point of view of physical optics, the clouds are an example of a very opaque medium. Radiation properties of such mediums are determined by the values of scattering and absorption of radiation by separate particles.

In ([1]) general formulae which describe the radiation properties of cloud particles are given.

Cloud drops are usually considered to be large and scattering upon them to be neutral in relation to solar radiation, and this is generally true but for some details discussed in § 2. This scheme allows to estimate correctly both the value of albedo and its dependence on the thickness and water content ([2]). Spectral dependences appear when it is necessary to estimate absorption. The estimation is made by the «layer of precipitated water» method ([3,4]).

Thermal radiation transfer in clouds is generally studied with the help of the same values both for the characteristics of thermal radiation scattering and for

(*) Main Geophysical Observatory named after A. I. Voyeykov, *Leningrad*, USSR.

those of solar radiation scattering, while the absorption is studied by the « layer of precipitated water » method ([3,5]).

In spite of the considerable descrepances existing between the taken in this scheme elementary-scattering characteristics and the computation data which will be shown later in this paper, the estimates of radiation properties of a cloud as a whole prove to be valid for thick clouds. The cause of this phenomenon lies in the fact that radiation properties of an optically thick cloud weakly depend on the elementary process characteristics.

When a beam of light enters a cloud, it undergoes a great number of scattering as if it were in the model of KIRCHHOFF's absolute blackbody and finally it is completely absorbed by the drops. The distance from the cloud edge, R^*, where the phenomenon takes place, we shall call the thickness of an active layer of radiation.

Of course, this value is determined by the chosen characteristics of an elementary action. If the thickness of a cloud is $H \gg R^*$, its properties little depend on characteristics of the elementary process, which is like the case when radiation properties of KIRCHHOFF's blackbody model with a sufficiently small opening do not depend on the material the walls of model are made of. It should be clear now that an accurate computation of elementary scattering characteristics is needed to estimate the thickness of R^* — an active layer of radiation — and to analyse some special problems: spectral albedo, spectral coefficient of brightness, etc.

Properties of optically thin clouds with $H \lesssim R^*$ are wholly determined by the elementary action of scattering.

The above conclusion is confirmed by the comparison of the computed by MÖLLER ([6]) clouds radiation properties with the virtual data. The assumption of absolute blackness of clouds proves to be valid for the low and middle layers. This leads to an overestimation of the cloud radiation in the upper layer by the factor about 2 [by 84%, see ([7]), p. 8].

Let us now discuss in detail spectral characteristics of the elementary scattering both in the shortwave and the longwave regions, and then conclude what advantages they offer concerning the clouds spectral properties. It is clear that stronger dependence should be expected in the longwave region.

Our main purpose is to study them.

2. *Scattering pattern of a cloud drop in the shortwave range.*

In this region the cloud drop is a large transparent sphere. When the light is scattered by particles, the spectral changes in scattering arise both due to diffraction and the changes of optical characteristics of the particle matter with the wavelength. The former occurs in dependence on characteristics of scattering from ρ ($\rho = 2\pi a/\lambda$), while the latter depends on the refraction coefficient m ($m = n - ix$).

For finitely large particles it was precisely proved ([1]) that formulae of geometrical optics of the sphere are the first to differ from zero in the expansion of exact formulae in the series by $1/\rho$. This is valid except the directions $\beta = 0, \pi$, and those of rainbows forming the countable number of angles.

In these angles the diffraction effects remain even at the first approximation.

With the exception of directions close to $\beta = 0$ (where we find half of the light scattered by a particle) and those close to the first rainbows, effects of diffraction are neglegible for all the other scattering angles.

In these directions the spectral dependence of scattering (for $\rho = \infty$) will arise only due to the dependence of m on λ.

Detailed calculations have been carried out ([8]) of spectral scattering patterns of the large waterdrops, the scattered light polarization and the rainbows spectral polarization with the help of the geometrical optics formulae taking into account the data of $m(\lambda)$ for liquid water.

Let us discuss the spectral range $\lambda = 0.35 - 1.1\,\mu$. In this case m of the liquid water is real at any point and varies within the limits of 1.3200 to 1.3450. Tables of scattering patterns are given ([8]) separately for both states of polarization « p » and « s », considering five beams of geometrical optics. The tables refer to the scattering angles $\beta = 0, 1, 2, 5\,(5)\,180^\circ$, for six m

1.3200	1.3350
1.3250	1.3400
1.3300	1.3450

The tables ([8]) allow to estimate the accuracy of the neutral drop model, where they usually take $m = 1.3300$.

It is found that the scattering on a drop may be considered neutral, with the accuracy $\pm 10\%$, for all the scattering angles except for the range of $60 - 95^\circ$.

In the above range relative changes of scattering intensity reach 80% with the variation of m (according to $m = 1.3300$).

The coloured arcs polarization has been computed for the first three rainbows ([8]). It proves to be great ($80 - 90\%$) and somewhat increasing from the red to violet rays.

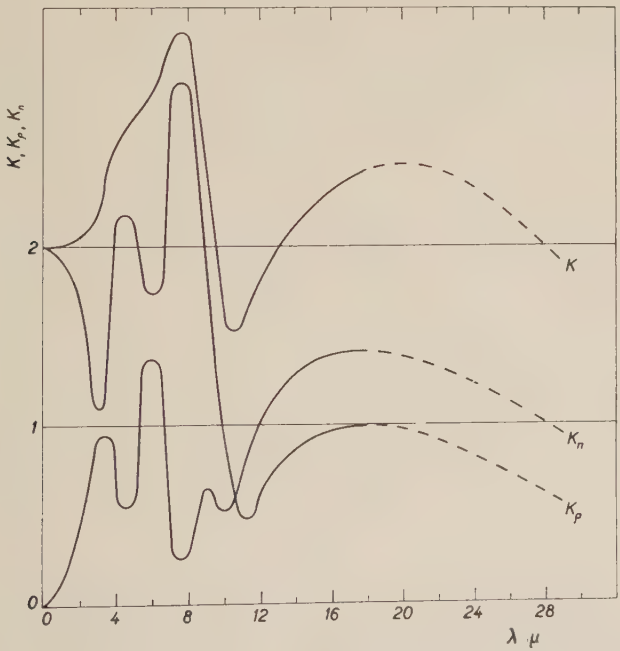

Fig. 1 - *The coefficients of attenuation K, scattering K_p and absorption K_n of a cloud drop for thermal radiation.*

3. *Radiation characteristics in the longwave region.*

a) *Relative role of drops and vapour* — Let us compare attenuation coefficients α^* and α per 1/km in vapour and drops respectively.

For a monodisperse cloud with water content q, particles radii a, vapour and water density σ^* and σ respectively, absorption coefficient in vapour $K(\lambda)$, attenuation coefficient on drops $K(\rho)$, we obtain

$$(1) \qquad \begin{cases} \alpha^* = K(\lambda) \cdot \sigma^* \\ \alpha = \dfrac{3q}{4a\sigma} K(\rho). \end{cases}$$

The respective significance of α^* and α is determined by the relation of temperature and water content. In general these are values of the same order. However, in the important spectral range of 8 — 20 μ, where the main part of the longwave thermal flux is concentrated, the attenuation in vapour is considerably less than that in drops. When crossing the layer of a monodisperse cloud 10 m thick, when $q = 0.5$ g/m^3, $a = 10$ μ. $t = 0^\circ$ C, the attenuation of the thermal radiation flux is 80% due to drops and only 20% due to vapour. This typical example shows that the vapour should be taken into consideration for accurate computation.

Table 1.

λ_μ	ρ	K	K_ρ	K_n	K_ρ'
3	13.121	2.004	1.110	0.894	0.1276
3.4	11.578	2.466	1.541	0.925	0.1348
4.5	8.747	2.646	2.146	0.500	0.1307
6	6.560	2.870	1.743	1.127	0.0273
7	5.623	3.299	2.595	0.704	0.0467
8	4.920	3.201	2.967	0.234	0.0425
9	4.374	2.4921	1.8626	0.6295	0.0505
10	3.936	1.4998	0.9248	0.5750	0.0136
11	3.578	1.233	0.4653	0.7677	0.00808
12	3.280	1.766	0.6321	1.134	0.0166
13	3.028	2.028	0.7922	1.236	0.0245
15	2.624	2.263	0.8869	1.376	0.0342
18	2.187	2.249	1.013	1.416	0.0457
52	0.7570	0.9598	0.1449	0.8149	0.0603
63	0.6248	0.7413	0.1041	0.6372	0.0470
83	0.4743	0.5810	0.06685	0.5142	0.0309
100	0.3936	0.2399	0.01895	0.2210	0.00892
117	0.3364	0.1700	0.01039	0.1596	0.00502

b) *Cloud drop characteristics* — It is difficult to estimate the radiation properties of cloud drops in the longwave range due to the fact that cloud drops can be considered neither « large » nor « small » in the spectral range of 3 — 100 μ and consequently it is impossible to use for them the simple formulae describing

the two finite cases. For example, the value $\rho = 2\pi a/\lambda$ will be about 4 for a drop of the radius $a = 6.265\,\mu$ which is typical for cloud drops and for the wavelength $\lambda = 10\mu$, close to which lies the maximum of blackbody thermal radiation at the cloud temperature. We can see ([1]) that this is a case of diffraction when computations should be made by precise formulae.

We have carried out the computations for a monodisperse cloud, containing drops of the radius $a = 6.265\,\mu$. While doing that we took into consideration variations of ρ, and water optical properties m with the change of λ [([1]), p. 35].

The results of this complicated computation are given in Table 1 (K, K_n, K_ρ are the coefficients of attenuation, absorption, and scattering of a drop respectively in parts of its geometrical section) and in Fig. 1.

The curves for K and K_ρ are alike. Spectral changes of water properties are added to the usual diffraction course of attenuation and scattering. A deep minimum with $\rho = 3.6$ ($\lambda = 11\,\mu$) corresponds, particularly, to a relatively weak reflexion and absorption of these waves by water.

c) *Absorption, radiation, accuracy of the « layer of precipitated water » method* — Spectral properties of liquid water manifest themselves in the absorption coefficient K_n. Large maxima at about $3\,\mu$ and $6\,\mu$ and the gap in the range of 7-9 μ well correspond to the intensive absorption bands and the « window of transparency » in the liquid water spectrum. It is of interest that the absorption coefficient becomes greater than unity at $\lambda = 6\,\mu$ and for $\lambda > 11\,\mu$. This means that the amount of radiation absorbed by a particle is greater than that « falling » on it. This unusual phenomenon is caused by diffraction when a particle « sucks up » the energy of electromagnetic field.

Let us now examine cloud drop radiation (Fig. 2, curve 1). The curve of the blackbody radiation is given for comparison (curve 2). Characteristic phenomena are the radiation maximum at $6\,\mu$ and the region beyond $11\,\mu$.

Table 2.

λ_μ	α 1/cm	$3/4\,\frac{K_n}{a}$ 1/cm
3	7330	1070
6	2140	1350
9	700	754
12	2590	1358
18	2990	1695
52	1160	976
83	710	616
117	360	191

It should be emphasized that in these intervals a drop radiates more than the blackbody. It should be added that spectral properties of a separate drop are identical to those of the layer of drops forming an optically «thin» cloud layer.

Table 2 allows to estimate the accuracy of the « layer of precipitated water »

method, which is generally used for the analysis of radiation absorption by a fog or a cloud layer.

Since an intensive scattering occurs in the fog the difference in attenuation of the fog layer and that of the equivalent layer of precipitated water is obvious. We want to emphasize that a considerable difference exists also in the case of pure absorption. The equivalence of the fog layer to that of precipitated water means the equality of the coefficient of radiation absorption in liquid water α to the value $3/4\, K_n/a$.

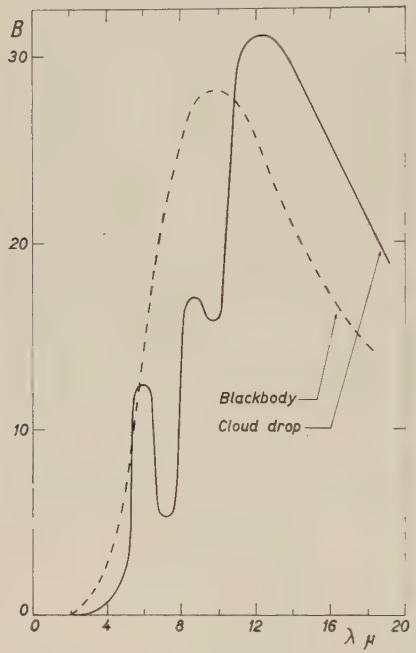

Fig. 2 - *Thermal radiation.*

A comparison of these two values is given in Table 2.

We can see that the absorption in a layer of precipitated water substantially differs from that in the fog. Approximate values for $\lambda = 3\,\mu$ differ from the true ones by the factor 7.

4. *Thermal radiation transfer in clouds.*

a) *Backscattering coefficient* — We shall use the simple method of SCHWARZSCHILD for a study of the thermal radiation transfer in a cloud of a finite optical thickness.

For the fluxes upward ($I_\uparrow$) and downward ($I_\downarrow$) we have

$$\mp \frac{dI_{\downarrow,\uparrow}}{dz} = -\alpha^* I_{\downarrow,\uparrow} + \alpha' I_{\uparrow,\downarrow} + \alpha_n B(z) \tag{2}$$

H is the thickness of a cloud. The flux $I_\downarrow = I_0$ comes on its upper boundary, while the flux $I_\uparrow = I^0$ comes on its lower boundary. $B(z)$ is the blackbody radiation function, α^*, α' and α_n are coefficients of attenuation, backscattering and absorption, calculated per unit volume of a cloud.

Here the meaning of the attenuation coefficient differs from that in the case of « thin » layers. It can be determined through α' and α_n by the formula

$$\alpha^* = \alpha' + \alpha_n \tag{3}$$

α_n is computed through the absorption on particles and water vapour, while α' is estimated by integrating the scattering pattern in the range of scattering angles β from $\pi/2$ to π. It is convenient to bear in mind that when the scattering pattern is unknown and the amplitudes of partial waves are computed as b_l and c_l, then from the known formulae [(1), pp. 55-56] it may be readily concluded that

$$K_\rho' = \frac{2}{\rho^2} \operatorname{Re} \left\{ BC^* + \Sigma \eta_{l,m} \right\} + \frac{1}{2} K_\rho . \tag{4}$$

Here K_ρ' is the backscattering coefficient on a particle (in parts of πa^2)

$$B = \sum_l f_l b_l \qquad C = \sum_l f_l c_l .$$

where $f_l = 0$ when l is even, and

$$f_l = \frac{(-1)^{\frac{l-1}{2}} \, l!!}{2^{\frac{l-1}{2}} \, [(l-1)/2]!}$$

if l is odd,

$$\eta_{l,m} = (c_l c_m^* + b_l b_m^*) \frac{(m+1)(l+1)[m f_m f_{l-1} - l f_l f_{m-1}]}{l(l+1) - m(m+1)} .$$

The results of computing K_ρ' by these formulae are given in Table 1 (column 6).

An advantage of SCHWARZSCHILD's method as compared with accurate methods lies both in its simplicity and in the fact that it is not necessary to know the whole value of scattering pattern as it is sufficient to know the value of K_ρ', i.e. the distribution of a diffused flux between the front and the back hemispheres.

d) *Radiation boundary layer* — The equation of transfer (2) can be solved as follows:

$$\begin{cases} I_\downarrow(z) = [I_0 - B(H)] \, e^{x(z-H)} + \mu [I^0 - B(0)] \, e^{-xz} + B(z) \\ I_\uparrow(z) = \mu [I_0 - B(H)] \, e^{x(z-H)} + [I^0 - B(0)] \, e^{-xz} + B(z) \end{cases} \tag{5}$$

where $\mu = \alpha'/2\alpha_n$.

The fluxes incoming into a cloud fade at the depth

$$R^* = \frac{3}{x} = \frac{3}{\alpha_n \sqrt{1 + 4\mu}} . \tag{6}$$

Whatever may be the radiation flux entering the cloud it becomes a flux of the blackbody radiation at the temperature of the examined cloud level, at some distance R^* from the cloud edge.

Let us consider for example a cloud with the temperature $t = -8^\circ$ C and wa-

ter content $q = 0.5$ g/m^3. Values μ and R^* (metres) for the case are given in Fig. 3.

The depth of penetration of the radiation R^* is different for various λ.

Since $\mu \ll 1$, R^* depends only on the absorption on drops and in vapour. In the regions of 4, 5, and 8 μ the absorption is small. Such a radiation penetrates into a cloud deeper than any other.

Consequently a cloud may be divided into two parts according to the character of the radiation processes, i.e. the inner part where the fluxes penetrating a cloud upward and downward are close to the radiation fluxes inside the blackbody, and the boundary layers where we find the spectral deformation falling from the outside radiation into the blackbody radiation. The boundary layers are active in relation to radiation, while the inner regions are passive. Radiation crosses them without any qualitative changes.

In the case of a thick cloud we obtain a simple formula for the radiation balance fluxes, $R(z)$.

$$R(z) = I_\downarrow - I_\uparrow = \beta \frac{dT}{dz} \qquad \beta = \frac{2}{(\alpha^* + \alpha')} \frac{dB}{dT}. \tag{7}$$

Thus, the radiation balance is proportional to the temperature gradient. Its value is very small. For example, at $t = 0^\circ$ C, $\nabla T = 5^\circ$/km, $q = 0.05$ g/m^3 we find for

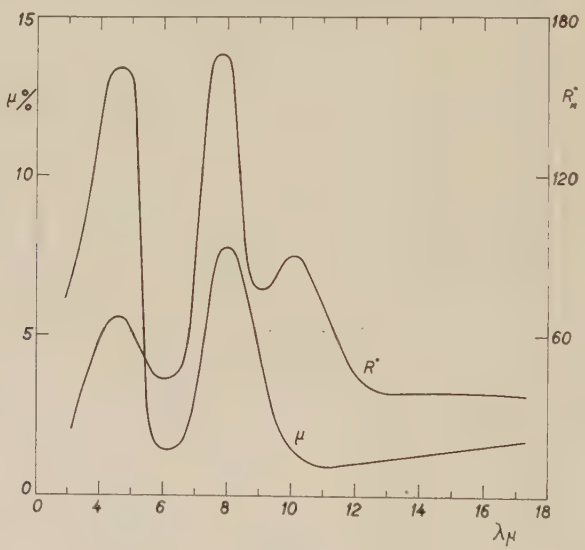

Fig. 3 - μ = *Albedo*, R^* = *Thickness of radiation boundary layer.*

the integral radiation balance $R = 0.01$ cal/cm^2 min. For large q it is even smaller. The fact of equality of the radiation balance inside a thick cloud to zero has been corroborated by V. L. Gaevsky who has made direct measurements of thermal radiation fluxes in clouds with the help of an aircraft ([11]).

e) *Longwave albedo* — For an optically « thick » cloud ($H \gg R$) the fluxes

on the lower and upper boundaries are respectively

$$\begin{cases} I\downarrow(0) = \mu I^0 + B(0)(1-\mu), \\ I\uparrow(H) = \mu I^0 + B(H)(1-\mu). \end{cases} \tag{8}$$

The flux coming to the cloud from below is I^0. It can be seen from (8) that the flux returned by the cloud consists of two parts. The first part is proportional to I^0, while the other is proportional to PLANCK's radiation function. The value μ in (8) is obviously the longwave albedo. The curve $\mu(\lambda)$ in Fig. 3 shows that the albedo in the examined case has two maxima for 5 μ and 8 μ equal to 13% and 8% respectively. On the average it is 2% for the whole spectrum.

f) *Radiation* — It may be seen from the formulae (5) and (8) that the radiation of the system certainly does not exceed the blackbody radiation, if the finite optical thickness is considered.

5. *Conclusion.*

Spectrum of clouds and fogs should be taken into consideration for the study of real polydisperse clouds. It has been found that in various cases it is well described by the general formula of four parameters:

$$f(a) = Aa^{\mu} e^{-\beta a^{\gamma}}. \tag{9}$$

This formula agrees also with HAGEMAN's data on the distribution of drops in fogs near the earth ($\mu = 8$, $\gamma = 0.5$) ([12]), SCHUMAN's data ($\mu = 2$, $\gamma = 3$) ([13]), the data of HRGIAN & MAZIN for clouds ($\mu = 2$, $\gamma = 1$) ([14]), etc.

The above results may be readily generalized for polydisperse clouds if we consider (9) and use the approximate method of estimating spectral characteristics for drops of different sizes, which has been developed in ([7]).

REFERENCES

([1]) SHIFRIN K. S.: *Light scattering in opaque medium*, GITTL, 1951. — ([2]) FRITZ S.: J. Meteor., 11, 291-300, 1954. — ([3]) HEWSON E. W.: Quart. J. Roy Met. Soc. 69, 298, 1943. — ([4]) FRITZ S.: J. Meteor. 15, 51-58, 1958. — ([5]) FEIGELSON E. M.: Isvestia AN, Geophysics, N 4, 1951. — ([6]) MÖLLER F.: *Handbuch der Geophysik*, 8, Kap. 11, 696, 1942. — ([7]) SHIFRIN K. S.: Trudy GGO, N 46 (108), 5-33, 1955. — ([8]) SHIFRIN K. S. & RABINOVITCH J. I.: Isvestia AN, Geophys. N 12, 1957. — ([9]) SHIFRIN K.S.:Doklady AN SSSR, 44, N 4, 1954. — ([10]) SHIFRIN K. S.: Trudy GGO N 46 (108), 34-58, 1955. — ([11]) GAEVSKY V. L.: Trudy GGO, N 46 (108), 59-69, 1955. — ([12]) SHIFRIN K. S. & BOGDANOVA N. P.: Trudy GGO, N 46 (108), 1955. — ([13]) SCHUMAN T.: Quart. J. Roy. Met. Soc., 66, 195, 1940. — ([14]) HRGIAN A. X. & MAZIN I. P.: Trudy CAO, N 7, 1952.

(*Received 5th January* 1961)

EIN EINFACHER NIEDERSCHLAGSINDIKATOR

von D. PAFFRATH (*)

Zusammenfassung — Der Niederschlagsindikator bewirkt bei einem normalen elektrischen Schreiber einen Ausschlag, durch den Beginn, Ende und Dauer eines Niederschlages festgelegt sind und der darüber hinaus bei schwachen Niederschlägen auch deren Intensität anzeigt.

Summary — By a simple measuring equipment beginning, ending and duration of precipitations are recorded with a common recorder. Furthermore, the intensity of weak precipitation is measured.

Résumé — Un appareil simple donne le commencement, la fin et la durée des précipitations en registrant ces moments avec un enrégistreur usuel. Il mesure en plus l'intensité des précipitations très faibles.

Für gewisse Untersuchungen (z.B. auf dem Gebiet der atmosphärischen Elektrizität) ist es wichtig, Beginn und Ende aller Niederschläge auch des feinsten Nieselns oder von nur wenigen Schneeflocken, möglichst genau zu erfassen. Die normalen meteorologischen Instrumente (Regenschreiber nach HELLMANN u.a.) versagen hier bekanntlich; und es besteht überhaupt die Schwierigkeit, weniger als ein Tropfen auf 10 m^2 (und schon diese geringe Menge ist ein Niederschlag) meßbar zu erfassen. Es bleibt also nur die meßtechnische Forderung, ein Gerät zu finden, mit dem man den ersten und letzten Tropfen bezw. Schneeflocke eines Niederschlags auf eine bestimmte Auffangfläche ermitteln kann.

Ob zwei in der letzten Zeit bekannt gewordene Niederschlagschreiber dieser Forderung genügen, scheint zweifelhaft zu sein. Bei beiden kommt es darauf an, daß der in einem Auffanggefäß gesammelte Niederschlag erst wieder zu Tropfen geformt wird, die abfallen und dann einen elektrischen Kontakt schließen. Bis zur ersten Anzeige des Niederschlags vergeht demnach eine mehr oder weniger lange Zeit, die von den Eigenschaften des Auffanggefäßes und von der Intensität des Niederschlags abhängt. Aus den Veröffentlichungen ist zu entnehmen, daß mit dem Gerät von ADKINS (1959) noch Niederschläge von 0.015 mm/min und mit dem von FINK (1960) noch 0.004 mm/min erfaßt werden können. Dabei arbeitet das erstgenannte mit einem umfangreichen elektronischen Verstärker, der auf einen

(*) Deutscher Wetterdienst, Meteorologisches Observatorium *Aachen*, jetzt: Flugwissenschaftliche Forschungsanstalt e.V. (FFM) *München, Flughafen Riem.*

gewöhnlichen Stromschreiber geschaltet wird, während im letztgenannten ein Transistor die Impulse verstärkt und ein Schreiber besonderer Bauart die Aufzeichnung liefert.

Nach einem Vorschlag von G. Fries werden Tropfen eines ausreichenden mechanischen Impulses durch einen in den Wind gedrehten Telefonhörer aufgenommen, dessen Stromimpulse verstärkt und integriert einem normalen Schreiber zugeleitet werden; die Auffangfläche kann hier leicht vergrößert werden. Für leichtes Nieseln, sacht fallenden Schnee und ausnässenden Nebel ist auch dieses Verfahren ungeeignet.

Ein Indikator, der ohne Zeitverzögerung arbeitet und der auch in seiner Empfindlichkeit nicht von speziellen Eigenschaften der Niederschlagsteilchen (wie dem mechanischen Impuls) abhängt, beruht auf einer zuerst wohl von J. Wiesner (1895) angegebenen und durch W. Kopp (1949) ausgebauten Methode des Auffangens der Tropfen auf einem chemisch getränkten Papier (z.B. Eosin), das durch die Flüssigkeit gefärbt wird. Dieses Verfahren liefert zugleich die Tropfengröße, sein Ergebnis ist gewissermaßen ein « Bild » des gefallenen Regens (Regenbildschreiber). Es hat den Nachteil, daß eine Aufzeichnung auf einem normalen elektrischen Schreiber, womöglich zusammen mit anderen Kurven, nicht möglich ist.

Das aber war im vorliegenden Falle gerade gefordert; auf die Erfassung der Tropfengröße im Einzelnen konnte dabei verzichtet werden. Notwendig war aber, daß der Niederschlagsindikator sehr einfach aufgebaut, robust im Betrieb und an sehr unterschiedliche Stromquellen und Schreiber anpaßbar sein sollte.

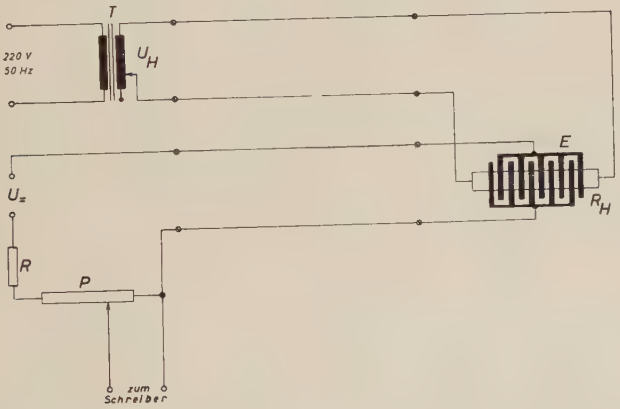

Abb. 1 - *Schaltung des Niederschlagsindikators.* Durch entsprechende Wahl der Grössen U, R, P kann das System an verschiedene Schreiber angepasst werden.

Die Aufgabe ließ sich relativ einfach lösen. Wir möchten nicht behaupten, daß das Prinzip andernorts noch nicht angewandt wurde; da aber eine Veröffentlichung darüber nicht zu existieren scheint, soll es im folgenden beschrieben und so allgemeiner nutzbar gemacht werden.

In seiner einfachsten Form wird der Niederschlagsindikator durch Abb. 1 dargestellt.

Auf einem von innen her elektrisch beheizten Zylinder R_H befinden sich zwei, elektrisch voneinander getrennte, einlagige Wicklungen aus blankem versilberten Draht (besser Platindraht), die sich gerade nicht berühren (Elektrodensystem E). Zwischen ihnen wird eine elektrische Spannung $U_=$, deren Höhe in weiten Grenzen wählbar ist, aufrecht erhalten, geliefert aus einer Batterie oder einem einfachen stabilisierten Netzanschlußgerät (Trockengleichrichter und Zener-Diode). Der erste auftreffende Regentropfen oder die erste durch die Beheizung geschmolzene Schneeflocke setzen den Isolationswiderstand von über 10^9 Ohm zwischen den Windungen auf einige 10^4 Ohm herab. Dadurch wird der Spannungsabfall an einem regelbaren Vorwiderstand P stark verändert, und der hieran angeschlossene Schreiber zeigt einen Ausschlag.

Bei geringen Niederschlagsintensitäten liefert das Gerät außer dem Zeitpunkt des Beginns und Endes auch eine Angabe über die Intensität des Niederschlags: der Widerstand zwischen den Windungen ist vom Grad der Benetzung abhängig. Insofern liefert der Indikator bis zur vollständigen Benetzung gewissermaßen eine « integrale » Anzeige, die erst durch die Beheizung « differentiellen » Charakter annimmt. Der Meßbereich ist dadurch begrenzt, daß schließlich die gesamte Lücke zwischen den Drähten andauernd durch neu auftreffende Tropfen naß gehalten wird. Die Größe des Meßbereiches — und zwar sowohl seine untere wie seine obere Grenze — hängt also u.a. wesentlich von der Beheizung ab. Daher kann man z.B. den Meßbereich durch stärkere Beheizung zu höheren Niederschlagsintensitäten verschieben.

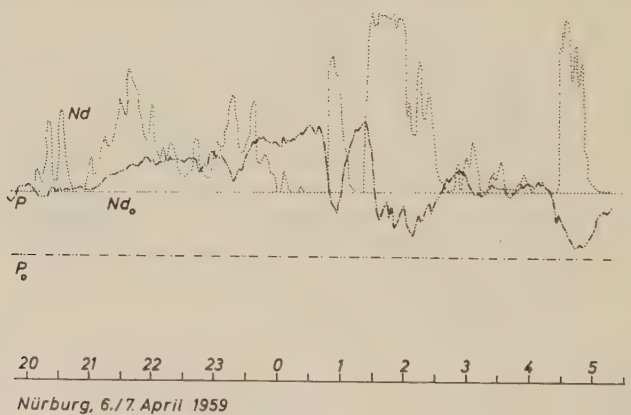

Abb. 2 - *Registrierung des Niederschlags* (Nd) *an der luftelektrischen Station Nürburg, 6./7.4.1959.* Bis gegen 22.30 h GMT Regen, danach Schnee (die feineren Schwankungen wurden bei der Umzeichnung unterdrückt). Die Abbildung zeigt ausserdem den Gang der positiv-polaren elektrischen Leitfähigkeit (P) der Atmosphäre.

Der Niederschlagschreiber kann gut zur Ergänzung des HELLMANN'schen Regenschreibers verwendet werden, dessen Meßbereich er nach geringen Intensitäten erweitert.

In dieser Form wurde der beschriebene Indikator mehrere Jahre lang bei der luftelektrischen Station Nürburg mit gutem Erfolg verwendet. Die hierbei benutzten Spannungen und Widerstände waren: $U_H = 5$ V, $R_H = 20$ Ohm, $U_= = 4.5$ V

(Taschenlampenbatterie), $R = 50$ kOhm, $P = 50$ kOhm; angeschlossen war ein 6-Farben-Kompensations-Punktschreiber.

Abb. 2 gibt ein Registrierbeispiel mit Regen, der gegen 22.30 h GMT in Schnee übergeht. Die Nullinie des Niederschlags $d(N_0)$ wurde zur Orientierung mit eingezeichnet. Sie wird vom Schreiber nur dann geliefert, wenn kein Niederschlag fällt.

Zu einer Abschätzung der Empfindlichkeit dieses Indikators kann man auf folgendem Wege gelangen: Jeder auf den Zylinder auftreffende Tropfen, der einen feuchten Fleck ergibt, dessen Durchmesser größer als der Abstand der beiden nebeneinanderliegenden Windungen (1 mm) ist, führt zu einer Registrierung. Ist n die Zahl der Tropfen, die während des ganzen Niederschlages pro Quadratmeter niederfallen und bedeutet f die senkrechte Projektion des Indikatorzylinders, dann ist die Wahrscheinlichkeit, daß der Zylinder von einem Tropfen getroffen wird: $w = n \cdot f$. Diese Beziehung ist um so genauer erfüllt, je größer n ist (man kann auch sagen: sie gilt im Mittel einer genügend großen Anzahl gleichartiger Niederschläge), denn die Tropfen fallen ja nicht gleichmäßig, sondern statistisch verteilt. Für die folgende Abschätzung soll näherungsweise eine gleichmäßige Tropfenverteilung angenommen werden. In diesem Sinne wird ein Niederschlag, der im ganzen nur aus $n = 1/f$ Tropfen pro Quadratmeter besteht, von dem Indikator mit der Wahrscheinlichkeit Eins angezeigt. Bei dem in Nürburg benutzten Indikator war $f = 15$ cm^2. Folglich wird ein Niederschlag mit der Wahrscheinlichkeit Eins registriert, wenn im ganzen 667 Tropfen auf den Quadratmeter fallen. Rechnet man mit kugelförmigen Tropfen von 2 mm Durchmesser (das sind die Tropfen, die mit Sicherheit zwei nebeneinanderliegende Windungen berühren; in Wirklichkeit dürften die Tropfen noch kleiner sein, da sie beim Auftreffen einen feuchten Fleck von wesentlich größerem Durchmesser bilden), dann entspricht das einem Niederschlag von insgesamt 0.0028 mm.

Ein Niederschlag, der mit der Intensität 0.0028 mm/min fällt, wird demnach im Mittel vom Indikator mit einer Zeitverzögerung von 0.5 Minuten angezeigt. Bei den in Nürburg gemachten luftelektrischen Untersuchungen waren Zeitverzögerungen bis zu einer Minute durchaus zulässig, d.h. von dem in Nürburg verwendeten Niederschlagsindikator wurden noch Niederschläge von weniger als 0.0014 mm/min mit einer mittleren Zeitverzögerung von einer Minute registriert. Bei den Geräten von Adkins und Fink tritt zu dieser statistischen Zeitverzögerung noch ein Zeitverlust, der durch das Sammeln des Niederschlags im Auffangtrichter bedingt ist. Die Empfindlichkeit des beschriebenen Indikators kann durch Vergrößern der Auffangfläche und durch Verkleinern des Abstandes zwischen den Windungen auf dem Zylinder leicht um den Faktor 10 bis 100 gesteigert werden.

Eine Erweiterung des Meßbereiches nach oben ließe sich nach einem Vorschlag von H. Dolezalek dadurch erreichen, daß man den Zylinder rotieren läßt und durch zusätzliche Beheizung der unteren Hälfte dafür sorgt, daß die Auffangfläche stets ganz trocken ist, bevor sie erneut exponiert wird.

Ein Nachteil ist, daß die Genauigkeit nicht sehr hoch ist und sich nur auf einem komplizierten Wege erheblich verbessern läßt. Für viele Zwecke aber wird die erreichte Genauigkeit vollauf genügen.

Über wissenschaftliche Ergebnisse, die unter Zuhilfenahme dieses Indikators in Nürburg erreicht wurden, wird gesondert berichtet.

Für die Anregung und für die Diskussionen möchte ich Herrn Prof. Dr. H. Israël und Herrn Dipl.-Phys. H. Dolezalek an dieser Stelle meinen besten Dank aussprechen.

LITERATUR

([1]) Adkins C. J., 1959: *A rate-of-rainfall recorder.* Quart. Journ. Roy. Met. Soc. *85* (1959), 419-420. — ([2]) Fink C., 1960: *Der Regenintensitätsschreiber.* Met. Rdsch. *13* (1960), 180-182. — ([3]) Fries G., unveröffentlicht, Auskunft beim Met. Obs. Aachen des Deutschen Wetterdienstes, entwickelt 1954. — ([4]) Kopp W., (1949): *Niederschlagsanalysen mit dem Tropfenschreiber.* 1. Tagung Met. Ges. Bad Kissingen. In: Ber. Dtsch. Wetterd. US-Zone *2* (1950), 241-247. — ([5]) Wiesner J., 1895: *Beiträge zur Kenntnis des tropischen Regens.* Sitz. Ber. Wien. Akad. Wiss. *104*, (I), 1397-1437.

(*Eingegangen am 17. März 1961*)

PERTURBATION EQUATIONS FOR THE TIME-AVERAGE STATE OF THE ATMOSPHERE INCLUDING THE EFFECTS OF TRANSIENT DISTURBANCES

by Barry Saltzman (*)

Summary — The time-average, or « stationary », state of the atmosphere can be regarded as a forced response to large-scale transient eddy transports of heat and momentum, as well as to fixed sources and sinks of heat and momentum resulting from small-scale transient eddy processes, non-adiabatic processes (e. g., radiation and phase transformations), topography, and friction. Perturbation equations governing this response are derived and a program of research based on the equations is proposed.

1. *Introduction.*

The influence of large-scale heat sources and sinks on the zonally-asymmetric stationary motions has been discussed by Smagorinsky (1953) and others, and the influence of mountains has been discussed by Charney & Eliassen (1949) and others. It is my purpose here to show how these treatments can be extended, within the framework of a single development, to include explicitly the effects of heat and momentum transfer by the transient disturbances. The method followed is similar in certain respects to that used by Kuo (1956) in his study of the zonally-symmetric motions.

2. *Fundamental equations.*

Using the notation,

λ = longitude
φ = latitude
p = pressure
t = time
$u = a \cos \varphi \, d\lambda/dt$ = zonal component of the wind
$v = a \, d\varphi/dt$ = meridional component of the wind
$\omega = dp/dt$ = individual pressure change
z = height above sea level of an isobaric surface
T = temperature
$\dot{p}$ = rate of heat addition per unit mass, due to radiation, conduction, water phase changes, and friction

---

(*) Department of Meteorology, Massachusetts Institute of Technology, *Cambridge* 39, *Mass.* Now at the Travelers Research Center, *Hartford, Conn.* (USA).

g = acceleration of gravity
$\Phi = gz$
a = radius of the earth
R = gas constant for air
J = mechanical equivalent of heat
C_p = specific heat at constant pressure
$R^* = R/J$
Ω = angular velocity of the earth
$f = 2\Omega \sin \varphi$ = Coriolis parameter
x = zonal component of the viscous force per unit mass
y = meridional component of the viscous force per unit mass,

and assuming hydrostatic equilibrium, we may write the fundamental equations governing u, v, ω, z and T in the form,

$$\frac{\partial u}{\partial t} + \frac{u}{a\cos\varphi}\frac{\partial u}{\partial \lambda} + \frac{v}{a}\frac{\partial u}{\partial \varphi} + \omega\frac{\partial u}{\partial p} - \left(f + \frac{u\tan\varphi}{a}\right)v + \tag{1}$$
$$+ \frac{1}{a\cos\varphi}\frac{\partial \Phi}{\partial \lambda} - x = 0$$

$$\frac{\partial v}{\partial t} + \frac{u}{a\cos\varphi}\frac{\partial v}{\partial \lambda} + \frac{v}{a}\frac{\partial v}{\partial \varphi} + \omega\frac{\partial v}{\partial p} + \left(f + \frac{u\tan\varphi}{a}\right)u + \tag{2}$$
$$+ \frac{1}{a}\frac{\partial \Phi}{\partial \varphi} - y = 0$$

$$\frac{\partial \Phi}{\partial p} + \frac{R}{p}T = 0 \tag{3}$$

$$\frac{\partial \omega}{\partial p} + \frac{1}{a\cos\varphi}\left(\frac{\partial u}{\partial \lambda} + \frac{\partial v\cos\varphi}{\partial \varphi}\right) = 0 \tag{4}$$

$$\frac{\partial T}{\partial t} + \frac{u}{a\cos\varphi}\frac{\partial T}{\partial \lambda} + \frac{v}{a}\frac{\partial T}{\partial \varphi} + \omega\frac{\partial T}{\partial p} - \frac{R^*}{pC_P}\omega T - \frac{\dot{q}}{C_P} = 0 \tag{5}$$

Let us now denote a long-time average (or an ensemble average, where the ensemble may be an individual season or month, for example) by a bar, and the instantaneous departure from this average by a prime, (i.e., $x = \bar{x} + x'$). Then if we neglect long term climatic fluctuations (which is to say, $\partial\bar{x}/\partial t = 0$) we can write equations (1) to (5) in the form,

$$\frac{u}{a\cos\varphi}\frac{\partial u}{\partial \lambda} + \frac{\bar{v}}{a}\frac{\partial \bar{u}}{\partial \varphi} + \bar{\omega}\frac{\partial \bar{u}}{\partial p} - \left(f + \frac{\tan\varphi}{a}\bar{u}\right)\bar{v} + \tag{6}$$
$$+ \frac{1}{a\cos\varphi}\frac{\partial \bar{\Phi}}{\partial \lambda} - X = 0$$

$$\frac{\bar{u}}{a\cos\varphi}\frac{\partial\bar{v}}{\partial\lambda}+\frac{\bar{v}}{a}\frac{\partial\bar{v}}{\partial\varphi}+\bar{\omega}\frac{\partial\bar{v}}{\partial p}+\left(f+\frac{\tan\varphi}{a}\bar{u}\right)\bar{u}+$$

(7)

$$+\frac{1}{a}\frac{\partial\overline{\Phi}}{\partial\Phi}-Y=0$$

(8) $$\frac{\partial\overline{\Phi}}{\partial p}+\frac{R}{p}\bar{T}=0$$

(9) $$\frac{\partial\bar{\omega}}{\partial p}+\frac{1}{a\cos\varphi}\left(\frac{\partial\bar{u}}{\partial\lambda}+\frac{\partial\bar{v}\cos\varphi}{\partial\varphi}\right)=0$$

(10) $$\frac{\bar{u}}{a\cos\varphi}\frac{\partial\bar{T}}{\partial\lambda}+\frac{\bar{v}}{a}\frac{\partial\bar{T}}{\partial\varphi}+\bar{\omega}\frac{\partial\bar{T}}{\partial p}-\frac{R^*}{C_{Pp}}\bar{\omega}\bar{T}-Q=0$$

where

$$X=\bar{x}-\left(\frac{1}{a\cos\varphi}\frac{\partial\overline{u'^2}}{\partial\lambda}+\frac{1}{a\cos\varphi}\frac{\partial}{\partial\varphi}\overline{u'v'}\cos\varphi-\right.$$

(11)

$$\left.-\frac{\tan\varphi}{a}\overline{u'v'}+\frac{\partial}{\partial p}\overline{u'\omega'}\right)$$

$$Y=\bar{y}-\left(\frac{1}{a\cos\varphi}\frac{\partial}{\partial\lambda}\overline{u'v'}+\frac{1}{a\cos\varphi}\frac{\partial}{\partial\varphi}\overline{v'^2}\cos\varphi+\right.$$

(12)

$$\left.+\frac{\tan\varphi}{a}\overline{u'^2}+\frac{\partial}{\partial p}\overline{v'\omega'}\right)$$

$$Q=\frac{\bar{\dot{q}}}{C_P}-\left(\frac{1}{a\cos\varphi}\frac{\partial}{\partial\lambda}\overline{u'T'}+\frac{1}{a\cos\varphi}\frac{\partial}{\partial\varphi}\overline{v'T'}\cos\varphi+\right.$$

(13)

$$\left.+\frac{\partial}{\partial p}\overline{\omega'T'}-\frac{R^*}{C_{Pp}}\overline{\omega'T'}\right).$$

Taking X, Y, and Q as known functions of λ, φ and p to be determined by observations, we can regard (6) to (10) as the fundamental « primitive » equations governing the time-averaged (i.e., stationary) state of the atmosphere.

3. *Perturbation equation for the zonally-asymmetric flow.*

We now resolve the average state into two components according to the relations,

(14)

$$\left\{\begin{aligned}\bar{u}&=u_0+u_1\\ \bar{v}&=v_0+v_1\\ \bar{\omega}&=\omega_0+\omega_1\\ \bar{\Phi}&=\Phi_0+\Phi_1\\ \overline{T}&=T_0+T_1\end{aligned}\right.$$

where the quantities having the subscript zero represent a basic state of zonal equilibrium in which

$$\left(f + \frac{u_0 \tan \varphi}{a}\right) u_0 = -\frac{1}{a}\frac{\partial \Phi_0}{\partial \varphi} \tag{15}$$

$$\frac{\partial \Phi_0}{\partial p} = -\frac{R}{p} T_0 \tag{16}$$

$$\frac{\partial}{\partial \lambda}(u_0, v_0, \omega_0, T_0, \Phi_0) = 0 . \tag{17}$$

By virtue of (15) and (16), which represent geostrophic and hydrostatic equilibrium, respectively, we have the thermal wind relation,

$$\left(f + \frac{2u_0 \tan \varphi}{a}\right)\frac{\partial u_0}{\partial p} = \frac{R}{ap}\frac{\partial T_0}{\partial \varphi}$$

and if we take $\partial T_0/\partial \varphi$ to be a constant this implies that

$$u_0 = U_s - \frac{R}{fa}\frac{\partial T_0}{\partial \varphi}\log\frac{P_S}{p} ,$$

where U_s is the value of u_0 at sea level and P_s is the value of p at sea level.

The values of $u_0(\varphi, p)$, $T_0(\varphi, p)$ and $\Phi_0(\varphi, p)$ are assumed to be an approximation to the observed zonally-averaged values of u, T and Φ, respectively, for the time interval or ensemble under consideration. The quantities $v_0(\varphi, p)$ and $\omega_0(\varphi, p)$, (which represent the zonally-symmetric mean meridional motions) and the quantities having the subscript one (which represent the zonally-asymmetric stationary disturbances) are all assumed to be of second order compared to u_0, T_0, and Φ_0. This breakdown is justified as a first approximation by the fact the normal motions for the hemisphere are predominantly in the nature of a zonally-symmetric polar vortex.

Two problems suggest themselves:

(i) to determine the symmetric components, v_0 and ω_0, as the « forced » motions which must be present in order that there exist dynamical consistency between the observed fields of u_0, T_0 and the zonally-averaged parts of X and Q (which we can call X_0 and Q_0),

and

(ii) to determine the zonally-asymmetric fields, u_1, v_1, ω_1, T_1, Φ_1, as the forced conditions which must exist in order that there be dynamical consistency between the observed fields of u_0, T_0 and the asymmetric parts of X, Y and Q (which we can call X_1, Y_1 and Q_1; i.e., $X = X_0 + X_1$, $Y = Y_0 + Y_1$ and $Q = Q_0 + Q_1$).

Aspects of the first problem were treated by Eliassen (1952) and Kuo (1956), and aspects of the second problem were treated by Charney & Eliassen (1949) and Smagorinsky (1953). We shall here formulate the governing differential equations for this second problem.

If, in accordance with the above remarks, we assume that the departures from the zonally-symmetric state defined by (15) to (17) are small enough that we can neglect terms involving their products, we can write the governing equations for

the departures in the form

$$\frac{u_0}{a\cos\varphi}\frac{\partial u_1}{\partial\lambda}+\omega_1\frac{\partial u_0}{\partial p}-Z_0v_1+\frac{1}{a\cos\varphi}\frac{\partial\Phi_1}{\partial\lambda}+X_1=0 \tag{18}$$

$$\frac{u_0}{a\cos\varphi}\frac{\partial v_1}{\partial\lambda}+\left(f+\frac{2\tan\varphi\,u_0}{a}\right)u_1+\frac{1}{a}\frac{\partial\Phi_1}{\partial\varphi}+Y_1=0 \tag{19}$$

$$\frac{\partial\Phi_1}{\partial p}+\frac{R}{p}T_1=0 \tag{20}$$

$$\frac{\partial\omega_1}{\partial p}+\frac{1}{a\cos\varphi}\left(\frac{\partial u_1}{\partial\lambda}+\frac{\partial v_1\cos\varphi}{\partial\varphi}\right)=0 \tag{21}$$

$$\frac{u_0}{a\cos\varphi}\frac{\partial T_1}{\partial\lambda}+\frac{v_1}{a}\frac{\partial T_0}{\partial\varphi}+\Gamma_0\omega_1-Q_1=0\,, \tag{22}$$

where

$$Z_0=\left(f-\frac{1}{a\cos\varphi}\frac{\partial u_0\cos\varphi}{\partial\varphi}\right)\equiv(f+\zeta_0) \tag{23}$$

and

$$\Gamma_0=\left(\frac{\partial T_0}{\partial p}-\frac{R^*}{C_{Pp}}T_0\right). \tag{24}$$

Φ_1 can be eliminated from (18) and (19) by forming the vorticity equation for our problem. In this elimination we assume (i) that $\zeta_0\partial\omega_1/\partial p$ is small compared to $f\partial\omega_1/\partial p$, (ii) that the « twisting term », $a^{-1}\partial\omega_1/\partial\varphi\cdot\partial u_0/\partial p$, can be neglected, (iii) that the vertical advection of vorticity, $\omega_1\partial\zeta_0/\partial p$ can be neglected, and (iv) that the vorticity of the asymmetric mean flow can be evaluated geostrophically (c.f., Kuo, 1959). Thus we obtain

$$\begin{aligned}&\frac{u_0}{a^2\cos^2\varphi}\frac{\partial^2 v_1}{\partial\lambda^2}+\frac{u_0}{a^2\cos^2\varphi}\frac{\partial}{\partial\varphi}\left(\cos\varphi\frac{\partial v_1\cos\varphi}{\partial\varphi}\right)-f\frac{\partial\omega_1}{\partial p}\\&\qquad+\frac{1}{a}\frac{\partial Z_0}{\partial\varphi}v_1=\frac{1}{a\cos\varphi}\left(\frac{\partial Y_1}{\partial\lambda}-\frac{\partial X_1\cos\varphi}{\partial\varphi}\right)=0\,.\end{aligned} \tag{25}$$

Using (20) and the geostrophic relation we can write the energy equation (22) in the form

$$\frac{u_0fp}{R}\frac{\partial v_1}{\partial p}-\frac{1}{a}\frac{\partial T_0}{\partial\varphi}v_1-\Gamma_0\omega_1+Q_1=0\,, \tag{26}$$

which together with (25) forms a closed linear system in v_1 and ω_1, with u_0, Z_0, Γ_0 and $\partial T_0/\partial\varphi$ to be specified as parameters.

We now combine (25) and (26) to obtain the governing differential equation for v_1:

$$\left\{ \frac{1}{a^2 \cos^2 \varphi} \left[\frac{\partial^2 v_1}{\partial \lambda^2} + \frac{\partial}{\partial \varphi} \left(\cos \varphi \frac{\partial v_1 \cos \varphi}{\partial \varphi} \right) \right] + k_1 (\varphi, p) \frac{\partial^2 v_1}{\partial p^2} \right.$$

(27)

$$\left. + k_2 (\varphi, p) \frac{\partial v_1}{\partial p} + k_3 (\varphi, p) v_1 = F (\lambda, \varphi, p) , \right.$$

where

(28) $$k_1 (\varphi, p) = - \frac{f^2 p}{R \Gamma_0}$$

(29) $$k_2 (\varphi, p) = - \frac{f^2}{R} \frac{\partial}{\partial p} \left(\frac{p}{\Gamma_0} \right)$$

(30) $$k_3 (\varphi, p) = \frac{1}{u_0} \left[\frac{1}{a} \frac{\partial Z_0}{\partial \varphi} + \frac{f}{a} \frac{\partial T_0}{\partial \varphi} \frac{\partial}{\partial p} \left(\frac{1}{\Gamma_0} \right) \right]$$

(31) $$F (\lambda, \varphi, p) = \frac{1}{u_0} \left[f \frac{\partial}{\partial p} \left(\frac{Q_1}{\Gamma_0} \right) + \frac{1}{a \cos \varphi} \left(\frac{\partial Y_1}{\partial \lambda} - \frac{\partial X_1 \cos \varphi}{\partial \varphi} \right) \right] .$$

It will be noted that the non-homogenous term F includes the effects of the large-scale transient eddy transports explicitly. These are to be considered as known quantities determined from observation. In this way the non-linearities associated with the non-steady motion are taken into account, the desireability of which was suggested previously by the writer (1959). The problem is to find, by solving (27) and the appropriate boundary conditions, the field of v_1 (and hence of u_1, ω_1, T and z_1) which is consistent with the empirical forcing function, F.

4. *General Boundary Conditions.*

At the « top » of the atmosphere $p = P_T \to 0$ and $\omega = 0$, and we have, from the energy equation (26),

(32) $$\frac{u_{0T} P_T f}{R} \frac{\partial v_1}{\partial p} - \frac{1}{a} \frac{\partial T_0}{\partial \varphi} v_1 + Q_{1T} = 0 ,$$

where the subscript T refers to values at the upper boundary. We may also require that at the upper boundary the kinetic energy per unit volume approaches zero.

We take the lower boundary to be the top of the « friction layer » which is a uniform distance, δ, above the surface of the earth defined by $z = h (\lambda, \varphi)$. We can assume that above $z = h + \delta$ the atmosphere is inviscid (i.e. $x = y = 0$). At $z = h + \delta$ there is, in general, vertical motion due to (*i*) uplifting over the topographical features and (ii) frictionally-induced convergence and divergence in the friction layer (Charney & Eliassen, 1949). Therefore, we can express the vertical motion at the top of the friction layer in the form,

(33) $$w_\delta = w_\delta^M + w_\delta^F$$

where the topographically-induced vertical motion is

$$w_\delta^M = \frac{u_\delta}{a\cos\varphi}\frac{\partial h}{\partial\lambda} + \frac{v_\delta}{a}\frac{\partial h}{\partial\varphi}, \tag{34}$$

and the frictionally-induced vertical motion is

$$w_\delta^F = \frac{D}{a\cos\varphi}\left(\frac{\partial v_\delta}{\partial\lambda} - \frac{\partial u_\delta\cos\varphi}{\partial\varphi}\right), \tag{35}$$

D being a constant and the subscript δ denoting values at the top of the friction layer.

From (33) we can write for $\omega_{1\delta}$ the relation,

$$\omega_{1\delta} = \overline{\frac{u_\delta}{a\cos\varphi}\frac{\partial p_\delta}{\partial\lambda}} + \overline{\frac{v_\delta}{a}\frac{\partial p_\delta}{\partial\varphi}} + \overline{w_\delta\frac{\partial p_\delta}{\partial z}} \tag{36}$$

$$= \overline{\frac{u_\delta}{a\cos\varphi}\frac{\partial}{\partial\lambda}\left[p_\delta + \left(\frac{\partial p}{\partial z}\right)_\delta h\right]} + \overline{\frac{v_\delta}{a}\frac{\partial}{\partial\varphi}\left[p_\delta + \left(\frac{\partial p}{\partial z}\right)_\delta h\right]}$$

$$+ \frac{gD\left(\frac{\partial p}{\partial z}\right)_\delta}{a\cos\varphi}\left(\frac{\partial v_{1\delta}}{\partial\lambda} - \frac{\partial u_{1\delta}\cos\varphi}{\partial\varphi}\right). \tag{37}$$

To further simplify we can set

$$p_\delta = P_\delta + p_\delta^* \tag{38}$$

where P_δ is the standard atmosphere pressure corresponding to $z = h + \delta$ and p_δ^* is the departure representing the surface synoptic variations of pressure. For a level earth P_δ is a constant representing the standard sea level pressure. In the case when topography is taken into account the variations of p_δ^* are small compared to the variations of $P_\delta(h)$ and can probably be neglected. In addition we may simplify (34), and hence (37), by writing

$$w_\delta^M = \frac{U_\delta}{a\cos\varphi}\frac{\partial h}{\partial\lambda}, \tag{39}$$

which is valid to the first order (U_δ is the basic zonal wind current at $z = h + \delta$).

With these approximations, at the lower boundary (26) becomes

$$\left\{\frac{U_\delta f P_\delta}{R}\frac{\partial v_1}{\partial p} - \frac{1}{a}\frac{\partial T_0}{\partial\varphi}v_1 - \frac{gD\left(\frac{\partial p}{\partial z}\right)_\delta\Gamma_0}{a\cos\varphi}\left(\frac{\partial v_1}{\partial\lambda} - \frac{\partial u_1\cos\varphi}{\partial\varphi}\right) =\right. \tag{40}$$

$$\left. = \frac{\Gamma_0 U_\delta}{a\cos\varphi}\frac{\partial}{\partial\lambda}\left[P_\delta(\lambda,\varphi) + \left(\frac{\partial p}{\partial z}\right)_\delta h(\lambda,\varphi)\right] - Q_{1\delta}(\lambda,\varphi).\right.$$

In the absence of sufficient data for the Southern Hemisphere it is not yet possible to integrate over the entire atmosphere, making it necessary to impose a boundary condition at the equator. One such condition can be specified by assuming symmetry between the Northern and Southern Hemisphere.

5. *Program of Research.*

The solution of (28) together with the boundary conditions can probably best be achieved by using finite difference procedures and numerical integration. The modern high speed computer has made an attempt at such an integration feasible. Before this can be done, however, an extensive observational study should be made to determine all of the components of F for which reliable hemispheric data exists. Such a study is now underway. It is to be hoped that integrations based on these empirical distributions will give insight into the comparative roles of the large-scale transient eddy transports and the fixed sources and sinks of heat and momentum due to other effects (i. e., small-scale eddy transport, non-adiabatic processes, deflections of currents by mountains, and friction) in maintaining the stationary perturbations.

We note that if we introduce specific humidity as an additional variable we can separate out for study the effects of the transient eddy transport of latent heat which are now included in F as a component of $\dot{q}$. Such a treatment will be discussed in a future paper.

In order to obtain some idea of the nature of the solution of (28) and the boundary conditions it will be of value to examine analytical solutions for simple distributions and geometries. The works cited in the list of references contain examples of this kind.

Acknowledgement — This research has been sponsored by the Geophysics Research Directorate of the Air Force Cambridge Research Center under Contract Nos. AF19 (604)-6108 and AF19 (604)-4969.

REFERENCES

Charney J. G. & A. Eliassen, 1949: *A numerical method for predicting the perturbation of the middle latitude westerlies.* Tellus, 1, 38-54. — Eliassen A., 1952: *Slow thermally or frictionally controlled meridional circulations in a circular vortex.* Astrophys. Norv., 5, 19-60. — Kuo H. L., 1956: *Forced and free meridional circulations in the atmosphere,* J. Meteor., 13, 561-568. — Kuo H. L., 1959: *Finite-amplitude three-dimensional harmonic waves on the spherical earth.* J. Meteor., 16, 524-534. — Saltzman B., 1959: *On the maintenance of the large-scale quasi-permanent disturbances in the atmosphere.* Tellus, 11, 423-431. — Smagorinsky J. 1953: *The dynamical influence of large-scale heat sources and sinks on the quasi-stationary mean motions of the atmosphere.* Quart. J. R. Met. Soc., 79, 342-366.

(*Received* 18 *February* 1961)

NULLSCHICHT UND TROPOPAUSE (*)

von W. Attmannspacher (**)

Zusammenfassung — An einer mittleren Zustandskurve der Atmosphäre wird gezeigt, daß auf Grund der Umkehr der Vertikalbewegung in der Nullschicht eine bereits vorhandene Tropopause aufgelöst werden und eine neue Tropopause entstehen kann. Die für Hoch- und Tiefdruckgebiete typischen Vertikalbewegungen ergeben die bei diesen Druckgebilden bekannten Tropopausentypen. Auch die starken vertikalen Verlagerungen der Tropopause sind so leicht erklärbar. Eine statistische Untersuchung bestätigt die theoretischen Überlegungen. Die Tropopausen werden in zwei verschiedene Entstehungsarten eingeteilt, die statische und die dynamische Tropopause.

Summary — It can be shown from an average distribution of the atmospheric temperature that because of a reversal in vertical movement in a null layer of first kind, the existing tropopause can be resolved and a new one arise. The typical vertical movement for low and high pressure structures in the process of strengthening and of stationary intensity respectively, results in already known tropopause types. The strong vertical movements of the tropopause are easily explained by the action of the vertical motion on the temperature field. According to their origin it has been suggested that the tropopause be separated into two basic types:

The *static tropopause;* to this type belongs the mixed tropopause which results from radiation conditions in an atmosphere in a state of repose, and the combined tropopause which occurs when the field of mixing and the area of vertical temperature increase from the upper layer of ozone downward, meet.

The second type originates because of dynamic events in the atmosphere and is thus called a *dynamic tropopause.*

1. *Einleitung* — Seit der Entdeckung der Stratosphäre und damit der Tropopause durch Teisserenc de Bort und Assmann im Jahre 1902 ist die Frage nach der Entstehung der Tropopause in der Meteorologie nicht mehr verstummt. Humphreys ([1]), Gold ([2]) und besonders Emden ([3]), waren die ersten, die sich theoretisch mit der Frage beschäftigten, wie dieser Knick im vertikalen Temperaturgradienten zwischen Troposphäre und Stratosphäre entstehen kann. Emden fand dabei (siehe Abb. 1), daß die Temperatur der Stratosphäre weitgehend dargestellt werden kann als Ergebnis der Aus- und Einstrahlung, während in der Troposphäre das Strahlungsgleichgewicht einen überadiabatischen vertikalen Tempe-

(*) Diese Arbeit wurde unterstützt vom US Department of the Army, European Research Office, unter Kontrakt Nr. DA-91-591-EUC-1668 OI 7330-61.

(**) Deutscher Wetterdienst, *Offenbach/Main.*

raturgradienten zur Folge hat, so daß Konvektion eintreten muß und eine Durchmischung der Atmosphäre in diesen Schichten entsteht. Mit Hilfe dieser Strahlungsberechnungen war es möglich, den Übergang von der Troposphäre in die Stratosphäre von dem Bereich mit einem negativen vertikalen Temperaturgradienten in ein Gebiet mit praktischer Isothermie darzustellen. Eine Tropopause in Form einer scharfen Inversion und die starken vertikalen Verlagerungen, d.h. die wetterbedingten Änderungen der Tropopause, konnten so nicht erklärt werden. Daß bei diesen Höhenschwankungen Vertikalbewegungen eine wesentliche Rolle spielten, hat bereits PALMEN [4] vor mehreren Jahrzehnten dargelegt [siehe auch [5]]. In der Literatur gehen die Ansichten über die Möglichkeit, daß die Advektion und die Vertikalbewegung eine Tropopause erzeugen können, zum Teil auseinander. So berechnet z.B. STALEY [6,7] den konvektiven Anteil zur Verschärfung oder Auflösung einer Tropopause und kommt zur Ansicht, daß die Vertikalbewegungen allein keine Tropopause erzeugen oder auflösen können. Dies ist richtig, wenn man — wie dies in der zitierten Arbeit der Fall ist — die Vertikalbewegung über die ganze Nordhalbkugel integriert und ihre Umkehr in der Nullschicht nicht berücksichtigt.

Es ist das große Verdienst DOPORTOS [8], rechnerisch und praktisch die Zusammenhänge zwischen v_z und Tropopause aufgezeigt zu haben. Er kam zu dem Ergebnis, daß die örtlichen Änderungen der Tropopause etwa halb durch die tatsächliche Vertikalbewegung, halb durch zonale Translation, auf deren Bedeutung bereits J. BJERKNES [9] aufmerksam gemacht hat, verursacht werden.

In seinen Arbeiten über die Nullschicht 1. Art (im Folgenden kurz Nullschicht genannt) hat FAUST [z. B. [10]] häufig auf den engen Zusammenhang zwischen Nullschicht und Tropopause hingewiesen. Der beim Nullschichteffekt erforderliche Massenfluß vom Tief zum Hoch bereitet zum Teil Denkschwierigkeiten, doch ist dieser Massenfluß seit nahezu 90 Jahren in der Synoptik bekannt, als C. LEY [11] und H. HILDEBRANDSEN [12] fanden, daß in rund 9 km Höhe die Cirren sich vom niedrigen Druck weg in Richtung des hohen Druckes bewegen. Auf diese Arbeiten wies bereits SCHNEIDER-CARIUS in seinem Buch « Wetterkunde Wetterforschung » hin [13]. LEY schrieb 1872 über die Beobachtung des Cirrenzuges: « Bei den höheren Strömungen befindet sich der höchste Druck im allgemeinen rechts eines Kurses, jedoch zeigen sie deutlich eine zentrifugale Tendenz über den Tiefdruckgebieten und eine zentripedale über den Hochdruckgebieten ».

2. *Theoretische Ueberlegungen* — In diesem Abschnitt soll versucht werden, auf Grund der in der Nullschicht ihr Vorzeichen wechselnden Vertikalbewegung bzw. durch die so erzeugten Temperaturänderungen die Entstehung bzw. Verlagerung der Tropopause schematisch darzustellen. Als Ausgangskurve wurde der vertikale Temperaturverlauf im p-T-Diagramm für Berlin, Jahresmittel 1949 bis 1953, auf Grund der in den Hauptisobarenflächen angegebenen Werte von HOLZAPFEL [14] benutzt. In diesen Mitteln sind die täglichen Wettereinflüsse weitgehend eliminiert. Diese mittlere Zustandskurve zeigt bis etwa 250 mb eine ständige Temperaturabnahme mit der Höhe und darüber nahezu Isothermie. Die Strahlungskurve von EMDEN stimmt in der Stratosphäre sehr gut mit dieser mittleren Kurve überein (Abb. 1). Eine Tropopause wäre hier um 250 mb anzunehmen. Auf Grund der von FAUST gefundenen mittleren Höhe der Nullschicht in Mitteleuropa [15], wurde an dieser Kurve in 267 mb die Existenz einer Nullschicht 1. Art angenommen. Es soll untersucht werden, wie sich die in Druckgebilden im

Mittel auftretenden Temperaturänderungen, bedingt durch Vertikalbewegungen, auf dieses mittlere Zustandsdiagramm auswirken. Die durch Absinken im Hoch bzw. Aufsteigen im Tief in der Troposphäre entstehenden mittleren Temperaturänderungen wurden einer Arbeit von FAUST ([15]) entnommen (Kap. VI, Tab. 1 bzw. 2). Die für Druckgebilde typischen Vertikalbewegungen treten, wie dort gezeigt wird, bei Druckgebilden in Verstärkung und im Falle der intensitätsmäßigen Stationarität auf. Es wurden zunächst die mittleren Temperaturänderungen ausgewählt für Tiefdruckgebiete (Hochdruckgebiete), bei denen am Boden der Druck um mindestens 5 mb gefallen (gestiegen) war bis zu jenem Zeitpunkt, an dem der Druck am Boden zum erstenmal um mindestens 5 mb stieg (fiel).

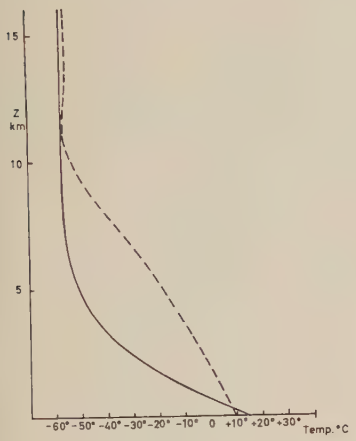

Abb. 1 - *Temperatur-Höhenkurven.*
(———) Bei Strahlungsgleichgewicht; nach EMDEN
(– – – –) Mittlere Werte (1949-53) für Berlin.

Diese mittleren Temperaturänderungen auf Grund der in den Druckgebilden typischen, in der Nullschicht umkehrenden Vertikalbewegungen wurden zu den Werten der mittleren Temperatur-Druckkurve Berlin addiert. Die mittleren Verhältnisse für ein stationäres Tief gibt Abb. 2 wieder. Die Abbildung entspricht dem mittleren vertikalen Temperaturverlauf bei Tiefdruckgebieten (Schlüsselziffer 5 des internationalen Tropopausenschlüssels). Es zeigt sich deutlich, daß praktisch in Höhe der Nullschicht eine Tropopause entstanden ist, die ausschließlich durch die Vertikalbewegung im Tiefdruckgebiet hervorgerufen wurde.

Die für Hochdruckgebiete gültigen Verhältnisse gibt Abb. 3 wieder. Hier hat sich die Tropopause durch die Vertikalbewegung im Hoch nach oben verlagert, sie kommt in diesem Fall nicht ganz 2 km oberhalb der Nullschicht zu liegen. Im Mittel liegt erfahrungsgemäß bei Hochdruckgebieten die Nullschicht 2 km unterhalb der Tropopause. Der Kurvenverlauf in Abb. 3 entspricht den mittleren Verhältnissen in Hochdruckgebieten. Er entspricht der Schlüsselziffer 1 des internationalen Tropopausenschlüssels.

In Abb. 2 und Abb. 3 wurde die in Nullschichthöhe liegende Millibarfläche konstant gelassen, da, wie HOLLMANN ([17]) und ATTMANNSPACHER ([18]) gezeigt haben, die Nullschicht eine Fläche konstanten Druckes, konstanter Temperatur und damit auch konstanter Dichte ist. Wenn man diese Abbildungen betrachtet, erhebt sich sofort die Frage, warum die Tropopause im Falle des Tiefs praktisch in der Nullschicht liegt, im Falle des Hochs rund 2 km darüber. Es läßt sich leicht zei-

gen, daß an diesem Unterschied der vertikale Temperaturgradient in Umgebung der Nullschicht schuld ist. Um dies zu demonstrieren, wurde in Abb. 4 angenommen, daß unterhalb und oberhalb einer tiefen Nullschicht ein stark negativer vertikaler Temperaturgradient vorhanden ist. D. h. die Nullschicht würde z.B. etwa in Höhe der 400-mb-Fläche liegen. Wie aus dieser Abbildung hervorgeht, ist es eine Frage der Größe der durch Vertikalbewegungen bedingten Temperaturände-

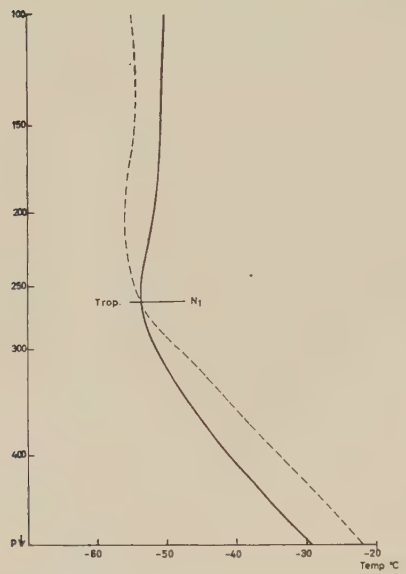

Abb. 2 - *Bildung einer Tiefdrucktropopause*:
(– – – –) Mittlere Temperatur-Druckkurve Berlin (1949-53)
(———) Modifizierte Kurve auf Grund mittlerer, durch Vertikalbewegungen zu beiden Seiten einer Nullschicht mit Aufsteigen darunter entstandene Temperaturänderungen. Trop = neue Tropopause.

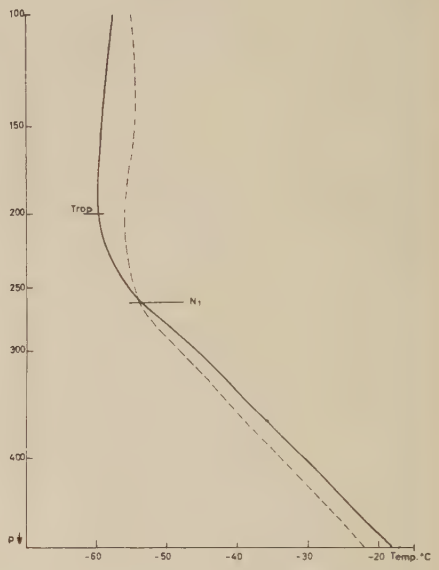

Abb. 3 - *Bildung Hochdrucktropopause*:
(– – – –) Mittlere Temperatur-Druckkurve Berlin (1949-53)
(———) Modifizierte Kurve auf Grund mittlerer, durch Vertikalbewegungen zu beiden Seiten einer Nullschicht mit Absinken darunter entstandener Temperaturänderungen.
Trop = neue Tropopause.

rungen, ob es zur Ausbildung einer tieferliegenden Tropopause kommt oder nicht. In dem hier angenommenen Fall liegt jetzt die Tropopause im Tiefdruckgebiet unter der Nullschicht und weit darüber befindet sich noch die alte Tropopause, die nicht durch den Einfluß des Druckgebildes entstanden ist. Im Fall der Hochdruck-Nullschicht (Abb. 5) liegt die neue Tropopause weit oberhalb der Nullschicht, die vorher vorhandene Tropopause existiert nicht mehr.

Was tritt dagegen ein, wenn die Nullschicht in einem Bereich liegt, in dem praktisch Isothermie herrscht? Bei einer Tiefdrucknullschicht entsteht so eine Tropopause (Abb. 6) unter der Nullschicht, im Hochdruckgebiet (Abb. 7) eine oberhalb derselben.

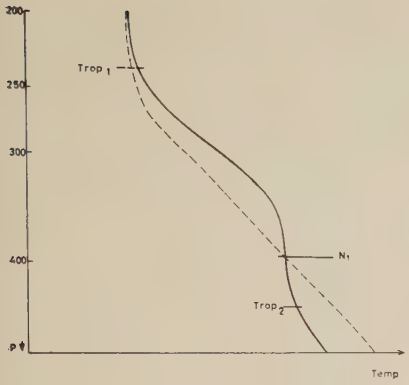

Abb. 4 - *Abhängigkeit des Abstandes Nullschicht-Tropopause vom vertikalen Temperaturgradienten - negativer Gradient:*
(– – – –) Mittlere Temperatur-Druckkurve Berlin (1949-53)
(————) Modifizierte Kurve auf Grund der Vertikalbewegungen zu beiden Seiten einer Nullschicht, unter der Aufsteigen herrscht.
$Trop_1$ = alte Tropopause.
$Trop_2$ = neuentstandene Tropopause.

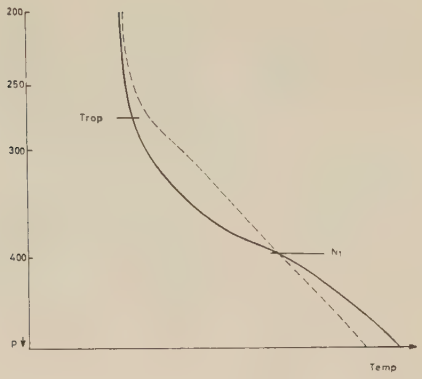

Abb. 5 - *Abhängigkeit des Abstandes Nullschicht-Tropopause vom vertikalen Temperaturgradienten - negativer Gradient*:
(– – – –) Mittlere Temperatur-Druckkurve Berlin (1949-53)
(————) Modifizierte Kurve auf Grund der Vertikalbewegungen einer Nullschicht, unter der Absinken herrscht.

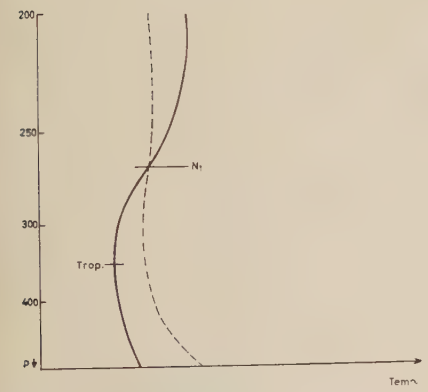

Abb. 6 - *Abhängigkeit des Abstanaes Nullschicht-Tropopause vom vertikalen Temperaturgradienten - positiver Temperaturgradient*:
(– – – –) Mittlere Temperatur-Druckkurve Berlin (1949-53)
(————) Modifizierte Kurve auf Grund der Vertikalbewegung an einer Nullschicht, unter der Aufsteigen herrscht.

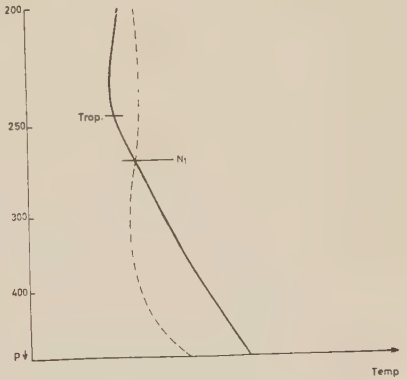

Abb. 7 - *Abhängigkeit des Abstandes Nullschicht-Tropopause vom vertikalen Temperaturgradienten - positiver Gradient*:
(– – – –) Mittlere Temperatur-Druckkurve Berlin (1949-53)
(————) Modifizierte Kurve auf Grund der Vertikalbewegung bei einer Nullschicht, unter der Absinken herrscht.

Es muß weiter das Problem betrachtet werden, was passiert, wenn die Druckgebilde altern. Wie von FAUST ([19]) gezeigt wurde, kehren sich die Vertikalbewegungen in Hoch- und Tiefdruckgebieten um, wenn Druckgebilde sich auflösen; d.h. im Hochdruckgebiet dominiert nun Ausfsteigen, im Tiefdruckgebiet Absinken. Dieser Vorgang ist schematisch in Abb. 8 für das Tief, in Abb. 9 für das Hoch dargestellt. Als Ausgangskurven dienten dabei die vorher in Abb. 2 und 3 erhaltenen mittleren Zustandskurven der beiden Druckgebilde. Um den mittleren Verhältnissen in der Natur möglichst nahe zu kommen, wurden beim Tief (Hoch) die Temperaturänderungen in den Hauptisobarenflächen vom Beginn des Druckanstiegs (-falls) am Boden um mindestens 5 mb bis zum nächsten Termin, an

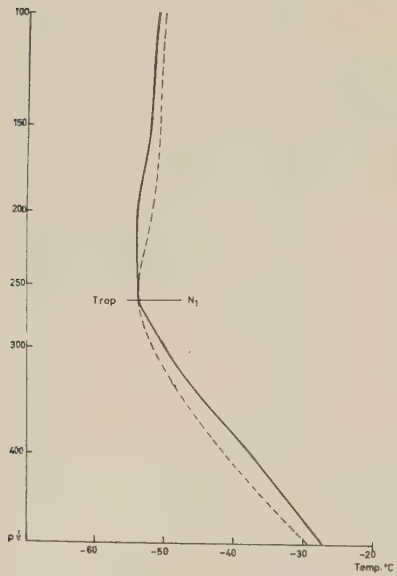

Abb. 8 - *Temperatur-Druckkurve im abschwächenden Tief*:
(– – – –) Temperaturbnahme mit der Höhe auf Grund der Wirkung einer Tiefdrucknullschicht (Abb. 2)
(————) Modifizierte Kurve durch Umkehr der Vorzeichen der Vertikalbewegung auf beiden Seiten der Nullschicht.

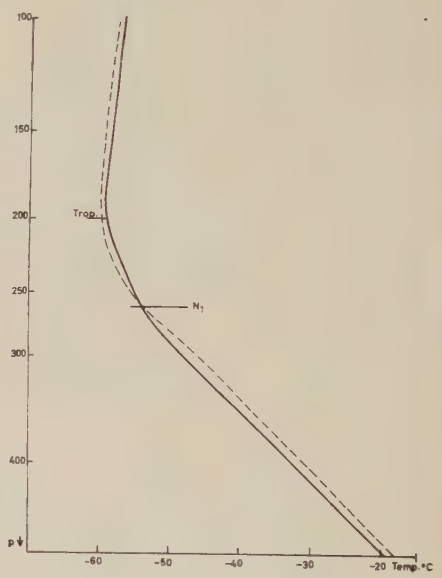

Abb. 9 - *Temperatur-Druckkurve im abschwächenden Hoch.*
(– – – –) Temperaturabnahme mit der Höhe auf Grund der Wirkung einer Wirkung einer Hochdrucknullschicht (Abb. 3)
(————) Modifizierte Kurve durch Umkehr der Vorzeichen der Vertikalbewegung auf beiden Seiten der Nullschicht.

dem der Druck am Boden um weitere 5 mb stieg (fiel) benutzt. Die Zahlen wurden ebenfalls der vorhin zitierten Arbeit entnommen. Wie die Abb. 8 zeigt, resultiert aus diesen Temperaturänderungen ein in der Natur häufig vorkommender vertikaler Temperaturverlauf, der im internationalen Schlüssel mit Nr. 3 bezeichnet ist. Der in Abb. 9 also bei der Auflösung eines Hochs entstehende vertikale Temperaturverlauf ist im internationalen Schlüssel nicht enthalten, er ähnelt jedoch weitgehend dem von SCHMAUSS ([20]) als Typ 3 bezeichneten Tropopausentyp.

Bei Abb. 2 und 3 und hier bei Abb. 8 und 9 liegen, wie bereits gesagt, mittlere Verhältnisse zu Grunde. Im Einzelfall sind weitaus stärkere Vertikalbewegungen möglich, d.h. der Gegensatz der vertikalen Temperaturgradienten oberhalb und unterhalb der Tropopause kann im Einzelfall (z.B. kräftiges Tief) wesentlich stärker sein als dies in den obigen Abbildungen zum Ausdruck kommt.

Bisher war immer davon die Rede, daß nur eine Nullschicht vorhanden war. Wie in einer früheren Arbeit ([21]) gezeigt wurde, ist es aber durchaus möglich, daß zwei, in seltenen Fällen sogar drei Nullschichten übereinander vorkommen können. Damit tritt die Frage auf, wie sich der vertikale Temperaturgradient in der Atmosphäre beim Vorhandensein von wenigstens zwei Nullschichten ändert. Ganz allgemein gibt es dabei 4 Haupttypen von Kombinationsmöglichkeiten, von denen jede wieder 2 verschiedene Ursachen haben kann, einmal ist es denkbar, daß sich eine hohe Nullschicht über eine tiefere schiebt, die andere Möglichkeit ist

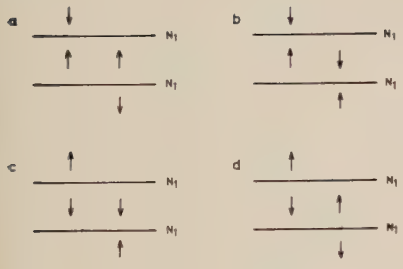

Abb. 10 - *Theoretische Grundmöglichkeiten der Kombination von 2 Nullschichten übereinander.*

Pfeile = Richtung der Vertikalbewegungen.

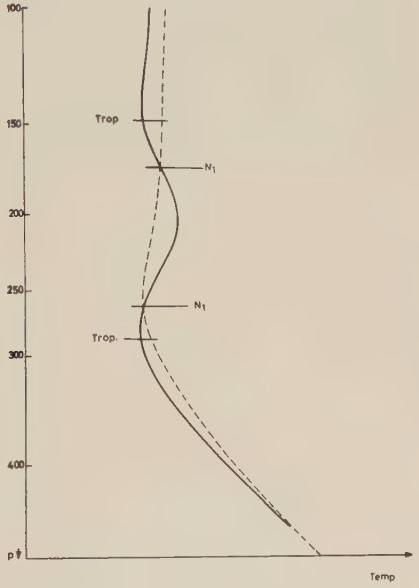

Abb. 11 - *Temperatur-Druckkurve bei 2 Nullschichten.*

Nullschicht mit Absinken darunter wandert über Nullschicht mit Aufsteigen darunter.

(– – – –) Druck-Temperaturkurve bei einer Tiefdrucknullschicht (Abb. 2)

(————) Modifizierte Kurve.

jene, daß die tiefere unter eine höhere wandert. In Abb. 10 sind die 4 Grundmöglichkeiten zusammengestellt, wobei die linken Pfeilpaare die Vertikalbewegung der oberen, die rechten jene der unteren Nullschicht wiedergeben. Wie in ([21]) gezeigt wurde, ist normalerweise eine hohe Nullschicht mit Absinken darunter, eine

tiefe mit Aufsteigen darunter verbunden. Diese Koppelung zwischen der Höhe der Nullschicht und der darunter vorhandenen Vertikalbewegung war bei einfachen Nullschichten gefunden worden, sie muß deshalb bei doppelten Nullschichten nicht unbedingt erfüllt sein. Es dürfte deshalb nicht nur theoretisch interessant sein, die Auswirkungen dieser 4 Grundmöglichkeiten auf den vertikalen Temperaturgradienten schematisch darzustellen.

Abb. 11 zeigt eine vertikale Verteilung der Temperatur, die typisch für eine zu einem intensitätsmäßig stationären Tiefdruckgebiet gehörende Nullschicht ist. Darüber schiebt sich jetzt eine weitere Nullschicht, unter der Absinken herrscht (Fall *c*). Die daraus resultierende Temperaturkurve zeigt, daß sich schließlich eine Tropopause oberhalb der höheren Nullschicht ausbildet, während die untere, ursprünglich bereits vorhandene Tropopause etwas nach unten verlagert wird.

Den Fall, daß eine tiefe Nullschicht mit Aufsteigen darunter unter eine hohe mit Absinken darunter wandert, gibt schematisch Abb. 12 wieder (auch hier handelt es sich um Grundmöglichkeit c). Die oberhalb der oberen Nullschicht liegende Tropopause bleibt darüber, wandert sogar noch etwas nach oben. Unterhalb der tieferen Nullschicht bildet sich eine neue Tropopause aus. Die Anordnung Tropopause/Nullschicht gleicht also jener der Abb. 11.

In Abb. 13 ist nun der Grundfall *a*) angenommen. Die Ausgangs-Druck-

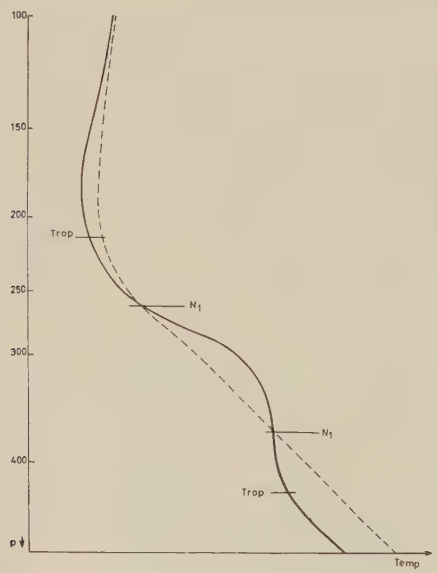

Abb. 12 - *Temperatur-Druckkurve bei 2 Nullschichten.*
Nullschicht mit Aufsteigen darunter schiebt sich unter Nullschicht mit Absinken darunter.
(– – – –) *p-T*-Kurve bei einer Hochdrucknullschicht (Abb. 3)
(———) Modifizierte Kurve.

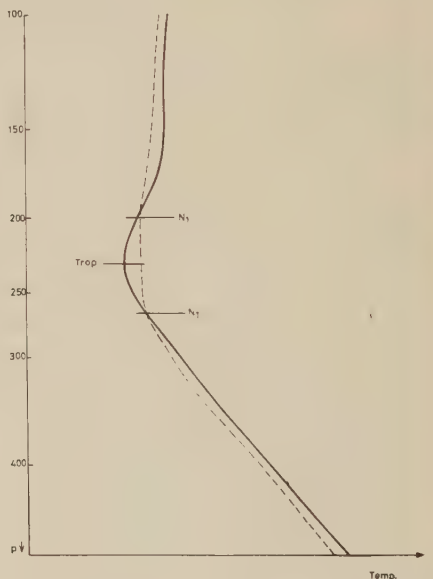

Abb. 13 - *Temperatur-Druckkurve bei 2 Nullschichten.*
Nullschicht mit Aufsteigen darunter scheibt sich über Nullschicht mit Absinken darunter.
(– – – –) *p-T*-Kurve bei einer Nullschicht im abschwächenden Tief
(———) Modifizierte Kurve.

Temperaturkurve entspricht jener der Abb. 8, also dem Fall des abschwächenden Tiefs. Darüber schiebt sich eine Nullschicht, unter der Aufsteigen herrscht. Wie diese Abbildung zeigt, entsteht keine neue Tropopause, die aus den Vertikalbewegungen sich ergebenden Temperaturänderungen verlaufen so, daß die Tropopause dieses Systems zwischen den beiden Nullschichten zu liegen kommt.

Abb. 14 gibt die Verhältnisse wieder, wenn über eine Nullschicht, die zu einem abschwächenden Tiefdruckgebiet gehört, eine sehr hohe Nullschicht, die Absinken unter sich hat, geschoben wird (Fall d). Oberhalb der oberen Nullschicht entsteht eine zweite Tropopause, so daß in der Gesamtanordnung zuerst eine Nullschicht, dann die erste Tropopause, darüber eine zweite Nullschicht und schließlich die zweite Tropopause auftreten.

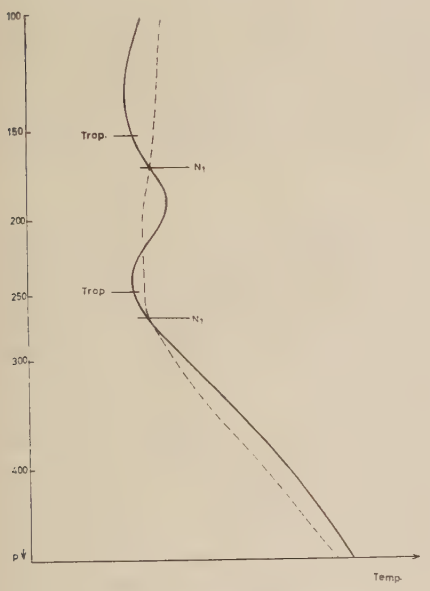

Abb. 14 - *Temperatur-Druckkurve mit 2 Nullschichten.*
Nullschicht mit Absinken darunter schiebt sich über Nullschicht mit Absinken darunter.
(– – – –) *p-T*-Kurve bei einer Nullschicht im abschwächenden Tief
(———) Modifizierte Kurve.

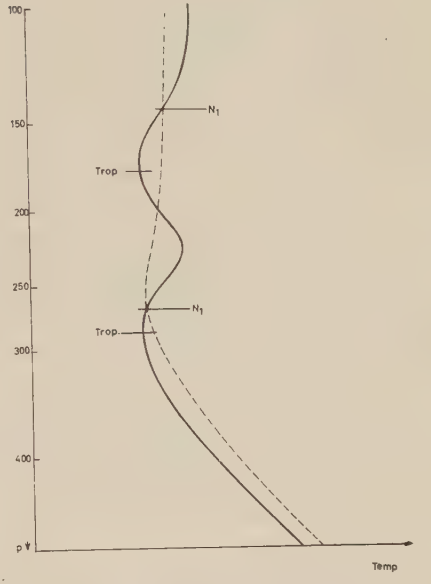

Abb. 15 - *Temperatur-Druckkurve bei 2 Nullschichten.*
Nullschicht mit Aufsteigen darunter schiebt sich über Nullschicht mit Aufsteigen darunter.
(– – –) *p-T*-Kurve bei einer Nullschicht im abschwächenden Hoch
(———) Modifizierte Kurve.

Die vierte Möglichkeit (Fall *b*) könnte ein abschwächendes Hochdruckgebiet darstellen, über das sich die Nullschicht eines heranziehenden kräftigen Tiefs schiebt. Physikalisch ist diese Kombination wenig wahrscheinlich, da die Nullschicht eines Hochdruckgebietes ja grundsätzlich höher liegt als die des Tiefdruckgebietes. Die schematische Kombination aus beiden Nullschichten gibt Abb. 15 wieder. Die untere Tropopause wird hier weiter etwas absinken, während sich unterhalb der oberen Nullschicht eine zweite Tropopause ausbilden kann.

Es sei noch einmal ausdrücklich darauf hingewiesen, daß es zur Ausbildung von 2 Tropopausen durch zwei Nullschichten generell nur dann kommen kann, erstens, wenn die Nullschichten weit genug von einander entfernt sind, so daß der geforderte Mindestabstand von zwei Tropopausen auch erreicht werden kann und zweitens, wenn die Vertikalbewegungen stark genug sind, um genug genügend große Temperaturänderungen hervorzubringen. Die letzte Bedingung gilt natürlich auch bei einfachen Nullschichten und einfachen Tropopausen.

3. *Statistiche Untersuchungen* — Bei der Bearbeitung von Nullschicht-Karten ([22]), die den Zeitraum vom 14.11.54-13.12.54 einschloß, war beim Herausschreiben der Windmaxima aller west- und mitteleuropäischen aerologischen Stationen auch die Höhe und Art der Tropopause festgelegt worden. Da nicht alle Windextreme Nullschichten repräsentieren, mußte geprüft werden, welche Maxima Nullschichten 1. Art darstellen und welche nicht; dies wurde von Frl. E. Soos ([22]) für die Höhen zwischen 850 mb und 100 mb auf Grund der Höhenkarten der Hauptisobarenflächen mit Hilfe eines einfachen Kriteriums ([18]) durchgeführt. Das so erhaltene Material wurde statistisch nach verschiedenen Auswahlprinzipien bearbeitet.

a) *Einfache Nullschichten bzw. einfache Tropopausen.*

Aus den vorhandenen Werten wurden alle Fälle mit einer Nullschicht herausgesucht und festgestellt, ob über den jeweiligen Stationen keine, eine einfache oder eine doppelte Tropopause vorhanden ist. Als Abstand zwischen N_1 und Tropopause wurden dabei maximal ± 3 km zugelassen. Das Ergebnis ist in Tabelle 1 zusammengestellt.

Tabelle 1 - *Einfache Nullschicht* 1. *Art* (Auswahlprinzip) *und Tropopause.*

Zahl der Tropopausen	Fälle	%
0	0	0
1	967	92
2	67	4

Die Tabelle zeigt, daß bei dem Vorhandensein einer Nullschicht fast immer auch eine Tropopause auftritt. Nimmt man die einfache Tropopause als Auswahlprinzip (Tabelle 2), so geht daraus hervor, daß jede einfache Tropopause in diesem Material zumindest mit einer Nullschicht verbunden war. In 94% waren es einfache, in 6% doppelte Nullschichten.

Bei der zugrundeliegenden Wetterlage handelt es sich um kräftig ausgebildete Südwest- bzw. Nordwest-Strömungen, bei denen durchweg eine Nullschicht über Mitteleuropa vorhanden war. Es darf demnach wohl angenommen werden, daß die Vertikalbewegungen bei dieser Lage stark genug waren, um genügend große Temperaturänderungen hervorzurufen, die, wie im vorigen Abschnitt gezeigt wurde,

nötig sind, um eine Tropopause zu erzeugen bzw. die vertikale Lage einer bereits vorhandenen Tropopause stark zu modifizieren. Beide Tabellen zeigen zumindest, daß das Auftreten von Nullschicht und Tropopause sehr eng miteinander gekoppelt ist.

Tabelle 2 - *Einfache Tropopausen* (Auswahlprinzip) *und Nullschicht* 1. *Art.*

Zahl der Nullschichten	Fälle	%
0	0	0
1	967	94
2	67	6

b) *Doppelte Nullschichten bzw. doppelte Tropopausen.*

Wie in der Arbeit von E. Soos dargelegt wurde, war es oberhalb 15 km schwer, den Nullschichtcharakter eines Windmaximums festzustellen, da in Höhe der 96 mb Fläche — und erst recht darüber — die Temperaturmessungen fehlerhaft oder überhaupt nicht vorhanden waren. Um nun beim Kollektiv der doppelten Nullschichten genügend Fälle zu erhalten, mußten alle Windmaxima oberhalb 15 km als repräsentativ für eine Nullschicht gerechnet werden, wenn sie quasi persistent waren, ihre Nullschichteigenschaft jedoch auf Grund fehlender oder zweifelhafter Temperaturmessungen nicht eindeutig festgelegt werden konnte. Es wurde zunächst ausgezählt, wie oft in den Fällen, bei denen über den einzelnen Stationen eine doppelte Nullschicht auftrat, einfache, zwei oder keine Tropopausen vorhanden waren (Tabelle 3).

Tabelle 3 - *Doppelte Nullschicht* 1. *Art* (Auswahlprinzip) *und Tropopause.*

Zahl der Tropopausen	Fälle	%
0	1	1
1	67	37
2	111	62

Die Werte zeigen, daß bei zwei vorhandenen Nullschichten praktisch immer eine Tropopause vorhanden ist. In 62% der Fälle sogar eine doppelte Tropopause.

Das umgekehrte Auswahlprinzip gibt Tabelle 4 wieder. Hier sind alle doppel-

ten Tropopausen zumindest mit einer Nullschicht, in 20% der Fälle mit zwei Nullschichten verbunden. Auch die in Tabelle 3 und 4 zusammengestellten Ergebnisse stimmen mit denen im vorigen Abschnitt angestellten Überlegungen überein.

Tabelle 4 - *Doppelte Tropopausen* (Auswahlprinzip) *und Nullschicht* 1. *Art.*

Zahl der Nullschichten	Fälle	%
0	0	0
1	43	28
2	111	72

Bei der Aufstellung der Werte mit doppelter Nullschicht und doppelter Tropopause zeigte sich, daß in verhältnismäßig vielen Fällen ($\sim 10\%$) die Entfernung zwischen Nullschicht und Tropopause bis zu 4 km betrug. Bei dieser Auszählung der doppelten Nullschichten und doppelten Tropopause wurde deshalb die Grenze zwischen Nullschicht und Tropopause auf ± 4 km herauf gesetzt. Ganz allgemein wurden nur solche Fälle gewertet, bei denen die zur Radiosonde gehörige Windmessung zumindest die Höhe der oberen Tropopause erreicht hatte. Damit ist natürlich für die obere Tropopause die Gewähr des Abstandes von 3 km bzw. 4 km von der dazugehörigen Nullschicht nach oben nicht gegeben, doch reichte die Windmessung der überwiegend größeren Zahl der Fälle in mehr als 3 km über die Höhe der oberen Tropopause hinaus. Interessant schien weiterhin bei den doppelten Nullschichten und doppelten Tropopausen die relative Lage der beiden Schichten zueinander. Eine entsprechende Auszählung gibt Tabelle 5 wieder.

Tabelle 5 - *Relative Lage bei doppelter Tropopause und doppelter Nullschicht* 1. *Art* (111 Fälle).

Nullschicht $\equiv 0$		0		0
	0		0	
	0	0		
Trop. $\equiv -$				
			0	0
%	9	3	84	4

Aus dieser Zusammenstellung geht klar hervor, daß bei der relativen Lage von zwei Tropopausen und zwei Nullschichten 1. Art, die Verteilung dominiert, bei der zuerst, von unten nach oben gesehen, eine Nullschicht, dann eine Tropo-

pause, darüber eine weitere Nullschicht und über der die dazugehörige Tropopause liegt. Diese Verteilung entspricht unserer Abb. 14, der zu Grunde liegt, daß sich über eine Nullschicht im Bereich eines abschwächenden Tiefs eine sehr hohe Nullschicht schiebt, unter der die Luft absinkt. Dieser Fall ist physikalisch durchaus sinnvoll, er entsprach den überwiegend bei dem betrachteten Wetterablauf vorkommenden Fällen. Die mit 9% vertretene Verteilung von doppelten Nullschichten und Tropopausen entspricht der im vorigen Abschnitt aufgeführten Grundmöglichkeit *c*. Das wäre also normalerweise die Verteilung, wie sie beim verstärkenden Tief und beim verstärkenden Hoch im Mittel vorhanden ist. Aus dieser Überlegung ergibt sich bereits, daß derartige Fälle verhältnismäßig selten sein müssen. Die in Spalte 2 der Tabelle 5 dargestellte relative Lage beider Schichten ist denkbar, wenn die Tropopause und die Nullschicht eines aktiven sich verstärkenden Tiefdruckgebietes über Nullschicht und Tropopause eines anderen verstärkenden oder zumindest stationären Tiefdruckgebietes sich schiebt. Das ist im normalen Wettergeschehen sicher nur selten der Fall, so daß die geringe Zahl des Prozentsatzes nicht verwunderlich ist. Die in der letzten Spalte der Tabelle 5 dargestellte relative Lage beider Schichten ist im Höhentemperaturdiagramm schwer meteorologisch sinnvoll realisierbar. Es wurden deshalb die vorliegenden 5 Fälle dieser Art noch einmal eingehend untersucht, und es stellte sich dabei heraus, daß das obere Windmaximum in allen 5 Fällen über 16 km hoch war, so daß eine Kontrolle auf seine Nullschichteigenschaften nicht mehr durchgeführt werden konnte.

Bei den einzelnen Nullschichten, die mit zwei Tropopausen verbunden waren, dominierte eindeutig der Fall, daß unter der unteren Tropopause die einfache Nullschicht 1. Art lag. Diese Verteilung kann damit erklärt werden, daß die in großen Höhen einsetzende Advektion warmer Luftmassen sehr häufig ihre Tropopause mitbringt. Es ist dabei durchaus möglich, daß die obere Tropopause durch eine Nullschicht entstanden ist, die im Ursprungsgebiet der Luftmasse längere Zeit wirksam war.

In allen Fällen mit einfacher Tropopause und doppelter Nullschicht war vielfach die zweite Nullschicht mehr als 4 km von der einfachen Tropopause entfernt, so daß hier von einem genetischen Zusammenhang zwischen dieser zweiten Nullschicht und der darunterliegenden Tropopause kaum mehr gesprochen werden kann. In den übrigen Fällen handelt es sich um einen alten, sich auffüllenden Kaltlufttropfen, über dem die Vorderseite einer neuen Störung zu liegen kam. Diese Kombination entspricht der Abb. 13.

Die zugrundeliegende Untersuchung der Nullschichten bezog sich auf Südwest- bzw. Nordwestwetterlagen. Um wenigstens größenordnungsmäßig erkennen zu können, wie die Verhältnisse bei anderen Wetterlagen sind, wurde noch folgende Statistik durchgeführt. Für den Aufstieg München wurden für die Jahre 1957 und 1958 alle Fälle herausgesucht, in denen zwei oder mehrere Windmaxima in der Vertikalverteilung des Horizontalwindes auftraten, und es wurde festgestellt, wie viele dieser doppelten Windmaxima mit einer oder zwei oder keiner Tropopause verbunden waren. Als maximale Entfernung zwischen Nullschicht und Tropopause waren wieder $\pm$ 3 km zugelassen. Es zeigte sich, daß von 530 Fällen 91% mit einer Tropopause, der Rest mit 2 Tropopausen auftrat. Es sei hier ausdrücklich betont, daß es sich bei diesen Windmaxima nicht um überprüfte Nullschichten handelt. Das umgekehrte Auswahlprinzip ergab, daß von 76 doppelten Tropopausen 74% mit zwei oder mehreren Windmaxima verknüpft waren, während der Rest nur ein Windmaximum zeigte. Die Darstellung der relativen Lage

der doppelten Tropopause und doppelten Nullschicht zueinander ergab 62 Fälle, bei denen die relative Verteilung der einzelnen möglichen Kombinationen, analog zu Tabelle 5, die gleichen relativen Verhältnisse lieferte, wie sie in dieser Tabelle bereits dargelegt wurden. Die zuletzt genannte Untersuchung bestätigt also die aus einem anderen Material gefundenen Ergebnisse. Sie läßt erkennen, daß ein Einfluß der Großwetterlage auf den grundsätzlichen Zusammenhang zwischen Nullschicht und Tropopause unwahrscheinlich ist.

4. *Zusammenfassende Betrachtung* — Die theoretischen Überlegungen haben gezeigt, daß man eigentlich von zwei grundverschiedenen Ursachen bei der Bildung einer Tropopause sprechen muß. Einmal kommt es in der ruhenden Atmosphäre zur Entstehung von Tropopausen, die man vielleicht als *statisch bedingte Tropopausen* bezeichnen könnte, bei denen man 2 Arten festlegen kann: An der Obergrenze der Durchmischungschicht einer im Strahlungsgleichgewicht befindlichen ruhenden Atmosphäre kommt es zur Ausbildung einer *Durchmischungs-Tropopause*. In der Stratosphäre herrscht dann nach Emden praktisch Isothermie. Bei Bestimmung des Strahlungsgleichgewichts einer Atmosphäre, in der Wasserdampf enthalten ist, erhält man, wie Möller ([23]) gezeigt hat, in der Stratosphäre einen Temperaturgadienten von ungefähr 0.3°/100 m. Die Obergrenze der Durchmischungsschicht ist ganz allgemein abhängig von der Einstrahlung am Erdboden und zwar in dem Sinn, daß sie bei stärkerer Zustrahlung höher liegt als bei geringerer Strahlung. D.h. es ergibt sich eine Breiten- und Jahreszeitenabhängigkeit dieser statisch bedingten Tropopause.

Die stark absorbierenden Eingeschaften der Ozonobergrenze und das so entstehende Temperaturmaximum in etwa 45 km Höhe sind seit längerer Zeit bekannt. Wie Faust und Attmannspacher ([24]) gezeigt haben, stellt diese Schicht den Energielieferanten für das zweite in sich geschlossene Zirkulationssystem innerhalb der Atmosphäre dar. Die Erwärmung in 45 km Höhe geht mit zeitlicher Verzögerung und unter Abschwächung der Amplitude [siehe auch ([25])] nach unten. Wenn nun die Obergrenze der Durchmischungsschicht und der nach unten wachsende von der O_3-Obergrenze ausgehende positive Temperaturgradient zusammentreffen, entsteht hier eine Tropopause, die als *Kombinationstropopause* bezeichnet werden könnte.

Durch dynamische Vorgänge im Zusammenhang mit einer Nullschicht 1. Art kann ebenfalls eine Tropopause entstehen, wie in vorstehender Arbeit gezeigt wurde, sie kann dementsprechend *dynamisch bedingte Tropopause* genannt werden. Liegen statisch bedingte Tropopause und Nullschicht nahe beisammen, wie z.B. in den gemäßigten Breiten, so kann die Nullschicht durch die umkehrende Vertikalbewegung und die so entstehenden Temperaturänderungen die statisch bedingte Tropopause zerstören und gleichzeitig die dynamisch bedingte Tropopause aufbauen. Liegen Nullschicht und statische Tropopause weit auseinander, so bildet sich im Bereich der Nullschicht eine dynamisch bedingte Tropopause aus, ohne daß dadurch die statisch bedingte Tropopause zerstört wird. Ein ähnlicher Vorgang scheint in den Subtropen vorhanden zu sein, da, wie Graves ([26]) für Porto Rico gefunden hat, in diesem Gebiet eine primäre Tropopause vorhanden ist, die der statisch bedingten Tropopause entsprechen würde, während eine darunter vorhandene Tropopause von Graves « sekundäre Tropopause » genannt, wetterabhängig ist, wie dies bei der dynamisch bedingten Tropopause der Fall ist. Bei den Subtropen muß allerdings beachtet werden, daß hier die thermisch direkte

Zirkulation dominiert, während in unseren Breiten die thermisch-indirekte Zirkulation maßgebend ist. Eine Untersuchung über die Bedeutung der Nullschicht in den Gebieten mit überwiegend thermisch-direkter Zirkulation wurde noch nicht angestellt, ist aber in diesem Zusammenhang unerläßlich.

Der Gedanke, daß die in der Atmosphäre so markant hervortretende Tropopause weitgehend von der Nullschicht abhängt, mag seltsam klingen. Er wird jedoch vertrauter, wenn man sich klar macht, daß die dynamischen Wettervorgänge von den dreidimensionalen Gradienten der meteorologischen Parameter p, T und ρ beherrscht werden. Wie in ([19]) gezeigt wurde, kann die vertikale Änderung des horizontalen Windes (v_h) als horizontale Komponente des Vektorproduktes $\nabla T \times \nabla p$ dargestellt werden:

$$\frac{\partial v_h}{\partial z} = \frac{R}{f p} \left[\nabla T, \ \nabla p \right]_{h\ Komp} \tag{1}$$

(R = Gaskonstante für Luft, f = Coriolisparameter $= 2\omega \sin \varphi$). Die Vertikalbewegung ergibt sich dann als z-Komponente dieses Vektorproduktes:

$$v_z = \frac{[\nabla T, \ \nabla p]_{z\ Komp}}{\rho f \left(\frac{\partial T}{\partial z} + \Gamma \right)} \tag{2}$$

$$\left(\rho = \text{Luftdichte}; \ \Gamma = \text{trockenadiabatischer Temperaturgradient} = \frac{g}{c p} \right).$$

In der Nullschicht liegen die beiden Vektoren ∇T, ∇p und damit auch $\nabla \rho$ parallel. In einem baroklinen Feld tritt somit eine Barotropie auf; daraus ergibt sich bereits die große Bedeutung der Nullschicht in der Dynamik des Wettergeschehens. In der Tropopause dagegen verschwindet das dreidimensionale Vektorprodukt keinesfalls, nur die z-Komponente des Temperaturgradienten wird 0, eine Größe, die lediglich für den absoluten Betrag der Vertikalbewegung von größerer Bedeutung ist.

Wie vorstehend gezeigt wurde, ist es zumindest im Prinzip möglich, die vertikale Verlagerung einer Tropopause, ihre Neubildung und vor allen Dingen die unterschiedlichen Tropopausentypen durch die Vorgänge im Bereich der Nullschicht 1. Art zu erklären. Bei den theoretischen Überlegungen wurde der Einfluß der Advektion absichtlich nicht berücksichtigt, der natürlich bei den statischen Untersuchungen mit enthalten war. Beide Untersuchungsmethoden ergaben weitgehende Übereinstimmung. Wie groß im Einzelfall bei der Bildung bzw. Verlagerung einer Tropopause der Anteil an Vertikalbewegungen allein ist, kann nur eine quantitative Untersuchung von Einzelfällen klar entscheiden, hierbei dürfte der Entwicklungszustand der Druckgebilde eine große Rolle spielen. Eine derartige Studie kann auch Aufschluß darüber geben, wie weit mit der aus der vorliegenden Arbeit sich ergebenden Tropopausentheorie die in der Natur vorkommenden Tropopausen sinnvoll erklärt werden können.

LITERATUR

([1]) Humphreys W. J.: *Vertical Temperaturgradient of the Atmosphere especially in the Region of the Upper Inversion.* Astrophys. Journal vol. XXIX, 14 (1909). — ([2]) Gold E.: *The Isothermal Layer of the Atmosphere and Atmospheric Radiation.* Proceed-

ings of the Royal Soc. of London, ser. A, vol. 82, 43 (1909). — (3) Emden R.: *Über Strahlungsgleichgewicht und atmosphärische Strahlungen.* Sitzungsberichte der math. phys. Kl. d. K. B. Ak. d. Wissenschaften 55 (1913). — (4) Palmén E.: *Die Beziehungen zwischen troposphärischen und stratosphärischen Temperatur- und Luftdruckschwankungen.* Beitr. z. Phys. d. fr. Atm. 17, 102 (1931). — (5) Chromow S. P.: *Einführung in die synoptische Wetteranalyse.* Springer, Wien, 380 (1940). — (6) Staley D. O.: *A Study of Tropopause Formation.* Beitr. z. Phys. d. Atm. 29, 290 (1957). — (7) Staley D. O.: *Some Comments on Physical Processes at and near the Tropopause.* Archiv. f. Meteorol., Geophys. and Bioklimat. Ser. A 10, 1 (1957). — (8) Doporto M.: *Dynamical Aspects of the Constancy of Air Density at 8 km.* Department of Industry and Commerce, Meteorol. Service, Geophys. Publ. Vol. III No. 6 Dublin (1951). — (9) Bjerknes J.: *Explorations de quelques perturbations atmosphériques à l'aide de sondages rapprochés dans le temps.* Geophys. Publ. 9, No. 9 (1932). — (10) Faust H.: *Nullschichteffekt und Frontalzonen.* Archiv f. Meteorol. Geophys. u. Bioklimat. Ser. A 6, S 338 (1954). — (11) Ley Cl.: *The Laws of the Winds. Part I London* (1872). — (12) Hildebrandson H. H.: *Atlas des Mouvements supérieurs de l'atmosphère.* (Stockholm 1877). — (13) Schneider-Carius K.: *Wetterkunde und Wetterforschung.* Karl Alber, Freiburg München (1955). — (14) Holzapfel R.: *Ergebnisse aerologischer Beobachtungen in Deutschland.* Ber. DWD Nr. 27 (1956). — (15) Faust H.: *Die Nullschicht, der Sitz des troposphärischen Windmaximums.* Meteorol. Rundschau 6, S 4 (1953). — (16) Faust H. & Attmannspacher W.: *Cell Structure of the Atmosphere.* Final Report 1959, Contract DA/91/508/EUC/387, Kap. VI. — (17) Hollmann G.: *Zur Frage des Vorzeichenwechsels der Vertikalbewegung beiderseits isobarer Flächen extremer Windgeschwindigkeit.* Meteorol. Rundschau 12, 137 (1959). — (18) Attmannspacher W.: *Extreme der horizontalen Windgeschwindigkeit und Vertikalwind.* Meteorol. Rundschau 12, 112 (1959). — (19) Faust H.: *Die Nullschicht bei Druckgebilden in Abschwächung.* Meteorol. Rundschau, im Druck. — (20) Schmauss A.: *Die Entdekung der Stratosphäre* 1902. Meteorol. Rundschau 5, 161 (1952). — (21) Attmannspacher W.: *Nullschicht und Wetter.* Mitteilungen des DWD Nr. 20 (1960). — (22) Sóos E.: *Windmaxima mit und ohne Nullschichtcharakter.* Meteorol. Rundschau 12, 118 (1959). — (23) Möller F.: *Die Wärmestrahlung des Wasserdampfes der Atmosphäre.* Gerl. Beitr. Geophys. 58, 11 (1941). — (24) Faust H. & Attmannspacher W.: *Die allgemeine Zirkulation der aussertropischen Breiten bis 60 km Höhe auf der Basis der Nullschichtkonzeption.* Meteorol. Rundschau 14, 6 (1961). — (25) Arnold A. & Lowenthal M. J.: *A sixteen-Month Series of Mid-Stratospheric Temperature Measurements.* Jour. of Meteor. Vol. 16, No. 6, 692 (1959). — (26) Graves M. E.: *The Relation between the Tropopause and convective activity in the subtropics.* Bull. Americ. Meteorol. Soc. 32, 54 (1951).

(*Eingegangen am 6. März* 1961)

MITTELFRISTIGE WETTERVORHERSAGEN MIT SYNOPTISCH-STATISTISCHEN METHODEN (*)

von Heinz Reuter (**)

Summary — The basic concept of synoptic statistical methods for construction of prognostic charts was outlined by the author in a previous paper. As a result of these investigations it was found that a high correlation exists between time and space means of contourheights of an isobaric surface (850 mb surface). As it has been shown later by Pichler this result may be interpreted by assuming that the geopotential fields obeys a numerical solution of the second order homogenous differential equation for wave propagation (hyperbolic equation) provided the phase velocity is given by $c = \Delta s/\Delta t \sqrt{2}$. Since Reuter has used for $\Delta s = 666$ km and for $\Delta t = 24$ hours the conclusion may be drawn that the phase velocity of the wave propagation has an order of magnitude of 5 m/sec. Actually for long waves in the westerlies such a value can be found on an average. The same method can be used for extended forecast procedures if the wave equation is set down for 5 days mean values. Theoretical considerations lead then to a prognostic formula for a 5 days mean chart (8a). This formula can be applied for a sufficient number of grid points in order to construct prognostic charts. The underlying assumption, namely that the mean geopotential field satisfies also a solution of the wave equation turns out to be quite accurate even if only average values of the phase velocity were used for the computation. The usefullness of the method is illustrated for two cases.

Das grundlegende Konzept der synoptisch-statistischen Methode für Konstruktion von Vorhersagekarten wurde bereits in einer früheren Arbeit (Reuter [1])] umrissen. In den letzten Jahren konnten einerseits durch praktische Erprobung der Methodik im Rahmen der zweimal wöchentlich von der Wetterabteilung der Zentralanstalt für Meteorologie in Wien herausgegebenen Mittelfristprognosen (Halbwochenprognosen) reiche Erfahrungen gesammelt werden, andererseits durch theoretische Untersuchungen [insbesondere Pichler ([2,3,4])] die Grundlagen erweitert und mathematisch genauer erfasst und studiert werden. Dadurch ist es möglich geworden, die synoptisch-statistische Methode mit Erfolg auszubauen.

Die Grundlagen der Methode lassen sich etwa folgendermassen formulieren. Die Tatsache, dass wir an Hand des in reichlichem Masse vorliegenden Beobach-

---

(*) Vortrag gehalten am 7. April 1961 auf der 9. Allgemeinversammlung der «Società Italiana di Geofisica e Meteorologia» (Genova, 6.8. April 1961).

(**) Prof. Dr. Heinz Reuter, Zentralanstalt für Meteorologie und Geodynamik, *Wien* XIX, Hohe Warte 38.

tungsmaterials die Änderungen der meteorologischen Feldgrössen (insbesondere der Druck- bezw. Geopotentialverteilung) in vorgegebenen Zeiträumen studieren können, ohne auf Einzelheiten der so äusserst komplizierten thermo-hydrodynamischen Gleichungen eingehen zu müssen, hat schon immer dazu verleitet, statistische Methoden bei der Wetterprognose zu verwenden, die uns einen Hinweis geben sollen, in welcher Weise die Natur selbst das schwierige Problem löst. Bei der synoptisch-statistischen Methode werden gewisse Korrelationen zwischen Anfangs- und Endverteilung meteorologischer Feldgrössen (Geopotentialverteilung einer isobaren Fläche) hergeleitet. Als Ausgangspunkt für die Aufstellung der Korrelationen gelten gewisse « synoptische Prinzipien ». Dabei handelt es sich

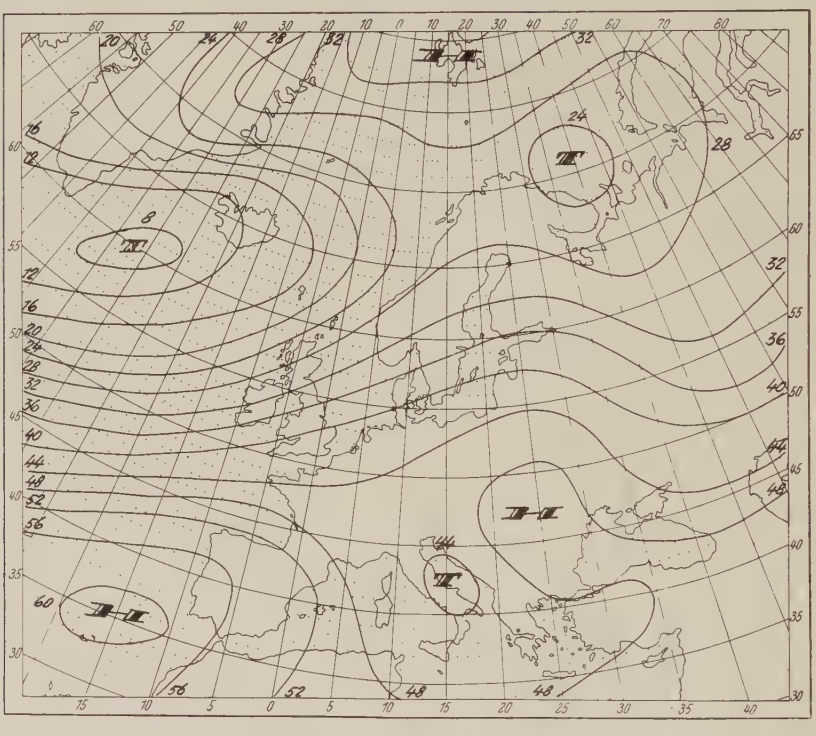

Abb. 1 - *850 mb 01 h — Mittelkarte 26. - 30. I. 1961.*

ähnlich den Prinzipien der theoretischen Physik um Erfahrungssätze, die durch die jahrelangen synoptischen Beobachtungen gewonnen wurden. Hier zeigt sich der Unterschied zu der in den letzten Jahren entwickelten numerischen Voraussage der Druckverteilung. Bei diesem Verfahren wird von den Prinzipien der theoretischen Physik (Energiesatz, Newtonsches Axiom, Erhaltung der Masse, etc.) ausgegangen. Wegen der auftretenden mathematischen Schwierigkeit bei der exakten Lösung der die atmosphärische Dynamik regelnden Differentialgleichungen wird bei der numerischen Methode auf mehr oder weniger realistische Modellgleichungen übergegangen (barotrope und barokline Modelle). Die synoptisch-statistische Methode fasst das Problem der Voraussage der Feldverteilung enger. Sie

stützt sich auf « synoptische Prinzipien », die natürlich implizit die physikalischen enthalten müssen aber sehr wahrscheinlich diejenigen Prozesse, die synoptisch bedeutsam sind, übersichtlicher und vor allem wesentlich einfacher beschreiben. Selbstverständlich besteht bei der Methode die grösste Schwierigkeit darin, solche synoptische Prinzipien aufzustellen und zu formulieren. In der bereits erwähnten Arbeit [Reuter (1)] wurde versucht, einige solcher Prinzipien als Arbeitsgrundlage aufzustellen. Inzwischen hat die Erfahrung gezeigt, dass die ursprüngliche For-

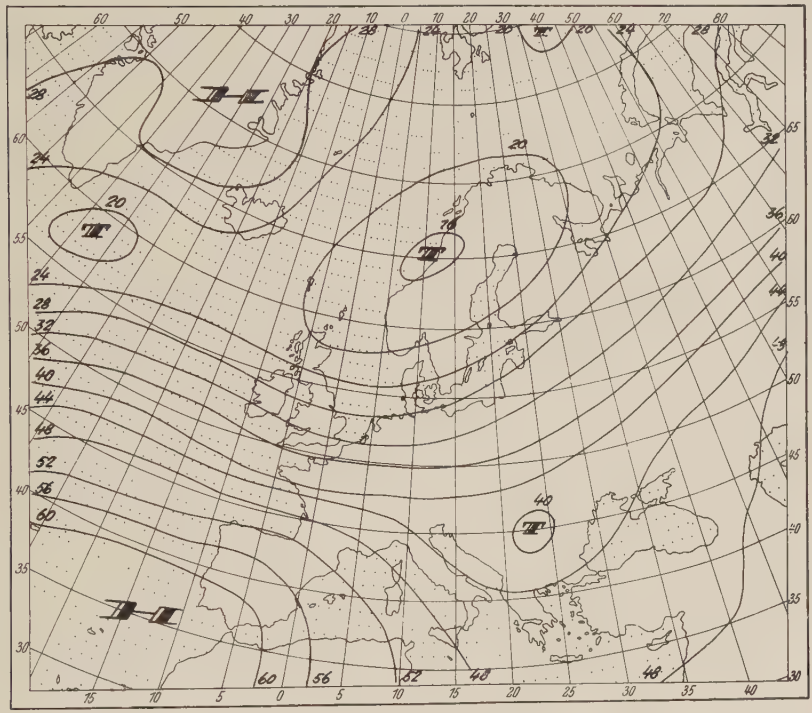

Abb. 2 - *850 mb 01 h — Mittelkarte 30. I. - 3. II. 1961.*

mulierung einer Verbesserung und Erweiterung bedarf. Als Ergebnis dieser ersten Untersuchungen muss aber festgehalten werden, dass es gelungen ist, eine hohe Korrelation zwischen räumlichen und zeitlichen Mittelwerten eines Geopotentialfeldes (850 mb und auch 500 mb Fläche) herzuleiten. Wir wollen dieses Ergebnis, das sich in den letzten Jahren an zahlreichen Fällen als zutreffend herausgestellt hat, als *Aequivalenzprinzip* bezeichnen. Es kann etwa in folgender Weise geschrieben werden:

Mit:

$$\hat{h} = 1/2\,[h\,(x, y, t + \Delta t) + h\,(x, y, t - \Delta t)]$$

$$\bar{h} = 1/4\,[h\,(x + \Delta x, y, t) + h\,(x, y + \Delta y, t) + h\,(x - \Delta x, y, t) + h\,(x, y - \Delta y, t)]$$

gelte:

$$\hat{h} = a\bar{h} + b \,. \tag{1}$$

Als Resultat einer grossen Anzahl von Fällen ergab sich für

$$a = 1.02 \,, \qquad \text{für} \qquad b = 0.09 \,.$$

Dabei verwendete REUTER ein Zeitintervall $\Delta t = 24$ Stunden und ein räumliches Intervall $\Delta x = \Delta y = \Delta s = 666$ km.

Wie das Äquivalenzprinzip zur Konstruktion einfacher Vorhersagekarten verwendet werden kann, wurde in den Arbeiten von REUTER ([1,5]) gezeigt. In seiner ursprünglichen Untersuchung sprach REUTER die Vermutung aus, dass das Äquivalenzprinzip zwischen räumlichem und zeitlichem Mittelwert einem Ausgleichs- oder Kompensationsprozess entspricht. Die theoretische Analyse von PICHLER ([4]) ergab jedoch, dass das Äquivalenzprinzip nur einen Wellenvorgang beschreibt, bei dem allerdings die Phasengeschwindigkeit durch das räumliche und zeitliche Inkrement vorgeschrieben ist. Wir wollen dies hier kurz an Hand der zweidimensionalen homogenen Wellengleichung zeigen. Sie lautet bekanntlich:

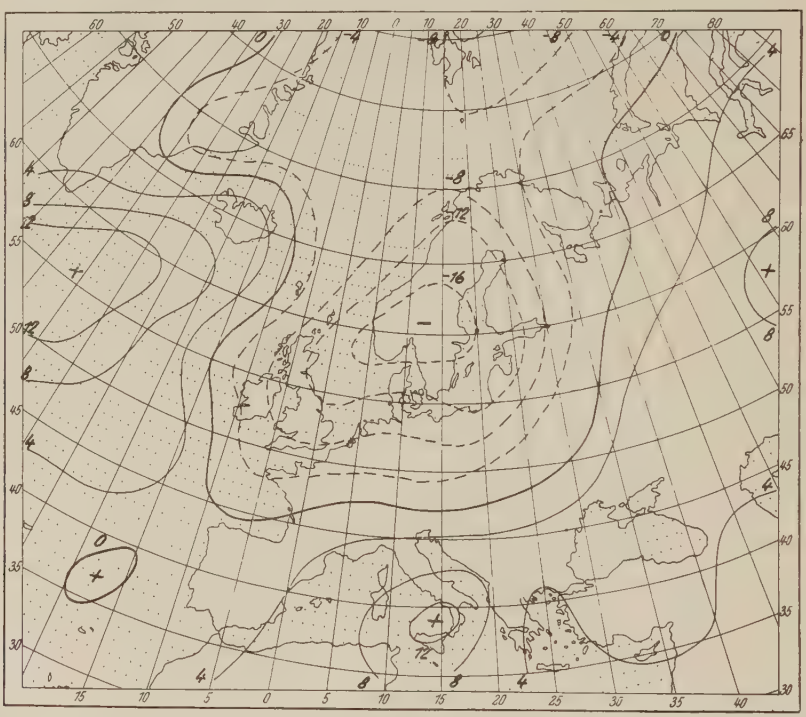

Abb. 3 - *850 mb 01 h — Vorhergesagte Änderung (26. I. - 30. I.) auf (30. I. - 3. II.)1961.*

$$\frac{\partial^2 h\,(x, y, t)}{\partial t^2} = c^2 \nabla^2 h\,(x, y, t) \,. \tag{2}$$

Bei Uebergang zu endlichen Differenzen schreibt sich (2) zu

(2a)
$$1/(\Delta t)^2 \cdot [h(x, y, t + \Delta t) + h(x, y, t - \Delta t) - 2h(x, y, t)] =$$
$$= c^2/(\Delta s)^2 \cdot [h(x + \Delta x, y, t) + h(x, y + \Delta y, t) + h(x - \Delta x, y, t) +$$
$$+ h(x, y - \Delta y, t) - 4h(x, y, t)]$$

was mit den früher eingeführten Abkürzungen für das räumliche und zeitliche Mittel auch

(2b)
$$2/(\Delta t)^2 \cdot (\hat{h} - h) = 4c^2/(\Delta s)^2 \cdot (\bar{h} - h)$$

oder

$$\hat{h} - h = (c/c_K)^2 \cdot (\bar{h} - h)$$

geschrieben werden kann, wenn unter

(3)
$$c_K = \Delta s/\sqrt{2}\,\Delta t$$

verstanden wird.

Man erkennt sofort aus (2b), dass das Äquivalenzprinzip (1) nur dann gelten kann, wenn $c = c_K$ ist.

Dies bedeutet aber, dass eine Äquivalenz zwischen räumlichem und zeitlichem Mittelwert nur dann erwartet werden darf, wenn die Feldgrösse $h(x, y, t)$ einen Schwingungsvorgang mit einer solchen Phasengeschwindigkeit befolgt, wie sie

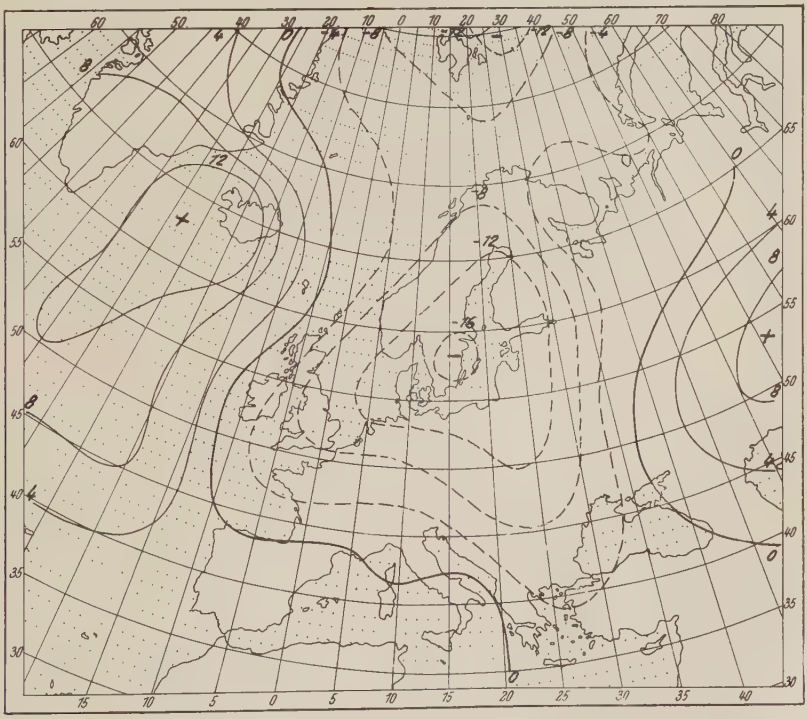

Abb. 4 - *850 mb, 01 h - Tatsächliche Änderung (26. I. - 30 I.) auf (30. I. - 3. II.) 1961.*

sich bei Vorgabe des räumlichen und zeitlichen Inkrementes aus (3) ergibt. Da REUTER bei seinen Untersuchungen für $\Delta t = 24$ Stunden und für $\Delta s = 666$ km wählte, lässt sich das Ergebnis der obigen Analyse auch mit folgenden Worten ausdrücken:

Im statistischen Mittel befolgen die Feldgrössen $h(x, y, t)$ einen Wellenvorgang mit einer durchschnittliche Phasengeschwindigkeit von 5.5 m/sek.

Die eben gegebene Ableitung eröffnet aber auch die Möglichkeit, andere Phasengeschwindigkeiten zuzulassen, indem entsprechende Änderungen an den zeitlichen Inkrementen vorgenommen werden. Natürlich können beide Inkremente nicht beliebig klein oder beliebig gross angesetzt werden, da gewisse numerische Stabilitäten einerseits und eine adäquate Beschreibung des Feldes andererseits

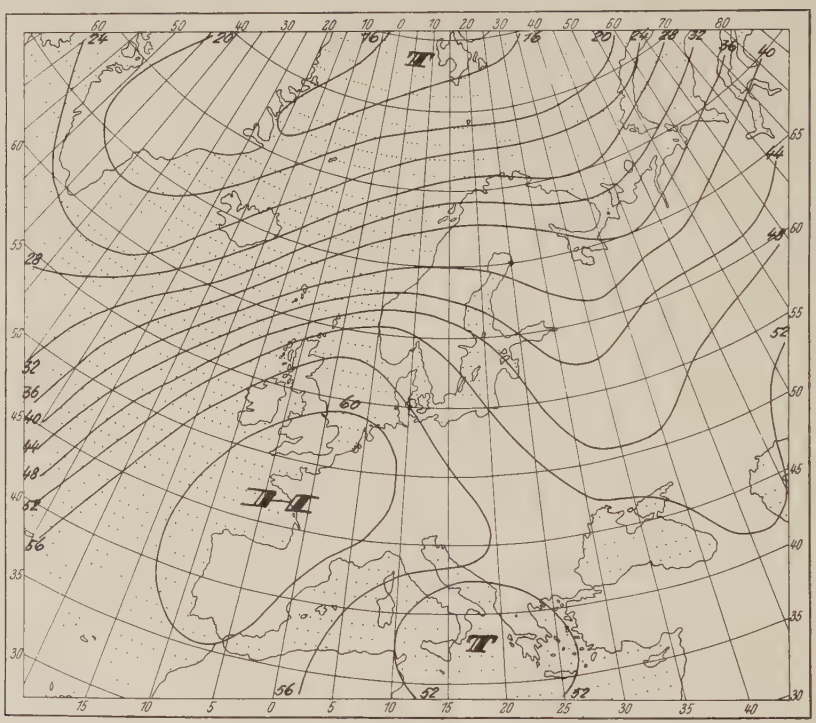

Abb. 5 - *850 mb, 01 h - Mittelkarte 2. - 6. III. 1961.*

gewährleistet sein müssen. Zur näheren Diskussion dieser Probleme sei auf PICHLER [4] verwiesen.

Bei der Aufgabe, das Äquivalenzprinzip auf einen konkreten Fall für den Zweck der Konstruktion von Vorhersagekarten anzuwenden, ist die grösste Schwierigkeit, die genaue Grösse der Phasengeschwindigkeit zu erhalten. Wird obiger Mittelwert verwendet, kann auch nur ein Durchschnittsergebnis erwartet werden. Daher hat PICHLER [4] versucht, zunächst mittels ROSSBYS Wellenformel aus dem Grundstrom und der beobachteten Wellenlänge der langen Wellen die Phasen-

geschwindigkeit abzuschätzen und hierauf das räumliche Inkrement nach (3) festzulegen. Dann kann mittels folgender einfacher Prognosenformel

$$h(x, y, t + \Delta t) = 2\bar{h}(x, y, t) - h(x, y, t - \Delta t) \tag{4}$$

bei hinreichender Anzahl von Gitterpunkten sehr einfach und rasch eine Vorhersagekarte konstruiert werden.

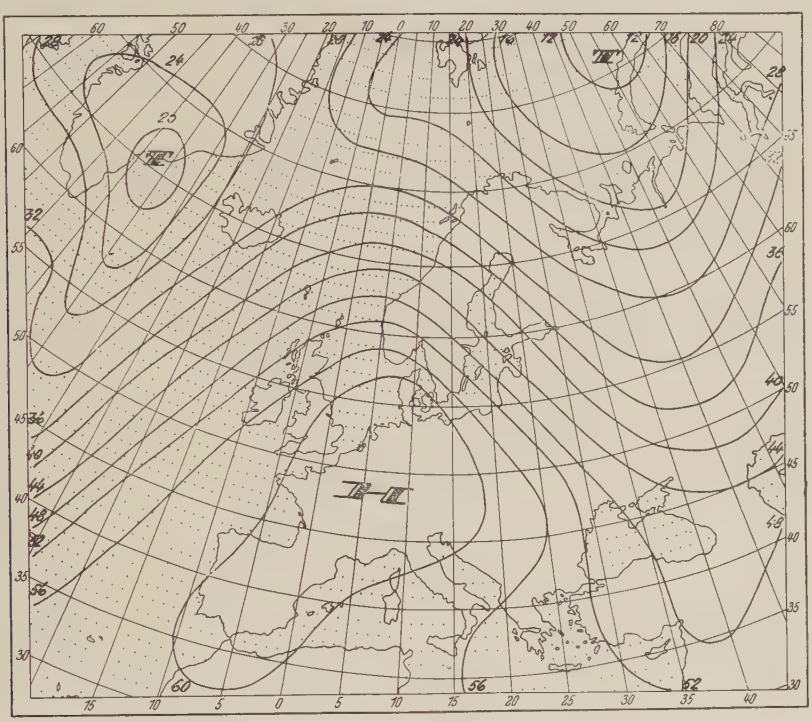

Abb. 6 - *850 mb, 01 h - Mittelwerte 6. - 10. III. 1961.*

Wir wollen jedoch hier von einer Anwendung der obigen Ueberlegungen auf mittelfristige Voraussagen sprechen, die eine Möglichkeit eröffnen, Niveauänderungen einer isobaren Fläche für eine 5-tägige Mittelkarte zu prognostizieren.

Zu diesem Zweck müssen wir voraussetzen, dass auch die zeitlich gemittelten Feldgrössen einem Wellenvorgang gehorchen. Dies erscheint nicht zu absonderlich, da speziell in klimatologischen Untersuchungen immer wieder auf die verschiedensten Perioden und Schwingungen hingewiesen wird, wenngleich die Realität solcher Vorgänge mitunter schwer nachzuweisen ist. Für die hier betrachtete Feldgrösse, nämlich die Höhe einer isobaren Fläche, hat bereits NAMIAS [6] vor längerer Zeit Wellenvorgänge postuliert, wobei ihm allerdings eine Ableitung der Phasengeschwindigkeit im Sinne der ROSSBYschen Formel als erfolgversprechend erschien. Er gab auch statistiche Resultate über die Variation dieser Phasengeschwindigkeit der langen Wellen in den verschiedenen Jahreszeiten bekannt.

In der folgenden Ableitung wollen wir unter ${}_n\hat{h}_m$ einen zeitlichen Mittelwert verstehen, der sich aus fünf im Abstand von 24 Stunden liegenden Werten zusammensetzt. Mit den Indizes sei angedeutet, über welchen Zeitraum die Mittelbildung erfolgt. Der Index 0 bedeute den Prognosentermin (letzter zur Verfügung stehender Wert), negative Indizes weisen in die Vergangenheit, positive in die Zukunft. Es gelte die Wellengleichung in der Form:

$$\frac{\partial^2 - {}_2\hat{h}_2}{\partial t^2} = c_m^2 \nabla^2 - {}_2\hat{h}_2 \tag{5}$$

Mit der obigen Bezeichnungsweise ist mithin unter ${}_{-2}\hat{h}_2$ ein zeitlicher Mittelwert zu verstehen, der aus den fünf Werten ${}_{-2}h$, ${}_{-1}h$, h_0, h_1, h_2 zu bilden wäre. Wir schrei-

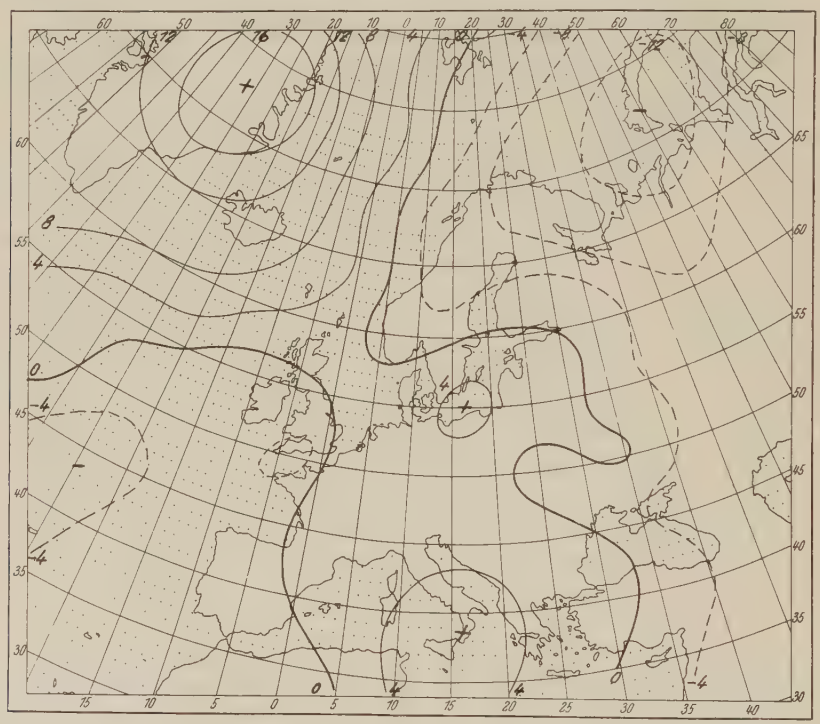

Abb. 7 - *850 mb, 01 h - Vorhergesagte Änderung (2. III. - 6. III.) auf (6. III. - 10. III.) 1961.*

ben nun analog zu den früheren Ueberlegungen die Gleichung (5) in endlichen Differenzen und erhalten:

$$2/(\Delta t_m)^2 \cdot \left[\frac{{}_{-4}\hat{h}_0 + {}_0\hat{h}_4}{2} - {}_{-2}\hat{h}_2 \right] = 4c_m^2/(\Delta s_m)^2 \cdot [\overline{{}_{-2}\hat{h}_2}^m - {}_{-2}\hat{h}_2] \tag{6}$$

Es sei noch besonders darauf hingewiesen, dass wir in (6) bei den Inkrementen und bei der Phasengeschwindigkeit den Index m angefügt haben, um darauf hinzu-

weisen, dass diese Grössen hier andere Beträge annehmen, als bei der analogen Wellengleichung für aktuelle Werte. Insbesondere muss beachtet werden, dass Δt_m in (6) ein Zeitintervall von 48 Stunden bedeutet. Das räumliche Inkrement Δs_m ist nunmehr derart zu wählen, dass die Phasengeschwindigkeit

$$c_m = \frac{'\Delta s_m}{\Delta t_m \sqrt{2}} \tag{7}$$

wird. Dann ist das Äquivalenzprinzip anzuwenden. Dies wirkt sich bei der räumlichen Mittelung entsprechend aus. Wir haben dies durch den Index m bei dem Querstrich der räumlichen Mittelung in (6) bereits angedeutet. Natürlich ist in

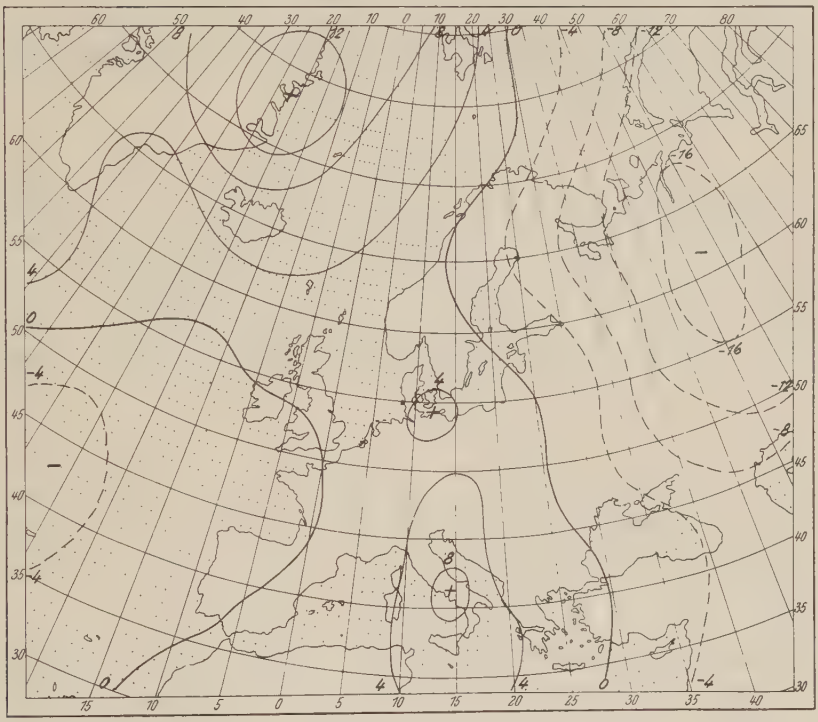

Abb. 8 - *850 mb, 01 h - Tatsächliche Änderung (2. III. - 6. III.) auf (6. III. - 10. III.) 1961.*

Wirklichkeit die genaue Grösse der Phasengeschwindigkeit nicht bekannt. Es muss daher mit Durchschnittswerten aus dem Erfahrungsmaterial gearbeitet werden.

Mit diesen Voraussetzungen schreibt sich die Prognosenformel für das zeitliche Mittelfeld analog zu (4) zu

$$\hat{h}_4 = 2\,\overline{\hat{h}_2}^{m} - \hat{h}_0 . \tag{8}$$

Zunächst kann diese Formel jedoch noch nicht verwendet werden, da der erste Term auf der rechten Seite von (8) zum Prognosentermin gar nicht bestimmbar ist, weil die zeitliche Mittelung bis zum Termin + 2 vorgreift, während tatsächlich nur die Werte bis zum Termin 0 als bekannt vorausgesetzt werden dürfen. Um hier Abhilfe zu schaffen, wenden wir nochmals die Wellengleichung an, diesesmal jedoch auf aktuelle Werte, die um ein Zeitintervall von 48 Stunden auseinanderliegen. Analog zu (4) gilt dann offenbar:

$$\frac{h\,(x, y, t + \Delta t_m) + h\,(x, y, t - \Delta t_m)}{2} = \bar{h}^{a}\,(x, y, t)\,. \tag{9}$$

Hier ist die räumliche Mittelung wieder mit einer anderen Gitterdistanz, als in (4) oder (8) vorzunehmen. Wir haben das durch den Index a beim Querstrich der räumlichen Mittelung angedeutet.

Setzen wir schliesslich (9) in (8) ein, so erhalten wir als endgültige Prognosenformel für das Mittelfeld:

$$\overset{(-m)}{{}_{0}\hat{h}_{4}} = 2\ \bar{h}^{a}\ (x, y, t) - {}_{-4}\hat{h}_{0}\,. \tag{8a}$$

Eine Anwendung der Formel (8a) verlangt, dass wir eine doppelte räumliche Mittelbildung an dem aktuellen Feld zum Prognosentermin 0 vornehmen. Wir müssten dazu genau genommen Kenntnis über die Phasengeschwindigkeit der Wellen im aktuellen und im Mittelfeld haben. Auch hier kann nur mit Erfahrungswerten gearbeitet werden. Die praktische Durchführung der doppelten Mittelung ist etwas zeitraubend. Daher wurde auf Grund einer Reihe von Fällen folgende empirische Beziehung hergeleitet

$${}_{0}\hat{h}_{4} - {}_{-4}\hat{h}_{0} = 1{,}2\,(h - {}_{-4}\hat{h}_{0})\,. \tag{8b}$$

Hierbei ist in h die räumliche Mittelung — wie bei den früheren Untersuchungen — mit einer Gitterdistanz von 666 km durchzuführen.

Zum Schluss sei die Formel (8b) an Hand zweier Beispiele verifiziert. Die Karten beziehen sich auf die 850 mb Fläche.

Abb. 1 zeigt die « Ausgangslage » als zeitliche Mittelkarte, gebildet aus den fünf aktuellen Werten vom 26. bis 30.Jan.1961. Abb. 2 veranschaulicht die « zukünftige » Entwicklung wieder als Mittelkarte für die Zeit vom 30.Jan. bis 3.Febr. 1961. Aus Abb. 3 und 4 sind die mit Hilfe von (8b) vorausberechneten und tatsächlich eingetroffenen Änderungen zu ersehen. Die Abb. 5 bis 9 zeigen die analogen Karten für den Fall der Mittelkarten vom 2. bis 6. März, bezw. 6. bis 10. März 1961.

Aus beiden Fällen kann ersehen werden, dass die Formel (8b) recht gute Ergnisse liefert. Eine serienmässige Erprobung wird derzeit durchgeführt. Die Ergebnisse werden später zusammen mit den entsprechenden Korrelationskoeffizienten veröffentlicht werden.

LITERATURVERZEICHNIS

([1]) Reuter H.: *Grundlagen einer synoptisch-statistischen Theorie der Druckänderungen*, Arch. Met. Geophys. Biokl. A, 10, 121 (1958). — ([2]) Pichler H.: *Zusammenhang*

zwischen räumlichem und zeitlichem Mittel eines Geschwindigkeitsfeldes in einer autobarotropen Strömung, Arch. Met. Geophys. Biokl., A, 11, 18 (1959). — ([3]) PICHLER H.: *Zeitliche und räumliche Mittelbildungen bei Rossby-Wellen.* Arch. Met. Geophys. Biokl. A, 12, 8 (1960). — ([1]) PICHLER H.: *Theorie der räumlichen und zeitlichen Mittelbildung einer beliebigen Feldfunktion und ihre Anwendung in der Meteorologie.* Arch. Met. Geophys. Biokl. A, 12 im Druck (1961). — ([5]) REUTER H.: *Erfahrungen mit einer neuen Methode der Mittelfristprognose.* Zeitschr. f. Met., 11, 299 (1957/58). — ([6]) NAMIAS J.: *Extended Forecasting by Mean Circulation Methods.* Washington, U.S. Weather Bureau, Febr. 1947.

(*Eingegangen am* 8. *April* 1961)

DER NEUBAU DER METEOROLOGIE

von Kurt Wegener (*)

Summary — The radiation as origin of the weather.

Résumé — Le temps, comme dépendant de la radiation solaire.

Als nach dem ersten Weltkrieg sich die Funkentelegraphie entwickelte und uns viele Wetternachrichten schnell verschaffte, hofften viele (auch der Verfasser) auf bedeutende Fortschritte der Wetterprognosen. Diese sind ein Maßstab dafür, wieweit wir die Vorgänge in der Atmosphäre richtig verstanden haben. Das Ergebnis war eine Enttäuschung.

Bisher war man von dem Druck- und Wärmefeld in Zyklonen (T) und Anticyclonen (H) ausgegangen.

Nun sind aber zweifellos Klima und Wetter der Breitengrade in erster Reihe von der Temperatur- oder Wellenstrahlung der Sonne abhängig, und diese Strahlung existierte in den meteorologischen Betrachtungen nicht. Wir wollen im Folgenden von der Strahlung ausgehen.

1. Die Unterschiede, die auf der gekrümmten Erdoberfläche durch die *Strahlung* geschaffen wurden, werden von der *Wärmeleitung* ausgeglichen. Der Boden ist hierfür zwar nutzlos, weil das meridionale Temperaturgefälle sehr klein ist. Aber die Luft wird infiziert, und sie ist beweglich und besorgt nun den « Austausch », indem sie *Wärme polwärts und Kälte äquatorwärts* verfrachtet. Diese Bewegung kann nicht geradlinig vor sich gehen infolge der sogenannten ablenkenden Kraft der Erdrotation, sondern wirkt in einer wirbelähnlichen kreisförmigen gekrümmten Bahn, in der man leicht die T und H der zünftigen Meteorologie erkennt.

Schwankung der Intensität der Strahlung bewirkt entsprechende Schwankung des Austauschs, so daß wir nun Anschluß an die zünftigen Vorstellungen gefunden haben. Die Bjerknes'schen Ideen bleiben anerkannt, gelten aber nur für das Innere der T und H, für den Austausch der in entgegengesetzter Richtung pol- und äquatorwärts gehenden Strömungen.

Schwankungen der Strahlung an der Erdoberfläche können von Vorgängen an der Sonnenoberfläche herrühren, also von Schwankungen der Solarkonstante. Man muß hoffen, daß einige Sternwarten, die dank der Entwicklung der Funkentelegraphie heute von der Zeitkontrolle befreit sind, sich der Aufgabe annehmen, für die ihnen die Physik in ihrem « schwarzen Körper » ein brauchbares Instrument

(*) Institut für Meteorologie und Geophysik der Universität *Graz*.

geliefert hat. Liegen 2 Sternwarten auf gleicher geographischer Länge, und messen sie gleichzeitig, so sollte es möglich sein, die Störung durch die Atmosphäre zu eliminieren, besonders, wenn man mit Serien-Beobachtungen arbeitet.

Die stärksten Schwankungen der an der Erdoberfläche eintreffenden Strahlung werden durch Wolken und Schneedecken hervorgerufen. Beide reflektieren nämlich 80 bis 90% der Strahlung. Für den Anfang wird es wohl genügen, die volle Sonnenstrahlung (bei wolkenlosem Wetter) gleich 1 zu setzen und die tatsächliche Bewölkung in Bruchteilen, also bei bedecktem Himmel gleich Null. Dies mag zunächst als roher Maßstab, in relativem Maß, für die Strahlung dienen. Mit dieser Strahlung läßt sich der aus ihr folgende « Austausch » (T und H) vergleichen.

Die Meere erwärmen sich durch die Strahlung sehr langsam infolge ihrer Strahlungsdurchlässigkeit. Wir können hier auf solche Einzelheiten nicht eingehen. Zunächst wird man wohl mit der groben Näherung auskommen, daß sie sich überhaupt nicht erwärmen, da es sich für die Prognose nur um Wochen handelt.

Ebensowenig soll uns die Frage interessieren, wie wir am zweckmässigsten die Stärke des « Austauschs » definieren: für uns handelt es sich um Prinzipien, nicht um Einzelheiten.

2. Bisher haben wir Messungen der Sonnenstrahlung nicht gebraucht. Bei einer Weiterentwicklung unseres « Neubaus der Meteorologie » werden sie nötig.

Zunächst ein kleines theoretisches Gesetz der Physik, der wir ja unsere Kenntnisse der Wellenstrahlung verdanken: wir können nur *Dimensionen* messen! Nun haben aber 3 ganz verschiedene Vorgänge, die Strahlung, die Wärmeleitung und die Reibung die gleiche Dimension, ohne daß wir sagen können, welchen der 3 Prozesse wir gemessen haben. Bei allen dreien messen wir cal/(Zeit-und Flächeneinheit).

Bei der Arbeit mit Raketen kam es zu zerstörender Erhitzung, als diese in einen jener unregelmässig, aber häufig von der Sonne ausgesendeten Elektronenhaufen gerieten. Mit mehr Mut als Überlegung erklärte man, dort sei die Rakete durch *Strahlung* erhitzt worden! Der Weltraum sollte also Strahlung aussenden! Eine solche Strahlung wäre längst an der Erdoberfläche gemessen worden. Offenbar waren den mutigen Entdeckern die zahlreichen Arbeiten über die Polarlichter, die wir dem Polarlicht-Observatorium in Tromsö, unter anderem au chder Arbeit von Robitzsch und dem Verfasser, aber vor allem der meisterhaften Arbeit von Vegard verdanken, unbekannt geblieben, was aus dem riesenhaften Anwachsen der Fachliteratur zu verstehen ist.

Die Haufen von Elektronen, die anscheinend von den « Fackeln » der Sonnenoberfläche entsandt werden, haben gelegentlich Lichtgeschwindigkeit. In der Haupt-Region des Polarlichts bilden sie zur Zeit des Sonnen-Untergangs im Herbst schnurgerade leuchtende Bänder, die spitz in die Richtung der Sonne weisen.

Gerät eine Rakete, ebenfalls bemüht, Lichtgeschwindigkeit zu erreichen, in einen solchen schnellen Elektronenhaufen, so kann die Reibung stark genug werden, um die Rakete zu verglühen. Aber von Strahlung sollte man hier nicht reden.

In dieser Zeitschrift war vom Verfasser unter dem Titel: « Die Kernfragen der Sonnenstrahlung in gedrängter Darstellung » (Vol. 43, 1959/II) die Frage kurz und deutlich behandelt worden.

Die Meteorologie ist leider auf dem Standpunkt Pouillet (1838) stehen geblieben und hat sich bis heute nicht um die Arbeiten der Physik über die Wellenstrahlung gekümmert. Nicht einmal Kirchhoffs Beweis (1859), daß man nur

einen Hohlraum als schwarzen, alle Strahlung absordierenden Körper ansehen könne, (womit POUILLET's Idee abgetan war) fand bei ihr Anerkennung. Vor einigen Jahren fand der Verfasser bei einer Tagung der Meteor. Gesellschaft in Berlin Gelegenheit, sich davon zu überzeugen, daß die vermeintlichen Spezialisten nicht die Kenntnisse hatten, die ihnen jedes Handbuch der Physik hätte übermitteln können. Brauchbare Beobachtungen fehlen infolgedessen, und es schien zweckmässig, zunächst auf Beobachtungen zu verzichten und nur die Kontinente zu betrachten.

Über den Tagesgang der Totalstrahlung, gemessen mit dem schwarzen Körper der Physik, hat der Verfasser in Revista Meteoros, Año 1, Junio de 1951 berichtet. Es fehlt noch: die Energieverteilung im Spektrum der Sonne mit Tagesgang. In der Meteorologischen Rundschau, der Fachzeitschrift der (west-) Deutschen Meteorologischen Gesellschaft, hat der Verfasser das Instrument beschrieben, das der deutschen Forschungsgemeinschaft gehört. Inzwischen hat aber das Auswärtige Amt, Bonn, den Verfasser, der Deutsch-Österreicher d.h. auf beide Staaten vereidigter Doppelstaatler war, ausgebürgert, und nun muß um die Zustimmung der deutschen Forschungsgemeinschaft zur Verwendung des Instruments gebeten werden.

(*Eingegangen am 25. Januar 1961*)

DER EINFLUSS VON BEWÖLKUNGSMENGE UND -ART AUF DIE GRÖSSE DER DIFFUSEN HIMMELSSTRAHLUNG (*)

von J. C. Thams (**)

Summary — During the last few years measurements of the diffuse radiation of the sky have been carried out at Locarno-Monti on the Southern slope of the Alps. The present paper deals with the influence of cloudiness and cloud forms on the amount of sky radiation. On the high level (C_H) sky radiation increases steadly with the amount of clouds; on the low level (C_L) there is at first an increase and than a decrease of sky radiation with cloudiness. Roughly we find the maximum of diffuse radiation at 6 to 8 tenths of the total cloudiness. In general the thickness of the clouds seems to be more decisive than the forms of the clouds. Haze has a remarkable influence.

The increase of the diffuse radiation of the sky by haze and clouds is very considerarable, especially with respect to all climatological purposes.

Zusammenfassung — Während der letzten Jahre sind am Südhang der Alpen in Locarno-Monti Messungen der diffusen Himmelsstrahlung ausgeführt worden. Die vorliegende Arbeit befasst sich mit dem Einfluss von Bewölkungsmenge und -art auf die Grösse der Himmelsstrahlung. Im hohen Niveau (C_H) nimmt die Himmelsstrahlung stetig mit wachsender Bewölkungsmenge zu; im tiefen Niveau (C_L) finden wir zuerst eine Zu-, dann eine Abnahme der diffusen Himmelsstrahlung mit der Bewölkungsmenge. Das Maximum liegt ungefähr zwischen 6-8 Zehnteln der Gesamtbewölkungsmenge. Im allgemeinen scheint die Dichte der Wolken entscheidender zu sein als die Wolkenart. Der Einfluss des Dunstes ist bemerkenswert.

Die Zunahme der diffusen Himmelsstrahlung durch Dunst und Wolken ist sehr beträchtlich, was besonders in klimatologischer Hinsicht von Bedeutung ist.

Riassunto — Durante gli ultimi anni sul pendio sud delle Alpi a Locarno-Monti sono state eseguite misure della radiazione diffusa del cielo. Questo lavoro si occupa dell'influsso della quantità e qualità della nuvolosità sulla intensità della radiazione diffusa del cielo. Al livello superiore (C_H) la radiazione diffusa del cielo aumenta in modo continuo con l'aumento della nuvolosità; al livello inferiore (C_L) troviamo dapprima un aumento, poi una diminuzione della radiazione diffusa del cielo con la nuvolosità. Il massimo giace pressapoco tra 6-8 decimi della quantità totale di nuvolosità. In generale sembra che la densità delle nubi sia più decisiva che la qualità delle nubi. L'influsso della caligine è notevole.

L'aumento della radiazione diffusa del cielo per effetto della caligine e delle nubi è considerevole, ciò che è importante specialmente dal punto di vista climatologico.

(*) Vorgelegt am 7. April 1961 auf der 9. Generalversammlung der « Società Italiana di Geofisica e Meteorologia » (Genova: 6.-8. April 1961).

(**) J. C. Thams, Osservatorio Ticinese della Centrale Meteorologica Svizzera, *Locarno-Monti.*

I. *Einleitung.*

Ein grosser Teil des bis heute veröffentlichten Materials über diffuse Himmelsstrahlung ist aus Werten der Globalstrahlung und der Horizontalkomponente der direkten Sonnenstrahlung berechnet worden. Registrierungen der Himmelsstrahlung selber liegen relativ wenige vor. Die grosse Bedeutung der Himmelsstrahlung, vor allem auch in klimatologischer Hinsicht, bedarf aber kaum besonderer Erwähnung. So sind denn auch während des Internationalen Geophysikalischen Jahres in der Schweiz nord- und südwärts der Alpen (Basel und Locarno-Monti) und im Hochgebirge (Davos) parallel laufende Registrierungen der Himmelsstrahlung vorgenommen worden. Diese Werte liegen zwar in Tabellen vor, sind aber sonst noch nicht weiter ausgewertet worden. Hier soll nur über Untersuchungen in Locarno-Monti berichtet werden und zwar beschränken wir uns auf den Einfluss von Bewölkungsmenge und -art auf die Grösse der diffusen Himmelsstrahlung. Diese beanspruchen am Alpensüdfuss insofern ein besonderes Interesse als durch den Einfluss des Nordföhns sehr hohe Intensitäten der direkten Sonnenstrahlung und damit sehr kleine Werte der diffusen Himmelsstrahlung an wolkenlosen Tagen erreicht werden. Diese Werte bilden den Ausgangspunkt unserer Betrachtungen.

Die genaueste Methode zur Messung der diffusen Himmelstrahlung besteht darin, dass ein kleiner Schirm der Sonne so nachgeführt wird, dass die Empfangsfläche der Thermosäule und die sie schützenden Glashalbkugeln ständig be-

Abb. 1a - *Der Abschirmungsring zur Messung der diffusen Himmelstrahlung mit dem Solarimeter Moll-Gorczynski.*

schattet werden. Ein solches Gerät ist z.B. seit vielen Jahren am Physikalisch-Meteorologischen Observatorium in Davos in Betrieb. Leider ist es sehr teuer, sodass man sich nach einer billigeren Lösung umsehen muss. Sie besteht darin, dass man im rechten Winkel zur Erdachse einen Abschirmungsring anbringt, der täglich ein Mal entsprechend der Sonnendeklination eingestellt werden muss (Abb. 1a und b). Der Durchmesser des von uns verwendeten Abschirmungsringes beträgt 90 cm, die Bandbreite 4 cm. Die mit dieser Einrichtung erhaltenen Werte

der Himmelsstrahlung müssen allerdings noch korrigiert werden, da ja nicht nur die Sonne selber, sondern auch Teile der Himmelsfläche ständig abgedeckt werden. Diesbezügliche Berechnungsgrundlagen finden sich bei W. SCHÜEPP ([1]) und A. J. DRUMMOND ([2]). Selbstverständlich lassen sich diese Korrekturen auch experimentell ermitteln. Es ist auf jeden Fall empfehlenswert, die Breite des Abschirmungsringes und seine Entfernung von der Thermosäule so zu dimensionieren, dass nicht zu grosse Teile der Himmelsfläche abgeschirmt werden, die Korrekturen also relativ klein bleiben.

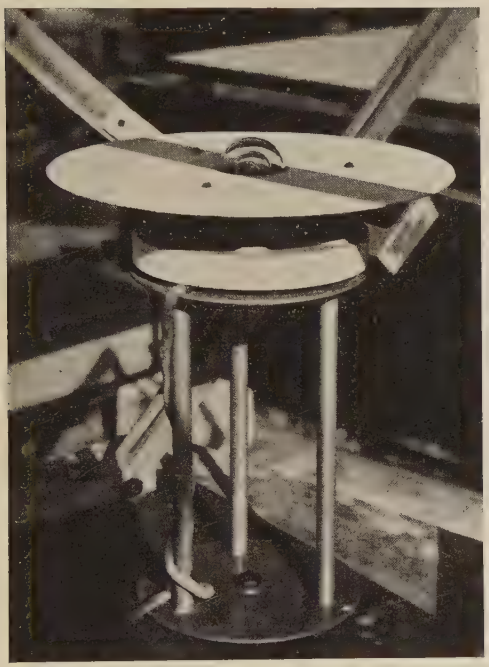

Abb. 1b - *Der vom Abschirmungsring auf Thermosäule und Glasglocken geworfene Schatten.*

Bei der Untersuchung über den Einfluss der Bewölkung auf die diffuse Himmelsstrahlung treten nun mancherlei Schwierigkeiten auf. Sie bestehen im folgenden:

a) Die Bestimmung der Bewölkungsmenge beruht auf Schätzungen; der individuelle Fehler kann daher gross sein. Das gleiche gilt für die Bestimmung der Wolkenarten. Hier wirkt noch besonders der Umstand erschwerend, dass in der synoptischen Meteorologie eher Himmelsansichten als fest begrenzte Wolkenarten verschlüsselt werden, ganz abgesehen von den häufigen Aenderungen des internationalen Codes. Man muss sich daher meistens mit einer Unterteilung der Wolken in solche des tiefen (C_L), des mittleren (C_M) und des hohen (C_H) Niveaus begnügen.

b) Schätzung der Bewölkungsmenge und Bestimmung der Art werden nur zu gewissen Terminen vorgenommen. Die zwischen den Terminen vor sich gehenden Aenderungen in der Menge und im Charakter der Bewölkung werden aber nicht erfasst. Als Beispiel sei hier auf die Abb. 2 verwiesen. Bei diesem relativ einfachen Verlauf der Himmelsstrahlung ist z.B. der Anstieg der Intensität um die

Mittagszeit durch keine Bewölkungsbeobachtung belegt. Da die Sonne erst nach 12 Uhr für ganz kurze Zeit zum Vorschein kam, können Intensitätsanstieg und Maximum nur durch eine Aenderung der Bewölkungsart, bezw. der Dichte erklärt werden. Diese Beispiele liessen sich beliebig vermehren. Kontinuierliche Registrierungen z.B. auf photographischem Wege wären technisch zwar möglich, sind aber mit erheblichen Kosten verbunden. Sie hätten aber den grossen Vorteil, dass auch die Verteilung der Wolken über dem Himmelsgewölbe miterfasst würde.

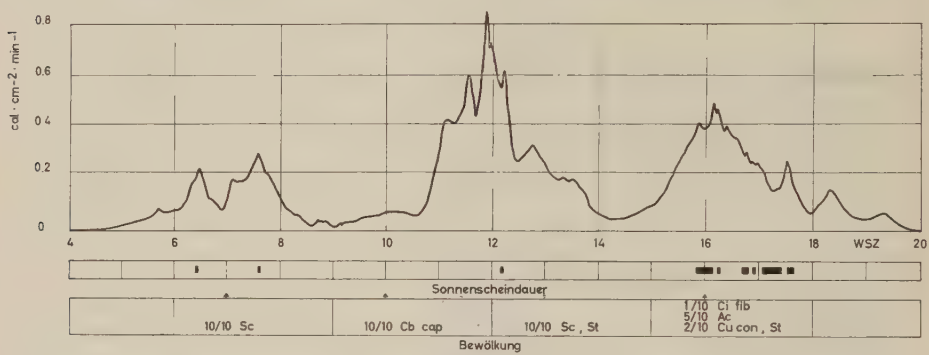

Abb. 2 - *Die diffuse Himmelsstrahlung am* 21. *Juni* 1959 *und die Unzulänglichkeit der Bewölkungsbeobachtungen.*

c) Die Zuordnung der Grösse der Himmelsstrahlung zu den verschiedenen Wolkenarten ist, namentlich bei grossen Bewölkungsmengen, nicht immer eindeutig. So können über tiefen Wolken mittlere, über diesen wiederum hohe Wolken liegen.

d) Wie wir später noch sehen werden, spielt in kleinen Meereshöhen der Dunst bei der diffusen Himmelsstrahlung eine nicht zu unterschätzende Rolle. Die Wirkung des Dunstes lässt sich aber von jener der Bewölkung meistens nicht trennen.

Im allgemeinen sind alle Bewölkungsbeobachtungen für eine genaue Interpretation der diffusen Himmelsstrahlung heute noch sehr unzulänglich.

II. *Material.*

Das hier für unsere Untersuchungen verwendete Material umfasst die Zeit vom April 1958 bis Dezember 1959. Diese Periode ist natürlich viel zu kurz, um aus ihr klimatologisch gesicherte Mittelwerte ableiten zu können. Das ist auch nicht unsere Absicht. Wir möchten mit dieser Bearbeitung vielmehr zeigen, wo die Probleme liegen, in welcher Richtung weitere Untersuchungen gemacht werden sollten und was man aus den bisherigen Messungen herausholen kann.

Für die Messung der diffusen Himmelsstrahlung wurde ein Moll-Gorczynski Solarimeter mit einem hochempfindlichen Schlagbügelgalvanometer (gesamte Messanordnung = Pyranograph) eingesetzt. Die Eichung erfolgte mit Hilfe eines zweiten, im Aufbau identischen Pyranographen, der die Strahlung von Sonne + Himmel auf die Horizontalfläche aufzeichnete. Es kamen zwei Eichmethoden zur Anwendung; *a*) der Vergleich der Pyranographen bei vollkommen bedecktem Him-

mel, mit und ohne Abschirmungsring des die diffuse Himmelsstrahlung messenden Pyranographen (Himmelspyranograph), *b*) der Vergleich der Pyranographen bei vollkommen wolkenlosem Himmel ohne Abschirmung des Himmelspyranographen. Die Methode *b* lässt sich allerdings nur bis zu bestimmten Intensitäten anwenden, da die Ausschläge wegen der grösseren Empfindlichkeit des Himmelspyranographen sonst zu gross werden. Der Pyranograph zur Messung der Strahlung von Sonne + Himmel ist fortlaufend mit einem Pyrheliometer nach der Abschattungsmethode geeicht worden. Auf das Problem der Eichungen des Himmelspyranographen soll in einer besonderen Arbeit eingegangen werden. Es mag hier jedoch erwähnt werden, dass die Ergebnisse recht befriedigend ausgefallen sind. Die von W. Schuepp berechneten Korrekturen für den Abschirmungsring sind in guter Uebereinstimmung mit den von uns experimentell gefundenen.

Die Sonnenscheindauer wurde, wie üblich, mit einem Sonnenscheinautographen Campbell-Stokes registriert. Bewölkungsmenge und -art wurden an folgenden Terminen bestimmt: 7h30, 10h30, 13h30, 16h30 und 21h30 MEZ, am Abendtermin jedoch nur die Bewölkungsmenge; auch die ungefähre Verteilung der Wolken über der Himmelsfläche wurde zu den angegebenen Zeiten aufgezeichnet.

III. *Ergebnisse.*

Wie wir bereits erwähnt haben, bilden die Werte der diffusen Himmelsstrahlung an praktisch wolkenlosen und möglichst dunstfreien Tagen den Ausgangspunkt unserer Betrachtungen. Meistens handelt es sich hier um Nordföhn-, gelegentlich auch um Antizyklonallagen.

Die Auswahl ist nicht sehr leicht, da schon bei relativ geringen Dunstgraden die diffuse Himmelsstrahlung stark zunimmt. Es wäre besser, von ganz bestimmten Trübunsgraden auszugehen, wie sie durch Messungen der direkten Sonnenstrahlung mit Filtern berechnet werden können. Leider sind die Trübungsfaktoren in Locarno-Monti nur für einen Teil des Materials berechnet worden und ausserdem sind nicht an allen wolkenlosen Tagen Messungen der direkten Sonnenstrahlung ausgeführt worden. Wir glauben aber, dass auch bei dieser vereinfachten Methode die wesentlichsten Resultate klar zum Ausdruck kommen.

Ausgangspunkt sollen hier zunächst die *Tagessummen* der diffusen Himmelsstrahlung an extrem klaren Tagen sein. Die mittleren monatlichen Tagessummen sind für Locarno-Monti in Tabelle 1 zusammengestellt. Sie sind sehr klein und entsprechen, von den Wintermonaten abgesehen, Werten, wie sie nach einer Zusammenstellung von Inge Dirmhirn ([3]) in etwa 1500 m/M angetroffen werden.

Tabelle 1 - *Mittlere Tagessummen der Himmelsstrahlung in cal · cm^{-2} in Locarno-Monti und auf 1500 m/M.*

	I	II	III	IV	V	VI	VII	VIII	IX	X	XI	XII
Locarno-Monti 380 m/M	30	37	49	63	71	73	72	67	55	40	30	27
1500 m/M	27	34	50	63	72	78	76	66	55	42	31	23

Dieses Resultat stimmt gut mit den hohen Werten der direkten Sonnenstrahlung an Nordföhntagen am Alpensüdfuss überein (4).

1. *Diffuse Himmelsstrahlung und Bewölkungsmenge* — Um den Zusammenhang zwischen Himmelsstrahlung und Bewölkungsmenge zu erfassen, kann man einmal von der Grösse der relativen Sonnenscheindauer, zum anderen von der geschätzten Bewölkungsmenge ausgehen, was zu recht verschiedenen Resultaten führt. Der Grund hierfür liegt nicht nur darin, dass die Bewölkungsmenge lediglich an bestimmten, relativ weit auseinander liegenden Terminen festgestellt wird, sondern vor allem an der Art der Schätzung der Bewölkungsmenge. Die bekannte Beziehung $S + B \sim 100$ (S = relative Sonnenscheindauer, B = Bewölkungsmenge, beide in Prozenten ausgedrückt), gilt nur für Wolkenarten, die so dicht sind, dass auf dem Streifen des Sonnenscheinautographen keine Brennspur mehr hervorgerufen wird, im Grunde also nur für Wolken des tiefen und teilweise auch für jene des mittleren Niveaus. Bekanntlich hat man bis zum internationalen meteorologischen

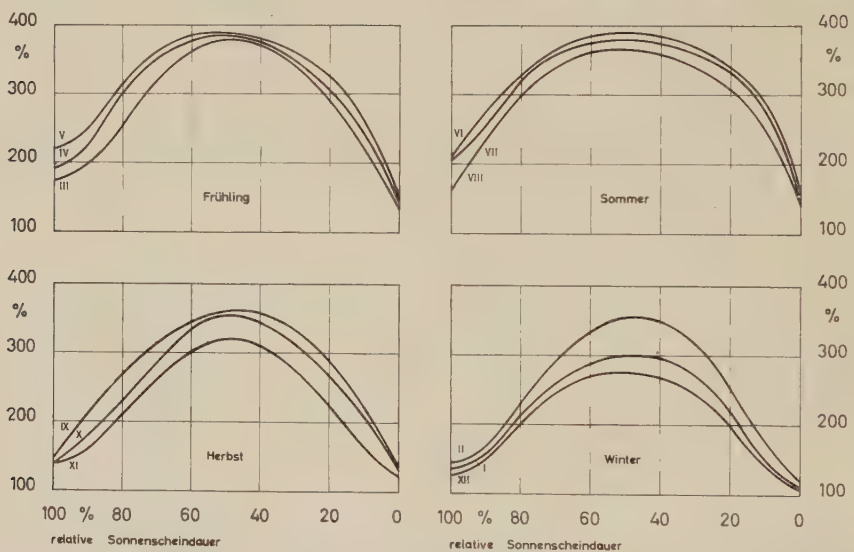

Abb. 3 - *Die Tagessummen der diffusen Himmelsstrahlung bei verschiedener relativer Sonnenscheindauer in Locarno-Monti in Prozenten des Wertes bei ganz klarem Himmel, getrennt nach Monaten und Jahreszeiten.*

Kongress in Wien im Jahre 1873 bei der Schätzung der Bewölkungsmenge Rücksicht auf die Dicke der Wolkenschichten genommen; nach 1873 aber in den meisten Ländern — die Schweiz bildet hier eine Ausnahme — nicht mehr, was sich an vielen Stationen des internationalen klimatologischen Netzes in einer « künstlichen » Zunahme der Bewölkungsmenge auswirkte (5). Um jedoch den Einfluss von Bewölkungsmenge und -art auf die diffuse Himmelsstrahlung zu erfassen, darf man selbstverständlich keine Rücksicht auf die Dicke der Wolkenschichten nehmen, muss also z.B. bei einem über der ganzen Himmelsfläche sich erstreckenden Cirrostratus einen Bedeckungsgrad von 10 Zehnteln angeben. Um sowohl den gut begründeten Wünschen des Klimatologen, nach denen die Bewölkungsmenge in

erster Linie ein Ausdruck der Sonnenscheindauer sein sollte, als auch den Erfordernissen der Strahlungsklimatologie zu entsprechen, wäre eine dreifache Schätzung der Bewölkungsmenge (tiefe, mittlere und hohe Bewölkung) das Gegebene. Bei dem hier zur Bearbeitung gelangenden Material wurde die Bewölkungsmenge ohne Rücksicht auf die Dicke der Wolkenschichten geschätzt.

In Abb. 3 ist nun der Zusammenhang zwischen diffuser Himmelsstrahlung und relativer Sonnenscheindauer (R) dargestellt. Die Tagessummen der Himmelsstrahlung an ganz klaren Tagen sind gleich 100% gesetzt. Der Charakter der Kurven ist in allen Monaten mehr oder minder der gleiche. Vom wolkenlosen Himmel ($R = 100\%$) erfolgt ein rascher Anstieg bis etwa 50% relativer Sonnenscheindauer und dann ein ebenso starker Abstieg bis zum bedeckten Himmel. Dass bei $R = 100\%$ die Himmelsstrahlung wesentlich grösser als 100% ist, muss der Wirkung des Dunstes zugeschrieben werden. Er ist natürlich am Alpensüdfuss besonders gross in den Sommermonaten. Während im Herbst und Winter der wolkenlose Himmel praktisch ebenso viel Strahlung abgibt wie der bedeckte, liegen im Frühling und Sommer die Werte für $R = 0\%$ viel tiefer. Von Mai bis August dürfte es sich zur Hauptsache um Wolken mit ausgesprochenem vertikalen Aufbau, also grosser Dichte, handeln.

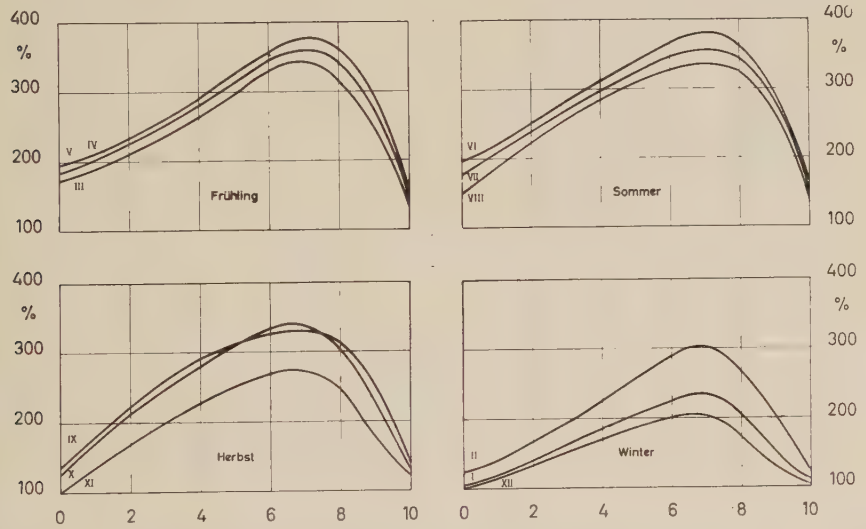

Abb. 4 - *Die Tagessummen der diffusen Himmelsstrahlung bei verschiedener Bewölkungsmenge in Locarno-Monti in Prozenten des Wertes bei ganz klarem Himmel, getrennt nach Monaten und Jahreszeiten.*

In Anbetracht des nicht sehr umfangreichen Materials sehen wir davon ab, auf Einzelheiten im Kurvenverlauf einzugehen; sie erscheinen nicht genügend gesichert. Dass im Frühling und Sommer die Maxima deutlich höher als im Herbst und Winter liegen, wurde auch von Inge Dirmhirn festgestellt. Auffallend ist auch, dass die Kurven der Monate November, Dezember und Januar, sowie die von September, Oktober und Februar besser zusammenpassen als die der eigentlichen Herbst- und Wintermonate.

Einen modifizierten Charakter zeigen die Kurven, wenn man an Stelle der relativen Sonnenscheindauer die Bewölkungsmenge aufträgt (Abb. 4). Die Maxima finden sich in allen Monaten zwischen 6-8 Zehnteln Bewölkungsmenge. Auch ist der Anstieg annähernd linear, der Abfall gegen den bedeckten Himmel sehr steil. Der Gewinn an Himmelsstrahlung bis zum Maximum ist immerhin erheblich und erreicht im Frühling und Sommer im Mittel etwa 350%. Dieser Wert wird natürlich auch durch den Umstand bestimmt, dass als Ausgangspunkt extrem klare Tage genommen wurden und nicht nur wolkenlose mit mehr oder minder starkem Dunst. Aber hierdurch wird nur ein Teil der hohen Werte der Himmelsstrahlung erklärt. Viel entscheidender ist die durch sorgfältige Untersuchungen erhärtete Tatsache [5], dass der Anteil der hohen und mittelhohen Wolken an der Gesamtbewölkung in Locarno-Monti besonders gross ist. Im übrigen zeigen die Kurven ähnliche Charakteristika wie jene, bei denen der Zusammenhang mit der relativen Sonnenscheindauer dargestellt ist.

2. *Diffuse Himmelsstrahlung und Bewölkungsart* — Um den Einfluss der Wolkenart auf die Himmelsstrahlung zu ermitteln, wurden die Wolken nur in solche des hohen (C_H), des mittleren (C_M) und des tiefen Niveaus (C_L) eingeteilt und die Tage herausgezogen, an welchen nur Wolken in einem dieser drei Niveaus vorhanden waren, also z.B. nur Cirren.

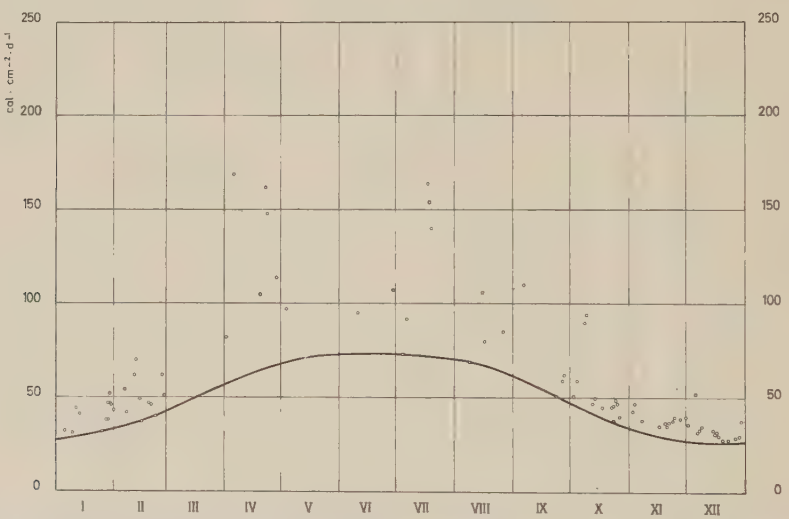

Abb. 5 - *Die Tagessummen der diffusen Himmelsstrahlung in cal · cm^{-2} an wolkenlosen Tagen mit und ohne Dunst in Locarno-Monti* (Ausgezogene Kurve: Werte bei Nordföhnlagen).

Doch bevor wir diese Ergebnisse diskutieren, sei hier noch kurz auf die Wirkung des Dunstes eingegangen.

Dieser kann die diffuse Himmelsstrahlung, namentlich in den Sommermonaten, ganz erheblich steigern, was eindrücklich aus der Abb. 5 hervorgeht. In dieser Darstellung sind die Tagessummen der Himmelsstrahlung (cal · cm^{-2}) an praktisch wolkenlosen Tagen eingezeichnet, d.h. es wurden auch noch Tage miteinbezogen,

an denen nur Spuren von Wolken beobachtet wurden. Die Kurvenlinie gibt die Werte der diffusen Himmelsstrahlung an extrem klaren Tagen wieder.

In der Abb. 6 finden sich nun für Locarno-Monti, geordnet nach den Wolkengruppen C_H, C_M und C_L, die Tagessummen der Himmelsstrahlung in Prozenten der Werte bei ganz klarem Himmel. Es wurden hier einzelne Tageswerte und nicht Mittelwerte eingetragen, um eine Vorstellung von der Streuung zu geben. Bei den Wolken des hohen und des tiefen Niveaus wurden durch die Punkteschar, den Schwerpunkten entsprechend, andeutungsweise Kurven gezogen. Es lässt sich folgendes feststellen: Bei den Cirren nimmt offensichtlich die diffuse Himmelsstrahlung mit zunehmender Bewölkungsmenge etwa linear zu, der grösste Wert dürfte bei bedecktem Himmel zu erwarten sein, vielleicht abgesehen von einem ungewöhnlich dichten Cirrus. Da mit den Cirren meistens auch starker Dunst auftritt,

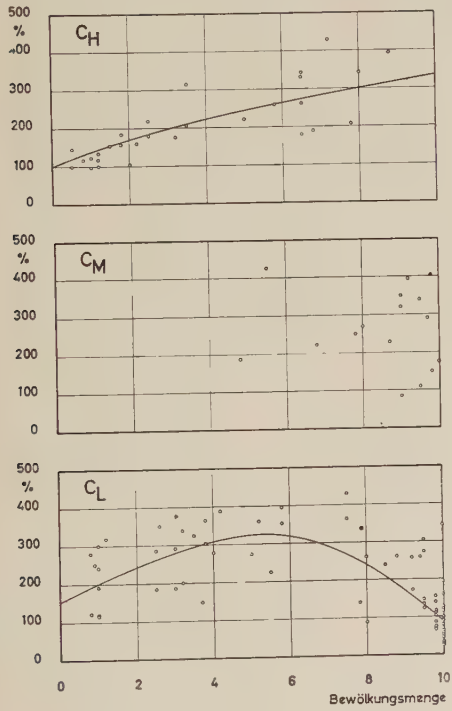

Abb. 6 - *Die Tagessummen der diffusen Himmelsstrahlung bei verschiedener Bewölkungsmenge in Locarno-Monti in Prozenten des Wertes bei ganz klarem Himmel, getrennt nach C_H, C_M und C_L.*

kann ihr Beitrag zur Vermehrung der diffusen Himmelsstrahlung nicht sicher ermittelt werden. Für die Wolken des mittleren Niveaus sind leider nur wenige Werte verfügbar und die meisten finden sich zwischen 8 und 10 Zehnteln Bewölkungsmenge. Auffallend ist hier die grosse Streuung, was insofern nicht überrascht, als namentlich der Altostratus von sehr wechselnder Dichte sein kann. Auch bei den Wolken des tiefen Niveaus ist die Streuung noch erheblich. Der Kurvenverlauf der Mittelwerte ist jenem nicht unähnlich, wie er für den Zusammenhang von diffuser Himmelsstrahlung und relativer Sonnenscheindauer gefunden wurde, (siehe Abb. 3). Bei ganz dichter tiefer Bewölkung liegen zahlreiche Werte weit unter 100%. Aus zeichnungstechnischen Gründen konnten bei der Bewölkungsmenge 10 Zehnteln

TABELLE 2 - *Maximalwerte der Tagessummen der diffusen Himmelsstrahlung in cal·cm⁻² in Locarno-Monti.*
SS = Sonnenscheindauer in Stunden, *R* = relative Sonnenscheindauer, *T* = Globalstrahlung, *D* = diffuse Himmelsstrahlung, $D/T\%$ = relative Globalstrahlung, $D/D_k\%$ = Tagessumme der diffusen Himmelsstrahlung in Prozenten der Tagessumme bei ganz klarem Himmel

Datum	*SS*	$R\%$	T cal · cm^{-2} d^{-1}	D cal · cm^{-2} d^{-1}	D/T %	D/D_k %	Tag. - Mitt. Bew. - Mge (Zehntel)	Bew.-Mge von bis	Bewölkungsart und weitere meteorologische Daten	Stärkes des Dunste
1958										
25. April	3.2	25	408	337	83	503	9.0	8 — 10	Ci fib, Ci spi, *Ac tr*, Sc, St, Cu med	1 — 2
10. Mai	3.8	29	430	343	80	490	9.9	9 — 10	*Ci fib*, *Ci spi*, *As*, *Ac*, Sc, Cu med, Cu hum	1 — 2
6. Juni	2.6	19	452	382	85	523	9.2	9 — 10	*Cs*, As, *Ac tr*, Cu med, Cu con	0
26. Juli	4.6	34	481	339	70	477	8.4	7 — 10	Cs, Ci fib, Ci spi, Ac tr, Sc, Cu, Himmel weisslich	0 — 1
1. August	9.4	71	513	299	58	421	2.5	2 — 4	Ac acgen, *Sc*, *Cu med*, *Cu con*, Himmel weisslich	2
5. September	3.4	28	287	218	76	363	7.6	1 — 10	Ci fib, *Sc*, *St*	1 — 2
21. Oktober	4.7	50	226	151	67	397	7.4	3 — 10	*Cs*, *Ci fib*, *Ci spi*, Ac, Sc, St	0
26. November	6.8	92	165	121	73	432	3.8	2 — 6	Ci fib, Ci spi, Ac, Sc, Cu hum	0
9. Dezember	0.3	4	96	85	89	327	7.9	4 — 10	*Ci fib*, *Ci spi*, *Ac*, Sc	0 — 1
1959										
24. Januar	4.6	59	174	110	63	344	9.4	9 — 10	*Cs*, *Ci*, As, Sc, St	0
24. Februar	4.3	44	214	134	63	327	7.8	3 — 10	Ci spi, *Sc*, *St*	2
9. März	5.0	48	300	215	72	457	9.8	9 — 10	*Cs*, *Ci spi*, Ac, Sc, Cu	0
18. April	5.8	46	318	274	86	428	8.2	5 — 10	Ci, *Ac*, Ac len, Sc, St	0 — 1
7. Mai	7.6	58	516	310	60	443	6.1	1 — 10	Ci fib, Ci spi, *Ac*, *Ac cogen*, Cu con	1 — 2
7. Juni	5.4	40	437	331	76	453	7.0	5 — 8	Ci fib, *Ac*, *Ac cogen*, Cu con	0 — 2
8. Juli	2.2	16	392	333	85	456	8.9	7 — 10	Ac, *Sc*, *St*, *Cu med*	0 — 1
8. August	4.9	38	438	326	74	472	8.5	6 — 10	Ci spi, *Ac*, *Ac op*, Sc, St, Cu med	1 — 2
14. September	5.4	47	373	271	73	493	6.8	4 — 10	As, Ac, Sc, St, Cu med, Cu con	1 — 2
15. Oktober	5.7	59	256	172	67	430	7.6	2 — 10	Sc, St	2
11. November	4.9	61	179	122	68	407	7.4	4 — 10	Ci spi, Ac, *Sc*	1 — 2
20. Dezember	1.7	24	110	91	83	350	8.5	6 — 10	Ci fib, Ci spi, Ac	0

nicht alle Punkte eingetragen werden; zahlreiche Werte sind mehrfach belegt. Betrachten wir noch einmal zusammenfassend die Abb. 6, so müssen wir feststellen, dass *jede* Bewölkungsart der drei Niveaus, bis zu mehreren hundert Prozenten zur Vermehrung der diffusen Himmelsstrahlung beitragen kann. Das scheint also weniger eine Angelegenheit der Wolken*art* als vielmehr der Wolken*dichte* zu sein.

Zu interessanten Ergebnissen führt auch die Untersuchung der Frage, unter welchen Bedingungen die höchsten Tagessummen der diffusen Himmelsstrahlung erreicht werden. In Tabelle 2 sind die entsprechenden Werte aufgeführt. Aus dieser Zusammenstellung kann man unter anderem folgendes entnehmen: Im allgemeinen ist das Tagesmittel der Bewölkungsmenge (es wurden hier die Terminbeobachtungen von 7h30, 10h30, 13h30 und 16h30 verwendet) sehr gross. Ein roher Vergleich von relativer Sonnenscheindauer und Bewölkungsmenge lässt aber schon erkennen, dass ein beträchtlicher Teil der Wolken genügend transparent gewesen sein muss, um die relativ grossen Sonnenscheindauern zu ermöglichen, die an diesen Tagen zu verzeichnen sind.

Das wird auch durch eine Betrachtung der Bewölkungsart bestätigt. Die vorherrschenden Wolkenarten (kursiv gedruckt) sind die des hohen und mittleren Niveaus, wobei allerdings bemerkt werden muss, dass auch der Dunst an den meisten Tagen sehr stark war. Charakteristisch ist überdies die Vielfalt der auftretenden Wolkenarten. Der höchste Wert wurde am 6. Juni bei Cs und AC tr mit 523% erreicht. Bildet man das Verhältnis von Himmelsstrahlung zur Gesamtstrahlung von Sonne + Himmel (D/T in Prozenten), dann erkennt man sehr klar, welche Bedeutung die Erfassung der diffusen Himmelsstrahlung für die kurzwellige Einstrahlung hat. Wir haben auch die Bedingungen, unter denen die niedrigsten Werte der diffusen Himmelsstrahlung auftreten, einer näheren Prüfung unterzogen. Durchwegs handelt es sich um Niederschlagstage bei geschlossener Wolkendecke. Relativ oft herrscht an diesen Tagen gleichzeitig Nebel. Die meisten Werte liegen weit unter 100%, der tiefste Wert wurde am 28. Oktober 1959 mit 26% festgestellt. Die Untersuchungen über den Einfluss von Bewölkungsmenge und -art würden sich noch wesentlich erweitern lassen, wenn man nicht nur von den Tagessummen der diffusen Himmelsstrahlung, sondern von den Momentanwerten der Strahlung an den einzelnen Terminen der Bewölkungsbeobachtungen ausgehen würde, wie das P. Bener [6] gemacht hat. Leider liegen in Locarno-Monti für die Sommermonate unserer Untersuchungsperiode noch nicht genügend gesicherte Tagesgänge der diffusen Himmelsstrahlung an sehr klaren Tagen vor, um diese Vergleiche durchführen zu können.

In dieser Arbeit sind nur einige der augenfälligsten Resultate mitgeteilt worden. Es wäre von Interesse, weitergehende Studien über den Einfluss der Wolken auf die Himmelsstrahlung zu machen; so z.B. darüber, in welcher Art sich die Verteilung der Wolken auf der scheinbaren Himmelsfläche auswirkt, ob gewisse Wolkenarten einen nur diesen eigenen Kurvenverlauf ergeben, welchen Einfluss die Dichte und die vertikale Mächtigkeit einer Wolkendecke auf die Grösse der diffusen Himmelsstrahlung haben. Für den Flugwetterdienst wäre es sehr vorteilhaft, wenn man z.B. von der sehr einfach zu messenden diffusen Himmelsstrahlung auf die vertikale Mächtigkeit von Nebel- und Hochnebelschichten schliessen könnte. Auch der Zusammenhang der diffusen Himmelsstrahlung mit der Sicht, dem Dampfdruck, den Kondensationskernen, dem Trübungsfaktor und der Luftverunreinigung wäre untersuchenswert. Aufschlussreiche Beziehungen ergeben sich auch zwischen der diffusen Himmelsstrahlung und der Globalstrahlung.

Die vorliegenden Untersuchungen stellen einen Beitrag zu den in der Schweiz durchgeführten Strahlungsmessungen während des Internationalen Geophysikalischen Jahres dar, die in dankenswerter Weise vom « Schweizerischen Nationalfonds zur Förderung der wissenschaftlichen Forschung » unterstützt wurden.

LITERATUR

([1]) Schüepp W.: *Enregistrement séparé des composantes du Rayonnement solaire*, Bulletin du Service Météorologique du Congo Belge et du Ruanda Urundi, No. 8, Août 1952. — ([2]) Drummond A. J.: *On the Measurement of Sky Radiation*, Archiv für Meteorologie, Geophysik und Bioklimatologie, Serie B, Bd. 7, 1956, S. 413-436. — ([3]) Dirmhirn Inge: *Untersuchungen der Himmelsstrahlung in den Ostalpen mit besonderer Berücksichtigung ihrer Höhenabhängigkeit*, Archiv für Meteorologie, Geophysik und Bioklimatologie, Serie B, Bd. II, 1951, S. 301-346. — ([4]) Thams J. C.: *Die Intensität der direkten Sonnenstrahlung bei Nordföhn auf der Alpensüdseite*, Archiv für Meteorologie, Geophysik und Bioklimatologie, Serie B, Bd. 6, 1954, S. 139-151. — ([5]) Thams J. C.: *Zum Problem der Doppelschätzung der Bewölkungsmenge*, Vierteljahrsschrift der Naturforschenden Gesellschaft in Zürich, XCIII, 1948, S. 223-237. — ([6]) Bener P.: *Der Einfluss der Bewölkung auf die Himmelsstrahlung*, Verhandlungen der Schweizerischen Naturforschenden Gesellschaft, Zürich 1946, S. 88-89.

(*Eingegangen am* 14. *April* 1961)

MESSUNGEN DER HIMMELSSTRAHLUNG UND DEREN POLARISATIONSGRAD WÄHREND DER SONNENFINSTERNIS AM 15.2.1961 IN VIAREGGIO (ITALIEN)

von E. de Bary, K. Bullrich & D. Lorenz (*)

Summary — On the occasion of the total solar eclipse in Viareggio (Italy) measurements of intensity of sky radiation and polarization have been carried out at 90 degrees vertical distance from the sun. UV-, green- and red-filters have been used. The results showed a diminution of the intensity during the eclipse of about 3 powers of ten. The sky brightness in the point 90 degrees distant during the total eclipse was similar to the brightness when sun is 7 degrees below the horizon. About one minute before the total eclipse the degree of polarization diminuished to zero. — Furthermore photos of nearly the total sky were made using two cameras with wide angle lenses.

A) *Einleitung.*

Das Ereignis der Sonnenfinsternis am 15.2.1961 gab Veranlassung zu Messungen der Himmelsstrahlung und deren Polarisationsgrad. Ein vorläufiger Bericht darüber soll heute and dieser Stelle gegeben werden.

Die Messungen sollten in erster Linie einen qualitativen Einblick über den Betrag derjenigen Himmelsstrahlung bringen, welcher während der totalen Finsternis nur indirekt in die Atmosphäre und zum Beobachter gelangt.

Die Strahlung eines jeden Himmelspunktes setzt sich aus 2 Komponenten zusammen:

a) Die von der Sonne erhaltene und in der Atmosphäre direkt zum Beobachter gestreute Strahlung,

b) Die sekundär und von höherer Ordnung in der Atmosphäre gestreute Strahlung.

Die beiden Komponenten zusammen werden mit Mehrfachstreuung bezeichnet.

Während einer totalen Sonnenfinsternis kommt die primäre Streuung nicht mehr zur Wirkung, weil die Atmosphäre keine direkten Sonnenstrahlen erhält, sondern nur indirekte Strahlung, die durch mehrfache Streuvorgänge hervorgerufen wird, und die ihren Ursprung in den außerhalb des Schattengebietes liegenden

---

(*) Meteorologisch-Geophysikalisches Institut der Universität *Mainz.*

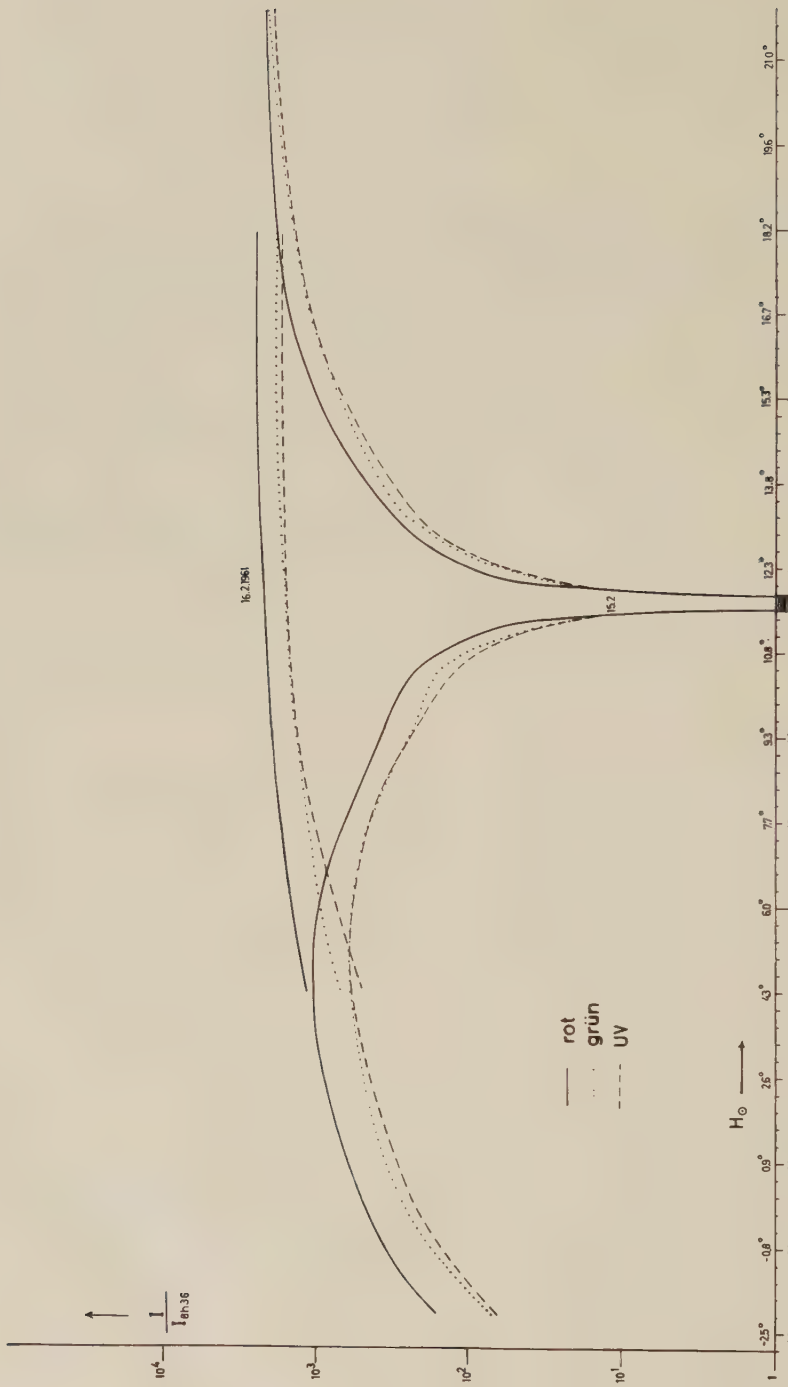

Abb. 1 - *Himmelsstrahlung im Sonnenvertikal in 90° Abstand von der Sonne am 15.2. und 16.2.1961 in Viareggio.*

Teilen der Atmosphäre hat. Die Himmelsstrahlung, die während der totalen Verfinsterung gemessen wird, ist daher ein Maß für den Betrag der Strahlung, die allein durch Steuung höherer Ordnung erzeugt wird.

B) *Messgeräte.*

a) *Photometrische Messmethode* — Es soll vorausgeschickt werden, daß das Photometer immer auf den im Sonnenvertikal in 90° Abstand von der Sonne liegenden Punkt gerichtet war. Das Gerät hatte einen Oeffnungswinkel von 14°. Als Meßelement diente ein Multiplier. Als Filter wurden ein Interferenzfilter für UV, ein Grünglas- und ein Rotglasfilter verwendet. Außerhalb der totalen Verfinsterung wurden für den grünen und den roten Wellenlängenbereich auch Interferenzfilter verwendet. Die Polarisation konnte mit Hilfe eines im Tubus des Photometers befindlichen drehbaren Polarisationsfilters bestimmt werden. Die verstärkten Intensitäten wurden an einem Multiflex Galvanometer abgelesen und auf Tonband gesprochen.

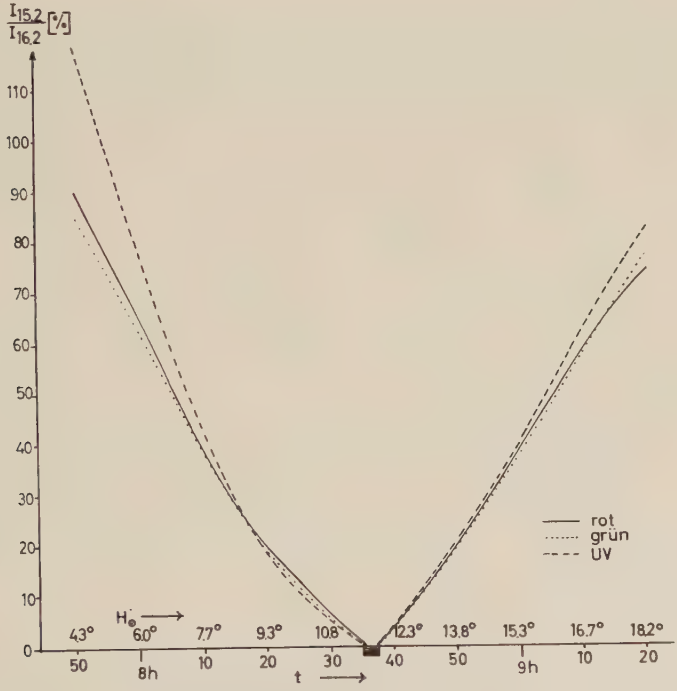

Abb. 2 - *Himmelsstrahlung im Sonnenvertikal in* 90° *Abstand von der Sonne am* 15.2.1961 *ausgedrückt in* % *der vom* 16.2. *im selben Zeitraum.*

b) *Photographische Messmethode* — Da die Phase der Totalen Verfinsterung nur etwa 2 Minuten dauerte, mußten die Photometermessungen auf einen einzigen Punkt des Himmels beschränkt werden. Um aber wenigstens einen Anhalt über die Gesamt-Leuchtdichte an anderen Stellen des Himmels zu bekommen, wurden

während der totalen Verfinsterung eine Reihe photographischer Aufnahmen des Himmels gemacht. Hierzu wurden 2 Kameras mit Superweitwinkel-Objektiven verwendet.

Mit je 3 Aufnahmen dieser Kameras konnte ein 80° - 90° breiter Streifen des Himmels von Horizont zu Horizont über den Zenith aufgenommen werden. Die Azimuth-Einstellung war dabei so gewählt, daß die Sonne etwa auf der Mittelsenkrechten der Bilder lag. Um die Reproduzierbarkeit der Aufnahmen zu gewährleisten, wurde jeweils ein Stück Film gleicher Emulsions-Nummer mitentwickelt, auf das ein Graukeil aufbelichtet war. Die Aufnahme-Zeitpunkte wurden auf Tonband gesprochen, so daß eine sekundengenaue Zuordnung zu den Photometermessungen möglich ist. Bei der Auswertung der Aufnahmen, die noch nicht abgeschlossen ist, wird der Helligkeitsabfall der Objektive rechnerisch berücksichtigt.

Den Firmen Agfa-Leverkusen, Leitz-Wetzlar und Schneider-Kreuznach, sei bei dieser Gelegenheit für ihre Unterstützungen gedankt.

C) *Messergebnisse.*

a) *Photometrische Messmethode* — Auf den Abbildungen 1-4 sind einige Ergebnisse der Messungen wiedergegeben, die am 14., 15. und 16.2.1961 in Viareggio bei Pisa ($\varphi = 43°44'$, $\lambda = 10°15'$, $H = 40$ m NN) durchgeführt wurde (*).

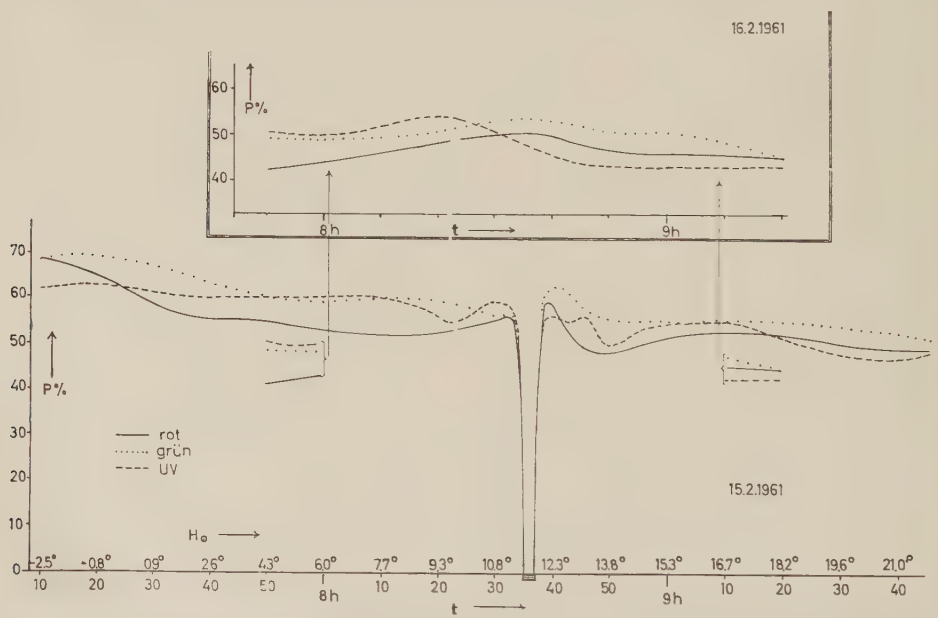

Abb. 3 - *Polarisationsgrad der Himmelsstrahlung im Sonnenvertikal in 90° Abstand von der Sonne am* 15.2. *und* 16.2.1961.

(*) E. Röd besorgte mit grosser Umsicht einen geeigneten Messplatz mit freiem Horizont. Für seine Hilfe, auch bei der Durchführung der Messungen, sei hier gedankt.

Auf Abb. 1 ist die relative Intensität der Himmelsstrahlung in den 3 genannten Wellenlängenbereichen während der partiellen und der totalen Sonnenfinsternis inAbhängigkeit von der Zeit bzw. Sonnenhöhe aufgetragen (logarithmischer Maßstab). Dabei wurden alle Meßwerte auf die Intensität während der totalen Finsternis bezogen. Sie haben also während der totalen Finsternis den Wert 1. Zum Vergleich sind die Meßergebnisse, die während des gleichen Zeitraumes am nachfolgenden Tag gewonnen wurden, beigefügt.

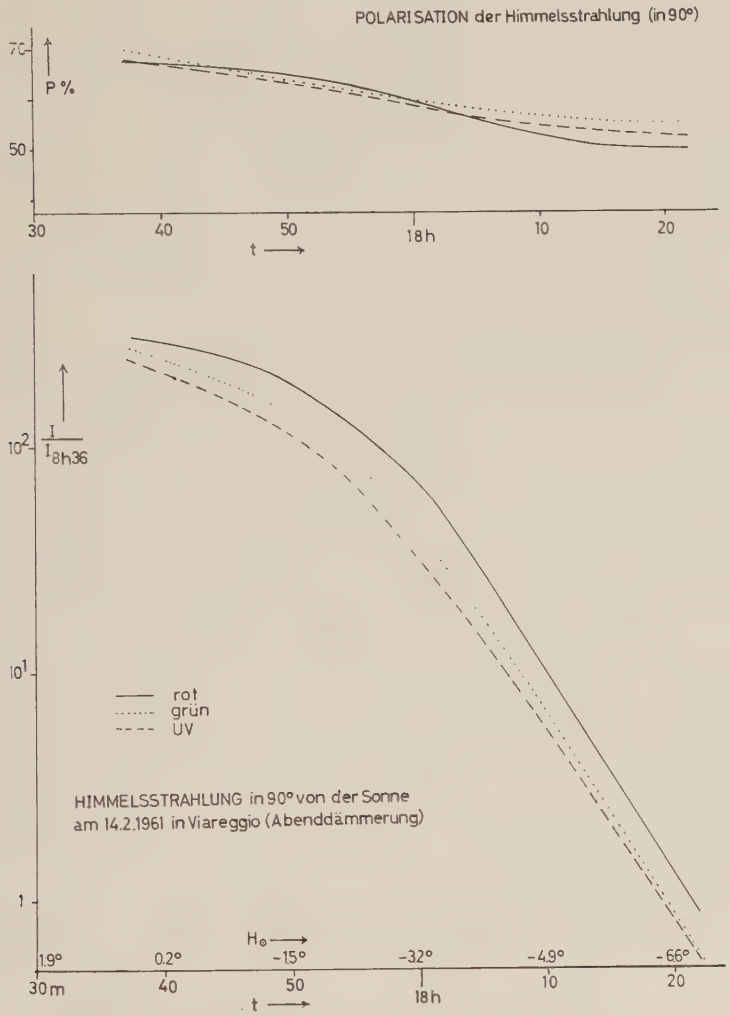

Abb. 4 - *Himmelsstrahlung und Polarisationsgrad der Himmelsstrahlung im Sonnenvertikal in 90° Abstand von der Sonne während der Abenddämmerung am* 14.2.1961 *in Viareggio.*

In Abb. 2 ist der Quotient der Ergebnisse vom 15. und 16.2, bezogen auf die Werte vom 15.2, wiedergegeben (linearer Maßstab). Wird annäherungsweise angenommen, daß die Trübungsverhältnisse an beiden Tagen ähnlich waren, so gibt

diese Darstellung einen anschaulichen Ueberblick über den Einfluß der Verfinsterung auf die Himmelsstrahlung. Erst wenn etwa 50% der Sonne durch den Mond bedeckt sind, setzt eine Verminderung der Himmelsstrahlung in Zenithnähe ein. Dabei ist angedeutet, daß die Strahlung im roten Wellenlängenbereich etwas stärker herabgesetzt wird, als im Kurzwelligen. Zunächst könnte erwartet werden, daß die Intensität im Rot relativ zunimmt, weil die zur Wirkung kommende Strahlung vom Sonnenrand röter ist als die von der abgedeckten Sonnenmitte. Andererseits ist während der totalen Verfinsterung der Einfluß der Streuung höherer Ordnung maßgebend, und dieser ist im Kurzwelligen größer als im Rot. Dieser Effekt der Streuung höherer Ordnug bewirkt während der totalen Sonnenfinsternis ein stärkeres Absinken der Himmelsstrahlung im roten Spektralbereich.

Auf Abb. 3 ist der gemessene Polarisationsgrad der Himmelsstrahlung im Sonnenvertikal in 90° Abstand von der Sonne wiedergegeben. Auffallend ist, daß der Polarisationsgrad, abgesehen von kurzzeitigen Schwankungen, bis zur totalen Verfinsterung konstant bleibt. Erst etwa 1 Minute vor dem zweiten Kontakt sinkt der Polarisationsgrad schnell ab. Während der Verfinsterung hat er den Wert 0 und schon etwa 1 Minute nach dem 3. Kontakt erreicht er wieder fast seinen normalen Wert.

Zum Vergleich sind auf der Abb. 3 die Werte des Polarisationsgrades mit aufgetragen, die am folgenden Tag zur gleichen Zeit gemessen wurden. Am 16.2. ist der Polarisationsgrad etwas niedriger als am 16.2. Die Ursache hierfür ist die etwas größere Trübung der Atmosphäre am 16.

Um die Meßergebnisse der Himmelsstrahlung und Polarisation während der Sonnenfinsternis mit solchen während der Dämmerung vergleichen zu können, wurden am Abende des 14. schon Himmelstrahlung und Polarisationsgrad, wiederum in 90° Abstand von der Sonne im Sonnenvertikal gemessen. Diese Messungen sind auf Abb. 4 dargestellt. Es ist zu sehen, daß die Intensitäten bei einer Sonnenhöhe zwischen — 6° und — 7° dieselben sind wie bei der totalen Sonnenfinsternis. Der Polarisationsgrad nimmt während der Dämmerung langsam ab, im Rot ein wenig mehr als im kurzwelligen Spektralbereich.

b) *Photographische Messmethode* — Aus den photographischen Aufnahmen läßt sich bereits ohne photometrische Auswertung während des Ablaufs der totalen Verfinsterung eine starke Änderung der Helligkeitsverteilung am Himmel erkennen. Sieist auf das Wandern des Mondschattens zurückzuführen. Die Helligkeit ist auf der Seite am größten, wo die Schattengrenze dem Beobachter am nächsten ist.

(*Eingegangen am* 11. *April* 1961)

SOME QUERRIES CONCERNING TROPICAL CYCLONES AND THEIR ORIGIN

by Ernest Gherzi S. J. (*)

Summary — The Author mentions some geographical data apparently neglected when one is considering the origin of a developing tropical cyclone.

Résumé — L'auteur avance quelques critiques au sujet de diverses techniques employées actuellement dans l'étude de l'origine des cyclones tropicaux.

The study of tropical cyclones has reached a tremendous development. It is almost impossible to get and read all the papers published, since the last war, on this always exciting subject.

We will give a short description of our impressions after the perusal of many of these recent investigations and will raise some questions to which, as far as we have been able to ascertain, no answer has yet been given, either because of a possible oversight or because of a somewhat « a priori » underating of established facts.

What had already been stated and demonstrated by Far Eastern meteorologists, forty years ago, namely that the tropical cyclones develop, without the usual cold and warm fronts of extratropical storms, in the interior of an homogeneous air mass (the Trade wind air mass) and that the main source of their energy is to be found in the latent heat of condensation, is now-adays accepted and at times given, strange to say, as a recent finding. Most meteorologists admit that the « hurricane » develops out of a preexisting surface atmospheric disturbance.

Although a confusion is still apparent in many articles about the origin of this preexisting surface disturbance and its intensification, all admit that a convection is the body of the hurricane. The height, the intensity and the diameter of the storm are, from the point of view of its thermodynamic nature, quite secondary considerations. Of course a more violent cyclone will cause greater destruction, but the meteorologist in his study of the atmospheric trouble is interested in its thermodynamic complex. A moderate and a full fledged hurricane are both of the same nature. The practice of distinguishing a tropical depression from a tropical storm and from a tropical cyclone or hurricane, has no thermodynamic foundation. It is a question of a greater or smaller intensity. Too often this subjective appreciation of the violence of the storm has been found wrong and dangerous. The intensity of these disturbances varies continuously and its real value can elude our analysis, owing to the lack of continuous and well located data around the center.

The fact that the central region of the cyclone can reach the upper or the mean troposphere levels, is also a secondary question, even for defining the intensity of the storm. Small tropical cyclones have been as violent as larger ones.

Too many times the forecaster, who had mentioned only a tropical depression for the next 24 hours, had to rush a special and belated warning stating that the so called « tropical depression » had suddenly become a violent hurricane.

(*) Geophysical Observatory, Brébeuf College, *Montreal, Canada.*

We know by oral communication how many mariners have been strongly outspoken against such a discriminative practice, most of the time based only on scattered weather reports. It has been found safer to simply state that the tropical cyclone was by such and such latitude and longitude and that its intensity was unknown.

The frequent relocation of centers has also caused distress to mariners who to comply with a warning giving the position of the storm to one tenth of degree (6 nautical miles) for the next 24 hours, had already altered their course. Others who had kept unchanged their route met the center of the cyclone where it should not have been.

But these unhappy events are not the subject we intend to discuss.

While it is admitted that convection is the real core of the tropical cyclone, we wonder why, more and more, meteorologists stick to the statement that the convection, which will gradually become a real cyclone, can develop only over the ocean's surface.

Extensive and daily maps of the hourly temperature of the ocean's surface water are unhappily not available to the public. One cannot check if the area of the ocean, where such and such storm formed, was really warmer than usual, and warmer than other more distant patches. The geographical dimensions of these warmer areas remain also unknown. A research made by outselves has shown that often, for instance in the Caribbean Sea, the ocean temperature had been rather high and nevertheless no tropical cyclone had made its appearance.

We would ask the meteorologist who accepts such a warmer than usual temperature as a requisite for the formation (not for the intensification) of the surface disturbance, which can develop into a hurricane, how he explains that the dimension of this disturbance is so restricted. How can a very small center form over the thousands of square miles of the ocean expanse, where the temperature was warmer. by two or at most five degrees Fahr., than the adjacent waters? This question has apparently never been considered, although to us it seems to be a vital one.

As it is generally admitted that in summer the whole surface of the ocean is a convective area, the meteorologist will mention an Easterly wave as being the triggering factor for the formation of a surface disturbance. But Easterly waves have very large dimensions when compared with the extent of that surface disturbance. And we will not insist on the fact that an Easterly wave has not been present prior to the appearance of many tropical cyclones. They apparently developed independently of any upper atmospheric action.

But why the possibility of a local restricted convection, developing over a small coral islands (and there are thousands of these in the in the hurricane belt), and being driven over the ocean surface by the Trade wind has never been considered? Why such a quite realistic atmospheric condition has never been quoted, when considering the formation of the preexisting disturbance, which the Coriolis force and other outside factors will transform into a cyclonic storm? We think that such a geographical consideration explains why over the western Pacific, dotted with thousands of small coral islands and lagunes, the tropical cyclones are more numerous than over the western Atlantic and why they are non existent to the west and east of southern America. Sophisticated reasons have been advanced concerning the existence of special ocean currents which would make impossible the formation of this type of storm.

Nevertheless the absence of islands in these south American tropical waters is a fact wich bears on the question raised.

Where, north or south and close to the equator, the islands are numerous the cyclones are frequent: where islands are less numerous the storms are few and where islands are absent tropical cyclones do not form. We would like to know the thermodynamic reasons for the rejection of the geographical consideration just formulated.

Such a negative stand of modern meteorologists seems to be untenable when one rembers that recent studies have shown that in the western Atlantic region, tropical cyclones were found to form over the Caribbean Sea, the Gulf of Mexico and close to the eastern coasts of Venezuela and Guiana. Other centers have been found not far from the Cape Verde islands or south of the Moroccan Coast. We do not see how such a recent finding could contradict the statement that the preexisting surface disturbance, due to develop into a real cyclone, may have formed over an island or a coastal strip. When we consider the temperature's value required for the formation of a substantial convection it is clear that, with an air temperature over the islands of 100° to 120° Fahr. and a maximum temperature of 90° Fahr. of the adjacent ocean, a surface disturbance will be formed much more violent than one which would develop over patches of the ocean with a temperature's difference of only 3° to 5° Fahr. This common sense reasoning, brought to the attention of meteorologists, has had no success. It has become a kind of axiom that the preexisting surface disturbance, required for the formation of the hurricane, can only be caused by an over-ocean convection and a « critical » value of the temperature for such a development has been fixed.

The statement that these few degrees temperature difference of the ocean waters can give a sufficient potential energy to the rising air of the convection formed does not prove that a convection, formed over very warm coral islands or tropical coasts and driven over the ocean by the prevailing Trade wind, would not possess the required potential energy.

It is not because it would be much stronger than a convection originated over the ocean that it should be discarded and in no case accepted as the possible origin of the preexisting atmospheric disturbance, required for the formation of a real hurricane.

Moreover, the fact that a tropical cyclone was first located in the open Atlantic waters does not prove that there, over the ocean surface, is the region where the preexisting disturbance formed and where the storm originated. Such a reasoning, latent in many articles, is, we believe, a wishful extrapolation.

In the same manner that an extratropical cyclone, formed inland, can take to the sea, driven by the westerlies, a thundery formation, developed over coral islands, can also move to the ocean expanses being driven by the Trade winds.

We still remember the first Atlas of hurricane tracks published in the United States for the western Atlantic. Almost none of those cyclones, the tracks of which had been initiated over the open waters, had been connected with the Cape Verde islands.

Later editions of the Atlas were clearly showing a continuous path from Cape Verde islands to the east coast of America. We are convinced that, if more ships reports had been received, those centers shown, even now-a-days, as having started in the open Atlantic would be found to have formed near west Africa or over the Dakar coast, like the famous New England hurricane of September 1938.

When at the occasion of cyclones located by the gallant reconnaissance planes over the open waters of the ocean, ships reports are lacking or badly scattered all around the center, one should refrain from pinpointing that region as the one where

the storm formed. The region of the ocean not crossed by our hurricanes tracks could not be accepted by mariners as an usually safe one.

Another item which is more and more interesting modern meteorologists is the energy transfer from the stratosphere into the upper troposphere, and that for explaining some aspects of the cyclonic column; for instance some higher than expected temperature's values. We are not the only meteorologist to oppose such an energy transfer from the very high atmospheric levels to the lower ones. The action exerted on the cyclonic column by the enveloping Trade wind air mass could be a sufficient explanation of facts contrary to the usually accepted model of the tropical cyclone.

And it is convenient to remind the reader that such an energy transfer has not always been established. Often upper atmospheric waves at the 200 or 100 mb level have quietly passed above the surface storm and no intensifiaction was produced.

Another aspect of the vortex of the cyclone which has seemigly been neglected is that of the inclination of the axis of the convection column while the hurricane is advancing or is stationary. Most of the studies published, as far as we have been able to understand, consider this column to remain vertical. An interesting research concerning the diameter of the expanding cyclone in the higher levels has recently been conducted but the possibility of a forward or backward inclination of the storm complex has generally been overlooked. We think that if the inclination of the axis of the cyclone were considered the contradictory values of the rainfall in different sectors of the storm could have a better explanation. The two dynamic centers of the hurricane have been given attention without any specific reference to the swaying of the central column, for instance, when the hurricane is making a « loop ». A more frequent and better checked observations of the types and motion of clouds should greatly help such a research. The up-to-now very few and badly distributed radio soundings, which are at hand around a cyclone, cannot replace the clouds' observations.

At a recent Caribbean hurricane Seminar the question of the future motion of the cyclone was raised. We advised the listeners to look for the place where,in the area defined by the centre and the enveloping 1000 mb isobar, the pressure was falling. The storm would move on that direction. We have never been able to find out if such a technique, so useful in the Far East, had ever been considered and practised in the western Atlantic or in the Gulf of Mexico.

At the same Caribbean hurricane Seminar we asked the local meteorologists not to minimize the experience gained elsewhere than in the western Atlantic. Of course many times phenomena already discovered and well established have been « found again ». Nevertheless the flowers of foreign gardens can be as nicely scented as those of our own parks and have blossomed in an earlier season (*).

(*Received 16th March 1961*)

(*) We add a few lines of a letter recently written by a Master of a well known American liner, plying over the Pacific.

« I wish I could say that the Japanese and our Americans in Guam were doing as good a job to-day on weather prediction as your people did. With high frequency radio and many more reports from ships, they should be expected to broadcast more accurate predictions. Unfortunately, as we old timers recognize, this is not the case » (3rd June 1960).

These somewhat too flattering words might perhaps help to consider our querries as something making sense.

CORRELATION OF PRECIPITABLE WATER VAPOUR VALUES OVER THE UNITED STATES WITH PHYSICAL AND CHEMICAL PARAMETERS.

Part I: SEASONAL TRENDS WITH PRECIPITATION AND ITS NITRATE CONTENT. GEOGRAPHIC CHANGES OF NITRATE (*)

by Alberto Montefinale & Henry M. Papée

Summary — The analysis of Reitan's data on precipitable water vapour in the atmosphere, and data of Junge on the nitrate content of precipitation, is extended onto a seasonal basis. Computations indicate consistency between precipitable water vapour, precipitation and its nitrate content, within a semiempirical law proposed, and especially for the warmer trimestres of the period July 1956 - June 1957. A simple expression correlating the atmospheric content of precipitable water vapour over stations situated between sea level and 580 ft of altitude, with temperature, is suggested and tested. Increasing trends of atmospheric nitrate with latitude are established for all seasons of the period examined.

1. *Introduction.*

It has recently been shown that correlation between total annual precipitation, its content in nitrates, and the precipitable water vapour, appears to occur throughout about 25 stations of the United States sampling network ([1]). Calculations leading to this observations were based on rainwater chemical composition-data due to Christian E. Junge ([2,3]) and on recent values on the content of precipitable water vapour in the atmosphere over a number of stations of the United States Weather Bureau [C.H. Reitan ([4])].

Our previous analysis was carried out with the use of a proposed simple semiempirical relationship and dealt with annual average parameters, and precipitable water vapour values between the station and the 525 millibar level. It was thought that, since both Reitan and Junge made available monthly and seasonal values respectively, an analysis such as the one previously given but pertinent to nitrate, on a trimonthly scale, and up to the 325 millibar level for precipitable water vapour, would be of interest. At the same time it was pointed out to us, that

---

(*) Contribution of the « Centro Nucleazione Aerosoli » of the National Research Council of Italy, Via Vettore 4 (Monte Sacro), *Rome*.

information on seasonal trends in nitrate distribution over the United States (cf. Ref. [5])] might give further insight into the origins of this atmospheric compound. While in fact it is known from JUNGE's work ([6,7]) that a substantial part of atmospheric nitrate is to be found on giant sodium chloride nuclei, it has been observed ([5]) that the amount of nitrate in precipitation is often stoichiometrically larger in the United States than that of sodium, especially at lower altitudes. It is well known that nitric oxides can be generated in the air by discharge phenomena, and since on the other hand it has been pointed out ([8]) that such phenomena may lead to activation of airborne particles towards nucleation, the question of origin and distribution of nitrate becomes of particular importance. Since latitudinal variations of NO_3 over the United States are indicated, the problem arises whether and to what extent the synthesis of the species is due for instance to possible « macroscopic » electric occurrences, or to discharge phenomena caused for example by drifting snow — a possibility which has recently been pointed out to us ([9]).

2. *The data.*

I. *Nitrates and precipitation* — Both « NO_3 », the concentration of nitrate in precipitation, and its product by the amount of water fallen, « R », may be thought of as representative of the nitrate distribution picture. « NO_3 » will depend not only on the amount of the substance formed in the atmosphere and present above the sampling station, but also on the amount of the precipitation fallen, and consequently on both the temperature and the precipitable water vapour, « π », available. On the other hand, the product « $R\ NO_3$ » may be thought of as being representative of the amount of nitrate in the atmosphere, since it is the total measure of the compound contained in the precipitation.

Values for « R » at JUNGE's stations were taken from the Monthly National Summaries of the United States Weather Bureau, for the period July 1956 - June 1957. Trimestrial sums were computed and average daily « R » values in centimetres $\times$ day^{-1} obtained and used in the analysis related to the « NO_3 » $\times$ « R » — « latitude » plots, except for one overall annual diagram where average daily « R » values obtained from an annual sum were used. The same procedure for « R » was applied in calculations involving the precipitable water vapour « π ».

Values for concentrations of nitrate in water collected during the period under examination were taken from Reference ([2]) and transformed into gramme-equivalents $\times$ litre^{-1}. Nitrate data at the following stations are quoted:

Below 100 *ft*:

Charleston	Nantucket	Boston
Hatteras	Tallahassee	Tampa
Jacksonville	Washington DC.	Mobile
Lake Charles	Palm Beach	

Between 500 *and* 1500 *ft*:

Acron	Fort Worth	Madison
Albany	Grand Rapids	Nashville
Burlington	Greenville	Roanoke
Columbia	Indianapolis	Sault Ste. Marie
Des Moines	Int. Falls	St. Cloud

Between 1500 *and* 3000 *ft*:

Amarillo	El Paso	Goodland
Bismarck	Glasgow	Grand Island
		Scottsbluff

II. *Precipitable water vapour and temperature* — Monthly and annual precipitable water vapour values pertinent to the atmosphere over a large number of the United States Weather Bureau Stations were recently published by REITAN ([4]) in the form of suitable maps. Those were based on an 11 year period of analysis, and the Author pointed out that there appeared to be no significant changes in « π » from year to year during this period. We felt that this interesting observation of REITAN allowed us to avail ourselves of data for our calculations which cover JUNGE's period of work, and we selected such stations as were common to the studies of both Authors quoted.

While REITAN's data are obviously altitude « self corrected » in that they give the amount of precipitable water vapour between the station and the 325 mb level, the task of comparing them with JUNGE's values required a temperature correction. Indeed, it can be expected that the precipitable water vapour will strongly depend on the temperature of the air, and that its « aptness » at condensation and subsequent precipitation will be temperature dependent. We found that a reasonably linear dependence exists between the average seasonal temperatures and « π » for about 14 of REITAN's stations situated below 580 ft. of altitude; that latitude correlates with temperature for the same stations and for the 4 trimestres, and that in consequence « π » correlates linearly reasonably well with latitude. We therefore again used an empirical latitude correction for precipitable water vapour, and reduced it for the purposes of our analysis to 35° N. This was done in the same way as previously described ([1]) in order to avoid the « potential temperature formula » by the use of which an alternative reduction of « π » to zero altitude could be calculated, and which appeared to give results of lesser consistency.

Whenever the temperature parameter was necessary, monthly values from the pertinent National Summaries of the United States Weather Bureau were taken and averaged over a trimestrial period. Those averages were then expressed in degrees Celsius or degrees Kelvin, according to the case.

Values obtained by both JUNGE and REITAN at the following stations were used for calculations relative to the « π » parameter:

Albany	Ely	Washington DC.
Albuquerque	Ft. Worth	Nashville
Bismarck	Grand Junction	St. Cloud
Boise	Hatteras	S. Diego
Brownsville	Int. Falls	Santa Maria
Caribou	Lake Charles	Sault St. Marie
Charleston	Las Vegas	Spokane
Columbia	Little Rock	Tampa
El Paso	Medford	Tatoosh Island
		Nantucket

3. *Results and discussion.*

I. *Nitrates* — Plots of nitrate concentration in precipitation vs. latitude, for stations situated to the East of the Rocky Mountains, are given in Figures 1 - 3.

Overall increasing trends for all trimestres can be observed both for stations at altitudes below 100 ft (and therefore near the seashore) and for those between 500-1500 ft of elevation (central United States). It can be seen that the experimental data appear to be less consistent at higher altitudes (Fig. 3), [cf. Ref. (5)]; $R\,NO_3$ latitude plots (Figs 4-6) seem to be generally of the same order of consistency and sign of trend as the ones previously discussed, with a greater uniformity perhaps in

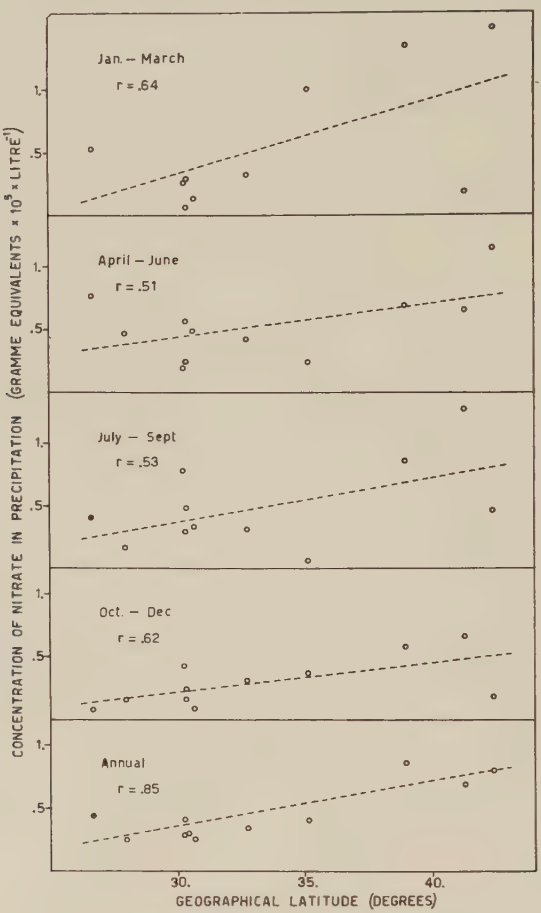

Fig. 1 - *Change of nitrate concentration in rainwater with latitude.* The sampling stations are situated east of the Rocky Mountains, and below 100 ft of elevation. Linear regression lines are drawn to illustrate trends.

the highest range of elevations considered (Fig. 6). Trends increasing with latitude can be noticed again and for all trimestres in the lower two ranges of elevation.

In order to gain further insight into the causes of the occurrences discussed above, parameters of linear regression were calculated for all seasonal groups of points in the lower to ranges of elevation. Values of the gradients and their standard devia-

tions are shown plotted against average pertinent trimestrial temperatures of stations in Figs 7-8. It can be noticed that whereas in case of « NO_3 » a decrease of nitrate concentration — latitude gradients with temperature, is indicated in the

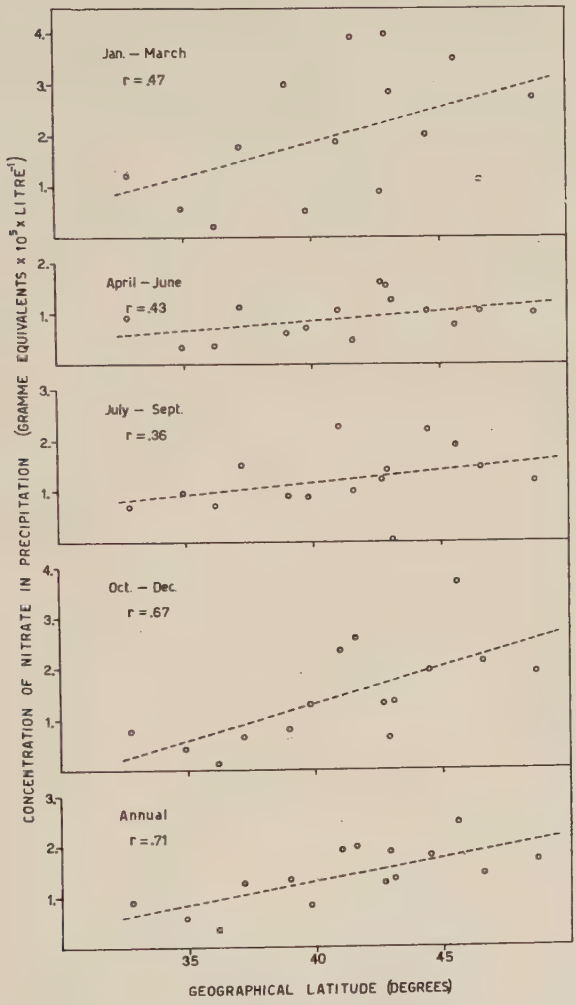

Fig. 2 - *Change of nitrate concentration in rainwater with latitude.* The sampling stations are situated east of the Rocky Mountains, and between 500 and 1500 ft of elevation. Linear regression lines are drawn to illustrate trends.

500-1500 ft range, this is not so for $R\,NO_3$. Such behaviour of the NO_3 and RNO_3 functions could be tentatively explained by assuming that the occurrence of nitrate, as suggested in the later part of this paper — may be associated with precipitation phenomena, and that if this is so, for low values of precipitable water vapour

due to low temperatures, larger amounts of « NO_3 » would be incorporated per unit volume of precipitation. It can readily be seen that if « NO_3 » was to be generated in prevalence by drifting snow, a similar behaviour of the gradients with temperature could be expected. Should this be the case, however, one would expect to have the nitrate incorporated and therefore immobilized at least in a substantial part, on surfaces of drifting snow crystals, and this would probably show only to a small extent in the experimental values, especially since JUNGE took care to have his rain gauges opened only during actual occurrences of precipitation. It

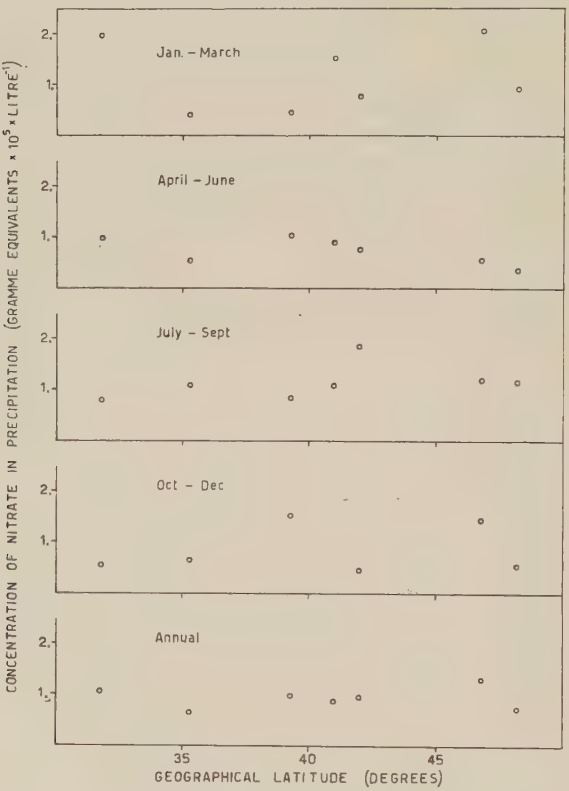

Fig. 3 - *Plot of the nitrate concentration in rainwater against latitude.* The sampling stations are situated east of the Rocky Mountains, and between 1500 and 3000 ft of elevation.

could furthermore be expected that if « NO_3 » in the atmosphere was not to be associated with phenomena which involve nucleation of precipitation, a *substantial* decrease in $d\mathrm{NO_3}/d\mathrm{lat}$ would occur during the colder season, due to a less ready collection of nitrate by the falling snow, than by the falling drops. We therefore are inclined to believe that the explanation of the main causes of the phenomena discussed is to be sought rather in such occurrences as may be associated with ge-

neral patterns of atmospheric circulation, as well as with such factors leading to the presence and permanence of nitrate in the lower strata of the atmosphere, as may be dependant on latitude.

The diagrams showing the behaviour of $dNO_3 / d\text{lat}$ and $dRNO_3 / d\text{lat}$

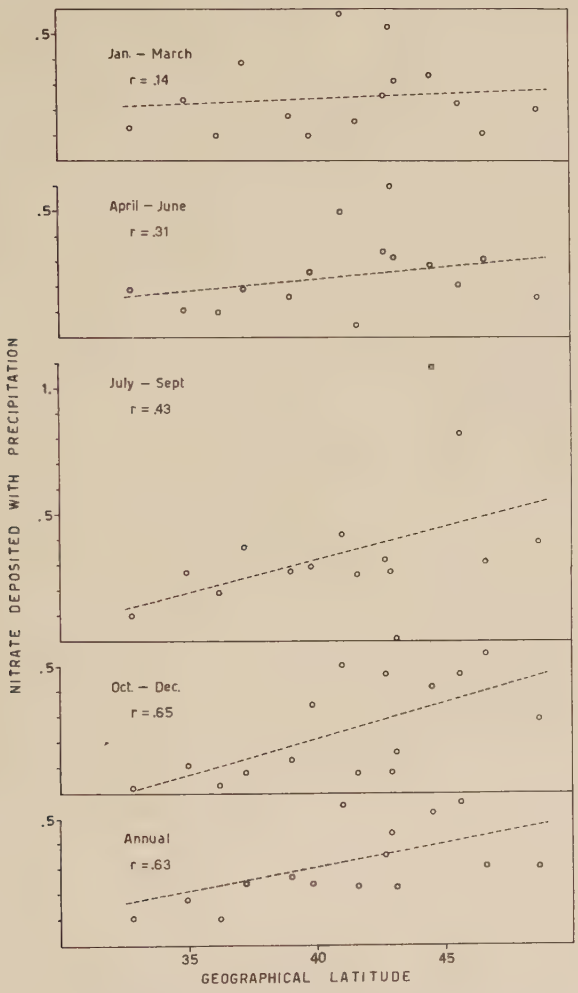

Fig. 4 - *Change of the product: average precipitation* (in centimetre per day) *by its nitrate content* (in gramme-equivalents $\times 10^5$ per litre) *with latitude* (in degrees). The sampling stations are situated east of the Rocky Mountains, and below 100 ft of elevation. Linear regression lines are drawn to illustrate trends.

with seasonal temperatures and *below* 100 ft of elevation can be tentatively explained along the same lines as for the 500-1500 ft range. The only substantial difference on hand appears to be the high value of $dRNO_3 / d\text{lat}$ in the first

trimestre; this may be due to higher precipitable water vapour local values near the sea.

II. *Temperature dependence of precipitable water vapour for stations below*

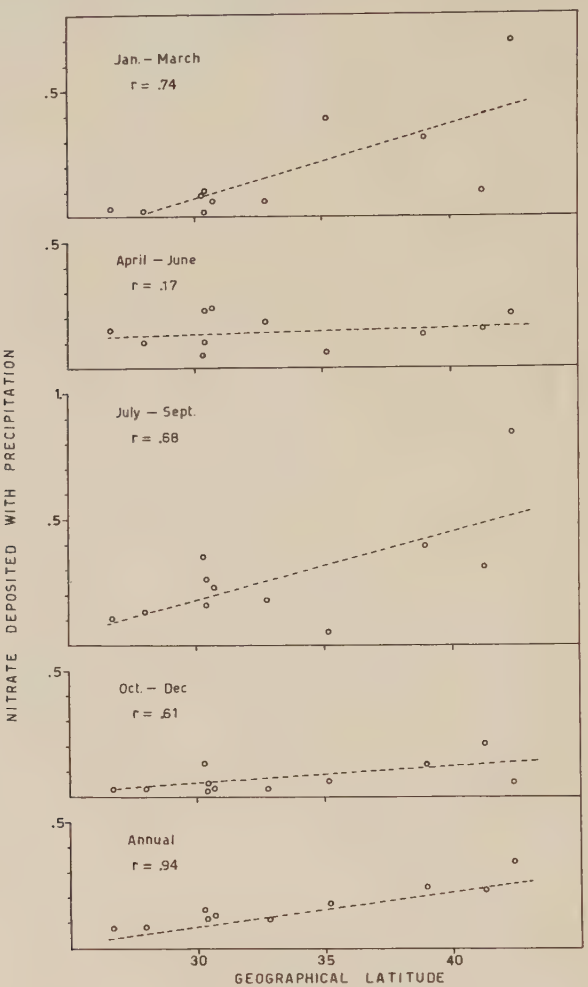

Fig. 5 - *Change of the product: average precipitation* (in centimetres per day) *by its nitrate content* (in gramme-equivalents $\times 10^5$ per litre) *with latitude* (in degrees). The sampling stations are situated east of the Rocky Mountains, and between 500 and 1500 ft of elevation. Linear regression lines are drawn to illustrate trends.

580 *ft* — The observation that the precipitable water vapour contained in the atmosphere above stations situated below 580 ft of altitude, consistently followed approximately linear trends with temperature for each of the 4 seasons, led us to an

attempt at understanding the cause of the phenomenon; especially since, in order to confront data by JUNGE with those of REITAN, reduction of all « π » values to an approximately common $T_{h\simeq 0}$ basis was required.

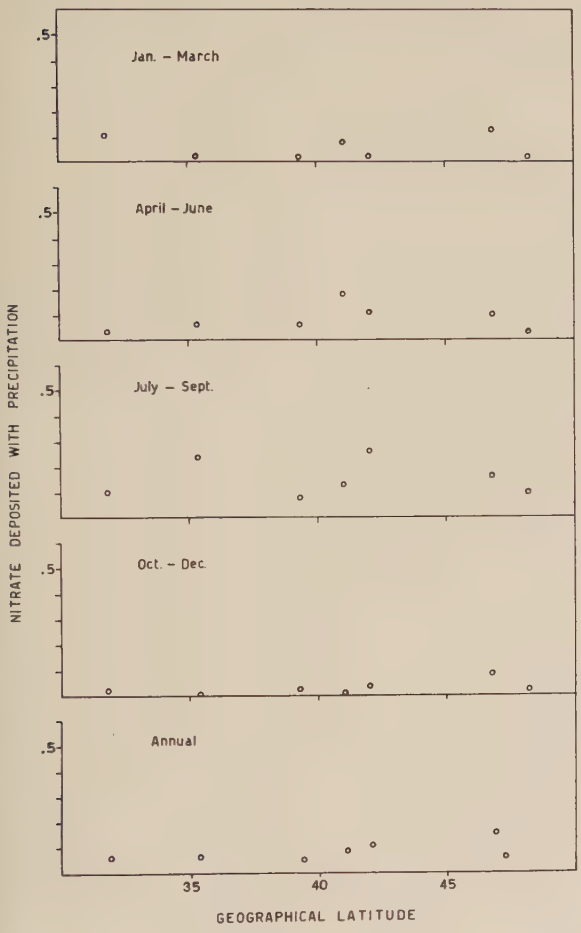

Fig. 6 - *Plot of the product: average precipitation* (in centimetres per day) *by its nitrate content* (in gramme-equivalents $\times 10^5$ per litre) *against latitude* (in degrees). The sampling stations are situated east of the Rocky Mountains and between 1500 and 3000 ft of elevation.

If a steady state distribution of precipitable water vapour with elevation h is assumed, than the concentration of water per unit volume of air, c, may be expected to vary with altitude according to:

(1) $$dc = -kcdh$$

where k is a constant. Eq. (1) integrates to:

(1′) $$c = c_0 e^{-kh}$$

where c_0, the concentration near the source, may be looked upon in terms of Clappey-

ron's equation. This leads to:

$$c_0 = \alpha \exp\left(-\frac{\Delta H}{RT_0}\right) \tag{2}$$

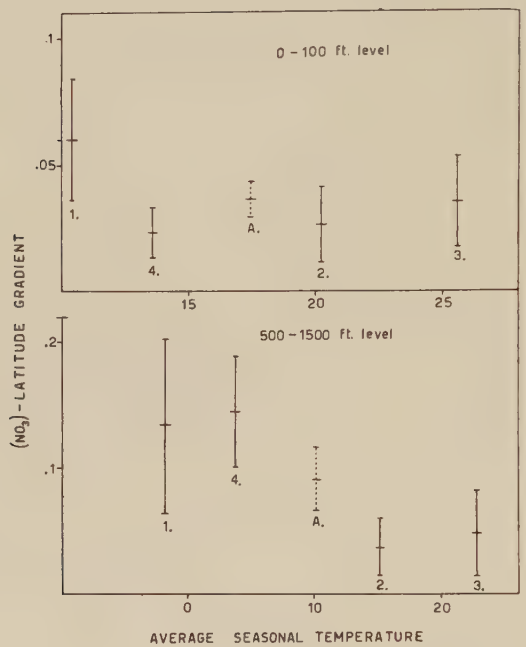

Fig. 7 - *Change of the gradient: nitrate in precipitation-geographical latitude* (in arbitrary units) *with average seasonal temperature of all stations considered* (in degrees C). Sequence numbers of trimestres are given with values.

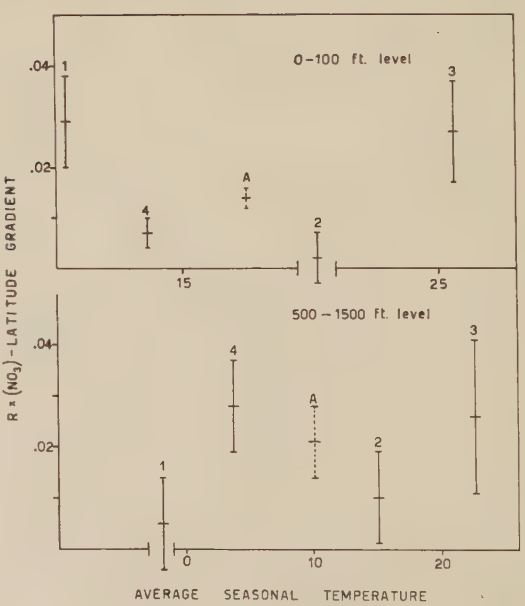

Fig. 8 - *Change of the gradient: Precipitation* × *nitrate content - geographical latitude* (in arbitrary units) *with average seasonal temperature of all stations considered* (in degrees C). Sequence numbers of trimestres are given with values.

where α is a constant, T_0 is the temperature of the source of water vapour, and ΔH and R are the latent heat of evaporation and the gas constant, respectively.

Substituting (2) into (1):

(2′) $$c = \alpha \exp\left(-\frac{\Delta H}{RT_0}\right) \exp(-kh)$$

However:

(3) $$d\pi = cdh$$

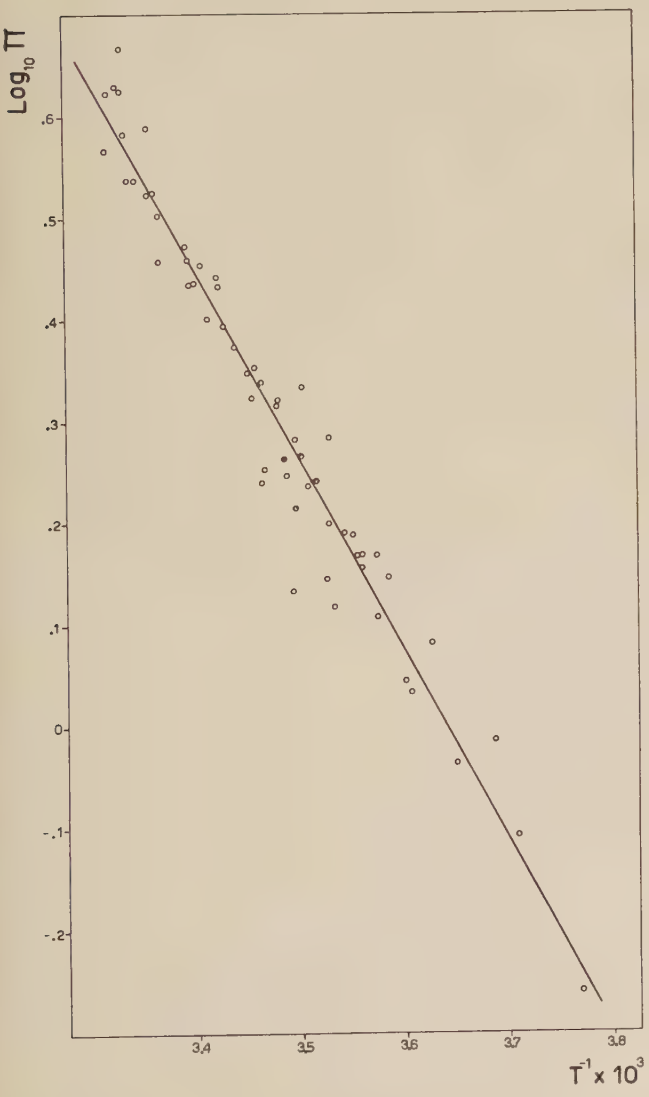

Fig. 9 - *Plot of the decimal logarithm of the average trimestrial precipitable water vapour up to the* 325 mb *level* (in centimetres of water) *against the inverse of the average trimestrial absolute temperature of stations* (degrees). Parameters at 15 of REITAN's stations situated below 580 ft of elevation are quoted, 4 points representing values of 4 trimestres are given for each station.

and the precipitable water vapour, between sea level altitudes ($h = 0$) and 325 mb ($h = H$; where for the practical purpose of this communication H is a constant), π_0, will be:

$$(3') \qquad \pi_0 = \int_0^H d\pi = \int_0^H \alpha \exp\left(-\frac{\Delta H}{RT_0}\right) \exp(-kh)\, dh .$$

A slight approximation enables this to be written:

$$(3'') \qquad \pi_0 = \alpha \exp\left(-\frac{\Delta H}{RT_0}\right) \int_0^H \exp(-kh)\, dh$$

which integrates to:

$$(4) \qquad \pi_0 = \alpha \exp\left(-\frac{\Delta H}{RT_0}\right) \left\{k^{-1}(1 - e^{-kH})\right\} .$$

Equation (4), after transformation, becomes linear in:

$$\log \pi_0 \quad \text{and} \quad T_0^{-1} .$$

Fig. 9 gives the plot of ($\log \pi$) against the inverse of temperature in absolute degrees for those of REITAN's stations which are situated below 580 ft of altitude. 4 points are given for every station, representing average temperatures of each season. There appears to be reasonable agreement with the general form of the equation proposed, especially in view of the approximations involved in deriving eq. (4), and the assumptions involved in the model. Table 1 gives the linear regression parameters obtained on individual seasonal and cumulative values in the system $\log \pi_0$ vs T_0^{-1}.

TABLE 1 - *Linear regression coefficients and their standard deviations for seasonal and cumulative-annual plots of* $\log_{10} \pi$ vs T^{-1} *for* 15 *of the U.S.W.B. stations where* π *up to the* 325 *mb level was measured.* The elevation of the stations is between 0 — 580 ft; π is expressed in centimetres and T in absolute degrees.

	January-March	April-June	July-September	October-December	Annual Cumulative
$\log_{10} \alpha$	$6._{47} \pm .4$	$6._{41} \pm .5$	$6._{48} \pm 1.$	$6._{37} \pm .5$	$6._{81} \pm .2$
Gradient $\times 10^{-3}$	$-1._{78} \pm .1$	$-1._{76} \pm .1$	$-1._{77} \pm .3$	$-1._{55} \pm .1$	$-1._{87} \pm .05$
Correlation coefficient	−.97	−.97	−.94	−.96	−.98

It appears to be of interest to point out that since the gradient should be equal to:

$$0.4343 \frac{\Delta H}{R}$$

— where ΔH stands for the latent heat of evaporation of water, and R is the constant of perfect gases — the value of « ΔH_{exp} » resulting from the cumulative annual data can be computed from the results obtained and its order of magnitude compared with data available (10). This leads to:

$$\Delta H_{exp} = 475.4 \pm 14 \text{ cal gm}^{-1},$$

in reasonable agreement with the reference quoted.

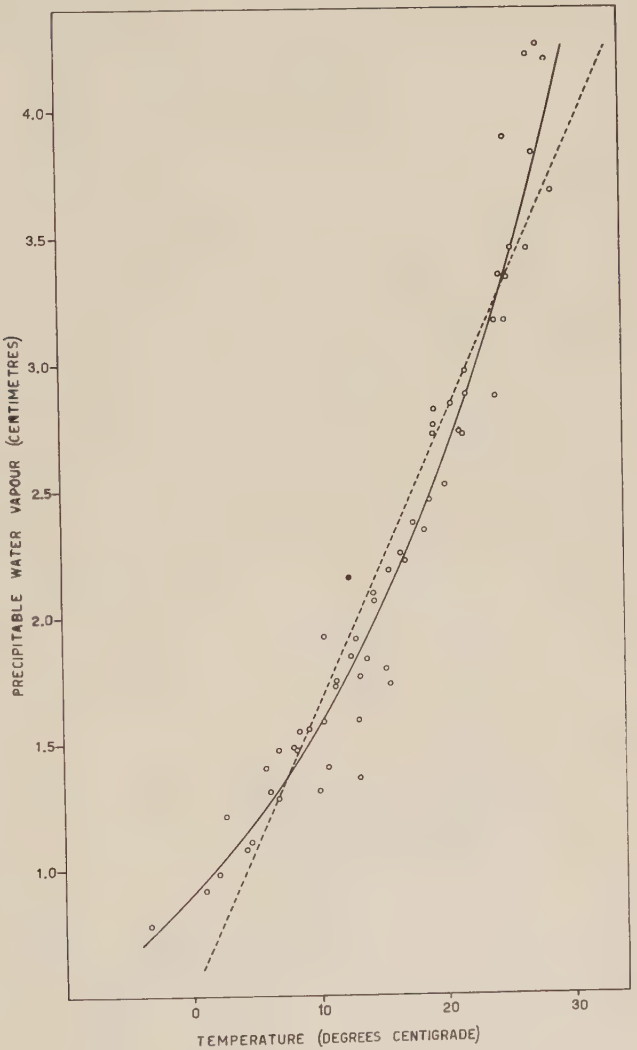

Fig. 10 - *Plot of average trimestrial precipitable water vapour up to the* 325 mb *level* (in centimetres of water) *against trimestrial average temperatures of stations.* Seasonal data at 15 of REITAN's stations situated below 580 ft of elevation are given.

Fig. 10 illustrates the experimental fit obtained by using the calculated parameters α and ΔH in a cumulative plot of π vs t. A least squares straight line is drawn for comparison; the standard deviations of the two functions computed are respectively:

0.203 and 0.277

Table 2 gives linear regression parameters obtained on individual *seasonal* values of π vs t, as well as parameters of the cumulative line. It can be seen from the results that fair linear consistency between seasonal data is approached.

TABLE 2 - *Linear regression coefficients and their standard deviations for seasonal and cumulative-annual plots of* π vs t, *for* 15 *of the U.S.W.B. stations where* π *up to the* 325 mb *level was measured.* The elevation of the stations is between 0 — 580 ft; π is expressed in centimetres and t in degrees centigrade.

	January-March	April-June	July-September	October-December	Annual Cumulative
Gradient $\times 10^2$.....	$7._{37} \pm .8$	$1_{1._{43}} \pm 1.$	$1_{4._{17}} \pm 2.$	$8._{66} \pm 1.$	$11._{46} \pm .5$
Intercept	$.8_2 \pm .09$	$.3_8 \pm .2$	$.0_5 \pm .5$	$.8_0 \pm .1$	$.5_{02} \pm .09$
Correlation coefficient	.93	.96	.89	.92	.95

III. *Correlation of precipitable water vapour with geographic latitude for stations below* 580 *ft and for the four seasons of the year* — As mentioned previously in this and an earlier communication (1) the reduction of π values to a $t_h \cong 0$ basis was carried out with approximation by availing ourselves of consistently linear dependencies between temperature and geographic latitude, for REITAN's stations situated below 580 ft, and by assuming that this correction can be extended within limits of error to stations at higher elevations in the United States. Diagrams on the basis of which the corrections were made are given in Fig. 11, the common base latitude chosen was that of 35° N and, for every seasonal group of points the adjustement of each experimental π value was carried out by multiplying it by the corresponding ratio of $(\pi_{35^\circ}) : (\pi_{lat})$. The latter was obtained from the π-latitude seasonal line, the parameters of which were calculated by least squares.

Table 3 gives linear regression parameters relative to π-latitude plots shown on Fig. 11.

TABLE 3 - *Linear regression coefficients and their standard deviations for seasonal and average annual plots of* π vs *geographic latitude for* 13 *of the U.S.W.B. stations where* π *up to the* 325 mb *level was measured.* The elevation of stations considered is between 0 — 580 ft; π is expressed in centimetres and the latitude in degrees.

	January-March	April-June	July-September	October-December	Annual Average
Gradient $\times 10^2$.....	$-9._{89} \pm .9$	$-9._{26} \pm .5$	$12._{36} \pm .8$	$-9._{76} \pm 1.$	$10._{14} \pm .6$
Intercept	$4._{90} \pm .3$	$5._{95} \pm .2$	$8._{07} \pm .3$	$5._{23} \pm .4$	$5._{95} \pm .2$
Correlation coefficient	−.96	−.98	−.98	−.94	−.98

When the regression parameters are plotted against pertinent seasonal average temperatures (Fig. 12) a generally constant trend of the gradients results except for a small summer deviation. Intercepts indicate an overall increase of π with temperature, as expected on the basis of what was previously discussed.

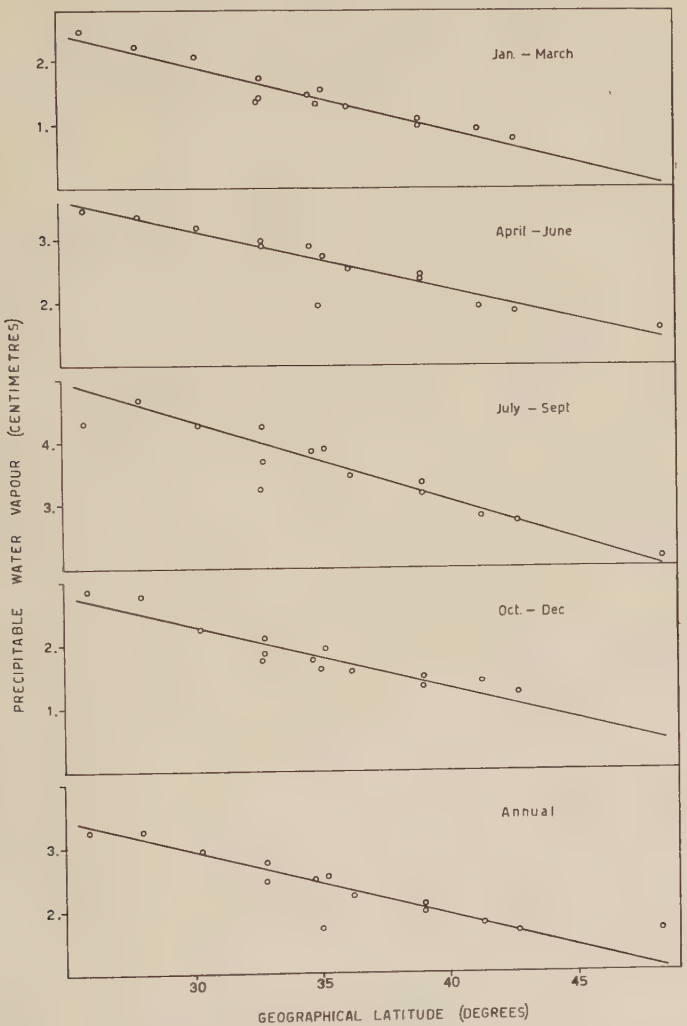

Fig. 11 - *Change of the precipitable water vapour contained in the atmosphere and up to the* 325 mb *level, over U.S. stations used by* Reitan *and situated below* 580 ft *of elevation, - with latitude.*

IV. *The correlation function*: π-R-NO_3 *for the* 4 *seasons* — Fig. 13 gives plots of precipitation against the latitude — corrected precipitable water vapour. Curves of this type, as pointed out previously ([1]), show trends in general agreement with

the integrated expression:

$$\frac{dR}{d\pi} = K(\alpha\pi - \beta R), \tag{5}$$

suggesting that the change of precipitation dR, due to a change of precipitable water vapour, $d\pi$, is proportional to the difference between parameters π and R, each of them multiplied by a suitable expression. This difference is looked upon as the amount of water in the atmosphere which bears direct influence upon precipitation.

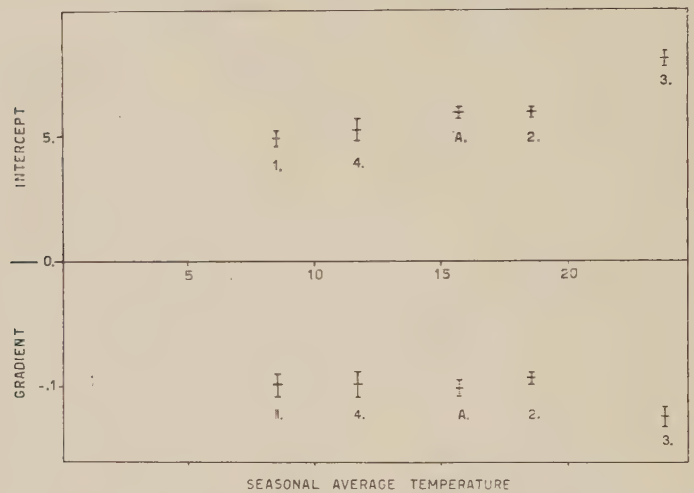

Fig. 12 - *Change of linear regression parameters* (arbitrary units) *pertinent to seasonal variations of precipitable water vapour up to the* 325 mb *level and for stations below* 580 ft *of elevation - with the seasonal average temperatures of all stations* (in degrees C). Sequence numbers of trimestres are given with values.

Examination of β indicates that it may be regarded as a constant of normalization for time of variable R, and has therefore the dimensions of time. α can be looked upon in approximation as a temperature dependent number to be determined over the sampling period considered, while K is a function depending on the amount of nuclei on the path of precipitation. Further insight into the meaning of α can be obtained from the following:

In C is taken to be the concentration of water vapour in a volume of air, and C^* a concentration at which occurrence of precipitation would start at a correspondingly fixed temperature T^*, then:

$$\frac{dR}{d\pi} = K(C - \beta R). \tag{5'}$$

It can be written, however, if variations of vertical temperature gradients from station to station are small:

$$\frac{C^*}{C} = \frac{T}{T^*} \tag{6}$$

and

(7) $$C^* = \tau\pi$$

with τ constant, therefore:

(8) $$C = \frac{T^*}{T}\tau\pi = \alpha\pi .$$

Parameter α is thus seen to depend on the inverse of absolute temperature.

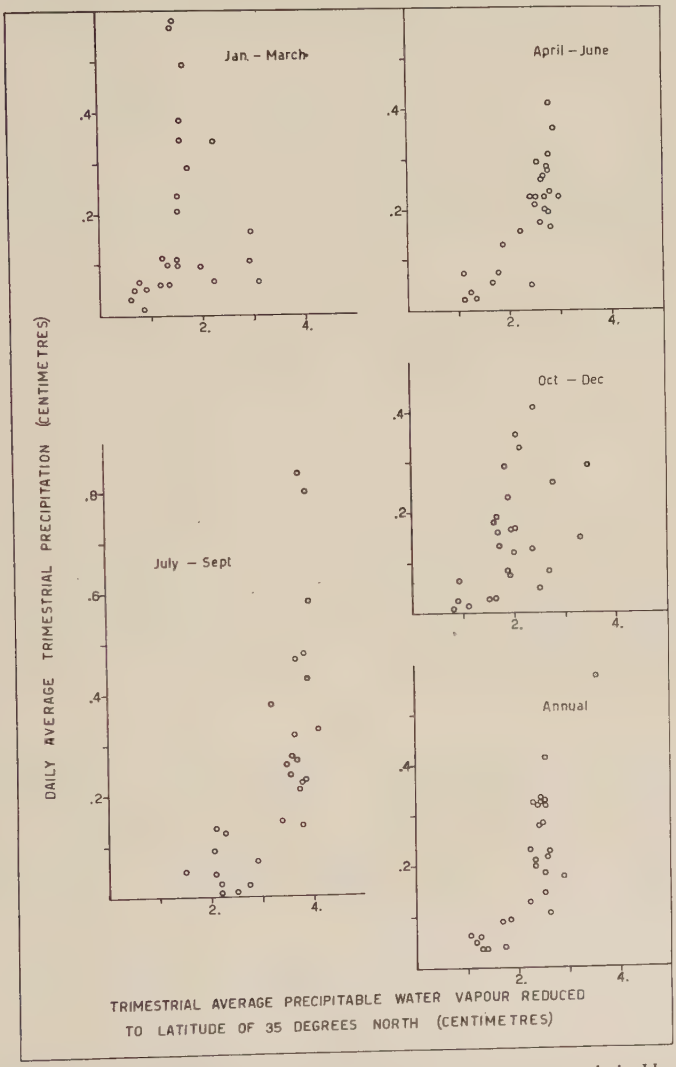
Jan. – March
April – June
July – Sept
Oct – Dec
Annual
DAILY AVERAGE TRIMESTRIAL PRECIPITATION (CENTIMETRES)
TRIMESTRIAL AVERAGE PRECIPITABLE WATER VAPOUR REDUCED TO LATITUDE OF 35 DEGREES NORTH (CENTIMETRES)

Fig. 13 - *Plots of daily average trimestrial precipitation against precipitable water vapour in the atmosphere* (linearly corrected for latitude). All stations common to the work of both JUNGE and REITAN are considered.

Equation (5) integrates, under the assumption that for $\pi = 0$, $R = 0$, to:

$$R = \frac{\alpha}{\beta}\left\{-\frac{1}{K\beta}\left(1 - e^{-K\beta\pi}\right)\right\}. \tag{9}$$

The derivative of (9) with respect to π can be written alternatively:

$$\frac{dR}{d\pi} = \frac{\alpha}{\beta}\left\{1 - e^{-K\beta\pi}\right\} \tag{5''}$$

and significantly approaches α/β for very high π values, whereas it is near to zero for small amounts of precipitable water vapour. Expanding eq. (9) in series one obtains:

$$R = \left(\frac{K\pi^2}{2!} - \frac{K^2\beta\pi^3}{3!} + ...\right). \tag{9'}$$

If K is now taken to depend directly on the total amount of a chemical substance in the atmosphere, and if that amount is assumed to be proportional to the quantity of the substance which was swept down and dissolved in rainwater, we have:

$$K = a\,(\text{«}Ch\text{»})\,R, \tag{10}$$

where « *Ch* » stands for the concentration of the chemical species in water of which an amount R has been collected.

Substitution of eq. (10) into eq. (9') and rearrangement gives:

$$\pi^{-2}\,\text{«}\,Ch\,\text{»}^{-1} = \alpha\left\{\frac{a}{2} - \beta\,\frac{a^2}{6}\,\text{«}\,Ch\,\text{»}\,R + ...\right\}. \tag{11}$$

Since previous work has shown that nitrate content in annual precipitation appears to show correlation with other parameters discussed above better than other chemical species, it was thought to extend our computations to seasonal data pertinent to that species. Linear correlation coefficients pertinent to plots of $(\pi^{-2}\,NO_3^{-1})$ vs $(NO_3\,R\pi)$ are given in Table 4, which also contains, for purposes of comparison, values of correlation coefficients of systems $R : \pi^2$ vs π [cf. eq. (9')], where aerosol influence was neglected.

TABLE 4 - *Linear correlation coefficients pertinent to equations* (11) *and* (9') *for the four seasonal and average annual values obtained from references* [2,3,4]. π is expressed in centimetres, R in centimetres day^{-1}, and nitrate in gramme-equivalents litre^{-1} $\times$ 10^5.

Function	January-March	April-June	July-September	October-December	Annual Average
$\pi^{-2}\,NO_3^{-1}$ vs $NO_3\,R\pi$	−.67	−.80	−.52	−.52	−.71
$R\pi^{-2}$ vs π	−.34	+.51	+.25	−.07	+.20

Eq. (9) can be written in our case:

$$R^2NO_3 = \frac{\alpha}{\beta}\left\{\pi' - \frac{1}{a\beta}\left(1 - e^{-a\beta\pi'}\right)\right\} \tag{11'}$$

where

$$\pi' = RNO_3\pi\ ;$$

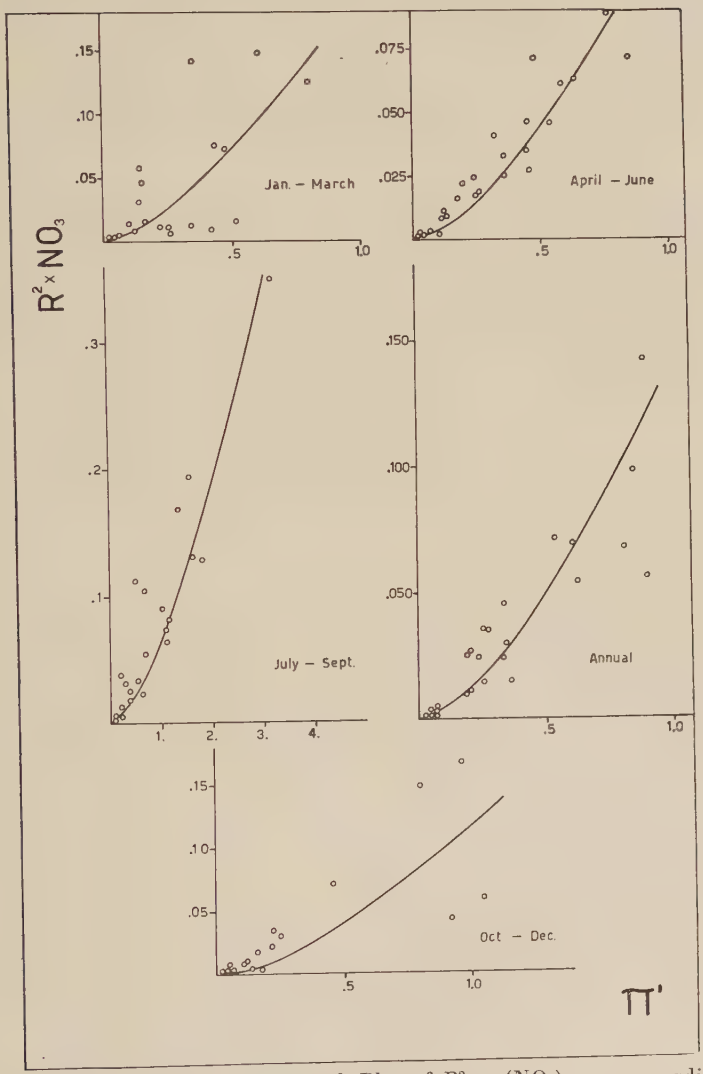

Fig. 14 - *Illustration of functions computed.* Plot of $R^2 \times (NO_3)$ vs π, according to equation (11), using parameters calculated.

$a\beta$ can be obtained as first approximation from eq. (11), since its value is equal to:

$$a\beta = \frac{3 \text{ slope}}{\text{Intercept}}$$

in a plot of $(\pi^{-2} NO_3^{-1})$ vs $(NO_3 R\pi)$. The value of $a\beta$ thus calculated is then substituted into eq. (11) which enables a good estimate of α/β to be obtained by leas squares from a line which is forced through the origin. $a\beta$ is subsequently re-checked by consecutive adjustements, using the S.D. of eq. (11) as a graphical monitor. Agreement between the two methods was found at all instances. Fig. 14 gives plots of $R^2 NO_3$ vs π' for the 4 seasons as well as a diagram computed on the basis of annual averages, while Table 5 gives the values of $a\beta$ and α/β obtained.

TABLE 5 - *Calculated seasonal and annual values of constants* $a\beta$ *and* $\frac{\alpha}{\beta}$ *of eqn.* (11).

Constant	January-March	April-June	July-September	October-December	Annual Average
$a\beta$	$5._{50} \pm 1.$	$3._{78} \pm .4$	$1._{26} \pm .3$	$3._{00} \pm .7$	$3._{28} \pm .5$
$\frac{\alpha}{\beta}$	$.2_{28} \pm .03$	$.1_{61} \pm .009$	$.1_{56} \pm .01$	$.1_{68} \pm .02$	$.1_{97} \pm .01$

Table 6 gives Standard Deviations of functions (9) and (11), for the periods of time under examination.

TABLE 6 - *Standard Deviations of functions given by equations* (9) *and* (11).

Function	January-March	April-June	July-September	October-December	Annual Average
R (eq. (9))	.20	.08	.13	.14	.10
$R^2 NO_3$ (eq. (11))	.03	.01	.03	.03	.015

According to what was previously pointed out and since β of eqn. (5) is constant, both α and α/β should be approximately linear with the inverse of absolute temperature. Analysis of the α/β values calculated and of those of the inverse of average quarterly absolute temperatures for stations below 580 ft (cf. Fig. 12) does not appear to contradict this.

Parameter a, eq. (10), and consequently to the product $a\beta$, will vary according to the definition of a, and « tend inverserly » to the elevation of the freezing level, and therefore inversely to the temperature of stations. This in fact can be observed from the values of $a\beta$ obtained, and average trimestrial temperatures.

It is interesting to observe that the consistency of the data within the equation proposed appears to decrease considerably with seasonal temperatures. It is possible that this may be due to either a lesser capacity of solid than liquid water to incorporate saline nuclei on its path, it may, however, means at the same time that, a mechanism of nuclei production or activation which does not reflect in nitrate formation gathers intensity in colder months, especially in the first trimestre ([11,12]). Another possible explanation could be thought of in terms of circulation of air masses containing once active and nitrate rich particles, which, due to low precipitable water vapour contents of winter atmosphere, travelled farther than in warmer seasons, but, while maintaining their nitrate content, decayed in activity before being brought down with precipitation.

4. *Conclusions.*

The present contribution is indicative of the fact that some correlation exists between atmospheric nitrate and precipitation. This means that NO_3 may to some extent be regarded as a tracer of phenomena capable of favouring nuclei formation or activation, unless of course precipitation occurrences result *regularly* in nitrate generation. It is our aim to extend our calculations to combinations of chemical species present in precipitation, in an attempt at improving correlation along the lines discussed.

Acknowledgements — We are indebted to Prof. V. Caglioti for his continuous encouragement and help, and to Prof. G. Fea for his interest in the problems studied.

REFERENCES

([1]) Papée H. M. & Montefinale A.: In press. — ([2]) Junge C. E.: *The distribution of ammonia and nitrate in rainwater over the United States.* Trans. Amer. Geophys. Union, 39, 241 (1958). — ([3]) Junge C. E. & Werby E. T.: *The concentration of chlorine, sodium potassium, calcium and sulphate in rainwater over the United States.* J. Meteor., 15, 417 (1958). — ([4]) Reitan C. H.: *Distribution of precipitable water vapour over the continental United States.* Bull. Amer. Meteor. Soc., 41, 79 (1960). — ([5]) Papée H. M. & Montefinale A.: *Change of the chlorine: sodium ratio in the atmosphere with altitude and distance from the source of sodium chloride, and the distribution of atmospheric nitrate over the United States.* Nature, 187, 1103 (1960). — ([6]) Junge C. E.: *The chemical composition of atmospheric aerosols I. Measurements at Round Hill field Station, June-July* 1953. J. Meteor., 11, 323 (1954). — ([7]) Junge C. E.: *Recent investigations in air chemistry.* Tellus, 8, 127 (1956). — ([8]) Papée H. M.: *Activated salt surfaces in ice nucleation and growth, and the formation of droplets.* J. Meteor., 16, 217 (1959). — ([9]) Godson W. L.: Private communication. — ([10]) Hodgman C. D.: *Handbook of Chemistry and Physics.* Chem. Rubber. Publ. Co., Cleveland, Ohio (1960). — ([11]) Georgii G. W.: *Neue Untersuchungen über den Zusammenhang zwischen atmosphärischen Gefrierkernen und Kondensationskernen.* Geofis. pura e appl., vol. 42, 62 (1959). — ([12]) Georgii H. W.: *Bemerkungen zu den « Januar Singularitäten » der Konzentration Atmosphärischer Gefrierkerne.* Ibid., Vol. 44, 249 (1959).

(*Received* 18*th March* 1961)

CORRELATION OF PRECIPITABLE WATER VAPOUR VALUES OVER THE UNITED STATES WITH PHYSICAL AND CHEMICAL PARAMETERS.

Part II: SEASONAL TRENDS WITH PHYSICAL VARIABLES (*)

by Henry M. Papée & Alberto Montefinale

Summary — Reitan's data on precipitable water vapour over about 45 stations of the U.S.W.B. network are correlated with altitude and average station temperature values. Computations are carried out following a simple proposed model which is found to be obeyed with reasonably good approximation on average monthly and seasonal scales.

1. *Introduction.*

We have shown in a previous contribution ([1]) that seasonal average distributions of precipitable water vapour over about 15 of such stations of the U.S.W.B., as are situated below the altitude of 580 feet, appear to obey a simple rule derived on the basis of Clapeyron's equation, with fair approximation. It is the aim of this paper to attempt an extension of calculations in question to all 45 stations situated at different altitudes, and for which values of precipitable water vapour were computed by Reitan ([2]).

Since precipitable water vapour in the atmosphere may be regarded as Nature's potential reservoir of precipitation, the need for a study of a suitable model clearly presents itself. Although the data used in this paper are pertinent to the North-American Continent, the possibility of application of some of their meaning to the case of Italy, and in view of the particular geographic position of the peninsula, appeared at the very start of the project.

2. *The data.*

Monthly precipitable water vapour values between stations and the 325 mb level were obtained from Ref. ([2]), and averaged both to a trimestrial and annual basis.

Average monthly temperatures of stations under study were obtained from the « National Summaries, Climatological Data » of the U.S.W.B., covering period:

(*) Contribution of the « Centro Nucleazione Aerosoli » of the National Research Council of Italy, *Rome*, Via Vettore 4.

July 1956 - June 1957. Those were averaged to a trimestrial and annual basis, and converted into absolute degrees. Elevations of stations, in feet, were obtained from the same source.

Monthly, seasonal and annual estimates were used as basis for computations in order to confront the results among eachother, and to gain indication as to what changes in consistencies of results may arise when periods of averaging are changed.

3. *Results.*

Symbols used.

$\frac{\Delta H}{R} = 4.268 \cdot 10^3$: Cumulative annual value obtained from Ref. (1)

z : Elevation of station (feet).

Z : Average elevation, in feet, of a circular plateau of 150 miles radius, of which the station considered is the center. Individual values used were obtained by planimetry of map.

T_0 : Temperature, in absolute degrees, of station at corresponding elevation = 0, computed from data at coastal stations, and assuming uniform change of temperature with latitude.

T^* : Temperature, in absolute degrees, of station at corresponding elevation = 0, and computed from actual temperatures of stations, which were reduced by $1.684 \cdot 10^{-3}$ degrees C per foot of elevation.

$T_=$: Temperature, in absolute degrees, at average height of a 150 miles radius plateau around station obtained in the same way as for T^*.

H : Altitude of the 325 mb level. This was considered a constant to the effects of precipitable water vapour distribution.

h : Altitude parameter.

A_0, k, α : Constants.

I. *First Approximation* — The consistency of linearity with which the logarithm of precipitable water vapour changes at low altitude points with the inverse of the temperature of station [trimestrial averages, see. Ref. (1)], leads to the analysis of a simple model of the type given in Fig. 1.

If the precipitable water vapour is taken to be generated exclusively at altitude zero and at constant temperature of the base, and to envelop the station in a manner uniform for a given level and monotonically decreasing in concentration with height, then, in line with Ref. (1):

$$\pi_h = \int_z^H d\pi = \alpha\, e^{-\Delta H/RT_0} \int_z^H e^{-kh}\, dh$$

$$\pi_h = \frac{\alpha}{k}\, e^{-\Delta H/RT_0} (e^{-kz} - e^{-kH}) . \tag{1}$$

Equation (4) of Ref. (1) deals with precipitable water vapour between sea level and level H, and can therefore be written:

$$\pi_0 = \frac{\alpha}{k}\, e^{-\Delta H/RT_0} (1 - e^{-kH}) = A_0\, e^{-\Delta H/RT_0}$$

where

$$A_0 = \frac{\alpha}{k}(1 - e^{-kH}) = \text{const.}, \tag{2}$$

hence

$$e^{-kH} = 1 - A_0 \frac{k}{\alpha}. \tag{2'}$$

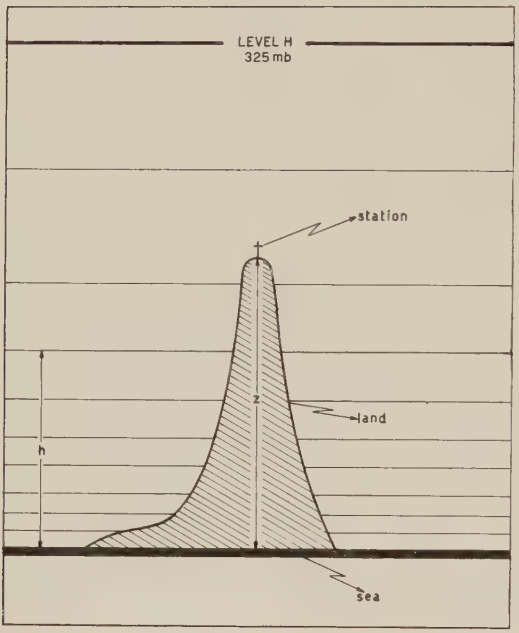

Fig. 1 - *Model of unperturbed distribution of precipitable water vapour generated at level zero altitude.* The concentration decreases monotonically with altitude because of steady state between vapour penetrating upward and water precipitating.

Substituting (2′) into (1) and rearranging:

$$\pi_h e^{\Delta H/RT_0} = A_0 + \frac{\alpha}{k}(e^{-kz} - 1). \tag{1'}$$

However

$$e^{-kz} = 1 - kz + \frac{k^2z^2}{2!} - \ldots\ldots; \tag{3}$$

if k is taken to be sufficiently small, two terms alone are considered; substitution of (3) into (1′) yields:

$$\pi_h e^{\Delta H/RT_0} = A_0 - \alpha z. \tag{4}$$

Values of T_0 were obtained from linear regression lines: temperature of station - latitude, for such stations used by REITAN which are situated below 580 ft of elevation [cf. Ref. (1)] and with the exception of those very near to mountains.

TABLE 1 - *Linear regression coefficients and their standard deviations for average monthly, seasonal and annual plots of temperatures* (in degrees C) *of* 17 *U.S.W.B. stations situated below* 580 ft *of elevation - against geographic latitude* (in degrees).

	Feb.	1st Trim.	May	2nd Trim.	Aug.	3rd Trim.	Nov.	4th Trim.	Annual
Intercept	$5_{7.71}$ ± 3.	$5_{3.41}$ ± 2.	$4_{8.01}$ ± 4.	$4_{4.65}$ ± 4.	$4_{4.21}$ ± 4.	$4_{4.71}$ ± 4.	$4_{8.55}$ ± 3.	$5_{0.44}$ ± 2.	$4_{3.69}$ ± 3.
Gradient	$-1._{40}$ ± .07	$-1._{28}$ ± .07	−.82 ± .1	−.74 ± .1	−.57 ± .1	−.61 ± .1	$-1._{04}$ ± .08	-1.1_0 ± .06	$-.7_9$ ± .07
Correl. Coeff.	−.98	−.98	−.87	−.88	−.77	−.80	−.96	−.98	−.94

Table 1 gives the results obtained which then served for the basis of computation of T_0.

Fig. 2 gives seasonal plots of $\pi_h \exp(\Delta H/RT_0)$ against z.

II. *Second appoximation* — Resolving eq. (4) with respect to π_h and taking the derivative with respect to T_0, one has:

$$\frac{d\pi_h}{dT_0} = \frac{\Delta H}{R}\frac{1}{T_0^2} e^{-\Delta H/RT_0}(A_0 - \alpha z). \tag{5}$$

If the ratio of differentials is taken to correspond approximately in our range of analysis to that of finite increments, then:

$$\Delta_1\pi_h \cong \frac{\Delta H}{R}\frac{1}{T_0^2} e^{-\Delta H/RT_0}(A_0 - \alpha z)\,\Delta T_0 \tag{6}$$

$$\Delta_1\pi_h \cong \frac{T^* - T_0}{T_0^2}\frac{\Delta H}{R} e^{-\Delta H/RT_0}(A_0 - \alpha z). \tag{6'}$$

Hence, from eq. (4):

$$\pi_h \cong e^{-\Delta H/RT_0}(A_0 - \alpha z) + \frac{T^* - T_0}{T_0^2}\frac{\Delta H}{R} e^{-\Delta H/RT_0}(A_0 - \alpha z), \tag{7}$$

which rearranges to:

$$\frac{\pi_h e^{\Delta H/RT_0}}{1 + \dfrac{T^* - T_0}{T_0^2}\dfrac{\Delta H}{R}} = A_0 - \alpha z. \tag{7'}$$

Fig. 3 illustrates the change of function (7') with altitude, for seasonal average data; comparison of figures 2 and 3 shows a considerably larger consistency of experimental values in case of expression (7') than in (4).

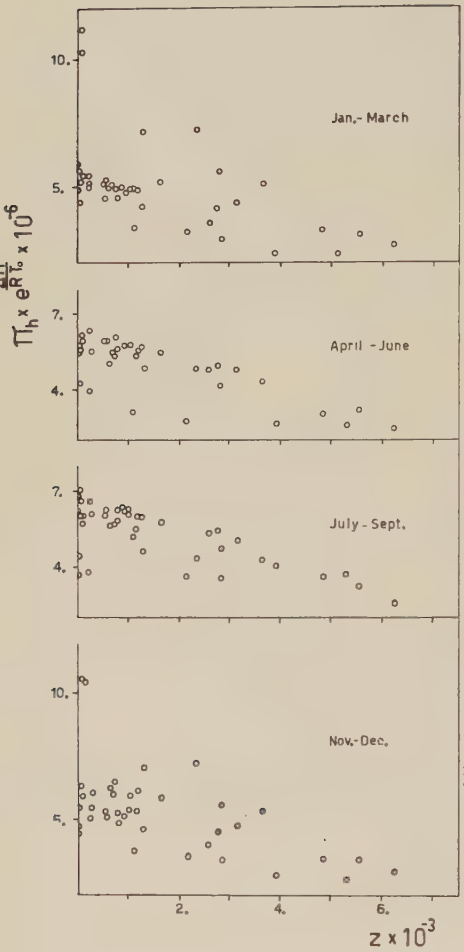

Fig. 2 - *First approximation. Change of the left hand side of eq.* (4) *with altitude of station* (*feet*). « Latitudinal » temperatures are used in exponential. Average trimestrial values are used in computation.

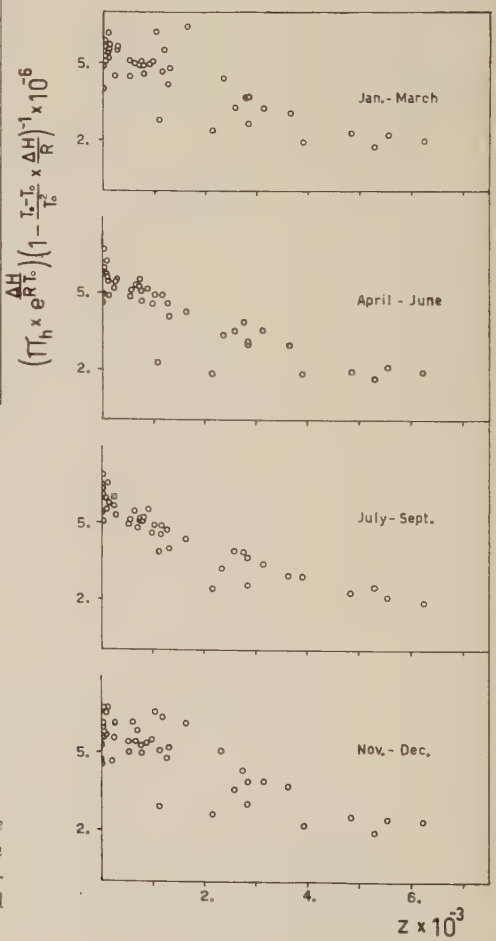
Jan.- March
April - June
July - Sept.
Nov.- Dec.
$\left(\Pi_h \times e^{\frac{\Delta H}{RT_o}}\right)\left(1 - \frac{T - T_o}{T_o^2} \times \frac{\Delta H}{R}\right)^{-1} \times 10^{-6}$
$z \times 10^{-3}$

Fig. 3 - *Second approximation. Change of the left hand side of eq.* (7') *with altitude of station* (*feet*). Effect of local temperatures is superposed on « latitudinal data ». Average trimestrial values are used in computations.

TABLE 2 - *Linear regression coefficients and their standard deviations for data computed according to equations* (4) *and* (7′), *and using the elevation of station for height parameter.* Seasonal data are pertinent to Figures 2-3. Average monthly, seasonal, and annual values respectively were used for computations.

	Linear regression according to eq. (4) (1st approx.)								
	Feb.	1st Trim.	May	2nd Trim.	Aug.	3rd Trim.	Nov.	4th Trim.	Annual
Gradient.	−517.4 ± 152.	−547.7 ± 125.	−513.4 ± 78.	−520.2 ± 68.	−484.4 ± 78.	−505.5 ± 68.	−590.1 ± 110.	−580.2 ± 115.	−545.7 ± 56.
Intercept $\times 10^{-6}$	$5._{66} \pm .3$	$5._{79} \pm .3$	$5._{58} \pm .2$	$5._{71} \pm .15$	$6._{15} \pm .2$	$6._{11} \pm .15$	$5._{81} \pm .2$	$6._{23} \pm .25$	$6._{02} \pm .12$
Correl. coeff.	−.46	−.56	−.71	−.76	−.69	−.75	−.63	−.61	−.83
	Linear regression according to eq. (7′) (2nd approx.)								
Gradient.	−525.7 ± 75.	−645.1 ± 64.	−723.1 ± 74.	−720.0 ± 58.	−726.8 ± 55.	−731.9 ± 52.	−592.9 ± 88.	−673.4 ± 72.	−722.1 ± 59.
Intercept $\times 10^{-6}$	$5._{26} \pm .2$	$5._{42} \pm .1$	$5._{37} \pm .2$	$5._{47} \pm .1$	$5._{76} \pm .1$	$5._{77} \pm .1$	$5._{72} \pm .2$	$5._{87} \pm .2$	$5._{92} \pm .1$
Correl. coeff.	−.73	−.84	−.83	−.88	−.90	−.91	−.72	−.82	−.88

Table 2 gives linear regression parameters pertinent to both cases [eqns. (4) and (7′)] for monthly average, seasonal, and average annual data.

If mixing of air masses over an area around the station considered is assumed, and if it is taken that the effect of that mixing will further smooth our values of π_h because of local, orographic factors, then Z, the effective altitude of a plateau around the station in question may be thought to be more representative of the altitude parameter in eq. (7′) than the height of the station.

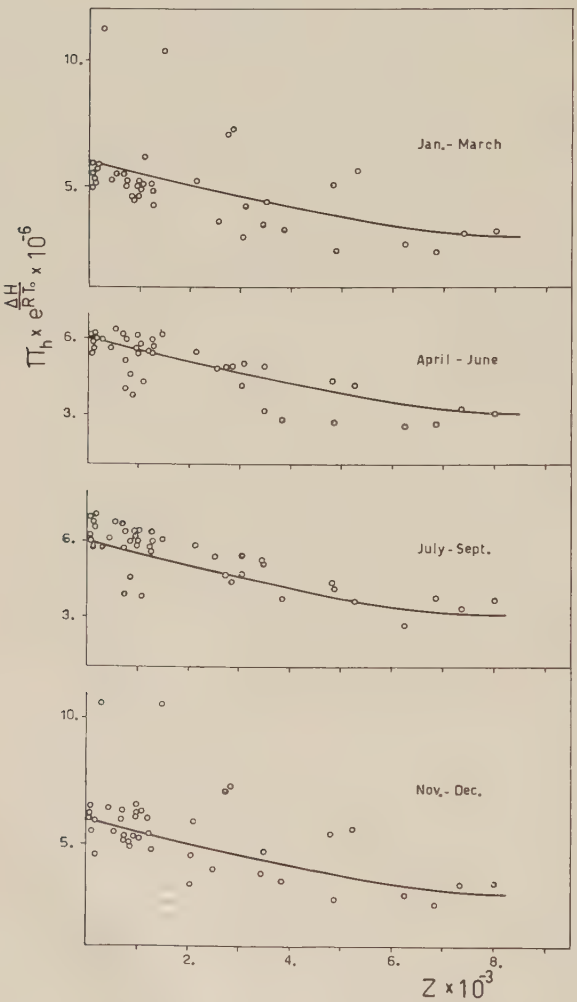

Fig. 4 - *First approximation. Change of the left hand side of eq.* (4) *with altitude of plateau around station* (*feet*). «Latitudinal» temperatures are used in exponential. Average trimestrial values are used in computations.

Values of average elevations of a circle of 150 miles of radius and with the station considered at center were computed planimetrically from a map. Seasonal results obtained are shown on Fig. 4,

where the left hand side of equation (4) is plotted against Z, the altitude of the plateau, and in Fig. 5, which shows plots according to eq. (7'). Monthly data are plotted on Figures 6 and 7.

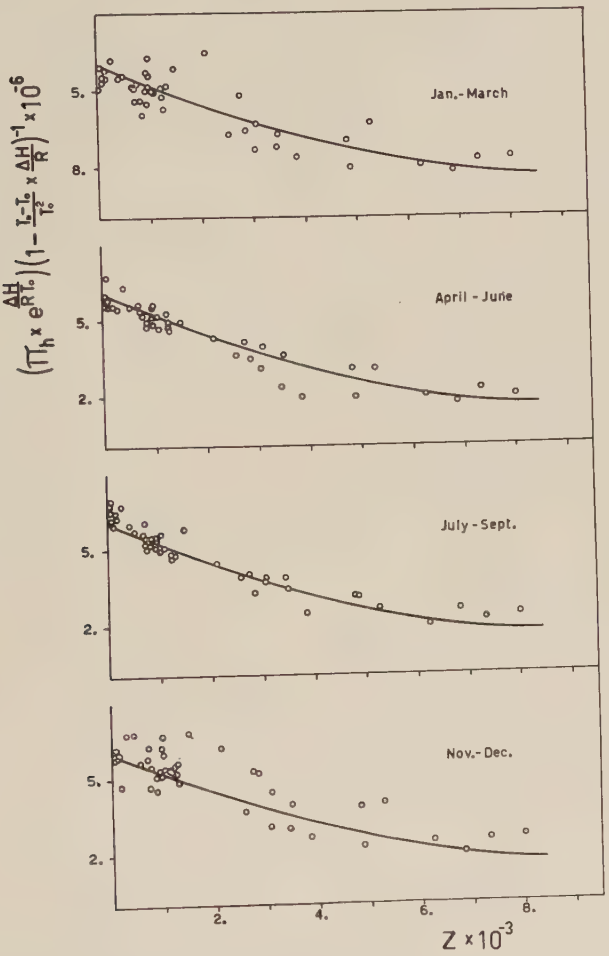

Fig. 5 - *Second approximation. Change of the left hand side of eq.* (7') *with altitude of plateau around station* (*feet*). Effect of local temperatues is superposed on « latitudinal » data. Average trimestrial values are used in computations.

III. *Third approximation* — *a*) If contribution of evaporation from a plateau situated at altitude Z is taken to superpose its value on that of atmospheric precipitable water vapour which « originated » at altitude zero, and according to the model on Fig. 1, then, following a reasoning similar to the previous

one, we have:

$$\Delta_2\pi_h = e^{-\Delta H/RT_=} \int_{H-Z}^{H} e^{-kh}\, dh \tag{8}$$

$$\Delta_2\pi_h = \frac{\alpha}{k}\, e^{-\Delta H/RT_=} (e^{kZ}\, e^{-kH} - e^{-kH}) \tag{8'}$$

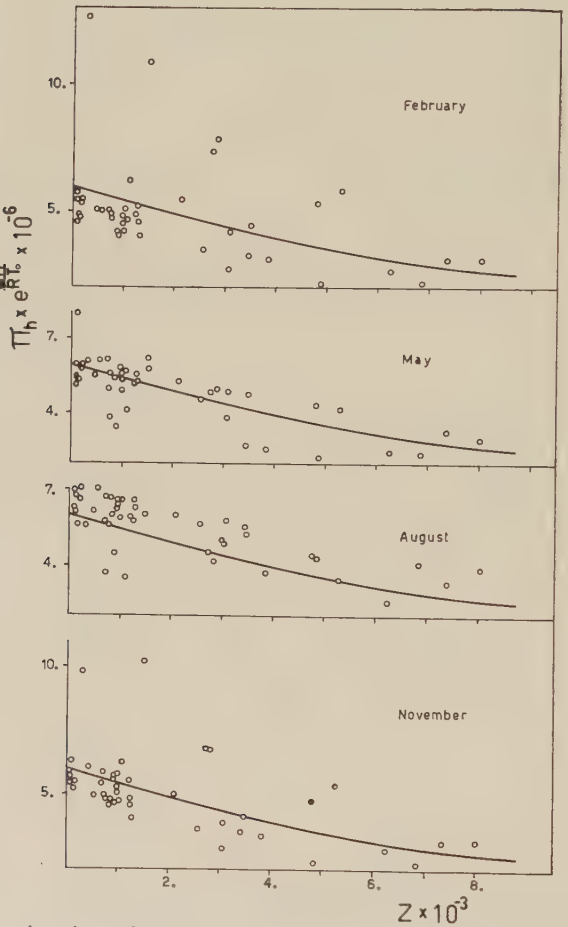

Fig. 6 - *First approximation. Change of the left hand side of eq.* (4) *with altitude of plateau around station* (*feet*). « Latitudinal » temperatures are used in exponential. Monthly values are used in computations.

Substituting eq. (2′) in (8′) and developing e^{kZ} in series (two terms):

$$\Delta_2\pi_h = Ze^{\frac{\Delta - H}{RT_=}} (\alpha - A_0 k)\,. \tag{8''}$$

Hence, in place of eq. (7) it could be written:

$$(9) \qquad \pi_h \, e^{\Delta H/RT_0} = (A_0 - \alpha z)\left\{1 + \frac{T^* - T_0}{T_0^2}\,\frac{\Delta H}{R}\right\} + Z\, e^{\Delta H/R \,\cdot\, (1/T_0 - 1/T_=)}\left\{\alpha - A_0 k\right\}$$

which rearranges to

$$(9') \qquad \frac{\pi_h \, e^{\Delta H/RT_0}}{1 + \dfrac{T^* - T_0}{T_0^2}\,\dfrac{\Delta H}{R}} - A_0 + \alpha Z = (\alpha - A_0 k)\left\{\frac{Z\, e^{\Delta H/R \,\cdot\, (1/T_0 - 1/T_=)}}{1 + \dfrac{T^* - T^0}{T_0^2}\,\dfrac{\Delta H}{R}}\right\}.$$

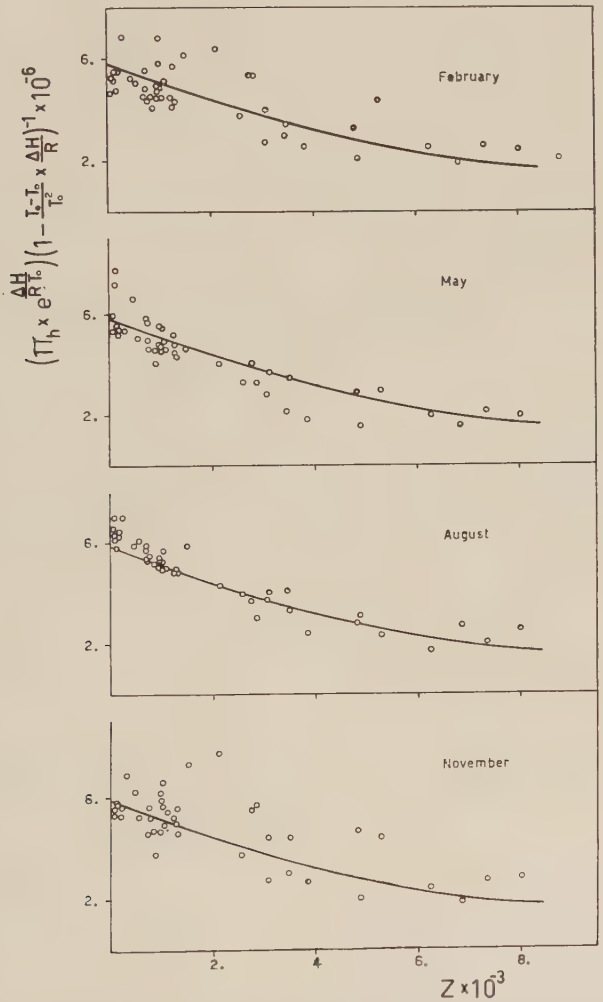

Fig. 7 - *Second approximation. Change of the left hand side of eq.* (7′) *with altitude of plateau around station* (*feet*). Effect of local temperatures is superposed on « latitudinal » data. Monthly values are used in computations.

The left hand side of this equation should therefore show a linear trend with the term in brackets on the right hand side. Analysis of this type of plots failed, however, to establish correlation for any of the 4 seasons.

b) The use of 3 terms in the development in series pertinent to expressions (1′) and (7) enables to write:

$$(10)\qquad \underbrace{\frac{\pi_h\, e^{\Delta H/RT_0} - A_0}{1 + \dfrac{T^* - T_0}{T_0^2}\dfrac{\Delta H}{R}}}_{\text{I}} = \underbrace{-\alpha + \frac{\alpha k}{2} Z}_{\text{II}} + \underbrace{\frac{e^{\Delta H/T \cdot (1/T_0 - 1/T =)}(\alpha + \dfrac{\alpha k}{2} Z - A_0 k)}{1 + \dfrac{T^* - T_0}{T_0^2}\dfrac{\Delta H}{R}}}_{\text{III}}.$$

Examination of Figures 4-7 allows an estimate of constant A_0 to be carried out with better approximation than both in Ref. ([1]) and the first approximation of this contribution. In view of the fact that monthly and trimestrial values plotted in Figs 4-7 follow practically very similar distributions in all four cases, A_0 was computed from linear regression on cumulative seasonal points situated between $Z = 0$ and $Z = 1500$. This permitted an estimation of the left hand side of eq. (10) to be carried out. Further analysis surprisingly indicated linear consistence between values of term I of eq. (10) and Z. Linear regression on terms I ad Z in the range of 1500-9000 ft where deviations due to small changes of Z are small, led to an estimation of both α and k. This in turn showed the value of the quotient α/k to be of the same order of magnitude as that of A_0. Eq. (2) explains this; it can be seen that with k sufficiently large, and since H is of the order of $28 \cdot 10^3$, the exponential in eq. (2) may become negligible with respect to unity, within limits of error.

Equation (8′) can anyhow be written after substitution of (2′):

$$(8''')\qquad \Delta_2 \pi_h = \left(\frac{\alpha}{k} - A_0\right) e^{-\Delta H/RT} + (e^{kZ} - 1),$$

hence, because of eq. (1):

$$(1'')\qquad (\pi_h + \Delta_2 \pi_2)\, e^{\Delta H/RT_0} = \Pi\, e^{\Delta H/RT_0} =$$

$$= A_0 + \frac{\alpha}{k}(e^{-kZ} - 1) + e^{\Delta H/R \cdot (1/T_0 - 1/T =)}\left\{\frac{\alpha}{k} - A_0\right\}(e^{kZ} - 1)$$

and since in our case $\alpha/k \cong A_0$

$$(1''')\qquad \Pi\, e^{\Delta H/RT_0} \cong A_0 + \frac{\alpha}{k}(e^{-kZ} - 1)$$

while for the temperature-corrected expression there is similarly:

$$\frac{(\pi_h + \Delta_2\pi_h)\, e^{\Delta H/RT_0}}{1 + \dfrac{T^* - T_0}{T_0^2}\dfrac{\Delta H}{R}} = \frac{\Pi\, e^{\Delta H/RT_0}}{1 + \dfrac{T^* - T_0}{T_0^2}\dfrac{\Delta H}{R}} =$$

(7″)

$$= A_0 + \frac{\alpha}{k}(e^{-kZ} - 1) + \frac{e^{\Delta H/R\,\cdot\,(1/T_0 - 1/T =)}(\alpha/k - A_0)\,(e^{kZ} - 1)}{1 + \dfrac{T^* - T_0}{T_0^2}\dfrac{\Delta H}{R}}$$

and

(7‴)
$$\frac{\Pi\, e^{\Delta H/RT_0}}{1 + \dfrac{T^* - T_0}{T_0^2}\dfrac{\Delta H}{R}} \cong A_0 + \frac{\alpha}{k}(e^{-kZ} - 1)\,.$$

The assumption that, within the limits of error and for the purpose of this contribution α/k is very near to A_0, leads to a test whether in the range of elevations of REITAN's stations the experimental data can be fitted according to equations (1‴) and 7‴). Substituting

(11)
$$\alpha = kA_0$$

into eq. (10), neglecting its III-rd term and rearranging, one obtains:

(10′)
$$\frac{\dfrac{\Pi\, e^{\Delta H/RT_0}}{1 + \dfrac{T^* - T_0}{T_0^2}\dfrac{\Delta H}{R}} - A_0}{A_0 Z} = -k + \frac{k}{2}Z\,.$$

If the left hand side term of this is called Y, constant k, as obtained by linear regression, is:

(12)
$$k = \frac{\Sigma Y_i\, \Sigma Z_i^2 - \Sigma Z_i\, \Sigma Z_i Y_i}{(\Sigma Z_i)^2 - n\Sigma Z_i^2}$$

which in turn leads to computation of α from eq. (11).

TABLE 3 - *Regression parameters pertinent to equations* (1‴) *and* (7‴). Values obtained were calculated using average *trimestrial* data for basis of cumulative computation.

Equation No.	$A_0 \times 10^{-6}$	α	$k \times 10^5$
(1‴)	$5_{.935} \pm .2$	$523.47 \pm 153.$	8.22 ± 2.3
(7‴)	$5_{.968} \pm .1$	$9_{38.77} \pm 85.$	$1_{5.73} \pm 1.2$

Table 3 gives the results computed by the use of the above procedure; parameters given are calculated from cumulative seasonal values; the lines drawn in Figures 4-5 are obtained on their basis and according to eqns. (1''') and (7''').

Analysis of monthly values leads to similar results. This is illustrated in Figures 6 and 7, where curves fitted in a manner described previously are drawn. Table 4 gives the pertinent parameters calculated using the four sets of monthly data cumulatively.

TABLE 4 - *Regression parameters pertinent to equations* (1''') *and* (7'''). Values obtained were calculated using average *monthly* data (February, May, August, November) for basis of cumulative computation.

Equation No.	$A_0 \times 10^{-6}$	α	$k \times 10^5$
(1''')	$5._{834} \pm .24$	$589.23 \pm 161.$	10.10 ± 2.3
(7''')	$5._{847} \pm .1$	$868.28 \pm 115.$	$1_{4.85} \pm 1.6$

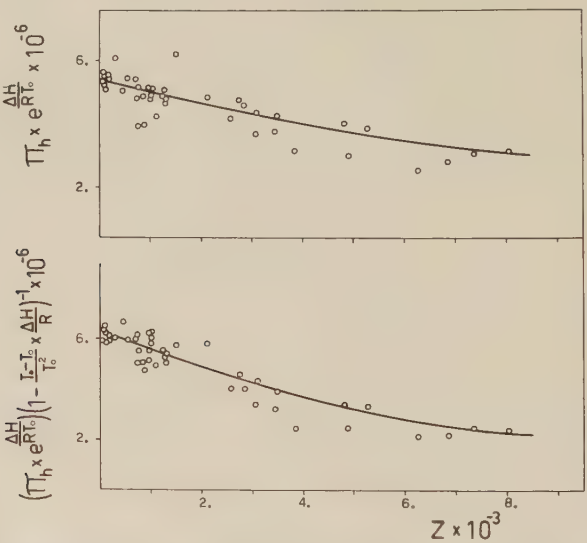

Fig. 8 - *First and second approximation patterns on data computed on annual average basis.*

Results obtained on the basis of the use of *annual average* parameters and according to both patterns under examination are shown in Fig. 8. The corresponding parameters are given in Table 5.

TABLE 5 — *Regression parameters pertinent to equation* (1‴) *and* (7‴). Values obtained were calculated using average *annual* data for basis of cumulative computation.

Equation No.	$A_0 \times 10^{-6}$	α	$k \times 10^5$
(1‴)	$6._{171} \pm .23$	$479.49 \pm 222.$	7.77 ± 3.3
(7‴)	$6._{246} \pm .16$	$818.23 \pm 198.$	$1_{3.10} \pm 2.8$

TABLE 6 - *Correlation coefficients pertinent to eq.* (1‴) *and* (7‴) *and between left hand side of equation, and* $(e^{-kZ} - 1)$, - *where Z is the elevation of the plateau.* Average monthly, seasonal, and annual values respectively were used for computations.

Eq. No.	Feb.	1st Trim.	May	2nd Trim.	Aug.	3rd Trim.	Nov.	4th Trim.	Annual
(1‴)	–.40	–.48	–.77	–.83	–.75	–.81	–.57	–.55	–.85
(7‴)	–.74	–.86	–.90	–.95	–.95	–.96	–.72	–.85	–.94

TABLE 7 - *Standard deviations and their percentual ratios to the average of experimental values for functions computed.* Average monthly, seasonal, and annual parameters respectively were used for computations.

Type of function	Deviation	Feb.	1st Trim.	May	2nd Trim.	Aug.	3rd Trim.	Nov.	4th Trim.	Annual
(1‴)	S.D.	.28	.24	.34	.29	.55	.40	.27	.26	.21
	S.D. %	28	23	17	15	19	14	21	19	12
(7‴)	S.D.	.19	.17	.35	.23	.32	.26	.23	.20	.21
	S.D. %	19	16	18	12	11	9	18	15	12

For the sake of comparison with consistencies of values calculated both on the basis of actual elevation of *stations* and the use of 2 terms in the development in series (Table 2), correlation coefficients between the left hand side terms of eqns. (1‴) and (7‴) and $(e^{-kZ} - 1)$ were computed, and are given in Table 6.

Standard deviations of the experimental precipitable water vapour values from data calculated from eq. (1‴) and (7‴) for all periods under examination and after substitution of pertinent constants (Tables 3-5) are given in Table 7.

4. *Discussion.*

Several improvements of the pattern of calculation carried out in this contribution, offhand appear possible. Thus it is evident that the estimation of a model of distribution of atmospheric precipitable water vapour based on integrated areas, the shape of which would be constructed according to periodical average movement of air masses, might prove superior to our basis of computation which relies on altitudes calculated from uniform circular plateaus.

Secondly, evapotranspiration over areas considered is entirely neglected in our considerations, and it of course appears that a suitable use of this parameter might improve the results obtained.

Thirdly, it can be seen that the temperature values used in this contribution are not altogether representative of the true conditions. It appears evident that for a temperature value to be representative over a given area so as to fit considerations applying to our model, periodical average temperatures at several points of the area in question should be taken and suitably transformed into a value pertinent to that area.

Lastly, it can be argued that the assumption of a stationary state distribution of precipitable water vapour over a whole continent is a somewhat coarse approximation.

We are fully aware of those and some other shortcomings of the model discussed here, although we feel confident that the weight of some of the points mentioned above would be smaller when applying the treatment to the Italian peninsula than it might be in the United States. However, in order to confront the results obtained with those resulting from other methods, a planimetric estimation of the standard deviations of values at 29 stations of the U.S.W.B. ([3]) was carried out. The average percent S.D. appears to be 20.9%, and we therefore feel that despite the simplicity of our model our own periodical average data (last row, Table 7 in particular) favourably compare with this.

It can be noticed that instabilities associated with colder periods of the year largely reflect in the data quoted in the first part of this contribution. This observation is substantiated by both the diagrams shown and the Tables illustrating the measure of dispersion of experimental values. It can furtherfore be noticed that consistencies of monthly values are inferior to trimestrial average and annual average data, although the pattern discussed is quantitatively very similar for monthly and seasonal averages (see Figs. 5-7), while annual average curves are higher.

A seemingly paradoxial aspect of the model quoted is that precipitable water vapour appears to distribute as if it was generated in its largest part at elevation zero, i.e. as if the contribution of evaporation from higher levels, and in the range considered, was so small as to be within limits of error. This is clearly occasioned by the dispersion of the experimental data which makes an exact estimation of both α/k and A_0 [eq. (1‴)] impossible. It is, however, felt that if sufficient experimental

material was on hand to enable a refinement of the treatment to be carried out, and if several measurements of precipitable water vapour carried out from altitudes larger than 8000 ft as well as some other data taken over oceans were available, a more accurate estimation of an overall contribution of evaporation from various levels could be carried out, possibly along a pattern similar to the one given here.

It has to be pointed out, however, that the possible causes of dispersion of precipitable water vapour values may be due at the same time to factors other than solely the ones discussed so far. It can be argued in fact that some higher values of π could partly be due to supersaturations with respect to overall equilibrium conditions, and that therefore introduction of suitable corrections based on the chemical content of precipitation might further improve consistencies. It is, in fact, interesting to note that deviations from the annual functions computed yield correlation coefficients of $-.49$ and $-.57$ with values of total annual precipitation, and total annual precipitation multiplied by its content in nitrates respectively [cf. Ref. (1)].

5. *Acknowledgements.*

The authors wish to express their thanks to Prof. V. Caglioti for his continuous interest in this work, and for his help.

The assistance of Mrs. L. Masironi in carrying out part of the calculations is gratefully acknowledged.

We feel especially grateful to the Division of Meteorological Research of the Italian Air Force, and its Director, Prof. G. Fea, for having extended their hospitality to the « Centro Nucleazione Aerosoli » during the initial stage of its work, as well as for much other help, assistance and stimulating discussions.

Both parts of this project were carried out with partial finantial support of the following organizations: « Società Generale Elettrica della Sicilia » and « Cassa per il Mezzogiorno ».

REFERENCES

(1) Montefinale A. & Papée H. M.: *Correlation of precipitable water vapour values over the United States with physical and chemical parameters. Part I. Seasonal trends with precipitation and its nitrate content. Geographic changes of nitrate.* Geofisica pura e applicata. Vol. 48, pp. 203-223 (1961). — (2) Reitan C. H.: *Distribution of precipitable water vapour over the Continental United States.* Bull. Amer. Meteor. Soc. 41, 79 (1960). — (3) Shands A. L.: *Mean precipitable water in the United States.* U.S.W.B. Technical Paper No. 10.

(*Received* 27 *March* 1961)

LIBRI NUOVI - REVIEWS - BUCHBESPRECHUNGEN
NOUVEAUX LIVRES - NUEVOS LIBROS

BENSON F. A. & HARRISON D.: *Electron-Circuit Theory*. In-8°, 371 pp. & num. figg. Edward Arnold (Publishers) Ltd, London 1959 (30 s.). — Il libro ha finalità didattiche ed è destinato specialmente agli studenti d'ingegneria, cosicchè gli sviluppi teorici sono sempre orientati verso le applicazioni. La materia è distribuita in 15 capitoli: Introduzione, Circuiti a corrente continua, Circuiti a corrente alternata monofase, Circuiti polifase, Quantità complesse, Uso delle grandezze complesse nei circuiti a corrente alternata, Teoremi ausiliari sulle reti, Circuiti accoppiati e trasformatori, Diagrammi circolari ed inversioni, Onde non sinusoidali, Circuiti polifasi non equilibrati, Carica e scarica di capacità, Circuiti a valvola termoionica, Circuiti per le comunicazioni, Macchine elettriche. Ciascun capitolo contiene alla fine una serie di problemi dei quali viene data la soluzione numerica. Dopo tre brevi appendici il libro termina con un indice analitico. La chiarezza del testo ed i numerosi esercizi numerici, spesso illustrati anche graficamente, rendono il libro assai efficace.

REDWOOD M. R.: *Mechanical Waveguides*. In-8°, 300 pp. & num. figg. Pergamon Press, Oxford 1960 (50 s.). — Il libro riguarda la propagazione delle onde acustiche ed ultrasoniche nei fluidi e nei solidi limitati. L'interesse maggiore dell'argomento riguarda la misura dell'attenuazione delle onde guidate nei materiali, allo scopo di dedurre le proprietà fisiche di questi. La trattazione della materia avviene in 13 capitoli: Propagazione nei mezzi illimitati; Riflessione e rifrazione delle onde su una interfaccia; Onde continue nei fluidi; Impulsi in onde guidate nei fluidi; Onde continue nelle piastre solide; Idem nei cilindri solidi; Teorie approssimate delle onde continue; Guide d'onda solide; Impulsi a settore stretto nelle guide d'onda solide; Impulsi a settore largo; Guide d'onda a multi-strati; Risonatori solidi; Mezzi anisotropi. Le cinque appendici del libro contengono vari complementi matematici. Ogni capitolo è integrato alla fine da una bibliografia selezionata.

PUTLEY E. H.: *The Hall Effect and related Phenomena*. In-8°, 263 pp. & num. figg. Butterworths, London 1960 (50 s.). — Il libro è dedicato allo studio delle proprietà di trasporto nei semi-conduttori. Vengono così descritti i metodi di misura dei principali effetti unitamente ad una discussione critica del loro significato, secondo i moderni concetti della fisica dello stato solido. Il testo è suddiviso in cinque parti: Processi di conduzione nei semi-conduttori, Descrizione e metodi di misura delle proprietà di trasporto: Conduzione in un solido isotropo; Il comportamento dei semi-conduttori tipici; Sintesi delle proprietà elettriche dei semi-conduttori. Il libro termina con un indice analitico ed uno degli autori.

BUDDEN K. G.: *Radio Waves in the Ionosphere*. In-8°, 542 pp. & num. figg., Cambridge University Press, 1961 (95 s.). — Il libro sviluppa in ogni dettaglio la teoria matematica della propagazione delle radio-onde nella ionosfera e della riflessione da parte di questa. Esso integra l'esposizione prettamente fisica della teoria magneto-ionica di J. A. Ratcliffe. La prima metà del testo è relativa alla teoria dei raggi, applicabile ai mezzi ionizzati omogenei ed alla riflessione delle radio-onde di alta frequenza ad incidenza verticale ed obliqua. Fra l'altro sono derivate le formole di Appleton-Hartree e della quartica di Booker, che vengono quindi ampiamente discusse. La seconda parte riguarda la teoria completa delle onde, da applicare quando l'approssimazione della teoria dei raggi risulta insufficiente: essa viene usata nella riflessione delle radio-onde di frequenza molto bassa, nonchè nello studio dei processi di riflessione, di accoppiamento fra onde caratteristiche e nel caso di penetrazione parziale. Gli ultimi capitoli si riferiscono alla funzione integrale di Airy, al fenomeno di Stokes, ai metodi numerici per de-

durre i coefficienti di riflessione ed al teorema di reciprocità. La bibliografia è posta in appendice ed occupa 13 pagine. L'esposizione risulta ovunque chiara e rigorosa; in breve, il libro rappresenta un'opera indispensabile per chi voglia accingersi allo studio organico della teoria della propagazione delle radio-onde e per i tecnici ai quali necessita risolvere con metodi fisico-matematici i problemi tecnici relativi.

Busbridge L. W.: *The Mathematics of Radiative Transfer.* In-8°, 143 pp. Cambridge University Press, 1960 (30 s.). — Il volumetto tratta alcuni problemi matematici che si presentano nella teoria dei processi radiativi attraverso l'atmosfera di una stella. Le prime 34 pagine sono riservate a richiami matematici, mentre la seconda parte riguarda le equazioni di Milne ed i procedimenti per la loro soluzione. In appendice vengono esposti alcuni argomenti complementari. Nell'insieme, il libro presenta vari pregi che lo rendono raccomandabile per lo studio teorico dei processi radiativi proprii dell'astrofisica.

Conrad W.: *Der Einfluss des geomagnetischen Feldes auf die kosmische Strahlung.* In-4°, 180 pp., 84 figg. & 6 tavv. f. t. Akademie-Verlag, Berlin 1959 (DM 54.50). — La monografia riunisce le attuali conoscenze sugli effetti che il campo geomagnetico esercita sulla radiazione cosmica. Si tratta di uno studio, sistematico ed accurato, sviluppato nelle tre parti seguenti: 1) Natura e comportamento della radiazione cosmica; 2) La radiazione cosmica nel campo magnetico terrestre supposto invariabile nel tempo; 3) Idem tenendo conto delle variazioni nel tempo del campo geomagnetico. In quest'ultima parte risaltano specialmente le trattazioni relative alle variazioni in funzione dell'attività solare. In appendice sono raccolte alcune cartine illustranti il comportamento delle « iso-cosme » sulla terra, anche in funzione della latitudine geomagnetica.

The Physical Society: *Reports on Progress in Physics*, Vol. XXIII, In-8°, 629 pp. & num. figg. The Physical Society, London S. W. 7, 1960 (21 s.). — Il volume riunisce dieci monografie, compilate da diversi specialisti, su problemi di attualità della fisica sperimentale e teorica. Eccone i titoli, col nome degli Autori: Proprietà ottiche delle pellicole sottili (O. S. Heavens), Teoria dei gruppi nella fisica dello stato solido (D. F. Johnston), Fotometria fotoelettrica (H. J. J. Braddick), Analisi sperimentale della struttura dei metalli (A. B. Pippard), Nuovi sviluppi nella spettroscopia interferometrica (P. Jacquinot), Nebulose planetarie (M. J. Seaton), Calcoli sulla struttura delle bande nei solidi (L. Pincherle), Cattura elettronica orbitale nei nuclei (R. Bouchez & P. Depommier), Misure di precisione nella spettroscopia con raggi gamma (G. A. Bartholomew, J. W. Knowles & G. E. Lee-Whiting), Reazioni indotte nell'elio (D. A. Bromley & E. Almquist). Come per i volumi precedenti, i contributi sono tutti di prim'ordine, sia per la chiarezza dell'esposizione come per l'organicità e la completezza delle trattazioni.

National Physical Laboratory: *Interferometry.* In-8°, 471 pp. & num. figg. Her Majesty's Stationery Office, London 1960 (s.i.d.p.). — È la raccolta delle relazioni presentate al Simposio sull'Interferometria tenuto a Londra dal 9 all'11 Giugno 1959. Le relazioni sono suddivise in cinque gruppi: Generalità, Misure assolute di lunghezze e sorgenti luminose per l'interferometria, Controllo ottico e misura della posizione relativa, Micro-onde ed interferometria dell'intensità, Interferometria spettroscopica e fotoelettrica. In generale ciascun rapporto è seguito dalla discussione cui esso ha dato luogo.

Information Processing. In-4°, 520 pp. & num. figg. Unesco, Paris, R. Oldenbourg, München-Butterworths, London 1960 ($ 25.00). — Il volume raccoglie gli Atti della Conferenza Internazionale sull'elaborazione numerica dei dati, organizzata dall'Unesco, che ebbe luogo a Parigi dal 15 al 20 Giugno 1959. Le relazioni presentate e qui pubblicate integralmente, con le relative discussioni, sono settantasette. Esse figurano raggruppate in sette sezioni: Metodi matematici di calcolo numerico; Linguaggio simbolico comune

alle macchine di calcolo numerico; Traduzione automatica delle lingue; Struttura e facoltà di adattamento delle macchine; Struttura logica delle macchine per il calcolo numerico; Tecniche future; Argomenti vari. La pubblicazione porta un decisivo contributo al progresso dei metodi per il trattamento meccanico dei dati, che è di fondamentale importanza anche ai fini della razionale e completa valorizzazione delle osservazioni geofisiche e meteorologiche.

Fultz D. & Al.: *Studies of Thermal Convection in a Rotating Cylinder with some Implications for Lange-Scale Atmospheric Motions.* In-4°, 104 pp. & 100 figg. American Meteorological Society, Boston 8, Mass., 1959 (s.i.p.). — Questa pubblicazione, che costituisce la No. 21 della serie « Meteorological Monographs », ha lo scopo di far conoscere i risultati delle esperienze eseguite all'Università di Chicago su modelli dell'atmosfera, realizzati con cilindri rotanti nel cui interno erano installate sorgenti o « pozzi » di calore. Vennero trovati due regimi convettivi principali, corrispondenti a grandi e piccoli valori del numero di Rossby.

Fournier F.: *Climat et Erosion.* In-4°, 201 pp. & num. figg. Presses Universitaires de France, Paris 1960 (NF 20.00). — Il libro offre ai lettori uno studio sistematico dei rapporti esistenti fra l'erosione del suolo operata dall'acqua e le precipitazioni atmosferiche. La prima parte (66 pagg.) è dedicata all'esame generale dei fattori in gioco, mentre le altre due costituiscono la parte originale del lavoro. In esse l'A. ricerca e trova delle relazioni numeriche e grafiche fra l'erosione del terreno e le precipitazioni (intensità e ripartizione nell'anno). Le correlazioni stabilite sono quindi sottoposte ad una critica statistica, tenendo conto dei fattori geomorfologici e geografici. Infine, l'A. valorizza le sue deduzioni valutando altresì l'erosione totale subìta da tutte le terre emerse. Il volume termina con una bibliografia delle opere che hanno servito per la compilazione del testo.

Berkner L. V. & Odishaw H.: *Science in Space.* In-8°, 458 pp. & num. figg. Mc Graw-Hill Book Co., Inc., New York & London 1961 (54 s. 6d). — La scienza dello spazio sta prendendo vita grazie al contributo di varie discipline, la cui evoluzione ha appunto portato alla conquista dello spazio. Va quindi segnalato con particolare favore il presente libro che raccoglie diverse monografie illustrative del medesimo contributo, ad opera di vari specialisti. La materia è distribuita in otto parti. Nella prima vengono anzitutto messi a punto i principali problemi relativi all'esplorazione dello spazio, con cenni ai risultati generali già raggiunti. Dopo il capitolo dedicato alla gravità (R. H. Dicke), la terza parte è relativa alla Terra, i cui problemi « spaziali » vengono trattati sia dal punto di vista geodetico (G. P. Woollard), sia da quello meteorologico (H. Wexler), come per lo studio dell'alta atmosfera (W. W. Kellogg, A. H. Shapley & O. G. Villard, Jr.). Nelle parti seguenti gli argomenti esaminati riguardano la Luna, i pianeti, la fisica delle particelle nello spazio, la radiazione cosmica, le fascie di van Allen, le aurore, nonchè il Sole e l'astronomia galattica ed extragalattica. Infine, si dànno alcuni cenni sulle conoscenze preliminari e sulle ipotesi relative all'influenza dello spazio sui fenomeni biologici. Un indice degli Autori ed uno analitico chiudono l'interessante volume.

Toperczer M.: *Lehrbuch der allgemeinen Geophysik.* In-8°, 384 pp. & 158 figg. Springer-Verlag, Wien 1960 ($ 15.25). — In conformità al titolo, questo libro ha finalità prevalentemente didattiche. Esso riguarda soltanto la Terra solida. La materia è suddivisa in cinque parti. La prima, dedicata alla Statica, contiene l'illustrazione dei metodi della Geodesia classica e di quella fisica, con particolare sviluppo della Gravimetria e dei metodi di interpretazione dei risultati relativi, in quanto si riferiscono alla costituzione della crosta terrestre. La sezione dedicata alla Dinamica tratta successivamente delle maree della crosta solida, degli spostamenti del polo terrestre, nonchè delle diverse forze geotettoniche. Alla Sismologia è dedicata la terza parte, dove sono

illustrati tutti i principali argomenti, dalla teoria della propagazione delle onde sismiche alla macrosismica, dalla teoria dei sismografi alla distribuzione geografica dei sismi ed alla loro occorrenza in senso statistico. Le novanta pagine seguenti hanno per oggetto il Geomagnetismo, il cui esame vien fatto organicamente sia da punto di vista teorico come da quello sperimentale, ossia con un'ampia discussione di tutti i risultati dedotti dalle osservazioni. L'ultima parte riguarda la costituzione interna della Terra, dove vengono trattati i problemi relativi alla sua età, alla sue condizioni termiche ed alle cause del campo geomagnetico. Nell'insieme, per la chiarezza e la sobrietà della esposizione, il libro rappresenta un ottimo trattato elementare di Geofisica ed esso viene quindi raccomandato agli studenti universitari, specialmente a quelli dei corsi per la laurea in Scienze geologiche.

Fanselau G.: *Geomagnetismus und Aeronomie*, Bd. II (*Geomagnetische Instrumente und Messmethoden*). In-4°, 648 pp. & 657 figg. Deutscher Verlag der Wissenschaften, Berlin 1960 (DM 123.–). — Questo secondo volume del trattato di « Geomagnetismo ed Aeronomia », compilato sotto la direzione del Prof. G. Fanselau, riguarda gli strumenti geomagnetici ed i metodi di misura relativi. I vari capitoli sono stati redatti da H. Wiese, H. Schmidt, O. Lucke e F. Frölich. Il volume è diviso in quattro parti. La prima ha per oggetto la teoria degli strumenti classici per la misura del campo geomagnetico ed occupa le prime 157 pagine. Nella sezione seguente sono illustrati, con ogni dettaglio, i metodi moderni di misura del Geomagnetismo (pp. 161-404), secondo una esposizione che comprende tutti o quasi gli strumenti sinora proposti ed applicati con successo. La terza parte riguarda i compiti ed i lavori che debbono svolgere gli Osservatori geomagnetici (pp. 407-488). Infine, nell'ultima sezione vengono esaminati i metodi di rilievo del campo geomagnetico, sia su terra ferma, come sul mare e dall'aereo (pp. 491-551). Un'ampia appendice (di oltre 70 pagine) è quindi riservata ai metodi sperimentali per la misura delle caratteristiche magnetiche dei materiali ed in particolare delle rocce. Ogni sezione è corredata alla fine da una bibliografia selezionata. Un indice analitico assai dettagliato chiude il volume. Il numero considerevole delle figure (in media una per ogni pagina di testo) documenta il dettaglio tecnico che caratterizza l'esposizione di ogni argomento trattato.

George J. J.: *Weather Forecasting for Aeronautics*. In-8°, 673 pp. & num. figg. Academic Press, New York & London 1960 ($ 15.00). — Il libro, compilato con la collaborazione di vari specialisti, ha finalità pratiche e riguarda particolarmente i metodi di previsione del tempo nel Nord America. Ciònondimeno, i richiami di meteorologia generale sono esposti con chiarezza e razionalità così da giustificare le applicazioni esposte, anche in condizioni diverse. La materia è distribuita in 18 capitoli: Il problema delle previsioni, Costruzione delle carte bariche previste, La previsione della ciclogenesi, Idem per i vari stadi di vita di un ciclone, Spostamento degli anticicloni sul Nord-America, Moto delle depressioni fredde a 500 mb, Spostamento dei fronti freddi al suolo, Analisi dei fronti caldi, Moto dei cicloni tropicali, Il metodo « Poor Man's » di previsione, Sintesi di una carta di previsione, La previsione della nebbia, Idem delle precipitazioni, Idem degli uragani, Idem delle grandi nevicate, La previsione del vento ai fini della navigazione aerea, L'impiego del Radar nelle previsioni, Le previsioni locali. La bibliografia, raccolta in appendice, comprende 114 citazioni. Nell'insieme il libro valorizza i metodi empirico-statistici di previsione, ai quali viene data importanza prevalente rispetto quelli fisico-sinottici.

Aitken M. J.: *Physics and Archaelogy*. In-8°, 181 pp. & num. figg. Interscience Publishers, New York & London 1961 ($ 6.00). — Il libro descrive i metodi fisici utilizzati o proposti per scopi archeologici, secondo un indirizzo in parte simile ai procedimenti in uso nella prospezione geofisica del sottosuolo a scopi minerari. La materia trovasi sviluppata in sette capitoli: 1) Generalità; 2) Metodi magnetici; 3) Il magnetometro

protonico; 4) Metodi elettrici a resistività; 5) Datazione, 6) Metodi radioattivi di datazione; 6) Datazione geomagnetica; 7) Analisi. Alla fine di ogni capitolo è riprodotta una bibliografia selezionata. La trattazione è chiara ed accurata, anche se le valutazioni quantitative sono fornite con richiami assai limitati di formule. Il libro riesce comunque di utile lettura anche al Geofisico.

Nalivkin V. D.: *The Geology of the U.S.S.R.*, In-8°, 170 pp. & 2 tavv. f. t. Pergamon Press, Oxford 1960 (30 s.). — Il libro, tradotto dall'originale russo a cura di J. E. Richey, fornisce al lettore le principali caratteristiche geologiche del territorio dell'U.R.S.S. La materia è distribuita in dieci capitoli: La piattaforma russa, La Siberia, Il bassopiano della Siberia Occidentale, Gli Urali, L'Artico Occidentale, La Geosinclinale di Angara, L'Asia Centrale, La Geosinclinale Mediterranea, Il limite Nord-Occidentale della Geosiclinale Mediterranea, La Geosinclinale del Pacifico. La carta geologica allegata, in due fogli, è alla scala di 1 : 7.500.000.

Bubnoff (von) S.: *Grundprobleme der Geologie.* In-8°, 234 pp. & 60 figg. Akademie-Verlag, Berlin 1959 (DM 14.00). — Si tratta di una ristampa invariata della precedente terza edizione. Essa venne curata dal Prof. H. Stille, al quale si deve anche la prefazione.

Péguy Ch. P.: *Précis de Climatologie.* In-8°, 348 pp. & 97 figg. Masson & Cie, Editeurs, Paris, 1961 (42 NF). — Cet ouvrage n'a pas d'équivalent dans la littérature scientifique de langue française. Sans doute, les connaissances concernant l'atmosphère inférieure avaient-elles fait depuis vingt ans en France — comme ailleurs — de très rapides progrès, mais les géographes français éprouvaient depuis longtemps quelques difficultés à insérer dans leur propre discipline certaines acquisitions des physiciens ou des biologistes. C'est ce qui a été tenté dans cet ouvrage. Après une rapide mise au point de ce qu'un géographe doit aujourd'hui connaître de la physique de l'atmosphère et de ses mouvements, l'auteur s'appuie tantôt sur la méthode statistique, tantôt sur la consideration de quelques lois physiques élémentaires pour préciser principalement les mille nuances de ce qu'il nomme l'« efficacité » des températures et des précipitations. Les questions de méthodologie climatique sont longuement développées. Mais le tout reste donné dans un cadre qui respecte volontairement les usages de l'enseignement géographique. Ecrit par un géographe, cet ouvrage est destiné avant tout aux géographes.

Direttore resp. Prof. Mario Bossolasco
Unione Tipografica - Autorizzazione del Tribunale di Milano del 18 Febb. 1949, N. 1155

you need up to date

Geophysics abroad

Ask SEISMOS

G. m. b. H.
Hannover-Germany

Since 1921 succesful all over the world

Magnetic-recording